Energy, Environment and Sustainable Development
1998-2002
Call identifier: EESD-ENV-99-2

Key Action 2: Global Change, Climate and Biodiversity
Area 2.4 European Component of the Global Observing Systems
RTD priority-2.4.1: Better Exploitation of Existing Data and Adaptation of Existing Observing Systems

Final report

Quantification and Interpretation of Long-Term UV-Visible Observations of the Stratosphere

Acronym: QUILT

Project number: EVK2-2000-00545
Contract N°: EVK2-CT-2000-00059
Date of preparation: 29 November 2004

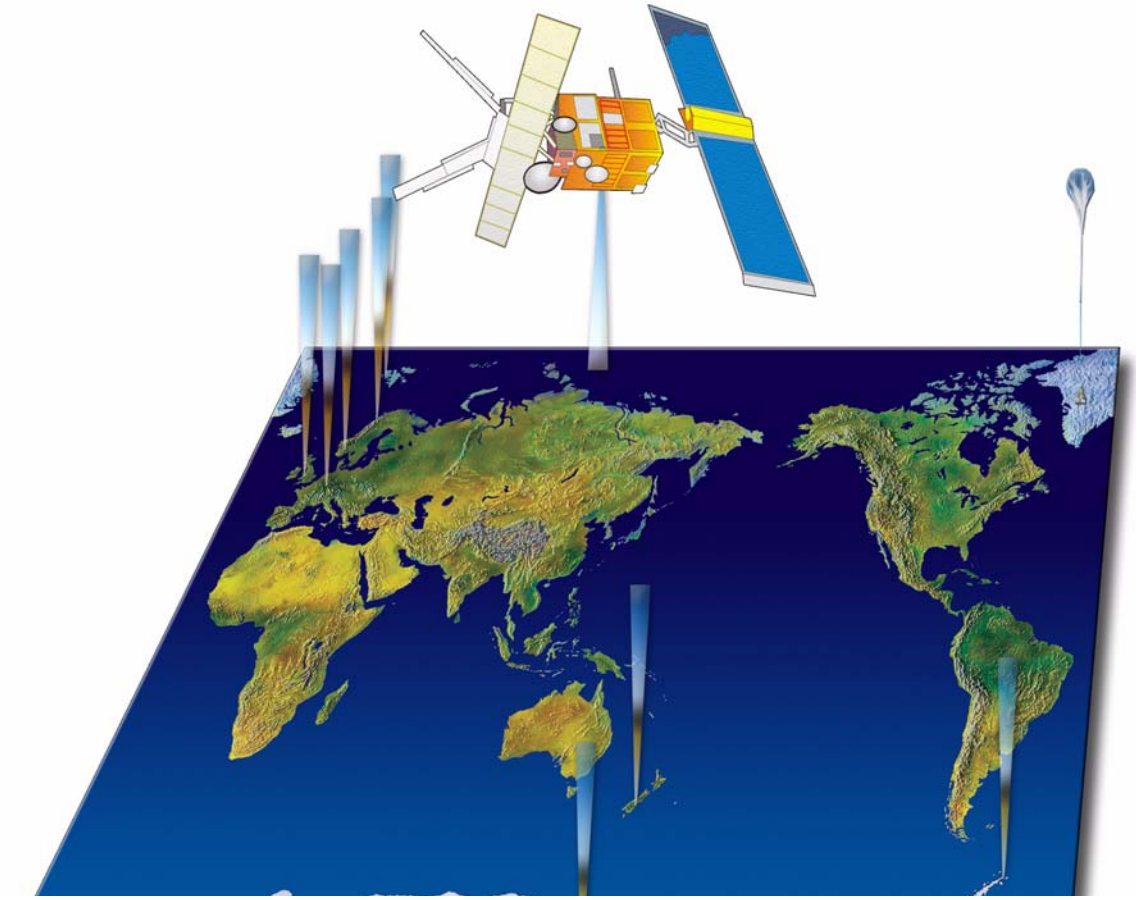

QUILT - Final Report

Project coordinator: Geir O. Braathen, Norwegian Institute for Air Research
Report edited by: Kerstin Stebel, Norwegian Institute for Air Research

Contributions from:

Norwegian Institute for Air Research (NILU), Kjeller, Norway
Geir O. Braathen, Kåre Edvardsen, Britt Ann K. Høiskar, Arve Kylling, Kerstin Stebel, and Kjersti K. Tørnkvist

Belgian Institute for Space-Aeronomy (IASB-BIRA), Brussels, Belgium
Caroline Fayt, François Hendrick, and Michel Van Roozendael

Institute of Environmental Physics, University of Bremen (IUP-UHB), Bremen, Germany
John P. Burrows, Sixten Fietkau, Thomas Medeke, Hilke Oetjen, Andreas Richter, Björn-Martin Sinnhuber, Mark Weber, and Folkard Wittrock

Service d'Aéronomie du Centre National de la recherche Scientifique (CNRS-DR5-SA), Paris, France
Florence Goutail, Aude Mieville, Franck Lefevre, Jean-Pierre Pommereau

The Institute for Environmental Physics at the University of Heidelberg (U-Heidelberg), Heidelberg, Germany
Andre Butz, Barbara Dix, Udo Frieß, Klaus Pfeilsticker, Ulrich Platt, Irene Pundt, Roman Sinreich, Christoph von Friedeburg, and Thomas Wagner

University of Leeds (UNIVLEEDS), School of Environment, United Kingdom
Martyn Chipperfield and Wuhu Feng

NERC-British Antarctic Survey (BAS), Cambridge, United Kingdom
Howard Roscoe and Laurent Denis

National Institute of Aerospace Technology (INTA), Torrejón de Ardoz, Spain
Manuel Gil, Monica Navarro, Olga Puentedura, and Margarita Yela

National Institute for Space Research (SRON), Utrecht, The Netherlands
Jos de Laat

Institute of Atmospheric Sciences and Climate (CNR-ISAC), Bologna, Italy
Daniele Bortoli, Giorgio Giovanelli, Ivan Kostadinov, Andrea Petritoli, and Fabrizio Ravegnani

Solar-Terrestrial Influences Laboratory, Stara Zagora Department, Bulgarian Academy of Sciences (STIL-BAS)
Rolf Werner

Acronym List

AMF	Air Mass Factor
CTM	Chemical Transport Model
DOAS	Differential Optical Absorption Spectroscopy
DSCD	Differential Slant Column Density
EASOE	European Arctic Stratospheric Experiment
EC	European Commission
ECMWF	European Centre for Medium-Range Weather Forecasts
ENVISAT	Environmental Satellite
ERS	European Remote Sensing Satellite
ESA	European Space Agency
EU	European Union
GATO	Global Atmospheric Observations
GB	Ground-Based
GCM	General Circulation Model
GOME	Global Ozone Monitoring Experiment
NDSC	Network for the Detection of Stratospheric Change
NRT	Near-Real Time
OA	Off-axis DOAS
ODP	Ozone Depletion Potential
ODS	Ozone Depleting Substances
PMT	Project Management Team
PSC	Polar Stratospheric Cloud
RTD	Research, Technological development and Demonstration
RTM	Radiative Transfer Model
SAGE	Stratospheric Aerosol and Gas Experiment
SAOZ	Système d'analyse par observations zénithales
SESAME	Second European Stratospheric Arctic and Mid-latitude Experiment
SCD	Slant Column Density
SCIAMACHY	Scanning Imaging Absorption spectrometer for Atmospheric Chartography
SYMOCS	System for Monitoring Compounds in the Stratosphere
SZA	Solar Zenith Angle
THESEO	Third European Stratospheric Experiment on Ozone
UKMO	United Kingdom Meteorological Office
UNEP	United Nations Environment Programme
VINTERSOL	Validation of INTER-national Satellites and study of Ozone Loss
VCD	Vertical Column Density
WMO	World Meteorological Organisation
WP	Work package
WWW	World Wide Web (Internet)

SECTION

6

Detailed report related to overall project duration

6.1 Background

In the Antarctic, springtime O_3 started to decrease dramatically in the early 1980's. From 1980 onwards the size of the "ozone hole", defined as that region having O_3 value below 220 DU, grew, and in addition it persisted for increasingly longer periods. After about 1989 the extent of depletion has stayed fairly constant with arguably some increase in size and duration. As a result of the halogen induced depletion cycles, it appears that throughout the 1990s, the stratospheric polar vortex air below approximately 25 km had very low values of ozone: the halogens being activated by the multi-phase or heterogeneous reactions of the so-called halogen reservoir species (eg. HCl, $ClONO_2$, HOCl, $BrONO_2$ etc.) on polar stratospheric clouds (PSCs), which form at relatively low stratospheric temperatures. The source of the halogens is primarily the anthropogenic release of chlorofluorocarbon compounds (CFCs), their substitutes, the HCFCs, the halons, methyl bromide and related compounds. The stratospheric dynamics above the Arctic in winter and spring is in comparison with that above Antarctica less predictable. It also appears that the ozone depletion in the polar vortex seems to be somewhat time lagged compared to that above Antarctica. Several winters winters in the 1990s associated with a strong and persistent polar vortex in the Northern Hemisphere and low temperatures have been characterised by severe Arctic ozone loss. Figure Figure 6.1.1-1 shows how the change from 1980 to 1997.

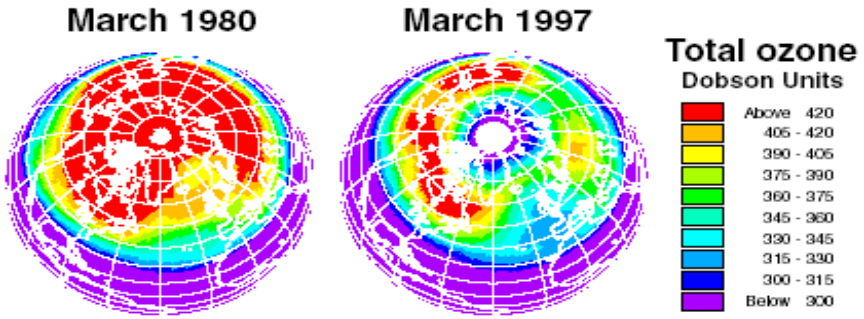

Figure 6.1.1-1. *Monthly mean total ozone over the Northern Hemisphere for the month of March for the years 1980 (left) and 1997 (right). Figures are based on data from TOMS on Nimbus-7 and on the Earth Probe.*

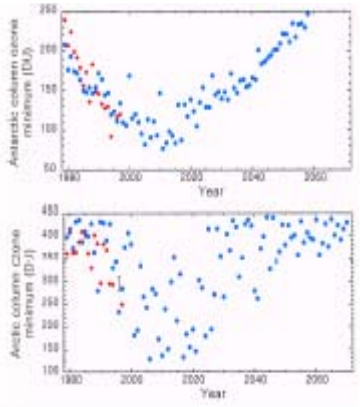

Figure 6.1.1-2. *GCM calculations coupled with stratospheric chemistry show than one can expect the ozone minimum in March to drop down to around 120 DU in certain winters between 2010 and 2019. In Antarctica one could expect ozone to drop down to 75 DU. Adapted from Shindell et al.*

The in the 1970's the typical behaviour of having an ozone "high" over the polar cap is in recent winters no longer the case. This pattern of stratospheric ozone behaviour resembles that observed over Antarctica, although the depletion is less severe. In general the most significant cases of ozone loss have been associated with unusually low temperatures in the Arctic stratosphere. Examples of this behaviour were in the winters and springs of 1995/1996, 1996/1997 and it appears that 1999/2000 is following this pattern. In contrast the stratosphere had an early warming in 1997/1998 and 1998/1999, and consequently the polar vortex was not stable. Nevertheless halogen activation and some associated ozone depletion could be observed in the polar vortex.

Recently a link between global warming and stratospheric ozone depletion has been made. The resultant cooling of the stratosphere appears to stabilise the polar vortex and increase ozone depletion. Simulations coupling general circulation models with stratospheric chemistry predict that the total ozone in the Arctic vortex in March can drop to 120 DU during the decade from 2010 to 2019 [Shindell, et al. 1998]. This is illustrated in Figure 6.1.1-2. Although these calculations are uncertain, they show that the coupling between ozone and climate can cause severe ozone depletion after the maximum in halogen loading has been reached.

At mid latitudes significant ozone depletion is also observed. The explanation of this phenomenon is not yet fully understood, having aspects of dilution of ozone poor air from the polar vortex, possible halogen activation and homogeneous gas phase catalytic destruction of ozone by halogen species in the middle and upper stratosphere. Several other factors that remain yet to be explained include:

- *The increasing trend of stratospheric NO_2. The trend is larger than expected from decreasing aerosol loadings, and models also appear to under estimate NO_2 in Polar Regions.*
- *What is the role of stratospheric iodine, i.e., IO, in stratospheric ozone depletion?*

In summary as a result of the non-linear complex nature of the atmosphere chemistry, transport models of the atmosphere in spite of large improvements in their accuracy in the last 25 years, continue to rely on the long-term measurement of atmospheric composition. For policymakers there is a clear need to continue and improve the accuracy of measurements of stratospheric constituents and combine these with models describing and predicting the behaviour of the stratosphere. The growing risk for future ozone loss increases the need for reliable atmospheric chemistry models. The objectives of QUILT specifically address this need. QUILT aims to combine not only validated global measurements of ozone and key stratospheric constituents and test the capability of the atmospheric models using existing data, but to extend and improve the data set for the period 2001 to 2003 when stratospheric halogen loading is predicted to reach its maximum. In addition it will continue to provide the user community with near real time data products from the European satellite instrument GOME.

References:

Shindell, D.T, D. Rind and P. Lonergan, Increased polar stratospheric ozone losses and delayed eventual recovery owing to increasing greenhouse-gas concentrations, Nature, 392, 589-592, 1998.

WMO (1998), Scientific Assessment of Ozone Depletion: 1998, Global Ozone Research and Monitoring Project, Report No. 44, ISBN: 92-807-1722-7.

6.2 Scientific, technological and socio-economic objectives

6.2.1 Scientific/technological objectives

Within the QUILT project several central outstanding issues within the field of stratospheric ozone depletion have been addressed:

1. To determine the abundances of stratospheric ozone, the key free radicals NO_2, BrO, OClO and IO throughout the period of 1990 to 2003 by analysing measurements made by the global ground-based ultraviolet/visible spectrometer network, existing balloon-borne ultraviolet/visible observations and by the European satellite instruments GOME and possibly SCIAMACHY.
2. To quantify the extent of chemical ozone depletion on a global scale during the 1990s and beyond, and to determine the relative contributions to this depletion of different chemical species. The cumulative chemical ozone-loss and its geographical extent will be determined.
3. To improve our knowledge of the latitudinal, seasonal and interannual trends of NO_2, BrO, OClO and possible IO, and to interpret the role of these species in terms of the long-term effects on stratospheric ozone.
4. To use the data and insight gained from the three points above to close the gap between measured and theoretically calculated ozone loss via the creation of the best possible synergy between existing measurements and models.

6.2.2 Socio-economic objectives

The European Dimension of the Problem

The thinning of the ozone layer is a global problem and therefore affects all of Europe. The substantial ozone loss that has been observed in the Arctic has affected Europe more than other regions of the Northern Hemisphere. This is due to the fact that the polar vortex often is shifted towards the European sector of the Arctic because of the Aleutian high (a high-pressure system that sits over Alaska and Eastern Siberia). Therefore, the depletion of stratospheric ozone is not a problem for a single nation or a small region. At the present moment, we are witnessing what potentially may become the most severe ozone-loss conditions yet observed in the European Arctic stratosphere. The problem is common to all European countries. It is of strategic importance to Europe to obtain a better understanding of the ozone layer problem. GCM calculations predict that the coupling of ozone and climate may lead to far more dramatic ozone loss during the decade from 2010 to 2020 than has been observed during the 1990s. It will therefore be of importance to further improve European atmospheric chemistry models in order to calculate future projections of stratospheric ozone-loss with greater accuracy.

The impact of carrying out the project at a European level is far greater than if it were to be carried out separately through isolated national projects. One reason for this is the need to combine data obtained by different experimental techniques. In order to get a complete picture of the processes that cause ozone depletion one needs to collect data on as many chemical compounds and atmospheric parameters as possible. This implies joining the skills, competence and instrumental technologies of several nations. There is no single nation in Europe that possesses the

range of instruments and theoretical models that are necessary to get a reasonable overview of the processes responsible for ozone depletion. QUILT consists of the entire range of UV-Vis techniques, the European NDSC UV-Visible ground-based stations in several countries, balloon-borne spectrometers, and 3-D CTM modelling techniques from three different nations (UK, France and the Netherlands). It is beyond the resources of one single nation to carry out such a complete observational and modelling project.

This project involves ten European research institutions. These institutions constitute a large part of the European know-how in the areas of UV-visible ground-based monitoring, balloon-borne measurement techniques, satellite measurements of stratospheric species, and associated modelling activities. In addition, UV-visible spectroscopy is also the most proven and validated method available for the detection of stratospheric ozone loss. The project aims at measuring stratospheric components that influence stratospheric ozone depletion over Europe. The compounds of interest include BrO, OClO, NO_2, O_3 and IO. These compounds are derived from a combination of both natural and anthropogenic sources. The project will focus more particularly on halogenated species that are of special interest and concern due to their relatively large anthropogenic contribution, as well as their strong ozone depletion potentials. Although this area of research can be considered as global in perspective, the emphasis will be placed on the European scale. This means that the research in this project directly or indirectly addresses problems common to all European countries: stratospheric ozone depletion, global change and factors leading to changes in surface level UV irradiance. The project also aims at the improvement of data products from European satellites, through the reinforcement of the existing collaboration between the ground-based and balloon communities, and the community of new satellite instruments.

The European Added Value of the Consortium

The research described herein cannot be carried out by one single country due to its trans-national dimension and geographical coverage, which means that the European approach adds value compared to a local, national or bilateral approach which would only shed light on limited aspects of the problem. The project needs to be carried out at a community rather than national level in order to combine and obtain sufficient skills and resources both in human, technological and financial terms. The consortium established incorporates the European ground-based UV-visible network, balloon-borne instrumentation, satellite data exploitation and 3D model investigations: obviously a service that can only be provided by a multinational group. Such activities must be conducted in order to aid in the evolution and implementation of EU environmental policy. The use of the NADIR data centre also contributes to the European added value. This data centre has been used with success in earlier ozone campaigns such as EASOE, SESAME, THESEO and EuroSOLVE. The research is also of strategic importance since it will contribute to putting Europe at the forefront in the international scene of ozone layer research. The NADIR data centre will play an important role in WP6000, whereby the QUILT consortium will provide a NRT data product service for the scientific and general community. Information consisting of both NRT measured data from the GOME satellite instrument and Arctic ground-based DOAS systems, as well as NRT 3D-CTM results on Arctic ozone-loss will be made available via the project webpages.

The project's contribution to EU policies

European countries and the European Union have responsibilities under the Montreal protocol of the Vienna Convention, its amendments and the Framework Convention on Climate Change. Knowledge about the state of the ozone layer constitutes the basis for negotiations and decisions on the political level concerning the phase-out of ozone depleting substances. The Intergovernmental Panel on Climate Change (IPCC) will consider aircraft impacts in its next report. For these reasons, it is essential that there is a strong, independent European scientific effort in stratospheric research. QUILT will contribute to the knowledge which is necessary to formulate a sound environmental policy which aims at protecting the environment by quantifying both chemically-induced ozone loss in the Arctic and at mid-latitudes. The improvement of computer models, which is one of the main goals of QUILT, is necessary for the prediction of future ozone loss. Such predictions will have implications for community policies on the phase-out of ozone depleting substances. Within the QUILT consortium, several validated European 3D-CTMs have been included.

Quality of life and health and safety

If it had not been for the existence of ozone observing networks the use of ozone depleting substances would have continued unabated and the thinning of the ozone layer would not have been discovered until severe effects were evident. For humans an increase in UV-B radiation can cause skin cancer, eye cataracts, sunburn, snow blindness, skin ageing and depression of the immune system. Non-melanoma skin cancer is one of the most common forms of cancer in humans and a relation with UV-B radiation has been established (WMO, 1998).

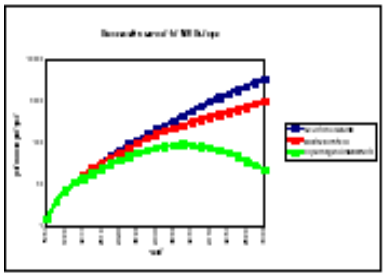

Figure 6.2.2-1. *Excess skin cancer incidence in North-West Europe under three different scenarios for ODS reductions. The blue curve shows the result for no action, the red curve for the first Montreal Protocol and the green for the Copenhagen amendments of the Protocol. Note the logarithmic scale on the y-axis. Adapted from Slaper et al.*

Figure 6.2.2-1 shows the excess skin cancer rate that would result under three different scenarios: 1) No reductions in emissions (or "business as usual") 2) The first Montreal Protocol and 3) The Montreal Protocol with the Copenhagen amendments.

Had no action been taken the skin cancer incidence would have increased to more than 2000 per million inhabitants per year in the year 2100. This represents a quadrupling compared to the actual skin cancer incidence. The first Montreal Protocol from 1987 would not have been enough to reverse this trend. Only with the London, Copenhagen and Vienna Amendments and Adjustments are the restrictions severe enough to prevent a run-away depletion of ozone (WMO, 1998). Since non-compliance is one of the most important current problems for the preservation of the ozone layer it is important that one continues to keep a close eye on the development. In addition to non-compliance there are others threats to the ozone layer: The increasing concentrations of greenhouse gases will lead to a cooling of the stratosphere, which will lead to a higher probability for PSC formation and hence halogen activation. Increasing amounts of water vapour in the stratosphere, due to air traffic and increased amounts of methane, will also contribute to more PSCs in the Arctic winter. All these negative developments call for a better understanding of the processes that cause ozone depletion and they give rise to a need for models that can predict the future development of the ozone layer under various scenarios. The results from QUILT will contribute to a better understanding of these processes and thereby to the improvement of models that predict future ozone change. Better models will enable us to better predict the consequences of various political actions to reduce ODS emissions and hence are important for the health and well-being of the citizens of Europe during the next century.

The research carried out within this project will contribute to improve the existing network capabilities for long-term monitoring of stratospheric oxygenated halogens, and to assess current 3D models in their ability to reproduce these observations. A new aspect of increasing importance will be the better exploitation

of the data from European satellites for studying stratospheric ozone trends as well as the effects of large-scale tropospheric pollution. This will lead to a better understanding of the mechanisms involved in ozone destruction in mid- to high latitude regions.

Preserving and/or enhancing the environment and the minimum use/conservation of resources

This aspect cannot be over emphasised. The main aim of such research is for the better understanding of natural processes that can directly contribute to the preservation and conservation of natural resources. The project proposed here improves the scientific underpinning of international and European environmental legislation such as the Montreal Protocol, the subsequent amendments and future revisions. Improvement in the quality of health and life/ecosystems, can be extended to cover also the preservation and enhancement of the environment. The ultimate goal of environmental legislation is to reduce the exposure of humans and ecosystems to toxic effects. A better understanding of the processes that influence stratospheric ozone can play a very significant role in this wide reaching social issue.

Marine recources:

UV-B radiation has been found to affect aquatic ecosystems, by limiting the production of phytoplankton and causing damage to the early development stages of fish, shrimp, crab, amphibians and other animals (UNEP, 1995). Phytoplankton form the basis of the food chain in the oceans; more than 30% of the world's human consumption of animal protein comes from the sea, with an even larger percentage in developing countries. One study (Smith et al. 1992) has shown that a reduced production of phytoplankton of 6-12% that occurred around the waters of Antarctica was directly related to an increase in UV-B resulting from the Antarctic ozone hole. As phytoplankton form a large sink for atmospheric CO_2 this may also influence atmospheric CO_2 concentrations and the enhanced greenhouse effect in the future, but this effect has not been demonstrated yet. The Barents Sea is the region in the world with the highest production of biomass. Damage on plankton in this area can have negative consequences on the fish that feed on these microorganisms. This will again have large economic effects for the fishing industries in Europe.

Agriculture:

The growth of terrestrial plants is also affected by UV-B radiation, even at present-day levels. There are large differences in UV-B response among species. Plants have several mechanisms to repair the effects of UV radiation and may, to a certain extent, adapt to increased radiation levels. UV radiation could affect the biodiversity of ecosystems by changing the balance of species. In agriculture, increased UV-B levels may decrease crop yield, which may necessitate the use of more resistant species or new cultures (UNEP, 1995). In order to assess the future UV climate in Europe one must have a good knowledge of the processes that lead to ozone depletion and modelling tools that can apply this knowledge in computer simulations of the future.

Other effects:

Increased levels of UV-B radiation may cause damage to materials, such as plastics, due to photo-degradation. This may limit the lifetime and quality of these materials and increase costs by requiring higher levels of light stabilisers or earlier replacement of the materials. In addition, UV radiation affects chemical processes in the lower atmosphere. It contributes to tropospheric ozone concentrations in polluted regions and influences the atmospheric lifetime and concentration of a large number of compounds, including several greenhouse gases.

References:

Smith, R.C, B.B.Prezelin, K.S. Baker, R.R. Bidigare, N.P. Boucher, T. Coley, D. Karentz, S. MacIntyre, H.A. Matlick, D. Menzies, M. Ondrusek, Z. Wan, K.J. Waters (1992): Ozone depletion: Ultraviolet radiation and phytoplankton biology in Antarctic waters, Science, 255, 952-959.

UNEP (1995): Environmental effects of ozone depletion, 1994 assessment, Ambio 3, 138-196.

WMO (1998), Scientific Assessment of Ozone Depletion: 1998, Global Ozone Research and Monitoring Project, Report No. 44, ISBN: 92-807-1722-7.

6.3 Applied methodology, scientific achievements and main deliverables

6.3.1 WP 2000: Improved UV-Visible data products

WP 2100: Ground-based off-axis DOAS measurements of BrO, NO_2 and IO

Applied methodology and scientific achievements

Ground-based differential optical absorption spectroscopy (DOAS) measurements of atmospheric trace gases in their traditional setup – measuring skylight scattered in the zenith – have a high sensitivity towards stratospheric absorbers. However, zenith-sky DOAS observation can be affected by trace gases in the troposphere, which potentially leads to an improper assessment of the stratospheric column:

1. Local pollution can cause strong increases in NO_2 column densities, and which can lead to an overestimation of the stratospheric column if the tropospheric fraction of the NO_2 profile cannot be determined with sufficient accuracy.

2. A systematic bias between BrO vertical columns measured from ground and from satellite [Van Roozendael et al., 2002] indicates the possible presence of a global BrO background in the free troposphere. BrO concentrations of (0.6 ± 0.2) ppt being present in the free troposphere are inferred from ballon-borne DOAS measurements [Fitzenberger et al., 2000], and this tropospheric BrO background is expected to have a significant impact on measurements of the total column.

3. Released from sea salt, the presence of high amounts of reactive bromine in the boundary layer during polar spring causes strongly increased column densities of BrO [Frieß et al., 2004; Oetjen et al., 2002; Wittrock et al., 2000]. These events lead to strong discrepancies between modelled and measured BrO when total BrO columns are compared [Sinnhuber et al., 2002] and exacerbates the interpretation of the seasonal variability of BrO in polar regions [Sinnhuber et al., 2002; Frieß et al., 2004b; Wittrock et al., 1996].

Multi- Axis- (MAX-) DOAS, a measurement technique that has become more and more popular in recent years, has the potential to discriminate between tropospheric and stratospheric absorbers. By observing scattered light not only from the zenith but also from sky close to the horizon, a long light path through the lowermost atmospheric layers and a strongly increased sensitivity to trace gases located close to the surface can be achieved (see Figure 6.3.1-1).

The main objective of this workpackage is the better assessment of purely stratospheric columns using ground-based MAX-DOAS measurements of atmospheric trace gases. This measurement technique allows separating tropospheric and stratospheric partial columns, which is essential for the interpretation of zenith sky measurements and may explain existing differences between stratospheric model results, ground based and satellite borne observations that are sensitive for the total atmospheric column.

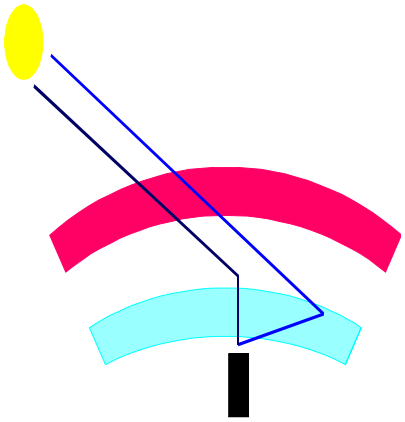

Figure 6.3.1-1. *Sketch of the measurement geometry used by the MAX-DOAS instruments. With a scattering height in the middle troposphere, the zenith viewing measurement (black) is weighted towards the stratosphere, whereas the horizon viewing measurement (blue) has a large sensitivity to the layers close to the ground. In first approximation, the stratospheric light paths are the same for both measurement geometries, enabling the boundary layer concentrations to be derived.*

During the QUILT project period, MAX-DOAS measurements of atmospheric trace gases have been performed at various locations, covering the Arctic, the northern mid- latitudes, the tropics and Antarctica, as well as 4 ship cruises from Bremerhaven to Antarctica onboard the Polarstern research vessel (see Table 6.3.1-1). In addition partner 2 (IASB), 3 (Univ. Bremen) and 5 (Univ. Heidelberg) particapated in the NDSC intercomparison in Andoya in February 2003 and in two campaigns within the FORMAT project with a MAX-DOAS setup.

Table 6.3.1-1. Ground-based MAX-DOAS measurements performed during the QUILT project period.

Lat	Lon	Location	Period	Participant
82.5	-62.3	Alert/Canada	04-06/2000	IUPHD
78.9	11.9	Ny-Ålesund/Spitsbergen	03/2000 - present	UHB
72.0	-38.0	Summit/Greenland	07/2003 - present	UHB
69.3	16	Andoya/Norway	02/2003	UHB, IUPHD and IASB
53.0	8.0	Bremen/Germany	10/2000 – present	UHB
49.4	8.7	Heidelberg/Germany	05-08/2003	IUPHD
47.3	10.6	Zugspitze/Germany	02/2002 – 07/2002	UHB
45.5	9.2	Milano area /Italy	07 – 08/2002 and 09/2003	IUPHD, UHB and IASB
43.9	5.7	OHP / France	01/2001 – 07/2002	IASB
8.3	-71.6	Merida / Venezuela	03/2004 – present	UHB
5.8	-55.2	Paramaribo/Suriname	06/2002 - present	IUPHD
-1.2	36.8	Nairobi / Kenya	09/2002 – present	UHB
-21.1	55.5	Reunion	07/2004 - present	IASB
-70.6	8.3	Neumayer/Antarctica	01/2003 - present	IUPHD
-77.8	166.7	Arrival Heights/Antarctica	10/1998 - present	IUPHD

As an example for the multi-axis DOAS technique we describe the instrumentation and data analysis used withing the Bremian DOAS network (BREDOM) in more detail:

Within the network a similar setups were build up at all stations (Ny-Ålesund, Bremen, Zugspitze, Merida, Nairobi)(see Figure 6.3.1-2). The main component is a grating spectrometer equipped with a 2-dimensional CCD detector. Light is transmitted from a simple telescope to the spectrometer through a quartz fibre bundle that also converts the spherical aperture of the telescope to the rectangular slit of the spectrometer. In addition, the quartz fibre bundle efficiently de-polarizes the light, an important quality as polarisation of skylight is changing during the day and grating spectrometers have different sensitivities towards parallel and perpendicular polarised light.

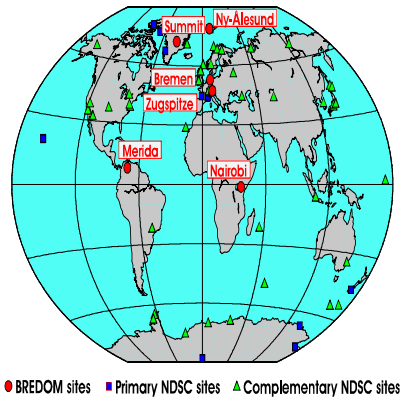

Figure 6.3.1-2. *The UV-Vis spectrometer network of the University of Bremen (BREDOM network)*

The telescope used is shown in Figure 6.3.1-3 and consists of two viewing ports, one to the zenith sky and another towards the horizon. A rotating mirror can be moved into the field of view of the zenith viewing fibre, directing the view towards the horizon at elevation angles between 0° and 30°. Usually, a sequence of 4 different horizon measurements and one zenith sky measurement is taken, each measurement averaging over roughly 1 minute, adding up to a total of 5 minutes for each measurement cycle. However, the instrument is fully programmable and other sequences can be selected for specific situations.

To assure high quality measurements, the instruments have to be kept as stable as possible and be calibrated on a regular basis. To provide calibration, the instruments are equipped with a HgCd spectral line lamp and a tungsten lamp in the telescope. Each night, calibration measurements are performed automatically, providing data for monitoring of system performance (spectral alignment, spectral resolution, radiance throughput) and for the correction of instrument parame-

ters in the data analysis (slit function, pixel-to-pixel variation). The spectrometer is housed in an insulated box that is maintained at constant temperature throughout the measurements; the CCD detector is cooled to provide low dark signal. As the telescope is usually situated outside of a building, it is heated to guarantee motor operations and to avoid accumulation of ice and snow on the optical ports.

Operation of the instruments is fully automated and data acquisition is controlled by a computer as a function of time and solar elevation. Data collection as well as instrument control is performed via internet connection. Depending on the location, computer time is adjusted via the internet of from a built in GPS receiver. Except in the case of hardware failure, the instruments run without maintenance for many months.

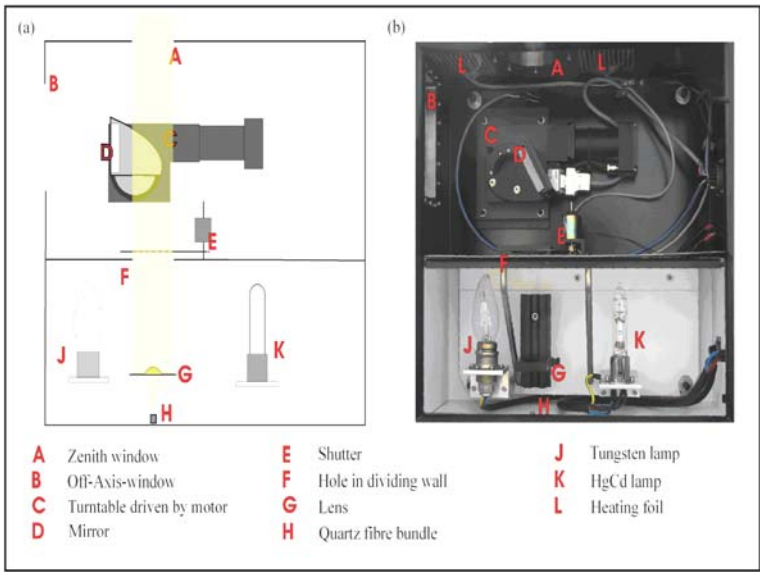

Figure 6.3.1-3. *Schematic (left) and photo (right) of the telescope used by the BREDOM instruments*

The basic quantity measured by the instruments are spectra between 320 and 600 nm at a spectral resolution of 0.5 to 1.5 nm. Measurements are taken at different solar elevations throughout the day and quasi simultaneously at different viewing angles. From the spectra, optical densities of a number of absorbers in the UV and visible spectral region can be retrieved using the Differential Optical Absorption Spectroscopy (DOAS) technique. In order to apply the DOAS retrieval, a background spectrum has to be selected to compensate for the strong Fraunhofer lines that are evident in solar radiation and also in scattered sun light. This background spectrum is either a zenith-sky measurement taken at high sun with the same instrument, or a measurement taken at the same time but in a different viewing direction. The result of the DOAS analysis is a quantity called slant column that corresponds to the integrated amount of the absorber along the (mean) light path through the atmosphere. If the background spectrum also contains atmospheric absorptions, the differential slant column, that is the difference in absorption between the two measurements is retrieved.

To convert this quantity into a geometry independent column, a radiative transfer model is used to simulate the light path through the atmosphere for a given situation, and to compute an enhancement factor (airmass factor) that provides the ratio between the measured slant column and the vertical column that is the absorber concentration integrated vertically from the surface to the top of the atmosphere.

Daytime BrO, NO_2 and IO slant columns measured at sites using both off-axis viewing and zenith-sky geometry (D5)

MAX-DOAS observations of BrO and its vertical distribution during surface ozone depletion at Alert

MAX-DOAS measurements of boundary layer BrO were conducted during the ALERT2000 polar sunrise experiment at Alert, Nunavut, Canada in April/Mai 2000 [Hönninger, 2002; Hönninger and Platt, 2002]. For the first time the MAX-DOAS method was applied to derive vertical profile information of BrO. BrO was observed at slant column densities (SCDs) of up to 10^{15} molecules/cm^2 during a 10-day period. The largest BrO SCDs were found by observing scattered sunlight from 5^0 above the horizon, and SCDs were decreasing with increasing elevation angles of the light-receiving telescope. For zenith scattered light the lowest absorption was recorded. Radiative transfer modelling and the calculation of air mass factors show that in most cases the bulk of the observed BrO was present in a layer of 1 ± 0.5 km thickness above the surface, e.g. in the boundary layer, and a corresponding BrO mixing ratio of 20-30ppt was inferred.

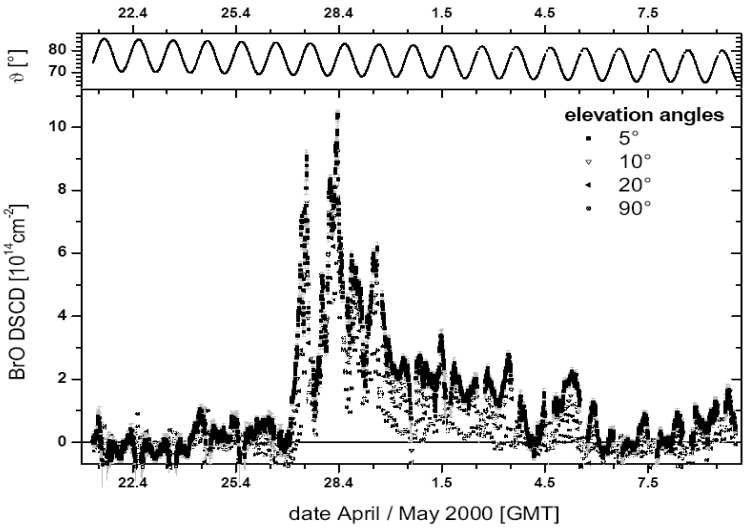

Figure 6.3.1-4. *BrO slant column densities measured during ALERT2000: the different telescope elevation angles are shown as different symbols. Adapted from Hönninger and Platt [2002].*

BrO has been measured using a spectrometer for the near UV in combination with a moveable telescope. Scattered sunlight has been observed sequentially from 6 different elevation angles (zenith, 60º, 40º, 20º, 10º, and 5º above the horizon). The BrO dSCDs measured during the ALERT2000 campaign are shown in Figure 6.3.1-4. A period of strong BrO enhancement occurs between Mai 26th and June 6th, with dSCDs reaching values of more than 10^{15} molec/cm^2. The dSCDs observed from different elevation angles show a clear separation, with higher values for lower elevations. This finding strongly suggests that the observed enhancement is due to BrO located close to the surface.

The vertical extent of the BrO layer has been estimated using Monte-Carlo modelling of the radiative transfer [Marquard et al., 2000]. A comparison of measured and modelled BrO SCDs under clear sky conditions as a function of elevation for different model layer heights is shown in Figure 6.3.1-5. The four different lines show the expected behaviour for a vertical extent of the BrO layer of 0.5, 1 and 2 km, respectively, and for an elevated layer between 1 and 2 km. A BrO layer height of 1 km at the ground is most compatible with the measure-

ments, whereas BrO layers of 0.5 and 2 km can be considered as lower and upper limits.

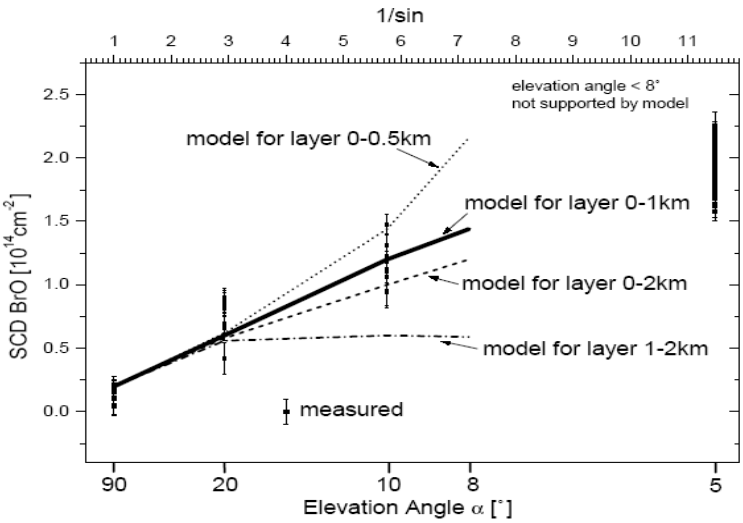

Figure 6.3.1-5. *Measured and modelled SCDs for the elevation angles used in the ALERT2000 campaign. SCDs are modelled for four different layers. Only data from a cloud-free day (4th Mai 2000) was used for this case study, the tropospheric BrO VCD was 2x10^{13} molec/cm^2. Adapted from Hönninger and Platt [2002].*

Multi-Axis DOAS observations of BrO and its vertical distribution at Ny-Ålesund

Since start of the Bremen DOAS UV/vis measurements in 1995 every spring epsiodes with high BrO in the boundary layer were observed. In contrast to zenith-sky measurements only it is possible to derive profile information of BrO with the MAX-DOAS method. This is illustrated in the following example.

Figure 6.3.1-6 shows in the upper panel the diurnal variation of BrO SCDs on April 12, 2002 above Ny-Ålesund. In particular in the morning there is a clear distinction between all different viewing direction of the instument. The lower panel shows the variation of the vertical column assuming two different scenarios for the BrO profile. The first one with no BrO in the troposphere yields in a good agreement between all elevation angles in the late evening. The second setting with 5 ppt in the boundary layer gives in excellent agreement between 2 and 6 am. Therefore one could assume BrO enriched air masses transported to Ny-Ålesund one day before. This is also supported by observations from GOME (Oetjen, 2002, Sommar et al., 2004).

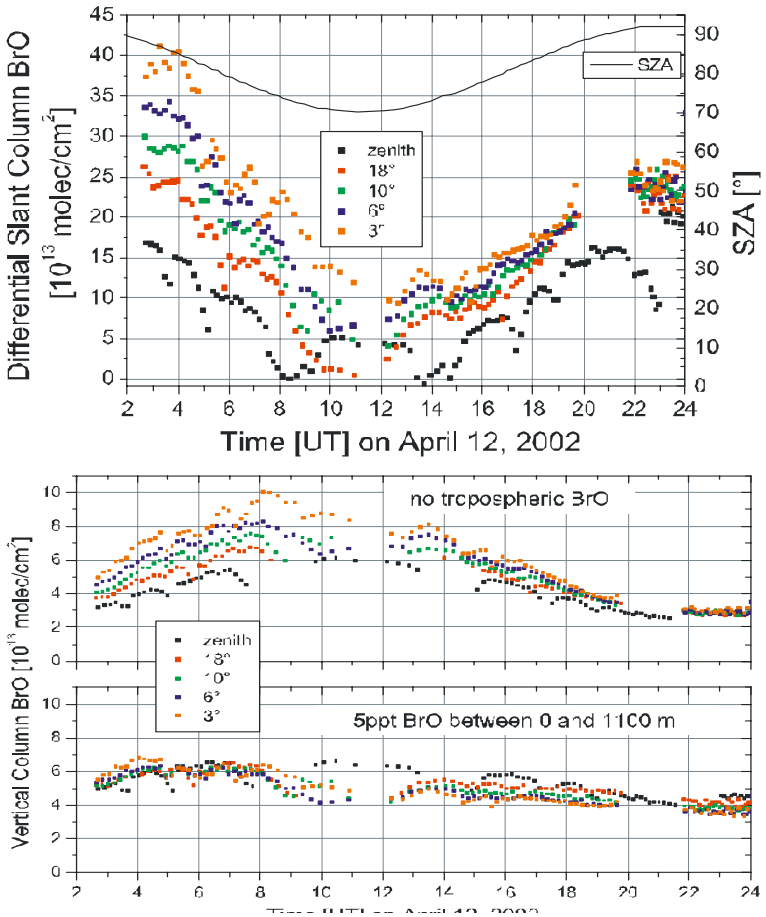

Figure 6.3.1-6. *The upper panel shows the diurnal variation of BrO DSCDs derived from spectra measured on April 12, 2002 in Ny-Ålesund. The lower panels show the vertical column calculated with different sets of AMF: the first one assuming no BrO in the troposphere at all, the other one asssuming 5 ppt in the boundary layer between 0 and 1100 m asl.*

The analysis of the BrO observations during the ALERT2000 campaign and in Ny-Ålesund have demonstrated that MAX-DOAS allows the determination of relatively precise concentration levels and layer heights of boundary layer BrO with relatively simple instrumentation.

Measurements of NO_2 vertical profiles with Multi-Axis DOAS in Heidelberg, Germany

MAX- DOAS measurements of NO_2 have been performed on the roof of the Institute for Environmental Physics building in Heidelberg/Germany from Mai to August 2003, using the UV/Vis DOAS system that has been also operated onboard the Polarstern research vessel. Using four moveable telescopes (three for the simultaneous measurement in the UV at different elevations, one for the visi-

ble wavelength range), the instrument has been pointing in western direction over the Rhein valley towards the city of Mannheim.

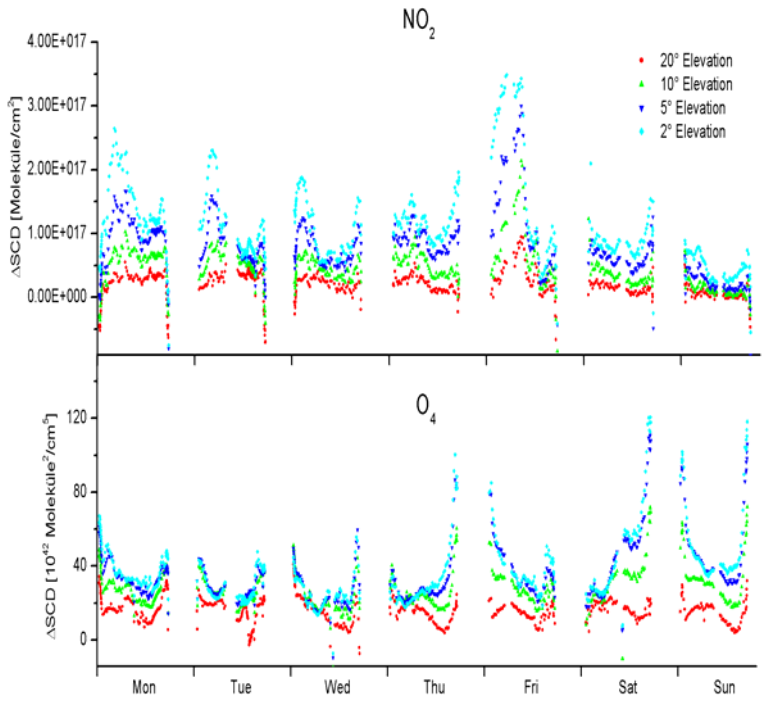

Figure 6.3.1-7. *NO_2 (upper panel) and O_4 (lower panel) differential slant column densities observed from Juli 7th to July 13th, 2003, in Heidelberg. The differential slant column densities are relative to the zenith observation at the same time, which removes the stratospheric part of the NO_2 column. Adapted from Sinreich [2003].*

Figure 6.3.1-7 shows one week of MAX-DOAS measurements during a period of highly increased NO_2. NO_2 dSCDs are determined relative to a zenith reference measured at the same solar zenith angle, which cancels out the stratospheric component of the slant column density since the stratospheric airmass factor is almost independent from the elevation angle. The NO_2 dSCDs are characterised by a distinct separation of the measurements at different elevation angles. NO_2 SCDs increase when pointing the telescope closer to the horizon, indicating the abundance of NO_2 in the lower troposphere. The NO_2 measurements at Heidelberg show a pronounced diurnal and weekly cycle: Peaks in NO_2 dSCDs occur during the rush hours in the morning and (to a smaller extent) in the evening, and only a small separation of the NO_2 dSCDs is present at the weekend. This strongly suggests that a large fraction of the observed tropospheric NO_2 is emitted by vehicles. Also shown in Figure 3 are the dSCDs of the oxygen dimer (O_4) as measured by the MAX-DOAS instrument. O_4 has a known vertical profile. It decreases exponentially with altitude, with a scale height of approximately 4km. MAX- DOAS measurements of the O_4 dSCD can therefore serve as a good qualitative indicator for the length of the light paths through the lower troposphere, and even contain quantitative information on the vertical profile and scattering properties of aerosols [Wagner et al., 2004]. In particular, a large separation of the O_4 dSCDs at different elevations indicates a clear atmosphere with low aerosol loading, while a small variation indicates the presence of high aerosol or low clouds.

Since the presence of aerosols alters the light path through the atmosphere, information on the aerosol extinction profile is essential for the interpretation of MAX- DOAS trace gas measurements. The aerosol extinction profile can be estimated by modelling the radiative transfer using different aerosol scenarios and

by comparing the modelled with the measured O_4 SCDs as a function of solar zenith angle and elevation.

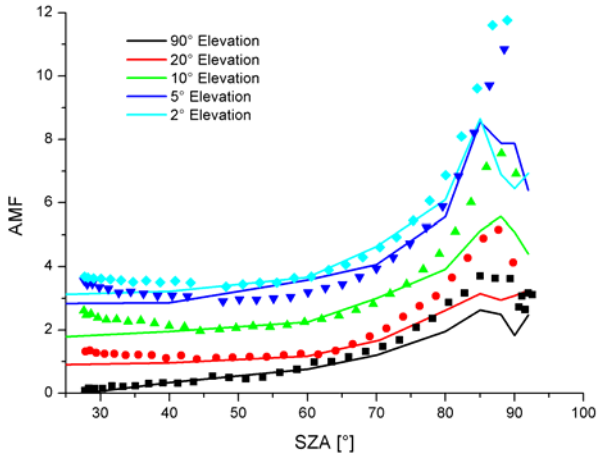

Figure 6.3.1-8. *Measured (symbols) and modelled O_4 airmass factors for an aerosol box profile with 2 km vertical extension and an extinction coefficient of 0.05 km^{-1}. The measurements were made on July 14th, 2003. Adapted from Sinreich [2003].*

Figure 6.3.1-8 shows measured (symbols) and modelled (solid lines) O_4 airmass factors under clear sky conditions. The best match between model and measurement is achieved for an aerosol box profile with a vertical extent of 2km and an extinction coefficient of 0.05km^{-1}.

A similar approach as for the aerosol extinction profile has been applied for the determination of the tropospheric NO_2 concentration profile: the tropospheric profile has been modified until best agreement between modelled and measured NO_2 SCDs has been achieved. When assuming a box profile, an NO_2 surface mixing ratio of 1.2 ± 0.2 ppb with a layer height of approximately 1500 m can be inferred.

The analysis of the MAX-DOAS NO_2 and O_4 measurements in Heidelberg have shown that MAX-DOAS is a suitable technique to gain information on the vertical profile of pollutants in urban areas. Furthermore, information on the aerosol extinction profiles can be extracted from measurements of the oxygen dimer.

MAX-DOAS measurements in Bremen, Germany

Measurements for a clear day in Bremen have been analysed using two different assumptions: a) enhanced NO_2 in the free troposphere and b) enhanced NO_2 in the boundary layer. As can be seen from Figure 6.3.1-9, measurements taken under different elevation angles give strongly disagreeing values with the first assumption, but nicely fall into line when enhanced boundary layer concentrations are assumed. When this approach is further refined, the vertical distribution of the NO_2 total column in the stratosphere, free troposphere and the boundary layer can be estimated, and two columns, a stratospheric and a tropospheric be determined.

Similar results can also be derived for BrO and HCHO in the case of enhanced boundary layer values.

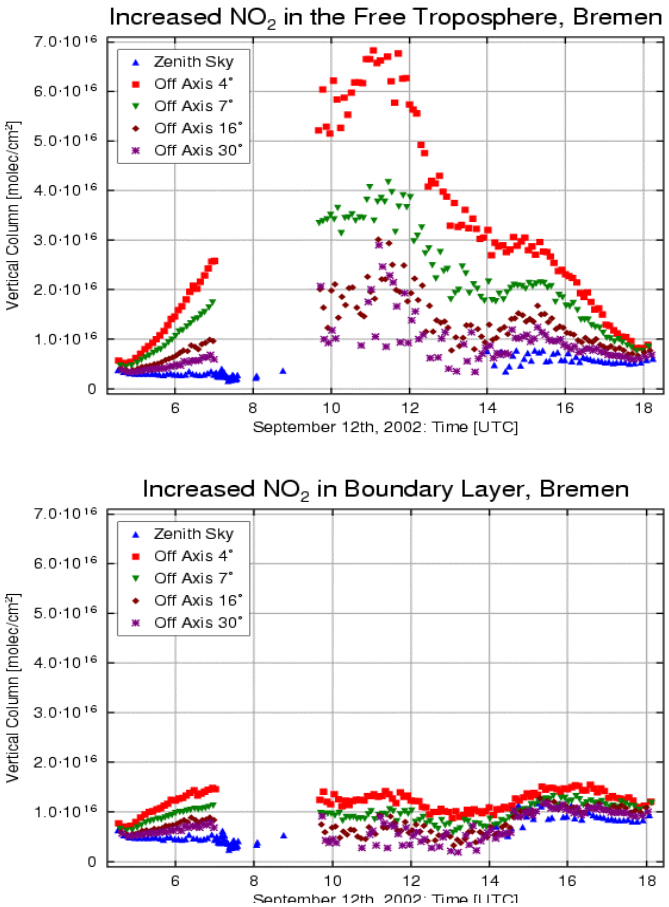

Figure 6.3.1-9. *Analysis of BREDOM NO_2 measurements in Bremen on 2002/09/12. The data have been analysed using two different assumptions: enhanced NO_2 in the free troposphere (upper panel) or enhanced NO_2 in the boundary layer (lower panel). As can be seen, only the latter assumption is compatible with the results from all viewing directions. using this approach, a rough estimate on the vertical distribution of the absorbers can be derived.*

MAX-DOAS measurements in Paramaribo/Suriname

As part of the ground-based SCIAMACHY validation network, a newly developed UV/Vis multi-axis DOAS instrument has been installed in Paramaribo/Suriname (5.8° N, 55.2° W), in Mai 2002. It is operated in collaboration with the Meteorological Service of Suriname (MDS). The measurement site is located at a coastal site close to the Atlantic Ocean. The ITCZ migrates twice per year over this tropical observation site. This allows to investigate the stratospheric composition at the location where the majority of the trace gases enters the stratosphere, and to sample air from both hemispheres.

First results of the measurements at this tropical site are shown in Figure 6.3.1-10, where two weeks of O_4 and NO_2 data are plotted. The large scatter in O_4 dSCDs is due to the presence of clouds, and the different values for different elevations indicate that the tropospheric light path is increasing with decreasing elevation angle. The same applies for NO_2 dSCDs, giving evidence that significant amounts of NO_2 are present near the surface. The diurnal variation of NO_2 is characterized by two peaks around 7:30am and 6:30pm local time, which are most likely due to the emission by traffic during rush hour in Paramaribo. Furthermore, there is a significant weekly cycle in NO_2 with a smaller tropospheric signal at the weekend. Since the stratospheric abundance of NO_2 in tropical regions is relatively small, it is of particular importance to determine the tropospheric column with high precision in order to gain the stratospheric part of the vertical column density.

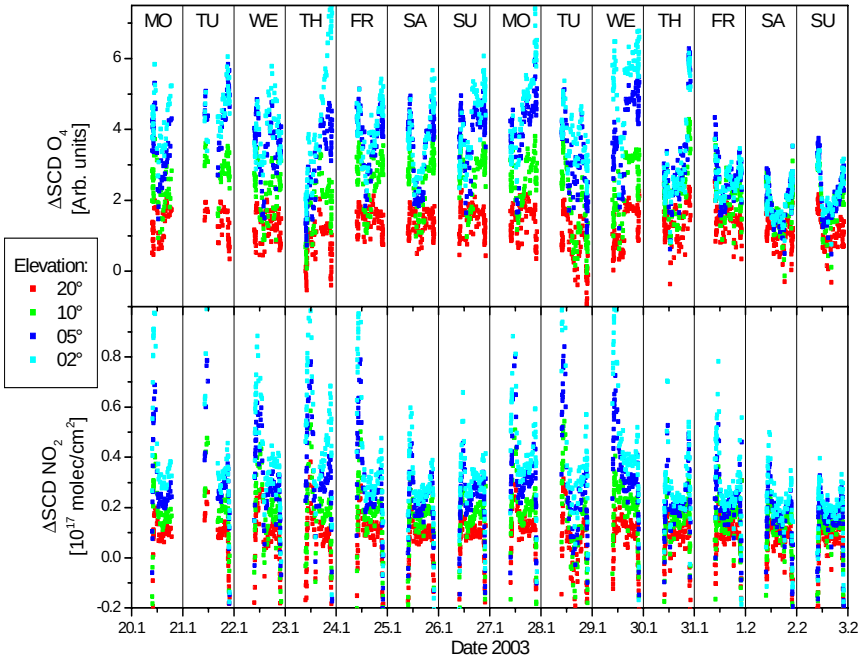

Figure 6.3.1-10. *Two weeks of O_4 and NO_2 measurements at Paramaribo, Suriname. Upper panel: dSCD O_4. Lower panel: dSCD NO_2. dSCDs are relative to the zenith observation at same SZA.*

MAX-DOAS measurements at Neumayer Station/Antarctica

The DOAS instrument at the German Antarctic research station Neumayer (70º S, 8ºW), which has been performing long-term zenith-sky measurements of ozone, NO_2, BrO, OClO, and IO since 1999, has been equipped with a newly developed multi- axis telescope in early 2003 (see Figure 6.3.1-11). The telescope unit is designed to operate in the cold and stormy environment of the Antarctic continent. It consists of a stainless steel housing equipped with a 100W heater. A quartz glass tube houses rotating quartz glass prisms, which allow to collect light from different elevation angles (zenith, 20º, 10º, 5º, and 2º). The optical components are kept free of ice by a continuous flow of warm air through the quartz glass tube. Furthermore, the telescope is equipped with halogen and mercury lamps for the automated measurement of calibration spectra during night.

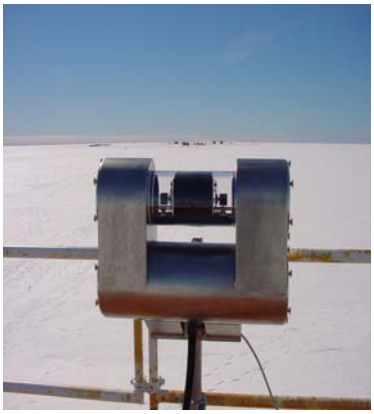

Figure 6.3.1-11. *The new multi-axis DOAS telescope at theNeumayer-Station, Antarctica.*

The main purpose of these multi-axis measurements is the investigation of the vertical distribution of tropospheric halogen oxides (BrO and IO), which are potentially released from sea salt (during Austral spring) and from biogenic processes in the ocean

The absorption structure of iodine oxide has already been identified in the zenith sky spectra recorded prior to the installation of the multi-axis telescope, and arguments based on photochemistry and the diurnal variation of the IO SCDs strongly suggest that the observed IO is located in the boundary layer rather than in the stratosphere [Frieß et al., 2001]. The likely source for the observed IO are biogenic processes leading to a release of short-lived organic iodine compounds from the ocean by macroalgae and phytoplancton.

Based on measurements using the new Multi-Axis telescope, more direct evidence for the presence of iodine oxide in the boundary layer has been found. Figure 6.3.1-12 shows the diurnal variation of IO on a clear day in March 2003. A strong increase in IO dSCDs with decreasing elevation angle is observed, strongly suggesting that the detected IO is present in the boundary layer. The IO dSCD strongly decreases during twilight (when only zenith sky measurements are performed), a feature that can be contributed to the rapid photochemistry of iodine

radicals, which are quickly converted to reservoir species ($IONO_2$, HOI) in the absence of sunlight.

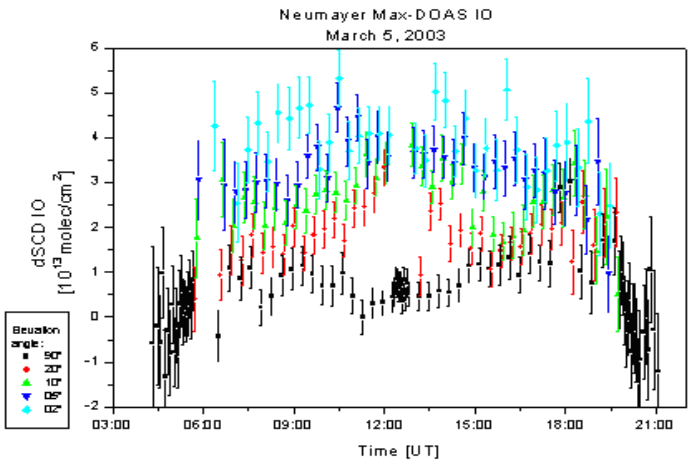

Figure 6.3.1-12. *Multi-Axis measurements of iodine oxide at Neumayer Station, Antarcita, on March 5, 2003 (preliminary data). The elevation angles of the observations are indicated by different colours as denoted in the legend.*

A quantitative estimation of IO concentrations using a radiative transfer model is still an outstanding issue. However, a simple geometric approximation based on the assumption that the majority of the scattering events occurs above the IO layer yields a vertical column density of roughly 10^{13} molec/cm^2, which corresponds to a mixing ratio of about 4 ppt for IO being uniformly distributed within the lowermost 1000m of the atmosphere. Model studies suggest that these concentration levels of iodine oxide have a significant impact on the boundary layer ozone budget, and IO is possibly the dominant sink for ozone in the Antarctic marine boundary layer.

MAX-DOAS measurements at Arrival Heights/Antarctica

The DOAS multi-axis instrument at Arrival Heights/Antarctica (77.8° S, 166.7° E) has been operated in cooperation with NIWA/Lauder almost continuously since 1998 [Frieß et al., 2002]. Scattered sunlight in the UV (330 – 420 nm) and visible (400 – 650 nm) wavelength region has been observed from four different elevation angles (10°, 15°, 20° and zenith) using a sun tracker system that keeps the relative azimuth angle between sun and viewing plane at a constant value of 20° in order to minimize azimuthal effects in the radiative transfer.

The analysis and interpretation of the existing data has mainly focused on both the vertical distribution of near surface BrO during Austral springtime and the possible abundance of BrO in the free troposphere above Antarctica in autumn.

Numerous events with highly elevated BrO SCDs, caused by heterogeneous release of reactive bromine from sea salt surfaces, were observed during springtime. In spring 2002, the measurements were intensified by additionally performing direct sunlight measurements [Schofield et al., 2004]. A comparison between multi-axis, zenith sky and direct light measurements during a period of several BrO enhancements is shown in Figure 6.3.1-13. The presence of BrO in the boundary layer can be clearly identified both by the MAX-DOAS measurements, which show a separation of the BrO dSCDs at different elevations, and by the direct light measurements, which strongly increase due to their high sensitivity for trace gases in the lower troposphere.

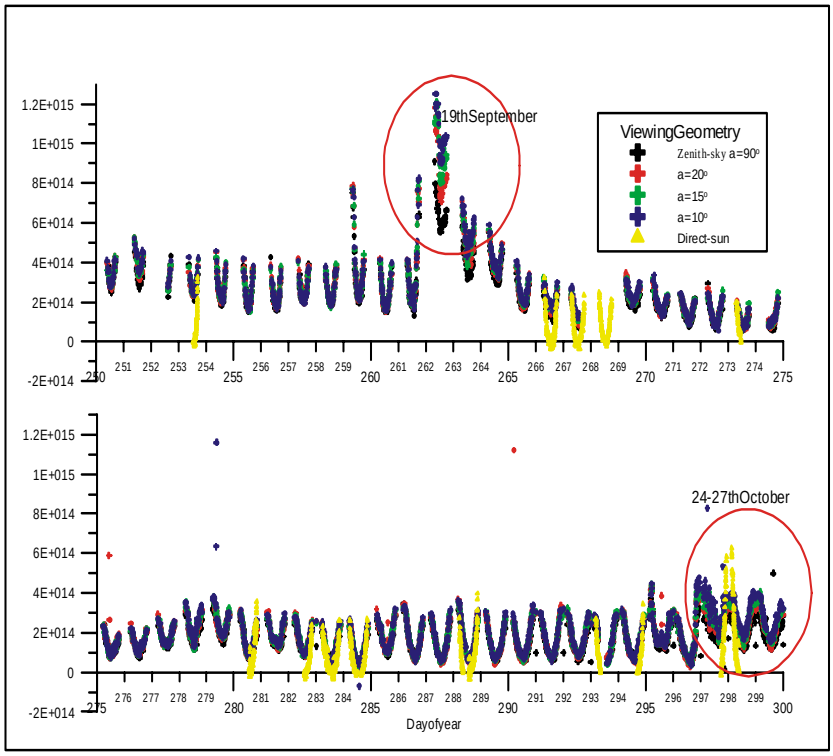

Figure 6.3.1-13. *Differential slant column densities for zenith sky, off axis and direct sun viewing geometries measured at Arrival Heights in spring 2002. The red circles drawing attention to two of the 'bromine explosion' events.*

This combination of off-axis, zenith sky and direct light observations allows to retrieve the diurnal variation of stratospheric as well as tropospheric BrO partial columns – and thus an improved estimate of the stratospheric column as well as information of the photochemistry of radical species such as BrO - with high accuracy using an optimal estimation algorithm developed at NIWA [Schofield et al., 2004]. Figure 6.3.1-14 shows the retrieved tropospheric and stratospheric BrO partial column densities as a function of solar zenith angle as inferred from the combined direct light and zenith sky measurements at Arrival Heights. The retrieved tropospheric BrO column density suggests that a significant amount of BrO is present in the free troposphere in the morning (~ $5x10^{13}$ molec/cm^2), while the values remain below the detection limit in the evening. This might reflect the (yet unknown) photochemistry of BrO radicals in the free troposphere.

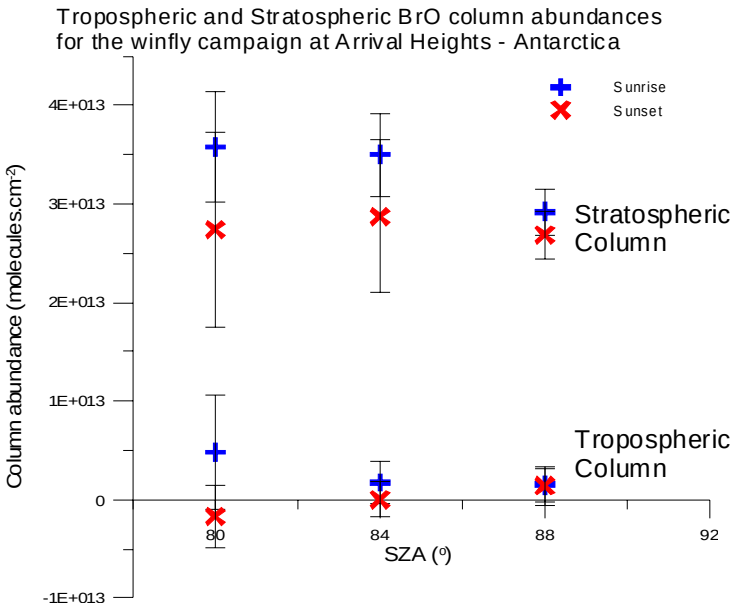

Figure 6.3.1-14. *Tropospheric and stratospheric partial columns at sunset (blue symbols) and sunrise (red symbols) derived from combined DOAS measurements of direct sunlight and zenith scattered skylight at Arrival Heights/Antarcitca using optimal estimation techniques.*

In order to further investigate a possible BrO background in the free troposphere, we have focused on the Multi-AXIS DOAS measurements during autumn, when no release of bromine from sea salt can be expected. Model simulations using the AMFTRAN radiative transfer model [Marquard et al., 2000] indicate that BrO being abundant in the free troposphere with a mixing ratio of more than 1 ppt should lead to a significant separation of the BrO dSCD measured at different elevation angles. Only small differences in the BrO dSCDs are observed under clear sky conditions, indicating that the observations at Arrival Heights are in agreement with BrO being abundant entirely in the stratosphere (see Figure 6.3.1-15). Based on all clear sky BrO data of autumn 2001, we performed a statistical analysis using multi-linear regression, which is possible since the observed BrO total column density is a linear combination of tropospheric and stratospheric slant column density. Our analysis yields BrO vertical columns of $(3.5\pm0.2)\cdot10^{12}$ molec/cm^2 in the troposphere and $(3.2\pm0.2)\cdot10^{13}$ molec/cm^2 in the stratosphere, in good agreement with the results from analysis of the combined direct light and zenith sky measurements described above.

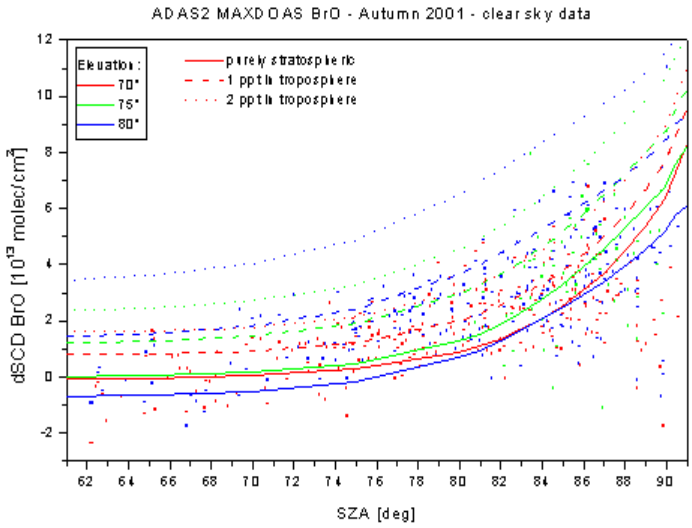

Figure 6.3.1-15. *Dots: BrO differential slant column density of BrO at Arrival Heights, during Autumn 2001 (clear sky data only), relative to the zenith sky observation at same SZA. Solid lines: Simulated diurnal variation of the BrO dSCDs for purely stratospheric BrO. Dashed and dotted lines: modelled dSCDs additionally 1 ppt and 2ppt BrO, respectively, uniformly distributed over the free troposphere.*

MAX-DOAS measurements onboard the Polarstern research vessel

A multi-axis UV/Vis DOAS instrument was operated onboard the German research vessel Polarstern during four cruises from Bremerhaven to Antarctica. These measurements offer the opportunity to determine latitudinal cross sections of both tropospheric and stratospheric trace gases (BrO, NO_2), ranging from northern mid-latitudes over the tropics to the south polar ocean.

Continuous measurements were performed during the Polarstern cruise from October 1st to October 21st, 2000 [Leser et al., 2003] with a time resolution of 5 min for the 5° geometry and 1 h for each complete MAX-DOAS series, respectively. Besides BrO, O_3, NO_2 and O_4 absorptions were measured simultaneously.

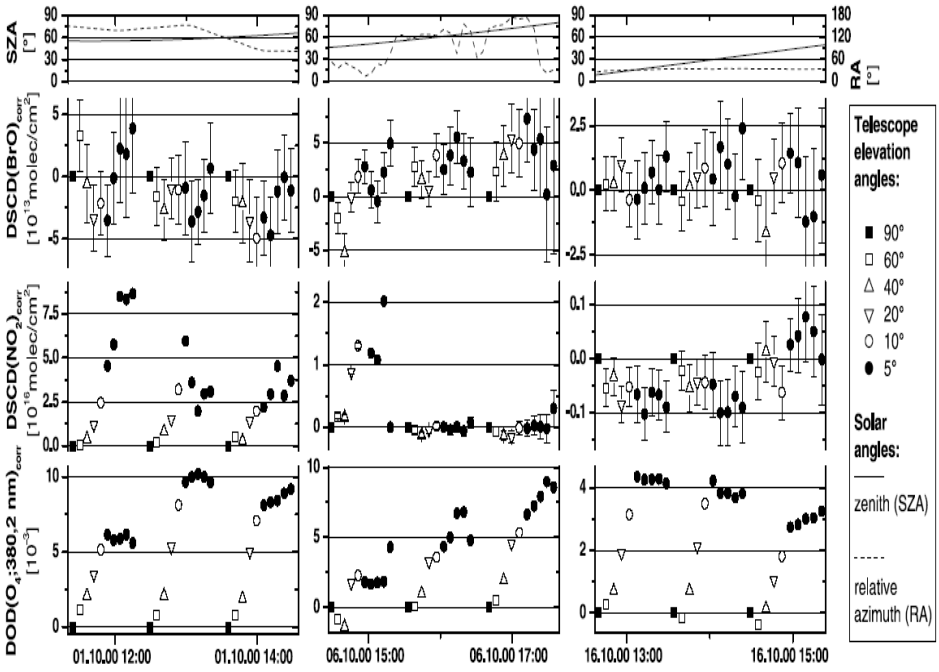

Figure 6.3.1-16. *Typical time series of DSCDs of NO_2, O_4, BrO, the SZA and the relative azimuth RA (azimuth angle between viewing direction and sun). Error bars denote 1 fit errors. Left panel: on October 1st the Polarstern was in the English Channel. The high DSCDs of NO_2 at low elevation angles relate to NO_2 abundance due to continental influence. Middle panel: The pattern of the BrO series on October 6th north of the Canary Islands is typical for BrO in the marine BL. Right panel: On October 16th in the remote Atlantic south-west of Africa both, NO_2 and BrO are below the detection limit.*

The O_4 measurements always increase with decreasing elevation angle as it is expected for an absorber close to the ground (see Figure 6.3.1-16, bottom). The large variations of O_4 show the influence of clouds on the radiative transfer. The NO2 measurements clearly show occasional presence of pollution in the lower troposphere. On October 1st the ship was still in the English Channel with the air being continentally influenced. As a result there are very high levels of NO_2 in the boundary layer visible as increasing DSCD with decreasing elevation angle (Figure 6.3.1-16, left). Around October 6th sometimes the wind was blowing the ship's exhaust plume into the viewing direction of the telescope as indicated by some measurements with high NO_2 DSCDs at low elevation angles. These NO_2 measurements had to be excluded from further evaluation. The right panel in Figure 6.3.1-16 (October 16th) shows an example of remote marine air. The NO_2 SCDs at low elevation angles are not higher than the zenith view absorption, but in some cases even lower resulting in negative DSCDs. This effect, occurring most of the time when there was no NO_2 abound, is still not understood.

While on most days the BrO DSCDs are not systematically changing with the elevation angle and not significantly differing from zero, from October 5th till noon of October 7th they show characteristics for BrO abundance in the boundary layer (see center panel of Figure 6.3.1-16). The BrO DSCD is increasing systematically at low elevation angles usually to levels significantly different from zero. Some MAX-DOAS series of this period were compared to other series taken at similar cloud conditions and solar zenith angles to rule out a correlation of the described signature with e.g., changes of the radiative transfer. At high elevation an-

gles the MAX-DOAS series of BrO show the same behavior as the O_4 measurements (e.g., the negative DSCDs before 3 pm on October 6th resulting from collecting light relatively close to the sun). Since O_4 is a typical absorber located close to the surface the similarity in the elevation angle dependence of both SCDs is another strong indication for near surface BrO abundance.

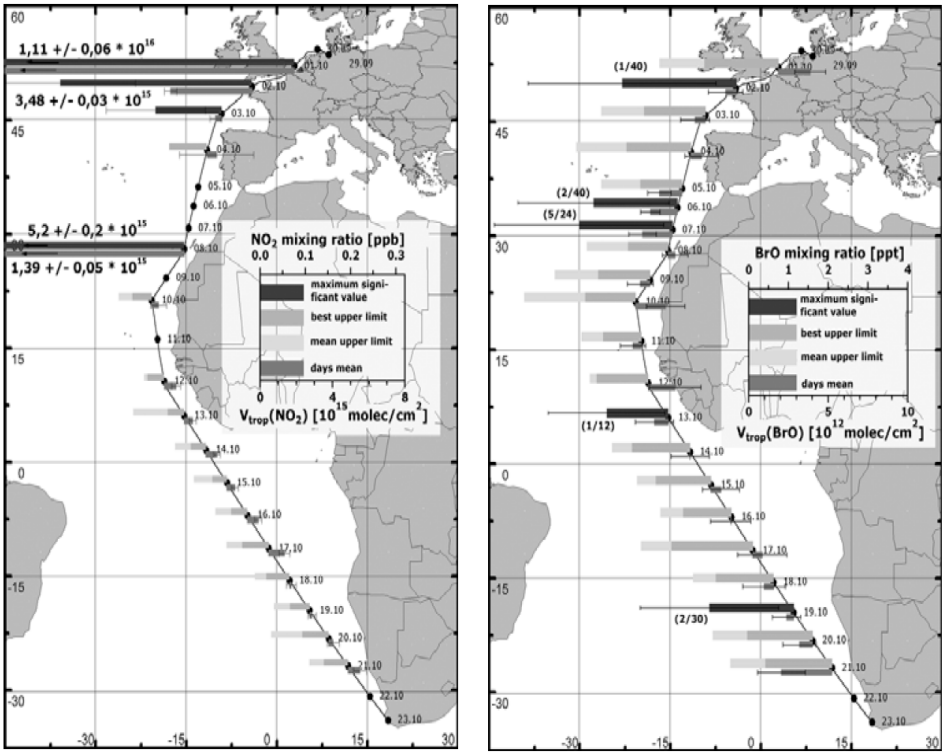

Figure 6.3.1-17. *Tropospheric VCDs of BrO and NO_2. Left: the NO_2 VCD was high in the English Channel and near the Canary Islands. Values affected by the ship's plume are omitted. Right: Except for 5 days the BrO DSCD of individual measurements was below detection limit. North of the Canary Islands for a period of two days several times BL BrO was identified by the systematic variation pattern of the DSCD with the elevation angle (see also Figure 11). In brackets significant and total number of data points are given for the respective days.*

Using a geometrical approximation for the airmass factor, tropospheric VCDs were calculated from the 5°-measurements. In Figure 6.3.1-17 for each day the highest VCD significantly different from zero are shown as well as the number of significant values (in brackets). For days not showing any significant trace gas levels upper limits are given. For the best upper limit the smallest error (2) of a single measurement and for the mean upper limit the mean error of each day is given (as VCD). The large variation of the upper limits originates from varying light intensity. In addition for each day time averages were calculated by weighting the individual measurements with their errors. Mixing ratios are calculated for the standard conditions at sea level. BrO could be detected directly in the mid-latitude marine environment for the first time. The highest significant individual measurement was 2.4 ± 2.1 ppt. Typical levels in the marine lower troposphere were <1 to 3.6 ppt in most cases. Besides the detection of NO_2 with mixing ratios up to 3.7 ± 0.2 ppb in the English Channel, upper limits for clean air in the Atlantic west of Africa of 24 to 100 ppt could be derived.

Figure 6.3.1-18 shows results of multi- axis UV/Vis DOAS NO_2 measurements performed onboard of the Polarstern research vessel during the cruise from Bremerhaven (Germany) to Cape Town (South Africa) in November 2001, conducted as part of the SCIAMACHY validation activitie. The latitudinal cross section of tropospheric NO_2 vertical column density was derived from the measured NO_2 SCDs using Monte Carlo radiative transfer calculations. Under the assumption that 15% of the tropospheric NO_2 resides in the lowermost 1 km of the troposphere, the analyses resulted in a maximum of the daily averages of the NO_2 mixing ratio in the marine boundary layer on November 10th at about 48°N 5°W in the British Channel of (0.36 ± 0.13)ppb. Such elevated NO_2 concentrations, which were also detected at the island of Tenerife, can be attributed to local pol-

lution. In more remote regions of the Atlantic slightly varying NO_2 mixing ratios around 80ppt were detected, with a minimum in the tropics, at about 6°N 16°W in the middle Atlantic with (60 ± 12)ppt..

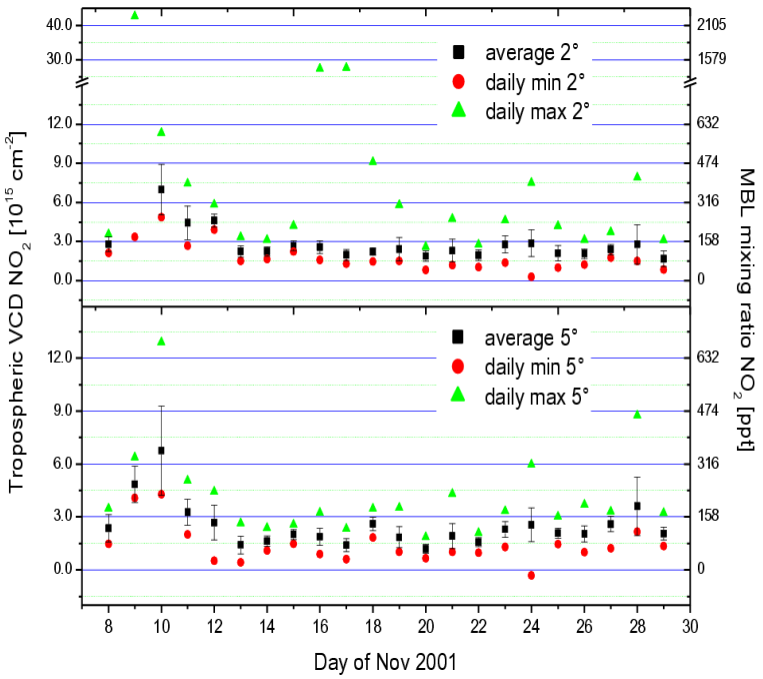

Figure 6.3.1-18. *Results of the Polarstern measurements: Daily averages, minimum and maximum values of the NO2 total tropospheric vertical column densities (up to 10 km) and the corresponding marine boundary layer mixing ratios up to one km assuming that 15% of the total tropospheric concentration resides in the first km. Upper panel: data derived from the 2° elevation measurements. Lower panel: data derived from 5° elevation measurements.*

Recommendations for off-axis instrumental set-up, spectral analysis and radiative transfer (D6)

Sensitivity studies for O_4 (Partner 3, University of Bremen)

When modelling the radiative transfer in the atmosphere, a number of parameters has to be set to realistic values. The most important ones are the viewing geometry, the position of the sun, wavelength, and the vertical profiles of absorbers, pressure and temperature. However, surface albedo and the atmospheric aerosol loading also have an impact on the results. For simplicity, all calculations in this work were made without consideration of clouds.

In Ny-Ålesund at least weekly profiles for the absorber ozone and daily temperature and pressure profiles of the atmosphere are available through ozone soundings and radiosondes, respectively. Above the burst height of the balloon the profiles are completed with values from a model climatology provided by the MPI. These profiles are used as realistic meteorological input for the model calculations.

In the following sections, the influence of multiple scattering, the relative azimuth, surface albedo, aerosols and the refraction on the O_4 AMF and consequently the calculated vertical column are investigated with model data. Such sensitivity studies are necessary to determine which parameters need to be known to which accuracy to derive realistic vertical columns from the measurements. The results are presented in the form of ratio between a reference airmass factor AMF_Ref of a standard scenario with the airmass factor AMF' obtained with one of the above mentioned parameters changed. This ratio indicates the error in the vertical column that is introduced when setting the respective parameter to an inappropriate value (Figure 6.3.1-19 - Figure 6.3.1-22). Whenever more information is necessary to illustrate the influence of one parameter, additional figures are shown.

Figure 6.3.1-19. *Effect of neglecting multiple scattering on the calculated vertical column of O_4. For an elevation angle of 6° the vertical column will be underestimated, if only single scattering is taken into account for the airmass factor.*

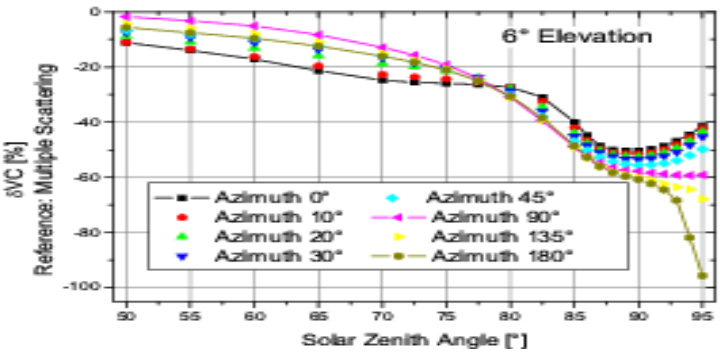

Figure 6.3.1-20. *Effect of the relative azimuth angle on the calculated VC. Shown is the error introduced in the vertical column of O_4 if an azimuth angle different from the 90° of the reference case is used in the airmass factor calculation.*

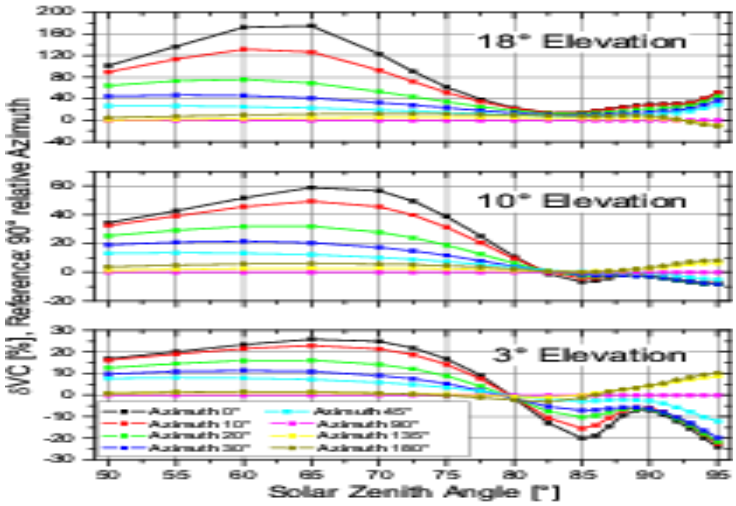

Figure 6.3.1-21. *Effect of the albedo on the calculated VC. Shown is the deviation introduced in the vertical column of O_4 if an albedo different from 0.5 of the reference is used in the airmass factor calculation.*

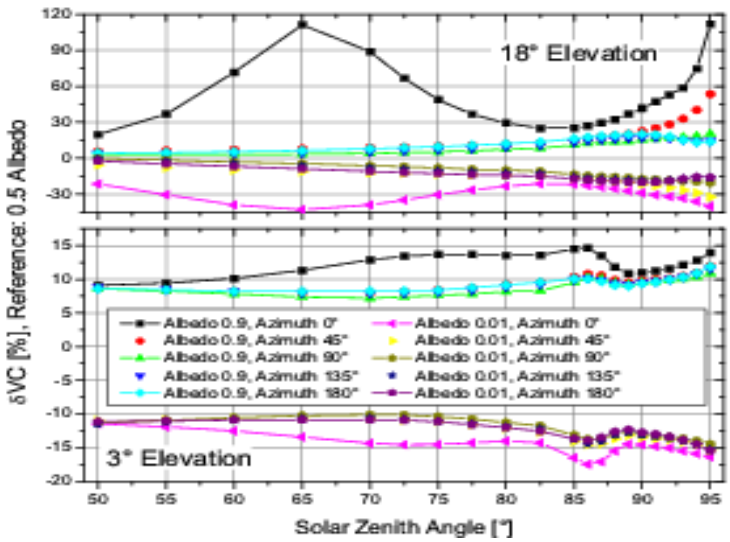

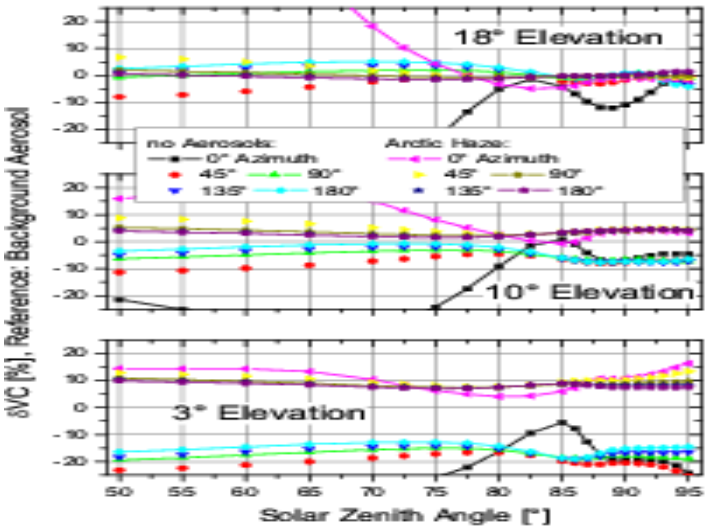

Figure 6.3.1-22. *Effect of the aerosol extinction profile on the calculated VC. Shown is the error introduced in the vertical column of O_4 if aerosol scenarios different from the background aerosol of the reference are used in the airmass factor calculation.*

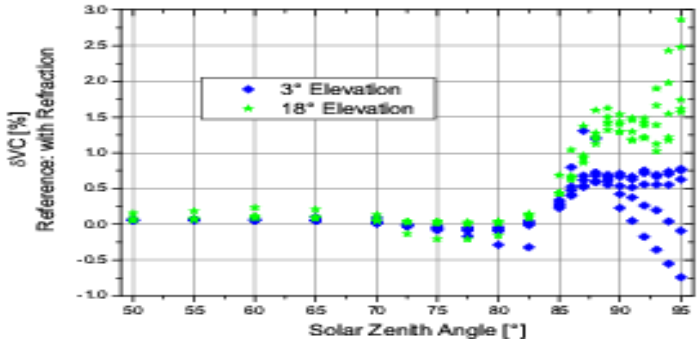

Figure 6.3.1-23. *Effect of neglecting refraction on the calculated VC. Only for solar zenith angles larger than 85° the introduced errors are larger than 0.5%.*

For the reference AMF, the atmospheric profile from 3 April 2002 was used and a Fraunhofer reference spectrum taken at 60° SZA in the zenith direction was assumed. All calculations shown have been done for 370 nm (the center of the O_4 fitting window), an albedo of 0.5, a background arctic aerosol (see Figure 6.3.1-24 and full multiple scattering and refraction. It is important to note, that the sensitivity studies are presented in the form in which the AMF will be applied to the actual measurement. therefore, not the absolute AMF but rather the difference in AMF between a horizon measurement and the background zenith measurement at 60° SZA is used nor the comparison with the reference scenario. This relative quantity sometimes was a larger sensitivity to changes in model parameters than the absolute AMFs, but as it reproduces the real measurement situation, it seems the appropriate choice.

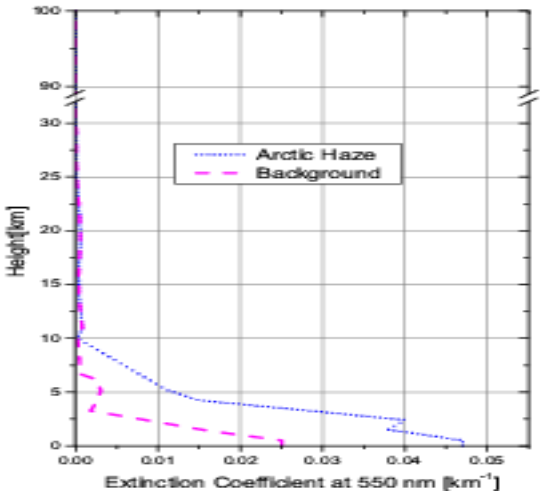

Figure 6.3.1-24. *Profiles of the aerosol extinction coefficient at 550 nm used for AMF calculations shown in Fig. 12.*

Multiple scattering

For a qualitative interpretation of MAX-DOAS measurements, simple geometric considerations have sometimes been used to estimate the airmass factors. However, in the troposphere multiple scattering at least for the used wavelength region cannot be ignored, and using a single scattering approximation introduces large errors. This is illustrated in Figure 6.3.1-19, there for an elevation angle of 6° the underestimation of the vertical column increases from a few percent at high sun to more than 50% at low sun depending on the relative azimuth. As is to be expected, the influence of multiple scattering increases with decreasing elevation angle (not khown). The reason for the large impact of multiple scattering is twofold: on one hand, the airmass factor for the zenith sky measurement increases with multiple scattering, thereby decreasing the difference between horizon and zenith measurement. On the other hand, the airmass factor for the horizon viewing mode is slightly increased by multiple scattering for high sun, but clearly decreased at low sun. The combination of both effects results in the behaviour shown in Figure 6.3.1-19.

Relative azimuth

When analysing the O_4 columns measured under different elevation angles on a clear day, it is apparent that the values do not only depend on solar zenith angle as in the case of zenith sky measurements, but also vary with the relative azimuth angle. This becomes apparent from Figure 6.3.1-25, which shows measurements of DSC from 26 April 2003. As the instrument is pointed towards the NNW, the relative azimuth varies over the day, and morning and afternoon measurements taken at the same SZA differ significantly. In order to evaluate the impact of the relative azimuth between measurement direction and the sun, airmass factors have been calculated for different elevation angles (3°, 10° and 18°) and then sorted according to the relative azimuth. The main effect is, that the AMF is significantly smaller when looking towards the sun, in particular for higher elevation angles (see Figure 6.3.1-26}). This is a result of the strong forward peak in Mie scattering, that reduces the effective light path in this geometry. The effect on the difference between the horizon AMF and the zenith AMF can be quite large as shown in Figure 6.3.1-20. Here, the error of the vertical columns is shown that is introduced when using a deviating azimuth instead of the correct relative azimuth of 90° in the AMF calculations. The azimuth effect is relevant for all elevation angles, and is largest for higher elevations and a small relative azimuth. For all azimuth angles pointing away from the sun the error is smaller than 10% for SZAs less than 93°.

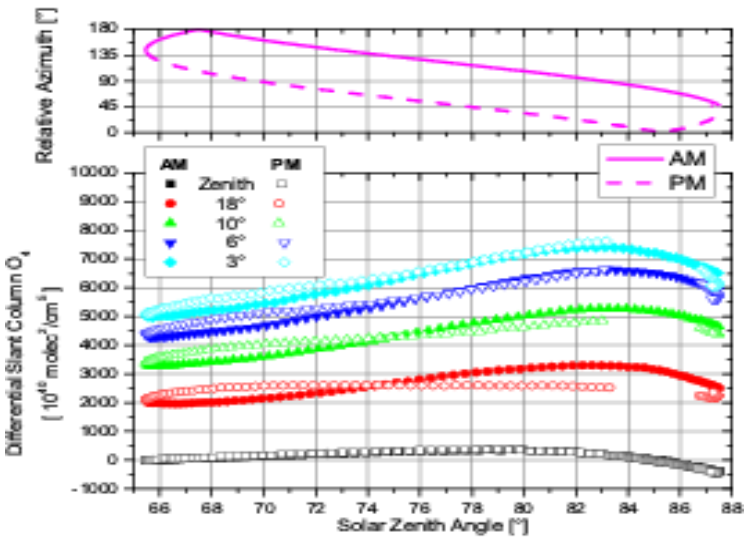

Figure 6.3.1-25. *Diurnal variation of the measured O_4 DSCs on 26 April 2003. As background the zenith sky noon spectrum from the same day was used. On this very clear day (only thin clouds in the late evening) the azimuthal dependency of the measured O_4 is clear*

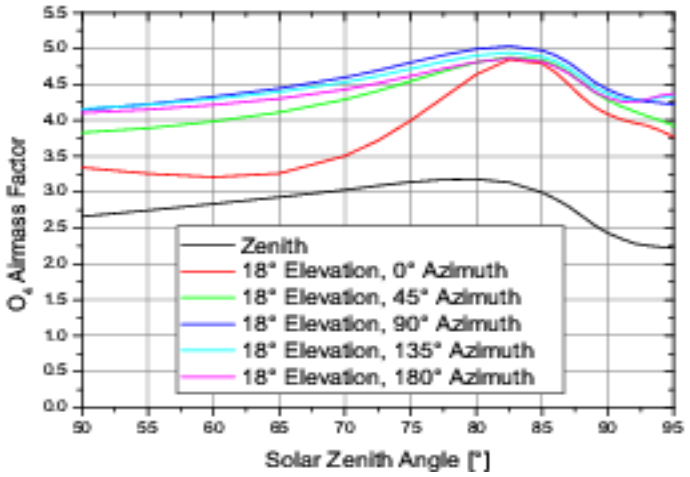

Figure 6.3.1-26. *Absolute airmass factors for O_4. Pointing the instrument towards the sun (0° relative azimuth)leads to decreasing differences between horizon and zenith sky AMF.*

From the results of this test we conclude, that it is preferable to joint a horizon viewing instrument away from the sun (This is not practicable at high latitudes!), and that the correct azimuth has to be taken into account in the AMF calculation.

Albedo

Surface albedo changes have a significant impact on the intensity of the diffuse radiation field close to the surface. In Ny-Ålesund, very different albedo values can be found depending on season and viewing direction, for example when comparing snow covered ground and open water. To study the impact of albedo on the AMF, calculations with the albedo of freshly fallen snow (0.9) and a very small albedo (0.01) are compared to a medium albedo of 0.5. For the lowest elevation angle (3°) the vertical column will be underestimated when a too small albedo is assumed and overestimated when the albedo is too high (Figure 6.3.1-21). At an elevation of 18° the same trend can be observed for the directions pointing away from the sun. However, for the direction towards the sun, i.e. 0° azimuth, using a wrong albedo has a big impact on the vertical column. For relative azimuths larger than 45°, the error introduced by using an inappropriate albedo is generally less than 20%.

Figure 6.3.1-27 shows the relative AMF, i.e. the difference between the actual AMF and the AMF of midday at 60° SZA. As can be seen, the difference is decreasing with increasing albedo. This results in a higher relative sensitivity of the off-axis measurements for a small albedo which at first glance is surprising. The reason for this unexpected behaviour is not so much the effect of high albedo on the low elevation measurements but an increased sensitivity of the zenith-sky viewing direction. For high albedo the number of photons scattered close to the ground is larger, making the zenith-sky measurements more sensitive to absorption in the troposphere.This reduces the difference in AMF between horizon and zenith-sky viewing directions.

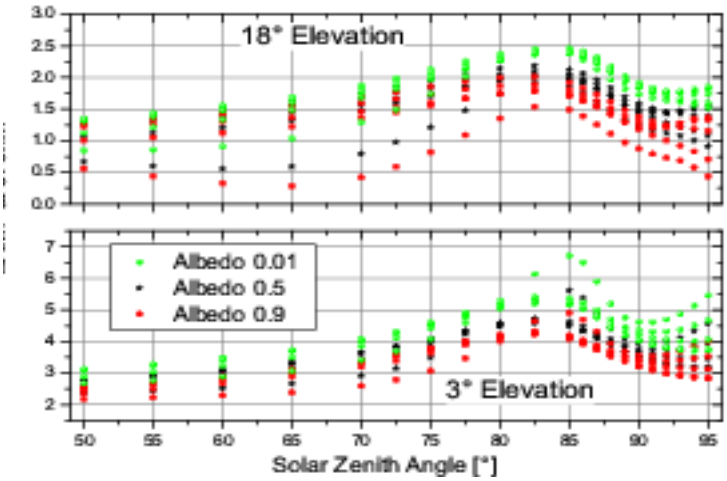

Figure 6.3.1-27. *Differences of AMF for O4 calculated with different albedos. All relative azimuth angles from previous figures are plotted but for clearness not with extra symbols indicated. All AMF are related to the zenith sky AMF calculated at 60° solar zenith angle. Although absolute AMF are getting larger for increasing albedo, the inverse behaviour is true for AMF differences between off-axis and zenith sky.*

In summary, the impact of albedo changes on the AMF is significant, in particular when looking towards the sun. Good albedo estimates are needed for the analysis (or have to be derived from the measurements themselves) and again it is simplifying the analysis if the telescope is pointed away from the sun.

Aerosols

The optical properties of aerosols are determined by their composition,their shape and relative humidity. For the impact on the AMFs, the vertical distribution of the aerosols also plays an important role. In general, increasing the aerosol extinction reduces the light path for the lower viewing directions but has little impact on the zenith directions, therebyreducing the difference in tropospheric absorption path for the different viewing directions. For the sensitivity studies, a simplified vertical extinction profile -- based on measurements in Svalbard during the ASTAR-Campaign 2000 was used. In the troposphere, a marine aerosol type was chosen, aged volcanic aerosol for the stratosphere and above that meteor dust. The standard extinction coefficient is shown in Figure 6.3.1-24. The relative humidity was set to 50% in the lowermost 5 km of the atmosphere.

In this study, only the total extinction was changed: The background scenario is compared with very strong extinction as would be observed in an arctic haze event and with no aerosols at all, i.e. zero extinction coefficient throughout the whole atmosphere. The results are shown in Figure 6.3.1-25 for three elevation angles. For the lowest elevation, the light path increases with decreasing extinction, and using a high aerosol scenario instead of the standard scenario will lead to a 10% overestimation of O_4. Similarly, using a Rayleigh atmosphere in the airmass factor calculations will lead to a 10--20% underestimation of the real column. For higher elevations, the sensitivity to aerosols decreases, but azimuth effects are more important. In particular, the 0° azimuth direction (pointed towards the sun) is very sensitive to changes in the aerosol extinction, mainly because the airmass factor for this direction is very close to the one of the zenith sky background measurement (see Figure 6.3.1-26).

Refraction

As a result of refraction in the atmosphere, the solar disc can be seen during dusk and dawn for some time even when it is geometrically below the horizon. In the SCIATRAN model, including refraction in the horizon viewing geometry is computationally expensive, and therefore the effect of neglecting refraction on the AMF was evaluated. As can be seen in Figure 6.3.1-23, the error in the vertical would be well below 1% at SZAs smaller than 80° depending on viewing geometry (elevation and azimuth) and increases for larger SZA. Thus, in most cases refraction is of minor importance.

Summary of the sensitivity study

The results of the model studies show, that multiple scattering can not be ignored, whereas refraction has only a minor impact on the results. The relative azimuth between sun and viewing direction has a significant effectand has always to be taken into account, in particular when the instrument is not pointed away from the sun and/or for measurements at high latitudes. The effect is much more pronounced when the realistic case of a zenith sky background spectrum with non negligible O_4 content is considered. Both, aerosol extinction and surface albedo can have a large effect on the airmass factors, and determining these parameters is crucial for a quantitative retrieval. The albedo can be adequately determined through weather observation or Web Cam pictures whereas the aerosol scenario persists to be an element of uncertainty. However, the measurements from different lines of sight can be used to get aerosol information as is shown in Heckel, et al., 2004 or in the following by partner 5. In all sensitivity studies, only one parameter was changed at a time to simplify interpretation. However, some of the parameters are clearly not independent from each other, and for example the effect of surface albedo might vary with aerosol extinction. Also, absorbers with a different vertical profile will not behave exactly as O4 does, in particular if they are confined to the boundary layer. However, the qualitative behaviour will be the same, and O_4 has the advantage of providing the opportunity to validate the model results.

Application of observations

An important test of the quality of the radiative transfer model used is comparison of modeled and measured O_4 vertical columns. In this section, vertical columns of O_4 on two selected days in 2002 and 2003 are shown, when weather conditions were stable and few clouds occured. Actual meteorological profiles and albedo settings have been used for the radiative transfer calculation. Starting with realistic aerosol scenarios the extinction profile and the composition of the different aerosol layers have been changed until closure of vertical columns of O_4 for all lines of sight has been reached.

In Figure 6.3.1-28, O_4 vertical columns are shown for 26 April 2003 and 13 July 2002. The first day was selected as it was exceptionally clear at least before 20:00 UT, the second as the NO_2 columns measured on that day show an interesting feature discussed in the next section.

When judging the quality of the O_4 vertical columns, threecriteria have to be examined: a) how well the different viewing directions agree in the vertical column, b) how constant the derived vertical column is over the day, and c) how well the measured vertical column agrees with the value derived from the independent sonde measurement.

Overall the agreement between the vertical columns obtained from the different viewing directions is excellent on both days. The small scatter in the data from 13 July 2002 is related to very thin clouds that were sometimes observed on that day.

The good agreement indicates, that the SCIATRAN model is capable of simulating the different light paths through the atmosphere with high accuracy.

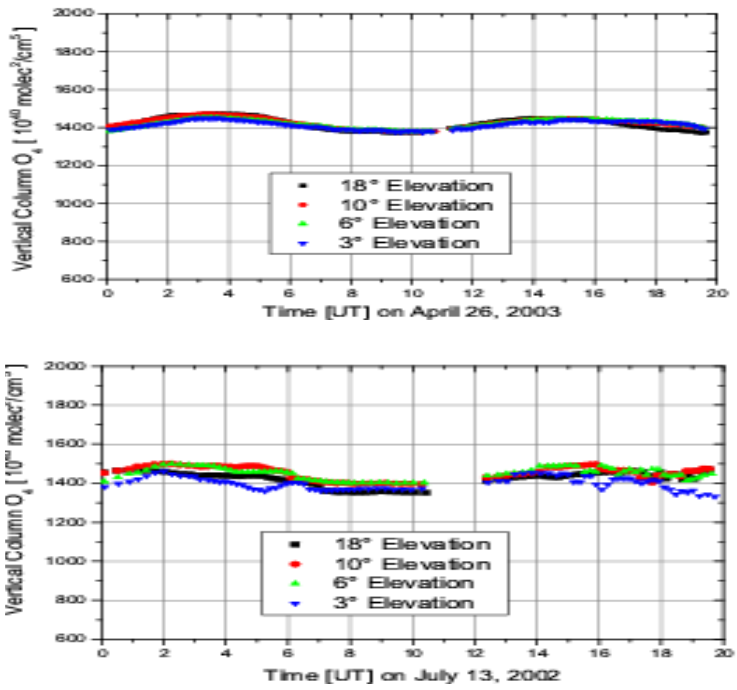

Figure 6.3.1-28. *Vertical columns of O_4 calculated for all off-axis directions from slant columns measured on two selected days.*

When looking at the variation of the retrieved O_4 vertical column over the day, a systematic pattern is apparent in the April measurements. This pattern with an amplitude of roughly $1*10^{42}$ molec^{2}cm^{-5} is observed on some but not all days. It is related to the relative azimuth and probably indicatesa mismatch between the aerosol phase function used in the model and the real value. However, the absolute variation is small (7% peak to peak) and does not have a big impact on the accuracy of the analysis.

The derived O_4 columns were also compared to the columns derived from sonde measurements. The latter yield $1.50*10^{43}$molec^{2}cm^{-5} on 23 April 2003, $1.44*10^{43}$ molec^{2}cm^{-5} on 30 April 2003 and $1.38*10^{43}$ molec^{2}cm^{-5} on 13 July 2002. As the temporal match is not perfect for April 2003, no direct comparison is possible. However, the derived value of $1.44*10^{43}$ molec^{2}cm^{-5} is close to the numbers measured before and after by the sonde. The same is true for the second measurement, that agrees with the sonde within 4%.

In summary, the results of the comparison between the retrieved O_4 vertical columns and the independent measurements is very favourable, and lends confidence to the model performance and the retrieval approach.

MAX-DOAS O_4 measurements as a new technique to derive information on atmospheric aerosols

Based on measurements conducted during the FORMAT II campaign in the Po Basin near Milan/Italy in September 2003, a detailed study on the potential of MAX-DOAS to derive information on atmospheric aerosols has been performed [Wagner et al., 2004]. The O_4 absorption between 335 and 367 nm was measured sequentially at different elevation angles using the same instrument as for the measurements in Heidelberg described above, but with the tree telescopes of the UV instrument pointing in different azimuthal directions (approximately north, south and west).

Like established methods e.g. sun radiometer and LIDAR measurements, MAX-DOAS O_4 observations determine optical properties of aerosol under atmospheric conditions. However, the novel technique has two major advantages: It utilizes differential O_4 absorption structures and thus does not require absolute radiometric calibration. In addition, O_4 observations using this method provide a new kind of information: since the atmospheric O_4 profile depends strongly on altitude, they can yield information on the atmospheric light path distribution and in particular on the atmospheric aerosol profile. From O_4 observations during clear days and from atmospheric radiative transfer modeling, we conclude that our new method is especially sensitive to the aerosol extinction close to the ground. In addition, O_4 observations using this method yield information on the penetration depth of the incident direct solar radiation. O_4 observations at different azimuth angles can also provide information on the aerosol scattering phase function. We found that MAX-DOAS O_4 observations are a very sensitive method: even aerosol extinction below 0.001 could be detected. In addition to the O_4 absorptions we also investigated the magnitude of the Ring effect and the (relative) intensity. Both quantities yield valuable further information on atmospheric aerosols. From the simultaneous analysis of the observed O_4 absorption and the measured intensity, in particular, information on the absorbing properties of the aerosols might be derived. The aerosol information derived from MAX-DOAS observations can be used for the quantitative analysis of various trace gases also analyzed from the measured spectra.

Figure 6.3.1-29 shows a simplified scheme of the atmospheric light paths relevant for MAX-DOAS observations for a given elevation angle. Also shown is the atmospheric height profile of the oxygen dimer O_4; due to its square dependence on the oxygen concentration its atmospheric scale height is only about 4 km. The most important effects of aerosols are:

a. Reduction of the visibility: Aerosols reduce the visibility of the atmosphere and thus decrease the direct light paths of the incident solar radiation and along the line of sight of the telescopes. These effects will, in general, reduce the observed O_4 absorptions.

b. Increased probability of multiple scattering: Aerosols increase the number of scattering events, especially in the case of extended clouds. This effect will in general lead to a simultaneous increase of the O_4 absorption for all viewing angles [Erle et al., 1995; Wagner et al., 1998, 2002].

c. Modification of the received intensity: Aerosol scattering increases the total amount of scattered photons and thus, in general, enhances the observed intensity. For high aerosol concentrations (especially also for thick clouds) this effect, however, can be (over-) compensated by aerosol extinction along the line of sight. Especially for absorbing aerosols the light intensity is further reduced. In contrast to Rayleigh scattering, aerosol scattering usually strongly prefers the forward direc-

tion. Thus the effect of aerosol scattering is significantly different for telescopes looking at different elevations and, especially, different azimuth angles.

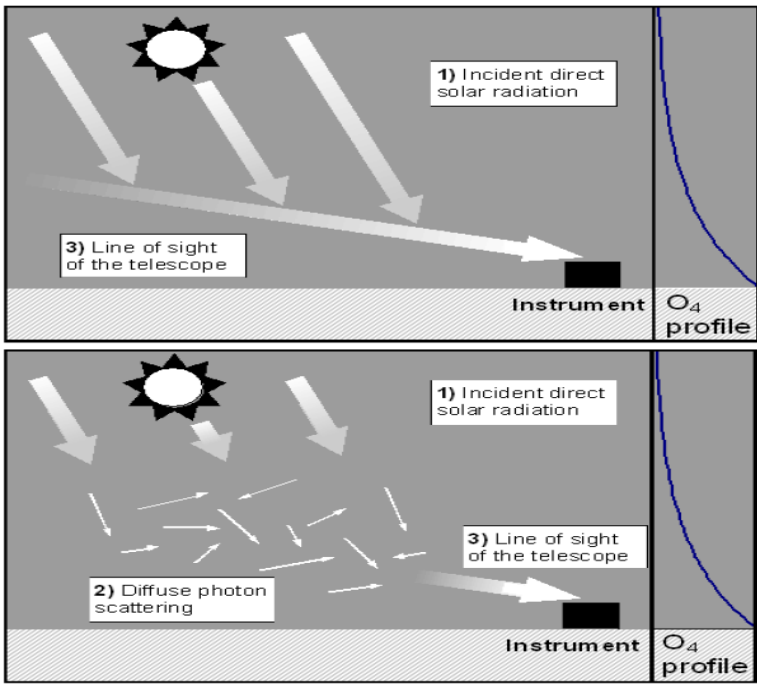

Figure 6.3.1-29. *Scheme of the different segments of the atmospheric light paths for MAX-DOAS observations. Top: for an optically thin atmosphere, e.g. for an atmosphere without aerosol scattering and observations in the visible spectral range the observed photons are mainly single scattered. The penetration depth of the direct sunlight is large (first segment); also the direct line of sight of the telescopes (third segment) is long. Bottom: If additional aerosol scattering takes place the direct line of sight of the telescopes decreases. Since the majority of the atmospheric O4 is located close to the ground the observed O4 absorption is then also significantly decreased. Additional aerosol scattering also decreases the penetration depth of the incident direct solar radiation. For very strong aerosol scattering (e.g. inside extended clouds) also a regime of diffuse multiple photon scattering can occur which can enhance the O4 absorption. Adapted from Wagner et al. [2004].*

These modifications of the atmospheric light paths change the relative composition of light paths having experienced different atmospheric O_4 absorptions and thus make MAX-DOAS O_4 measurements especially sensitive to the influence of aerosols.

For the analysis of MAX-DOAS O_4 observations, we focus on a measurement period of four mostly clear days during the FORMAT II campaign in Milan, Italy in September, 2003 (see www.nilu.no/format/). During these days the aerosol load of the atmosphere was strongly increasing. At the beginning, on September 14th, the atmosphere was very clear after a series of rainy days. The atmospheric visibility was very high and even the Monte Rosa mountain at a distance of about 120 km was clearly visible. During the following days the atmospheric visibility was steadily decreasing. Finally, even the southern edge of the Alpine mountains at a distance of only about 30 km was not visible anymore.

In Figure 6.3.1-30 the respective MAX-DOAS O_4 observations for the southern telescopes are presented. Except for the morning of September 15th, the diurnal variation of the O_4 absorptions is smooth and almost symmetric, indicating that the sky was clear throughout most of the period. Nevertheless, the magnitude of the O_4 absorption and also the amplitude of the diurnal variation of the O_4 absorptions change significantly during the following days, which can be attributed to the influence of additional aerosol scattering. Different aerosol effects can be distinguished:

a. Aerosol extinction reduces the direct light path along the line of sight of the telescopes. The higher the aerosol load is, the shorter is the distance from which photons can reach the telescopes on a direct path.

b. Aerosol scattering changes the penetration depth of the incident sunlight and thus the amplitude of the diurnal variation of the measured O_4 absorption.

c. At low aerosol levels (and in particular at relatively long wavelengths) the bulk of the light recorded by the spectrometer is only scattered once. However, for high aerosol concentrations, a layer can occur in which the photons undergo diffuse multiple scattering.

d. Additional aerosol absorption, however, decreases the absolute values of the observed intensity. Information on the absorbing properties of aerosols might thus be retrieved if both the measured O_4 absorption and the broadband intensity are taken into account for the interpretation of the MAX-DOAS observation.

e. The angular dependence of aerosol scattering differs significantly from that of molecular scattering. In particular aerosol scattering strongly prefers the forward direction. Thus the influence of aerosols on the observed O_4 absorption is different for different azimuth angles (at moderate to large SZA).

f. Not only the O_4 absorption but also the measured broad band intensity and the Ring effect are influenced by aerosol scattering in a significant and characteristic way, and thus contain useful information on atmospheric aerosols properties.

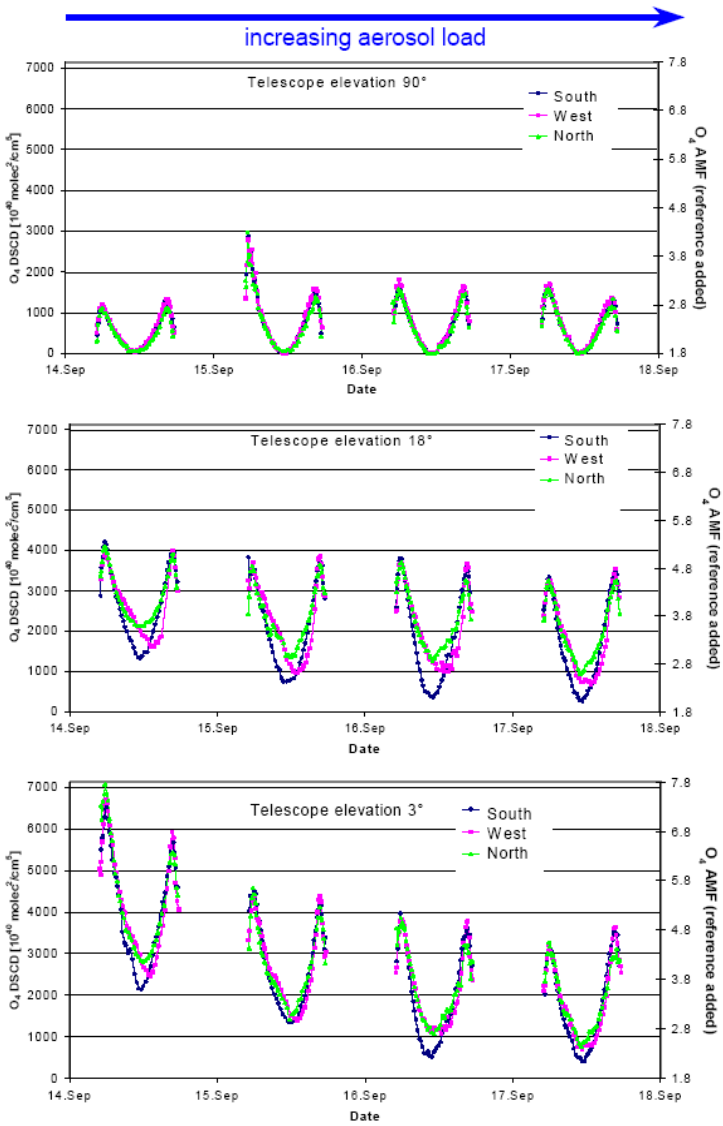

Figure 6.3.1-30. *Measured O_4 DSCDs for different azimuth angles (north, south, west) and selected elevation angles (zenith, 18°, 3°) for September 14 to 15. The zenith observations during the morning of September 15 were affected by clouds and should not be taken into account for the detailed interpretation of the time series. Adapted from Wagner et al. [2004].*

Using MAX-DOAS observations during clear days, we investigated several aspects of the aerosol influence in detail. These findings were also confirmed by atmospheric radiative transfer modeling and can be summarized as follows:

a. MAX-DOAS O_4 observations are very sensitive to the aerosol extinction close to the ground.

b. They are sensitive to the penetration depth of the incident solar radiation. Thus they can yield information on the altitude of the aerosol layer.

c. From the comparison of the observed O_4 absorption and the measured intensity, information on the absorbing properties of the aerosols might be derived.

d. Measurements at different wavelengths can characterize the wavelength dependence of the aerosol scattering, and thus yield information on the size distribution.

e. Not only the O_4 absorption can be analyzed but also the magnitude of the Ring effect and the (relative) intensity can be investigated. These quantities can also be used for the determination of aerosol properties. In addition, also the absorption of the O_2 molecule should be investigated.

f. Due to the differences in the polarizing properties of aerosols and Rayleigh scattering additional information on aerosol properties might be derived from observations of light with different polarization orientation.

g. From MAX-DOAS O_4 observations at different azimuth angles information on the scattering phase function can be derived.

h. MAX-DOAS O_4 absorptions are very sensitive: aerosol optical depths below 0.001 can probably be detected.

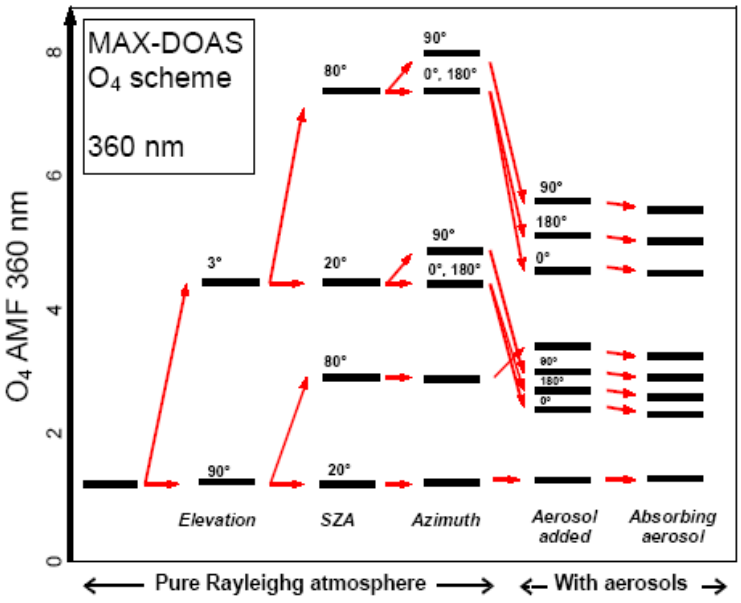

Figure 6.3.1-31. *Overview on the influence of aerosols on MAX-DOAS O_4 observations for 360 nm. Along the x-axis the possible MAX-DOAS geometries are shown (the first case is for a SZA of 20° and a telescope elevation of 90°). Even for a pure Rayleigh atmosphere a large variety of different O_4 absorptions is found. If aerosols are added these O_4 observations are modified in a characteristic way depending on the aerosol properties (the aerosol extinction was set to 0.5/km and the single scattering albedo was either set to 0 or 0.5). In contrast to the absolute intensity the influence of the aerosol single scattering albedo on the O_4 absorption is relatively weak. It should be noted that similar schemes for O_4 absorption bands at other wavelengths show different dependencies indicating additional information content of multi-wavelength MAX-DOAS observations. Also the observation of the O_4 absorption for light with different polarization might add valuable further information.*

Using optimal estimation to derive aerosol properties from ground-based MAX-DOAS measurements of O_4

Here we present first results from an optimal estimation retrieval code for the determination of aerosol properties based on ground-based MAX-DOAS measurements of the oxygen dimer O_4, which is currently under development. Our approach is similar to the analysis of airborne MAX-DOAS observations [Bruns et al., 2004]: information on the aerosol extinction profile and optical properties are retrieved using measurements of the optical depth of O_4 absorption bands at different wavelengths and using various observation geometries (lines of sight as defined by elevation angle, solar zenith angle, and azimuth angle). The retrieval algorithm is based on the optimal estimation technique, which derives a solution for the state vector (e.g., the aerosol extinction profile) given a particular measurement (e.g., measurements of O_4 optical depths). This kind of problem is usual-

ly under-constrained, which means that there are few measurements than retrieval quantities. Thus additional information on the state vector is necessary, which is provided by an a priori state vector, i.e. the knowledge on the state vector before the measurement is made. A priori information can be based, for example, on a climatology. The a priori state vector is then represented by the average state of the atmosphere and its variability. Using the Bayesian approach, the a priori state vector and the measurements are combined to derive the expected value of the state vector under the constraint that the measurement has been made, given the probability density function of the state vector. This approach yields the so-called maximum a posteriori (MAP) solution of the state vector.

Compared to the retrieval of trace gas vertical profiles, the retrieval of aerosol properties using observations of scattered sunlight is a very complex problem [Wagner et al., 2004]: the response of the measurements to a change in state vector (the weighting function) is independent from the state of the atmosphere in case of optically thin absorbers (which is the case for most atmospheric trace gases in the UV/Vis except ozone), which means that the solution can be determined in only one iteration. However, aerosols have a strong impact on the radiative transfer through the atmosphere since they act as scattering particles. The retrieval of aerosol properties is therefore a strongly non- linear problem. This makes it necessary to determine the MAP solution iteratively, a very time consuming procedure since the weighting functions have to be re-calculated in each step. Furthermore, aerosol concentrations in the boundary layer are highly variable, which means that the a priori state vector can provide only very loose constraints to the solution.

We use the radiative transfer model SCIATRAN as the forward model for the retrieval. O_4 slant columns densities are modeled using full spherical geometry and taking into account refraction and multiple scattering. Furthermore, SCIATRAN is able to calculate the radiance in specific lines of sight. Therefore measurements of the intensity from different lines of sight can be used as an additional source of information for the aerosol retrieval.

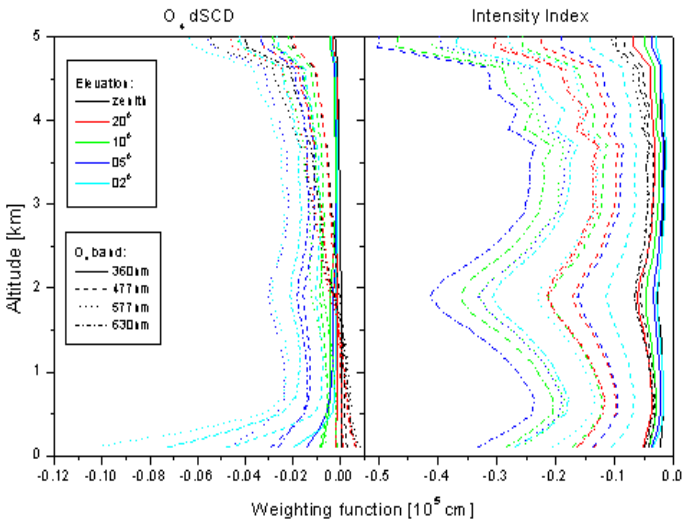

Figure 6.3.1-32. *Aerosol extinction weighting functions for the optical depth of O_4 (left panel) and the intensity index (right panel). Different colours indicate different elevation angles and different line styles indicate different wavelengths as denoted in the legend, respectively.*

Figure 6.3.1-32 shows aerosol extinction weighting functions for the O_4 differential optical depth (left panel) and the intensity index (right panel), i.e. the response of the measured quantities to a perturbation of the aerosol extinction profile at a particular altitude. The weighting functions are shown for four O_4 absorption bands in the UV/Vis spectral region between 360 and 630nm. The intensity index is defined the intensity in the centre of the O_4 absorption band, normalised to the respective intensity of the reference spectrum at the same wavelength. The weighting functions shown in Figure 6.3.1-32 are calculated for a

mid-latitude standard atmosphere using a rural aerosol profile with 23km visibility adapted from the LOWTRAN aerosol library. The calculations were performed for a solar zenith angle of 85.

The weighting functions for the O_4 optical depth in show a strong peak for the surface layer. The (absolute) peak values of the weighting functions at the surface increase with decreasing elevation angle, reflecting the increasing sensitivity of the measurements for aerosols close to the surface when pointing the instrument closer to the horizon. The O_4 weighting functions show a strong wavelength dependence, and the highest sensitivity is achieved using the 577nm O_4 absorption band. The sensitivity to aerosols is weakest in the near UV (360nm) since Rayleigh scattering becomes more dominant at shorter wavelengths, which causes a shorter direct light path along the line of sight. The weighting functions with respect to the intensity index show a pronounced peak around 2km, which means that using measurements of the intensity in the aerosol retrieval yields an improved sensitivity for aerosols at higher altitudes than if using measurements of the O_4 optical depth alone.

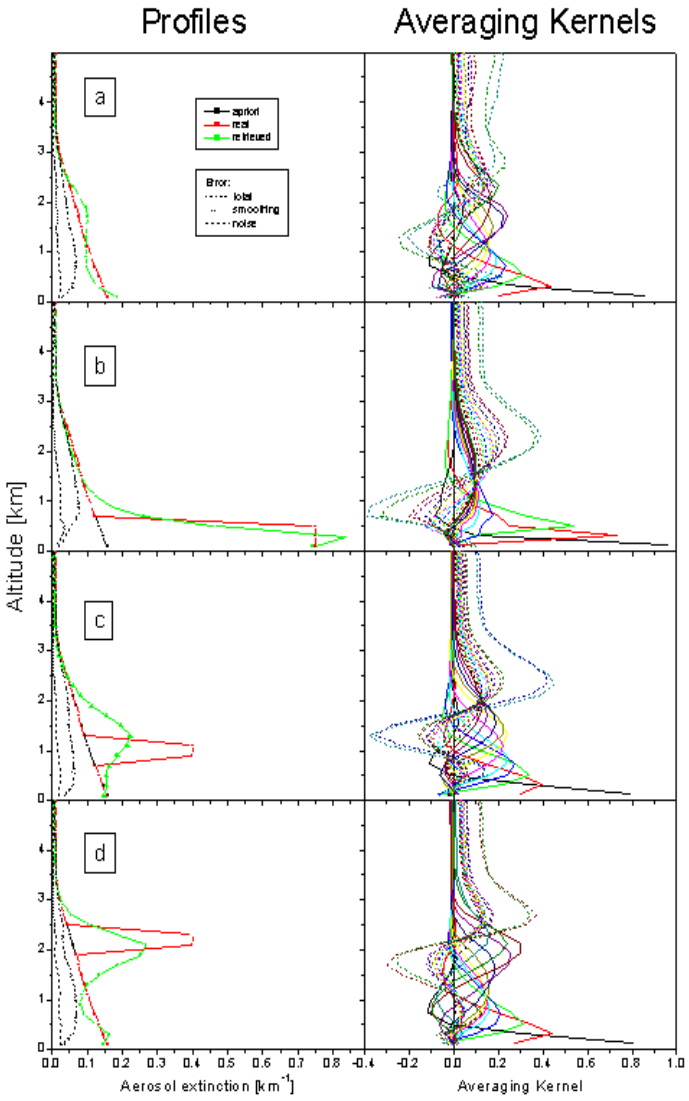

Figure 6.3.1-33. *Examples for the MAX-DOAS retrieval of aerosol extinction profiles in the lower troposphere, based on simulated measurements. Left panels: A priori (black solid line), 'true' (red line) and retrieved (green line) aerosol profiles for the LOWTRAN rural aerosol profile (a) as well as for increased aerosol layers at the surface (b), and around 1km (c) and 2km (d) altitude. Dashed, dotted, and dash-dotted lines show the different error contributions (total error, smoothing error and retrieval noise, respectively). Right panels: Corresponding averaging kernels for the different scenarios. The retrieval has been performed using both the optical depth of O_4 and the intensity index at four wavelengths (360, 477, 577, and 630nm), and for elevation angles of 90, 20, 10, 5, and 2, at a solar zenith angle of 85.*

Figure 6.3.1-33 shows some examples for the retrieval of aerosol profiles in the lowermost 5 km of the troposphere, based on simulated measurements for the LOWTRAN rural aerosol profile (panel (a)), as well as for increased aerosol lay-

ers at the surface and around 1 and 2 km (panels (b)-(d), respectively). Also shown are the respective averaging kernels (right panels), i.e. the sensitivity of the retrieved profile to the true profile. The retrieved profile can be regarded as the true profile, smoothed by the averaging kernel of the respective altitude, and the resolution of the retrieved profile can be quantified by the width of the averaging kernel. The following conclusions can be drawn for these case studies:

1. Aerosol profiles can be retrieved with a vertical resolution of approximately 500m at the surface and better than 1km up to an altitude of ~2km.

2. For an aerosol extinction constantly decreasing with altitude (case (a)), the measurement errors introduce some oscillation of the retrieved profile around the true profile.

3. Layers of enhanced aerosol extinction are well captured by the retrieval, in particular at the surface (case (b)), and to a lesser extend for elevated aerosol layers (cases (c) and (d)), where the retrieved profiles are much smoother than the true profiles and do not peak exactly at the nominal altitudes.

4. The peak values of the averaging kernels – and thus the vertical resolution of the retrieval - increase at altitudes where the aerosol extinction is increased.

To further investigate the information content of MAX-DOAS O_4 measurements regarding the retrieval of tropospheric aerosol profiles, we have performed aerosol retrievals for different aerosol loads by varying the aerosol extinction. This was done by multiplying the LOWTRAN rural aerosol profile with a scale factor between 0 and 20. The left panel in Figure 6.3.1-34 shows the retrieval error for the aerosol extinction in the lowermost 2.5 km of the atmosphere as a function of aerosol load. Further quantities useful for the assessment of the quality of the retrieval and the information content of the measurements are the degrees of freedom for signal and the entropy as shown in Figure 20. The degrees of freedom for signal is the number of independent quantities that can be inferred from the measurements, while the entropy S quantifies the information content of the measurement, i.e. 2^S is the number of different aerosol extinction profiles can be distinguished.

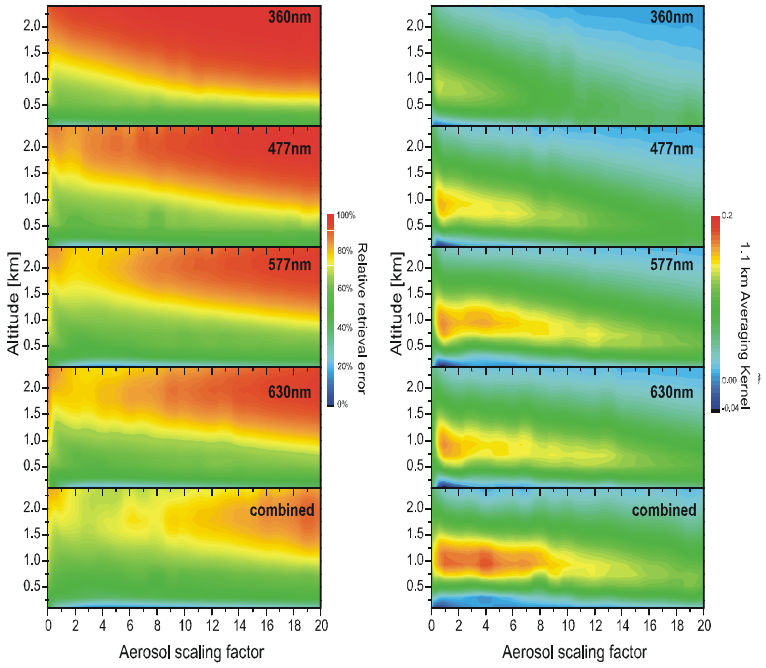

Figure 6.3.1-34. *Left panels: Relative error of the retrieved aerosol extinction profile as a function of altitude (y-axis) and aerosol load. The aerosol load is varied by multiplying the LOWTRAN rural aerosol profile with a scaling factor (x-axis). A scaling factor of zero refers to a pure Rayleigh atmosphere, a scaling factor of 1 to a visibility of 23km, and 20 to a visibility of ~1.2km. Right panels: Averaging kernel for the aerosol extinction retrieved at 1.1km as a function of altitude and aerosol scaling factor. The upper three panels show retrieval errors and averaging kernels when using the O_4 optical depths at single wavelength as denoted in the graphs, while the bottom panels show the results for the combined retrievals using all four wavelengths. The retrieval has been performed for a solar zenith angle of 85 and elevation angles of 90, 20, 10, 5, and 2.*

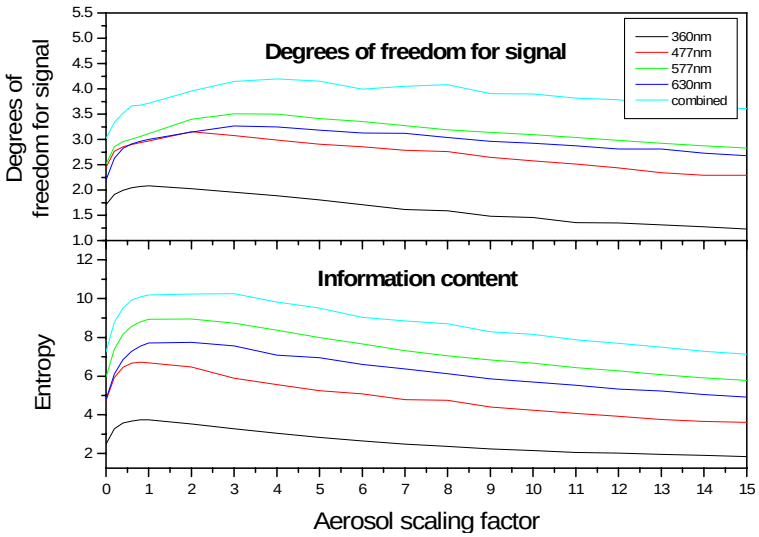

Figure 6.3.1-35. *Degrees of freedom for signal (top panel) and entropy (lower panel) of the aerosol profile retrieval for different aerosol loads. These quantities are shown for retrievals using a single O_4 absorption band at different wavelengths as denoted in the legend, and for the combined retrieval using all four O_4 absorption bands (magenta line).*

The following can be concluded from these results:

1. When using only a single O_4 absorption band for the retrieval of aerosol extinction profiles, the smallest errors and best vertical resolution is achieved when using the 577nm O_4 band.

2. A combined retrieval using the four O_4 absorption bands centred at 360, 477, 577 and 630nm significantly improves the quality of the retrieval in terms of vertical resolution and retrieval error.

3. Using all four O_4 absorption band in a combined retrieval allows to determine aerosol extinction profiles within a wide range of atmospheric conditions. The vertical resolution at 1km altitude is better than 1 km (Figure 6.3.1-34) for aerosol scaling factors between 0.5 and 8, corresponding to visibilities of approximately 3-50 km.

4. As expected, the aerosol extinction retrieved for the surface layer has the smallest relative error. The retrieval error remains less than 15% for visibilities between about 2.5 and 10km.

5. Smaller relative errors are achieved for altitude regions where the aerosol extinction is strongly enhanced (see the examples shown in Figure 6.3.1-33).

6. The information content of the measurements strongly depends on aerosol content. Degrees of freedom for signal and entropy are relatively low in very clear atmospheres (visibility > 50km) (see Figure 6.3.1-35).

7. The information content of the measurements strongly depends on the wavelength of the O_4 band used for the retrieval. The highest information content in terms of entropy and degrees of freedom for signal is achieved for the 577nm O_4 band. However, a significant improvement is achieved when using all four O_4 absorption bands in a combined retrieval.

This model study has shown that MAX-DOAS measurements of the oxygen dimer (in combination with intensity measurements) are suitable for the retrieval of aerosol extinction profiles in the lowermost 2-3 km of the atmosphere, i.e. in the region where the highest variability in aerosols is present. Using optimal estimation, aerosol extinction profiles can be determined with a vertical resolution of better than 1km. Furthermore, MAX-DOAS measurements of O_4 (in particular in combination with measurements of the relative intensity) offer the possibility to retrieve optical properties of aerosols, such as the amount of absorbing aerosol.

Separated tropospheric and stratospheric NO_2 column densities derived from off-axis measurements (D7)

Partner 2 (IASB) has carried out MAX-DOAS observations of HCHO and NO_2 at Observatoire de Haute Provence (see Figure 6.3.1-36) and at Reunion (see Figure 6.3.1-37). Both sites show a clear tropospheric signal for NO_2. The highest values of HCHO occur in summer probably due to biogenic emissions from forest at this site. A more detailed analysis of these data taking into account radiative transfer calculations (see WP 2500) will be available soon.

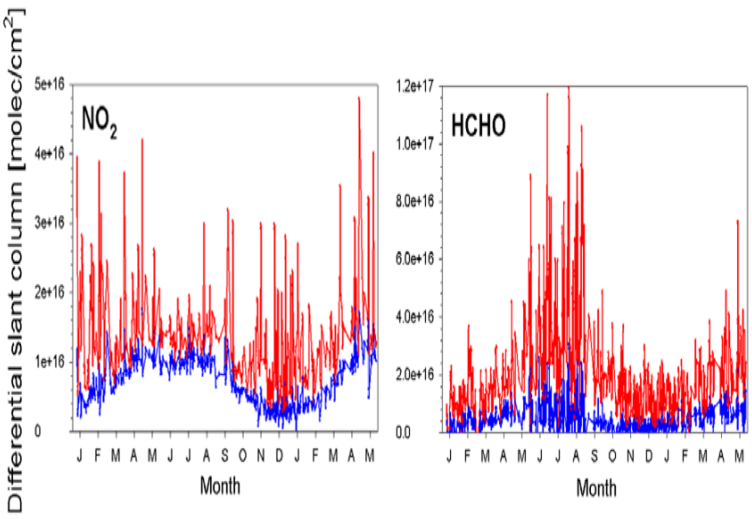

Figure 6.3.1-36. *Time-series of NO_2 and HCHO differential slant columns measured by BIRA-IASB at Observatoire de Haute Provence (44°N) from January 2001 until July 2002. Simultaneous observations (at 75°SZA, PM) in the zenith direction and at an elevation angle of 10° are represented with blue and red lines respectively. Slant column evaluations have been performed using daily noon zenith-sky reference spectra. Results are displayed for clear days where meaningful information on tropospheric contents can be derived from the excess absorption in off-axis observations in comparison to simultaneous zenith-sky values.*

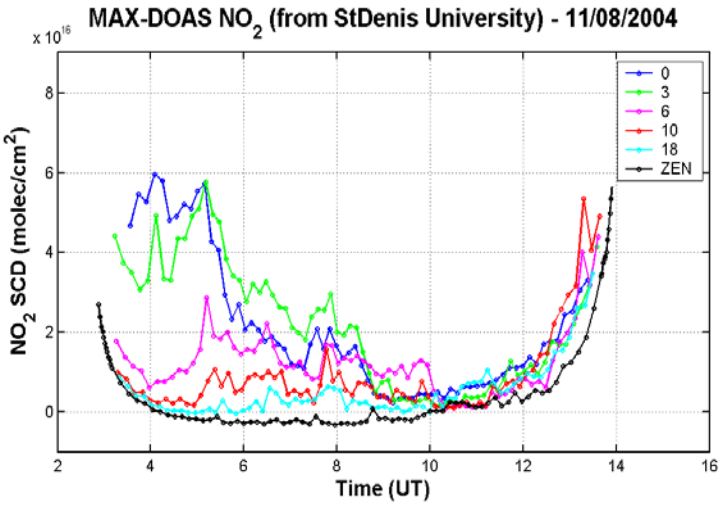

Figure 6.3.1-37. *Example of daily time evolution of the NO_2 slant column as measured in different viewing directions by the BIRA-IASB MAX-DOAS instrument at Reunion Island (22°S).*

Summary and conclusion

This work package might be one of the most successful in the project. Since the first test of off-axis measurements in 1998 by partner 3 in Ny-Ålesund and the installation of continuously running instruments in Arrival Heights by partner 5 and again Ny-Ålesund a lot of progress was obtained in interpreting these measurements and in finding new applications for this method. Several examples are illustrated above:

- measure halogen oxides in the boundary layer (D5)
- measure local pollution, e.g. NO_2 in the Arctic (D7)

Several sensitivity studies have illustrate the relevance of different atmospheric parameters on the analysis of off-axis observations (D6). Different instrumental setups have been developed showing that MAX-DOAS instruments can be built small and inexpensively. This makes them ideal to use in remote areas or e.g. on planes and ships.

In summary, Multi-Axis DOAS measurements are a promising tool for continuous measurements of several tropospheric species such as NO_2, BrO, SO_2, HCHO, and O_3. Quantitative analysis of the measurements depends on a number of parameters in the radiative transfer, and models such as those described in WP 2500 are now in a position to include all these factors with the necessary accuracy. In the near future other applications for off-axis or MAX-DOAS observations are likely:

- - monitoring of air pollution
- - monitoring of volcanoes
- - tomography of urban areas

It is also expected, that advances in software development raises new applications. While radiative transfer models are available to interpret MAX-DOAS data, the algorithms to derive vertical profiles of trace gases are still under development (some examples have been shown above).

References:

see Section 6.4: Main literature produces

Main deliverables

- *Daytime BrO, NO_2 and IO slant columns measured at sites using both off-axis viewing and zenith-sky geometry*
- *Recommendations for off-axis instrumental set-up, spectral analysis and radiative transfer*
- *Separated tropospheric and stratospheric NO_2 column densities derived from off-axis measurements*

WP 2200: NO_2 profiles with GB DOAS

Applied methodology and scientific achievements

Introduction

More than twenty ground-based zenith-sky spectrometers are routinely measuring stratospheric NO_2. They cover all latitudes and include the primary stations of the International Network for Detection of Stratospheric Change (NDSC). The slant columns observed at twilight are routinely used to determine vertical columns of NO_2, but the change in scattering height at the UV-visible wavelengths used to measure NO_2 allows a vertical profile to be retrieved. Although the information content of the profile is limited, at the very least it would replace the currently used standard vertical profile, thereby allowing self-consistent vertical columns to be determined. This will greatly improve the accuracy of trends in NO_2 deduced from ground-based measurements.

In WP2200, we designed a new program suite for operational retrieval of NO_2 profiles by any operator with data from any ground-based site, and two research suite with limited portability and access but which provides an independent check on the operational tool and allows other aspects of the retrieval to be investigated. The suites use classical optimal estimation to perform the retrieval, and use a Radiative Transfer Model (RTM) together with the output of a stacked chemical box model to calculate transfer functions between columns and profiles. The suites use climatologies to define the profiles of air and minor constituent densities for the RTM and to initialise the chemical model, and to provide an a-priori profile for the retrieval.

The results from the research suite strengthen our confidence in the reliability and robustness of retrieval of vertical profiles of stratospheric trace gases from ground-based zenith-sky observations. The technique offers new perspectives for validation of models, and of satellite and balloon-borne measurements.

The NERC-BAS operational retrieval suite

Each module of the retrieval suite has an executable, a parameter file that includes the definitions, and well defined input and output files. The parameter files can easily be extended to cover long data series from a site, with monthly or more frequent recalculation of chemical and RTM outputs.

A variety of climatologies are included in the suite. The chemical model is initialised with the output of the Cambridge 2D model run in the conditions of 1995, giving mixing ratios of twenty-five constituents plus temperature at 3.5 km vertical intervals, together with an initialisation tool to interpolate them to the latitude and date of the measurement site. The IASB NO_2 climatology from HALOE data can overwrite the NO_2 values from the 2D model. The RTM uses temperature and pressure from CIRA-1986 to calculate air densities, plus a standard profile of background aerosol extinction. The a-priori NO_2 profile can be chosen from the 2D model, the HALOE climatology, or profiles with Gaussian or uniform shapes.

The chemical model accounts for the chemical variation of NO_2 during twilight. It is a non-family version derived from the SLIMCAT 3D Chemistry-Transport Model with identical chemistry. It includes 52 constituents, and heterogeneous chemistry on liquid and solid aerosols. Aerosol amounts are based on the H_2SO_4 distribution and its temperature-dependent equilibrium with HNO_3 and H_2O. The time-step is chosen to be 1 minute. The model is run for 30 days to assure convergence of the NOy compounds within 0.1%, using the solar parameters from a single day throughout the run. It is run independently at each of the 17 pressure-hights of the 2D-model climatology. The output takes the form of a look-up table of NO_2 as a function of solar zenith angle (SZA) and altitude, of which Table 6.3.1-2 contains some examples.

Table 6.3.1-2. Ratios of NO_2 to NO_2 at solar zenith angle of 90°, at selected solar zenith angles and altitudes at sunset, for the measurements at OHP in June.

Altitude (km) SZA (°)	20	25	30	35	40
85	0.82	0.90	0.91	0.92	0.91
92	1.13	1.13	1.15	1.12	1.11
94	1.17	1.28	1.44	1.58	1.60
95	1.16	1.28	1.49	1.95	2.19

The RTM was developed at Service d'Aeronomie and British Antarctic Survey in the early 1990s for Air Mass Factor (AMF) characterisation. It calculates the transmission function by forward ray tracing in a fully spherical atmosphere in shells of 1 km thickness from the ground to 90 km. The model runs in single or double scattering, but a sensitivity study showed that the change from single to double scattering was four times smaller than that induced by a change of NO_2 profile, so single scattering is chosen. The NO_2 transmission in each layer above 18 km is chemically weighted using the look-up table calculated by the chemical model. The transmission function is then used to produce chemically modified weighting functions (Table 6.3.1-2).

Figure 6.3.1-38. *Left, Gaussian profiles of simulated NO_2 with various amplitudes, used in the Radiative Transfer Model for weighting function calculations. Right, weighting functions (transfer functions from slant columns to vertical profiles) of the Gaussian profile chosen as standard (A=1) at various values of Solar Zenith Angle between 60° and 94°.*

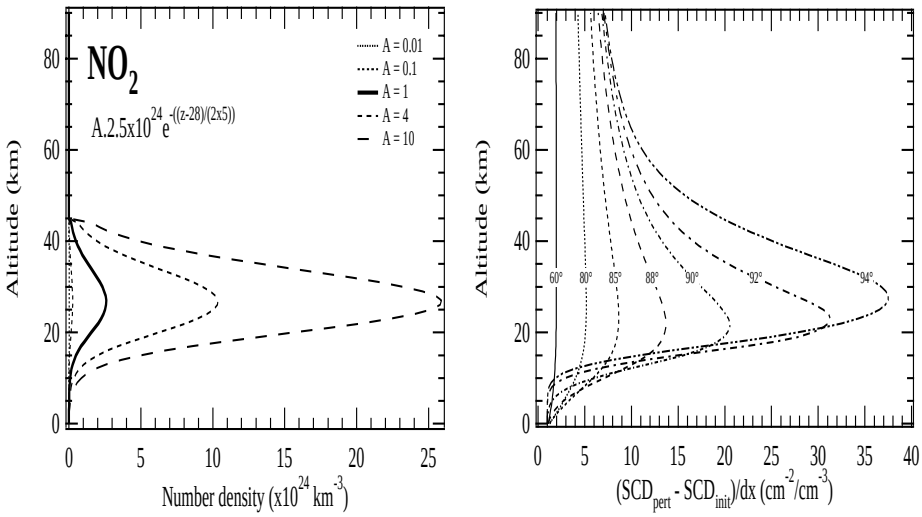

Vertical profiles are deduced from slant columns using an optimal linear inversion, resulting in a weighted mean between the a-priori vertical profile (a function of altitude), and the measurement series (a function of SZA) transferred into the vertical space by the matrix of weighting functions. The weights are the errors of the a-priori profile, and the error of each measurement similarly transformed. The vertical intervals can be specified, or chosen to equal the approximate vertical resolution given by the mean of the full width at half maximum of the averaging kernels. Limitations in the retrieval arise might arise from the chemical model stopping at 58 km, but above 45 km the weighting functions in Figure 6.3.1-38 show the information content becomes inherently small, so the profile tends towards the a-priori profile.

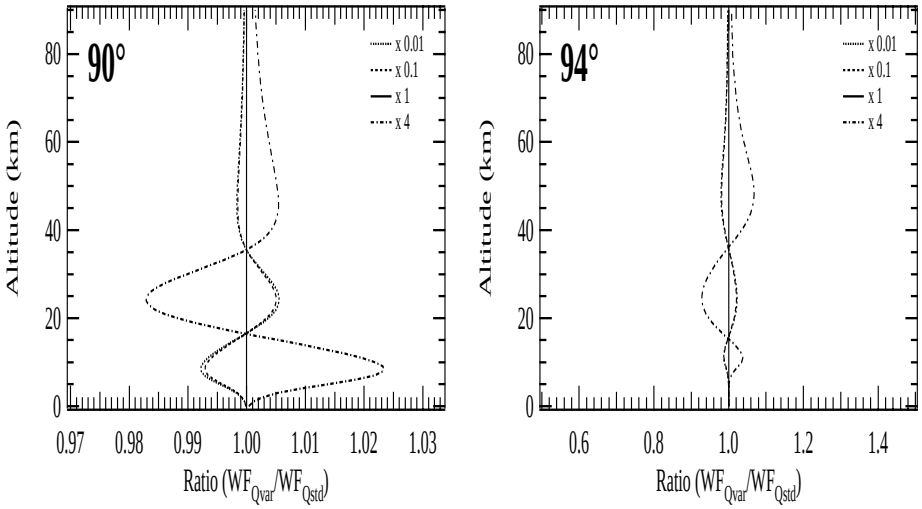

Figure 6.3.1-39. *Weighting function ratios using the NO_2 standard profile and others defined in Figure 1. Differences from unity increase with increasing solar zenith angle. For amounts of NO_2 four times the standard, the differences are ±7% at 94°, ±5% at 92° and ±2% at 90°.*

For constituents like ozone, weighting functions are affected by a small variation of the constituent amount, because typical atmospheric amounts of ozone render it optically thick, so weighting functions must be recalculated after a first retrieval iteration. The possible non-linearity of weighting functions of NO_2 was assessed in Figure 6.3.1-39, shows negligible effect at reasonable NO_2 values.

Initailly, we applied our retrieval procedure to two data sets, one with very good signal-to-noise ratio and one with poor. The instrument with good signal-to-noise ratio was the IASB spectrometer, measuring in June 1996 at Observatoire de Haute Provence (OHP, 44°N 6°E). This modern spectrometer uses a cooled detector of MOS technology. The time of year was chosen because of reliable periods with clear skies in the mornings, and because the stratospheric winds are weak so that stratospheric composition is slowly varying. Lack of cloud is important for a northern hemisphere site, otherwise one must take care to avoid even minor pollution episodes when measuring total NO_2.

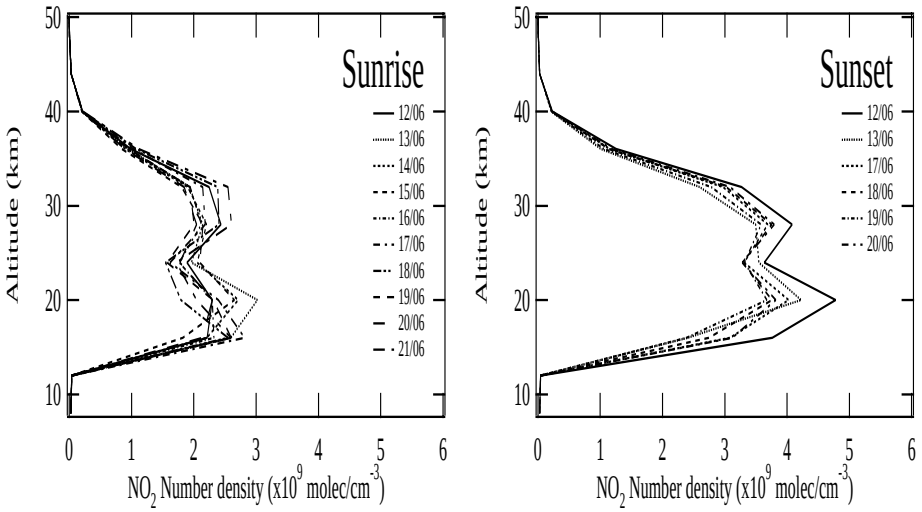

Figure 6.3.1-40. *Retrieved profiles at 44°N in June 1996, from the IASB instrument, which has good signal-to-noise ratio. T he day to day consistency of the results (variation of 25% at sunrise and 15% at sunset) at a time and place when stratospheric variability should be small, illustrates the high quality of the retrieval.*

The instrument with poor signal-to-noise ratio was the BAS spectrometer designed by CNRS in the late 1980s, still operated at Rothera (68°S 68°W). This spectrometer has a P-N junction rather than MOS detector, and it is uncooled to improve reliability and reduce power in remote locations. Sample results from

January 1997 are shown in Figure 6.3.1-41, the dates being chosen to be in late summer when the full range of SZAs are available at this polar latitude, but when NO_2 amounts are still large. In summer the stratospheric variability is again expected to be small.

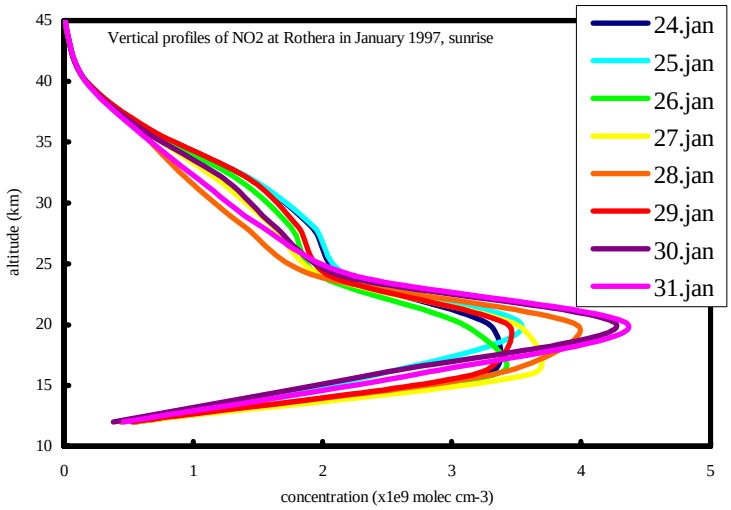

Figure 6.3.1-41. *Retrieved profiles at 68°S in January 1997, from the BAS instrument that has comparatively poor signal-to-noise ratio. Again, the day to day consistency of the results when stratospheric variability should be small illustrates the high quality of the retrieval despite the poorer signal-to-noise ratio. These results have been slightly smoothed in the vertical to guide the eye, unlike Figure 6.3.1-40.*

A balloon-borne UV-visible spectrometer from CNRS was flown close to OHP in June 1996, allowing a validation of the ground-based retrievals in Figure 6.3.1-40. The flight went from Tallard (45°N 6°E) to Toulouse (44°N, 2°E), recording spectra of the sun during occultation during sunset on 19 June and sunrise on 20 June. Profiles were retrieved by onion-peeling with much finer vertical resolution than that of the ground-based profiles. Figure 5 shows the comparison, with a standard deviation of the differences of 13% and much better agreement above 15 km where ground-based information content is greater. Smoothing the balloon-borne profile to the resolution of the ground-based profile would improve the agreement. Given the day-to-day variation in the NO_2 profile in Figure 6.3.1-42, the remaining small differences could be due to the difference in locations.

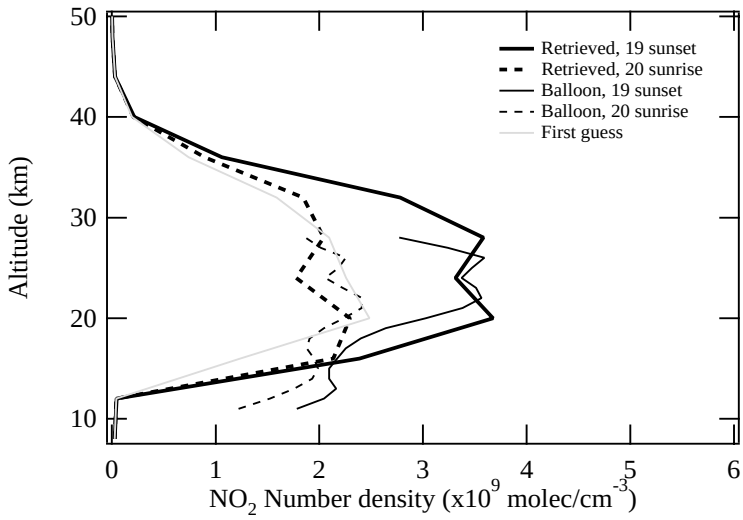

Figure 6.3.1-42. *Comparison between the profiles retrieved from the ground-based spectrometer in this work, and from the CNRS balloon-borne spectrometer, on 19 June 1996 at sunset and on 20 June at sunrise.*

The IASB research retrieval suite

As in the NERC-BAS suite, the IASB retrieval uses optimal estimation. The chemical model is the IASB model PSCBOX, initialised by output from a 1999 run of the 3D CTM SLIMCAT at the location and day of the year of the ground-based observations. The RTM is UVspec/DISORT in multiple scattering mode with ground albedo fixed to 25%, with the variation of the concentration of the absorbing species along the light path taken into account. The a priori profiles are from the output of the chemical model. Below the lowest altitude of the chemical model the NO_2 content in the a priori profile was made negligible, and above its highest altitude the US76 standard atmosphere completed any requisite profiles. The suite uses the SZA range from 75° to 94°, and in a novel feature it deduces the amount of NO_2 in the reference spectrum as well as the vertical profile. This avoids the need for a chemically modified Langley plot performed separately before the retrieval, although it can lead to difficulties in averaging the amount when using a single reference spectrum for a long data series.

The research suite was used to conduct an extensive set of validations, using ground-based measurements from IASB spectrometers at the NDSC station of Harestua and Andøya, and comparing to data from the balloon-borne spectrometers from CNRS and from Heidelberg, and the satellite instruments POAM III (Polar Ozone and Aerosol Measurement) and HALOE. These balloon and satellite instruments were chosen because they cover complementary altitude ranges (15 to 30 km for balloons, 20 to 45 km for satellites). Satellites also operate year-round, allowing a large number of coincident measurements with the ground-based observations.

Satellite and balloon-borne instruments also have good vertical resolution (1 to 2 km), but before comparing with ground-based results they must be smoothed by convolving with the ground-based averaging kernels: $\mathbf{x}_s = \mathbf{x}_a + \mathbf{A}\,(\mathbf{x}_c - \mathbf{x}_a)$, where $\mathbf{A}$ is the ground-based UV-visible averaging kernels matrix, $\mathbf{x}_a$ is the a priori profile used in the retrieval, and $\mathbf{x}_c$ is the balloon or satellite profile. The balloon and satellite profiles cover a limited altitude range but must be extended over the same altitude grid as the averaging kernels. Below, this is done by the a priori profile scaled to agree at the upper and lower measurement limits.

All the flights used for the CNRS balloon-borne comparisons originated in Kiruna (68°N, 21°E) and occurred at sunset. As the balloon data have not been corrected for photochemical variations along the line of sight, only the ascent data are taken into account for the comparisons. Five coincident events were found, three in summer (Harestua data) and two in early spring (Andøya data), although several days can separate the ground-based and balloon-borne observations. Due to the latitude difference of 8° between Harestua and Kiruna, their comparisons are only relevant in summer when the stratosphere is stable. Figure 6.3.1-43 shows good agreement for the cases of Harestua 13 & 28 August and Andøya 16 March, the profiles differing over the entire altitude range by less than 7%, 25%, and 21%, respectively. For both other coincident events, the relative difference is smaller than 25 % above 20 km but larger discrepancies are observed below (up to 70%). For Andøya 27 March, dynamical effects could be argued to explain the observed discrepancies since it is the end of the polar vortex season and the observations are 3 days apart, but the PV at 475 K shows that both measurements were outside the vortex. The vertical columns integrated over the balloon-borne height range show agreement of better than 17 % for each case (Table 6.3.1-3).

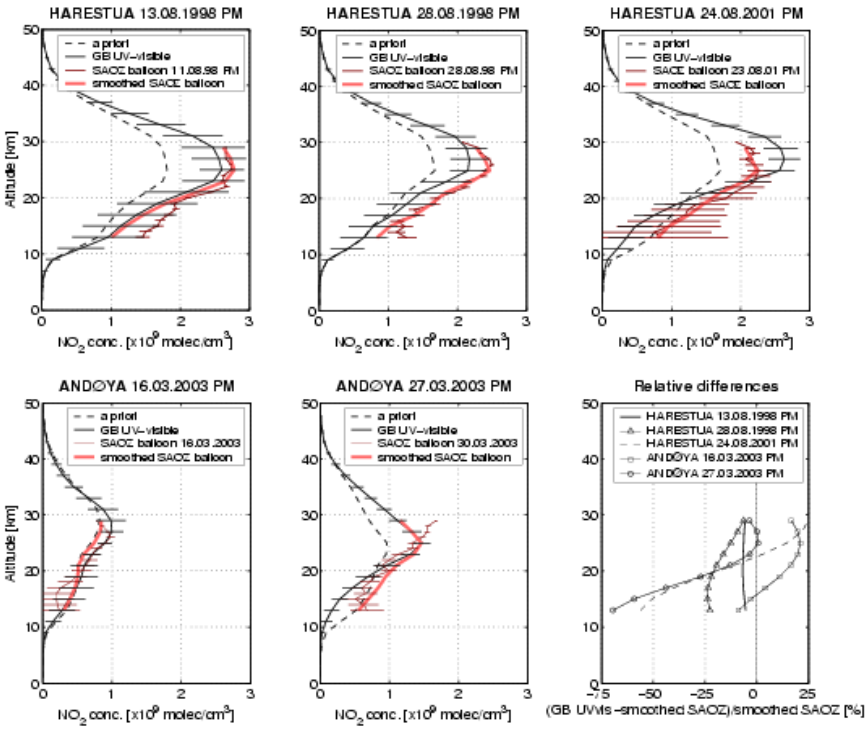

Figure 6.3.1-43. *Comparison between ground-based UV-visible profiles at Harestua (sunset, summer conditions) and Andøya (sunset, late winter-early spring conditions) and SAOZ balloon profiles. In the 5 cases, SAOZ balloons were launched from Kiruna. For direct comparison, SAOZ balloon profiles have been smoothed by convolving them with the ground-based UV-visible averaging kernels. The relative differences appear in the right lower plot.*

Table 6.3.1-3. 13-29 km NO_2 partial columns values calculated from coincident GB UV-visible and smoothed SAOZ balloon profiles at Harestua and Andøya at sunset. In the 5 cases, the SAOZ balloons were launched from Kiruna. The relative differences in % appear in the third row.

	Harestua			Andøya	
	13.08.98	28.08.98	24.08.01	16.03.03	27.03.03
(a) GB UV-visible [x10^{15} molec/cm^2]	3.13	2.43	2.51	1.06	1.43
(b) smoothed SAOZ balloon [x10^{15} molec/cm^2]	3.34	2.89	2.65	0.93	1.72
(a –b)/b x100 [%]	-6	-16	-5	+14	-17

The Heidelberg balloon-borne spectrometer has a cooled detector to provide high signal-to-noise ratio. Two flights originating from Kiruna are appropriate for comparison with Harestua ground-based data, on 19 August 1998 and 21 August 2001 at sunset. As for the CNRS balloons, only ascent data are used. For the second flight, the closest day of Harestua data is 2 days earlier. In Figure 6.3.1-44, the agreement for 1998 is excellent with differences of less than 4% over the whole altitude range, but in 2001 the ground-based profile exceeded the balloon-borne by up to 30% near 27 km. The partial column values in Table 6.3.1-4 reflect these differences.

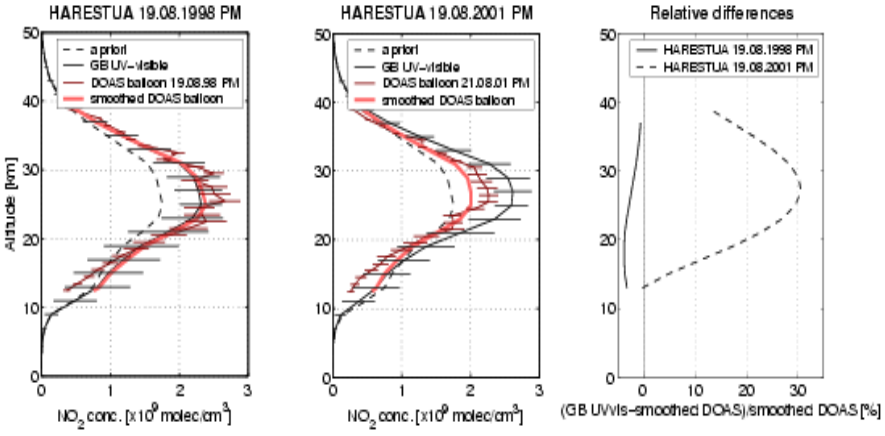

Figure 6.3.1-44. *Comparison between ground-based UV-visible profiles at Harestua and DOAS balloon profiles for two sunsets in summer conditions. DOAS balloons were launched from Kiruna. For direct comparison, DOAS balloon profiles have been smoothed by convolving them with the ground-based UV-visible averaging kernels. The relative differences appear in the right plot.*

Table 6.3.1-4. NO_2 partial columns from 13 to 37 km calculated from coincident ground-based and smoothed Heidelberg balloon-borne profiles at Harestua at sunset. In both cases, balloons were launched from Kiruna. The relative differences in % appear in the last row..

	19.08.98	19.08.01
(a) GB UV-visible [$x10^{15}$ molec/cm^2]	4.01	4.24
(b) smoothed DOAS balloon [$x10^{15}$ molec/cm^2]	4.10	3.41
(a –b)/b x100 [%]	-2	+24

POAM III is a solar occultation instrument launched on SPOT 4 satellite in 1998, measuring stratospheric profiles of NO_2 from 20 to 45 km at sunset via differential measurements at 439.6 nm (NO_2-on channel) and 442.2 nm (NO_2-off channel). Vertical resolution is about 2 km at altitudes below 40 km but is more than 7 km at 45 km. Retrievals do not include a correction for the variation of NO_2 along the line of sight. 76 coincident events (within 5° latitude and longitude of Harestua) were found between June 1998 and September 2000, with examples in Figure 6.3.1-45. Agreement is good in two examples, with differences less than 25 % over the whole altitude range, largest below 25 km where the ground-based values are smaller. This difference at low altitude is larger in the third example, reaching 40 %, and is clearly systematic as it persists when profiles are averaged (Figure 6.3.1-46). Except two days in 2000, the POAM II columns in Figure 6.3.1-47 are larger than ground-based columns by up to 26%, but the difference varies with year and season. Earlier POAM validations were compared to total NO_2 from ground-based instruments and were smaller because of POAM's limited height range, and the result is the same if Harestua total columns are used, emphasising the importance of vertical retrieval for such validation studies – without it, an opposite conclusion would be reached.

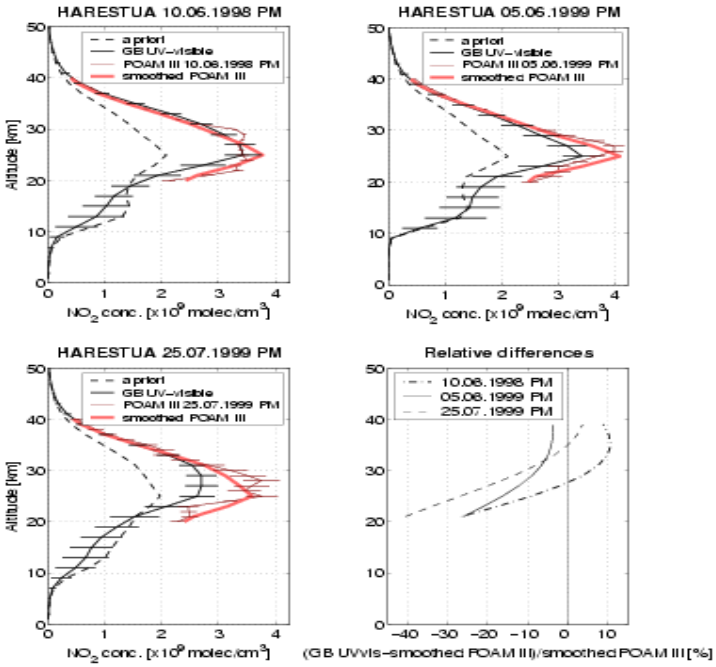

Figure 6.3.1-45. *Examples of comparison between ground-based UV-visible and POAM III profiles at Harestua (sunset conditions). For direct comparison, POAM III profiles have been smoothed by convolving them with the ground-based UV-visible averaging kernels. The relative differences appear in the right lower plot.*

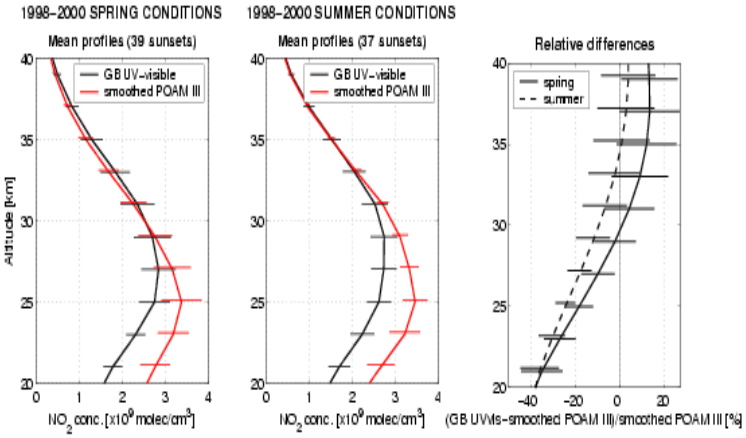

Figure 6.3.1-46. *Comparison of averaged ground-based profiles and smoothed POAM III satellite profiles at sunset in spring (left) and summer (centre) at Harestua between 1998 and 2000. The seasons are separated because of the difference in the polar vortex conditions. The relative differences appear on the right. Error bars are offset by 0.2 km for clarity.*

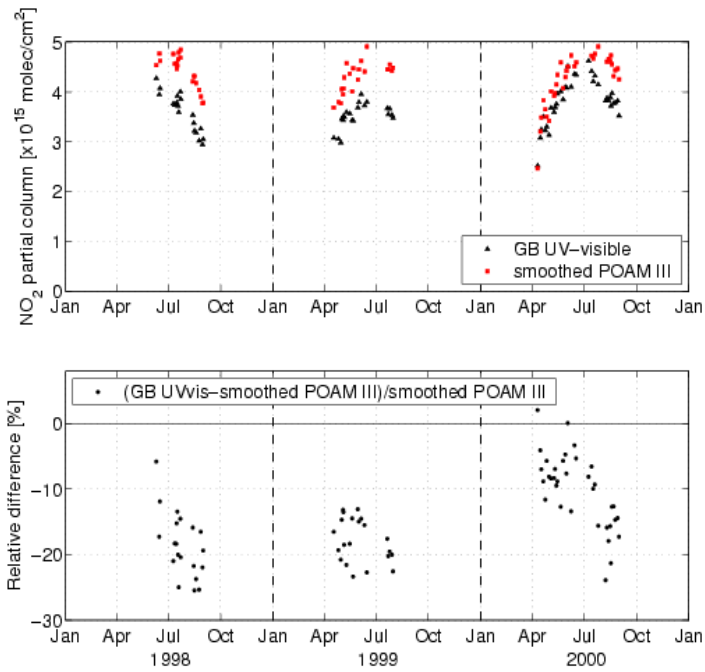

Figure 6.3.1-47. *Comparison of the sunset 20-37 km NO_2 partial columns calculated from the coincident ground-based UV-visible and smoothed POAM III profiles at Harestua for the period 1998-2000. The relative differences appear in the lower plot.*

HALOE (HALogen Occultation Experiment) was launched on UARS satellite in 1991. As for POAM III, it observes solar occultation. Vertical profiles of NO_2 are inferred from an infrared channel centred at 6.25 µm, and measurements extend from about 10 to 50 km. Large error bars are sometimes observed below 25 km, the error becoming larger as the altitude decreases, so only HALOE data above 20 km are used here. Vertical resolution is 2 km, and retrieval does include a correction for the line of sight changes of NO_2. 22 coincident events (3 at sunrise, 19 at sunset) were found for late winter-spring and 8 (6 at sunrise, 2 at sunset) for summer-early fall. Figure 6.3.1-48 shows the comparison, with good agreement above 28 km. Below, the ground-based profiles are systematically less than HALOE, as in POAM III comparisons, although the observed differences are here within profile variability of both profiles, and agreement with HALOE at sunset is significantly better than with POAM III (differences below 25 km smaller than 20% instead of being comprised between 20% and 40%). The partial column comparisons in Figure 6.3.1-49 show similar features, with ground-based values generally less than HALOE. The scatter is larger in late winter-early spring, when large dynamical effects occur above Harestua. As with POAM, earlier HALOE validations were compared to total NO_2 from ground-based instruments and were smaller, and we again find the same opposite result if total columns are used.

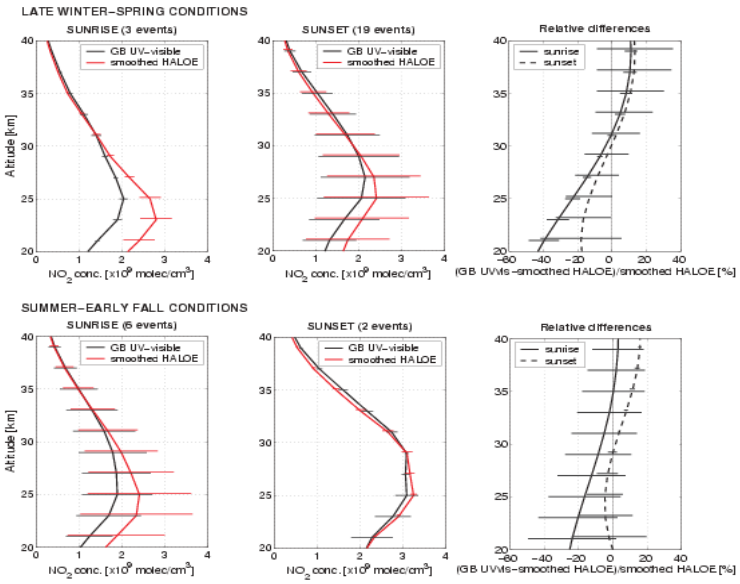

Figure 6.3.1-48. *Comparison of coincident ground-based and smoothed HALOE profiles separately averaged for sunrise and sunset for late winter-spring (upper plots) and summer-early fall (lower plots) at Harestua. Events cover the period from mid-June 1998 to mid-September 2001. The relative differences appear in the right-hand plots, where error bars are offset by 0.2 km for clarity.*

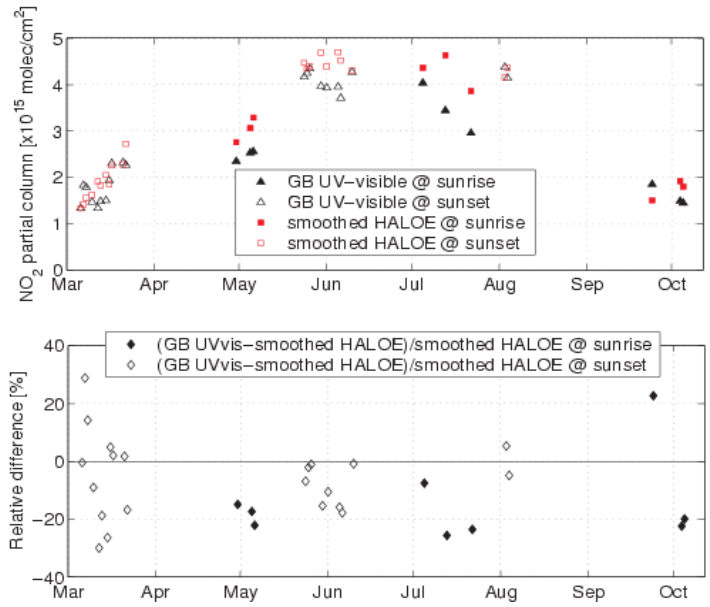

Figure 6.3.1-49. *Comparison of 20-37 km NO_2 partial columns from the coincident ground-based and smoothed HALOE satellite profiles at Harestua. Relative differences appear in the lower plot.*

The good agreement with both balloon-borne instruments suggests the disagreement with both satellite instruments at low altitudes is a problem with the satellite instruments at low altitudes, where HALOE error bars increase and POAM III neglects the correction for the line of sight variations. Neglecting the correction results in overestimation of NO_2 below 25 km, as follows for POAM III from the above argument. One estimate of the correction is 20% at 20 km, which would provide a partial explanation for the differences, though other estimates are smaller suggesting that the correction may have a large uncertainty. This uncertainty could also account for the difference in agreement with HALOE between sunrise and sunset, as the correction and so its uncertainty is much larger at sunrise than at sunset.

Errors

The total error of the retrieved profile is the sum of three errors: the error due to the smoothing of the true profile, the error due to the measurement noise, and the error due to systematic errors in the forward model.

As residuals from spectral fits are dominated by the random noise of the detector, the measurement covariance matrix $\mathbf{S}_\varepsilon$ is chosen diagonal with values corresponding to the statistical error from the spectral fits. The $\mathbf{S}_\varepsilon$ matrix being fixed, the a priori covariance matrix $\mathbf{S}_a$ can act like a tuning parameter. The variance value to be placed on the diagonal of the $\mathbf{S}_a$ matrix has been empirically determined and 10% was found to be the threshold value above which undesired oscillations in the retrieved profiles can occur. $\mathbf{S}_a$ also contains extra-diagonal terms in order to account for correlations between NO_2 values at different altitude levels. In the research suite these terms were added as Gaussian functions:

$$\mathbf{S_a}_{ij} = \sqrt{\mathbf{S_a}_{ii}\mathbf{S_a}_{jj}}\exp(-\ln(2)((z_i - z_j)/\gamma)^2) \qquad (1)$$

where z_i and z_j are the altitudes of i^{th} and j^{th} levels, respectively and γ is the half width at half maximum (HWHM). The choice of a correlation length of 8 km (γ = 4 km) is discussed below.

The smoothing error covariance matrix $\mathbf{S}_s$ can be calculated using:

$$\mathbf{S}_s = (\mathbf{A} - \mathbf{I})\,\mathbf{S}_x\,(\mathbf{A} - \mathbf{I})^T, \qquad (2)$$

where $\mathbf{S}_x$ is a realistic covariance matrix of the true NO_2 profile, **A** is the averaging kernels matrix and **I** is the unit matrix. For retrievals using the research suite, the variance of the true NO_2 profile placed on the diagonal of the $\mathbf{S}_x$ matrix has been estimated from HALOE NO_2 profiles at 55°N to 65°N over the five years from 1998 to 2002. 1368 profiles were selected, covering sunrise and sunset and February to October. The use of the HALOE data was limited to the 17-50 km altitude range, and variance values calculated at 17 and 50 km from HALOE data are assumed below 17 km and above 50 km. $\mathbf{S}_x$ also contains extra-diagonal terms in order to account for correlations between NO_2 values at different altitudes. These terms were added as Gaussian functions using the same expression and correlation length as for the $\mathbf{S}_a$ matrix.

The measurement error is defined as:

$$\mathbf{S}_m = \mathbf{G}\,\mathbf{S}_\varepsilon\,\mathbf{G}^T \qquad (3)$$

$$\text{with } \mathbf{G} = \frac{\partial \hat{x}}{\partial y} = \mathbf{S}_a\,\mathbf{K}^T(\mathbf{K}\,\mathbf{S}_a\,\mathbf{K}^T + \mathbf{S}_\varepsilon)^{-1}, \qquad (4)$$

where $\mathbf{S}_\varepsilon$ is the measurement error covariance matrix, and **G** is the contribution functions matrix expressing the sensitivity of the retrieved profile to changes in the measured NO_2 slant column abundances.

The forward model parameter error $\mathbf{S}_f$ is given by:

$$\mathbf{S}_f = \mathbf{G}\,\mathbf{K}_b\,\mathbf{S}_b\,\mathbf{K}_b^T\,\mathbf{G}^T, \qquad (5)$$

where **G** is the contribution functions matrix, $\mathbf{K}_b$ is the sensitivity of the forward model to perturbations of forward model parameters **b**, and $\mathbf{S}_b$ is the covariance matrix of **b**. $\mathbf{S}_f$ cannot be determined easily due to the large number of forward model parameters, so the matrix derived in an earlier study by K. Preston et al. was used.

Error profiles from the two suites are shown in Figure 6.3.1-50 and Figure 6.3.1-51. Smoothing error dominates in the research suite, due to its use of measured variability to define the smoothing-error's covariance. This may be philosophically inappropriate, and ongoing research will resolve the issue.

Figure 6.3.1-50. *Error profiles from the operational retrieval suite for the profile from OHP of 19 June 1996 at sunset.*

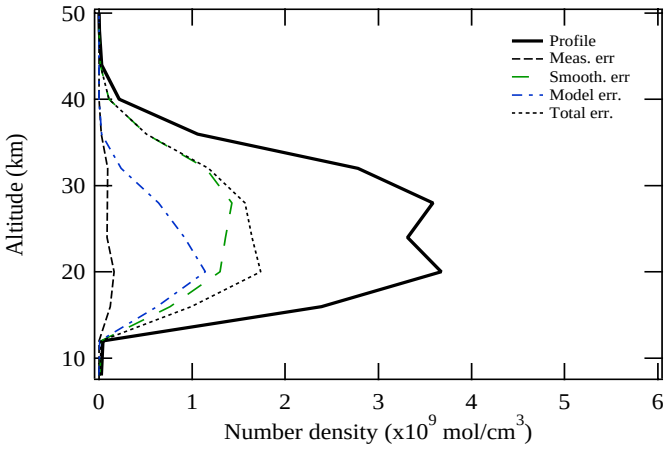

Figure 6.3.1-51. Example profiles of the retrieval errors and NO_2 natural variability from the research retrieval suite for the profile of Harestua May 25, 2001 at sunset.

Information content

The averaging kernel matrix **A** is the key parameter for characterization of vertical resolution and information content. Typical averaging kernels are shown in Figure 6.3.1-42, where those between 13 km and 33 km peak at their nominal altitude. Vertical resolution is 8 km at 13 km and reaches 20 km at 33 km.

The number of independent pieces of information that can be retrieved from the measurements can be estimated from the trace of **A**. **A** depends on the a-priori covariance matrix $\mathbf{S}_a$, and therefore on the correlation length between altitude levels used for the calculation of the extra-diagonal terms of $\mathbf{S}_a$. The impact of this correlation length is significant (Figure 6.3.1-43). The trace of **A** also depends on the SZA sampling and range of the measurements. Figure 6.3.1-43 shows that for optimal information content it is crucial to exceed 93°SZA and to sample at small intervals, important in the design of new instruments.

Figure 6.3.1-52. *Left: Typical example of ground-based NO_2 averaging kernel, for . sunset at Harestua on May 25, 2001. Plain diamonds indicate the altitude at which each averaging kernel should peak in an ideal case*

Figure 6.3.1-53. *Right: Trace of the averaging kernels matrix **A** as a function of the HWHM (γ), for sunset at Harestua on 25 May 2001. The maximum number of independent pieces of information is about 2, occurring at a correlation length (twice γ) of 8 km.*

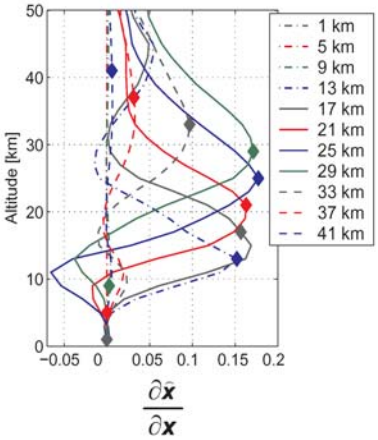

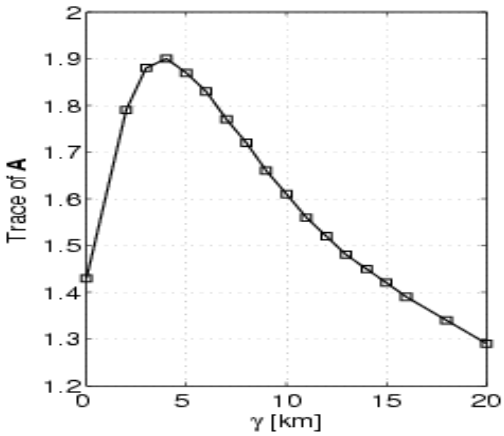

Figure 6.3.1-54. *Left: Typical example of ground-based NO_2 averaging kernel, for . sunset at Harestua on May 25, 2001. Plain diamonds indicate the altitude at which each averaging kernel should peak in an ideal case*

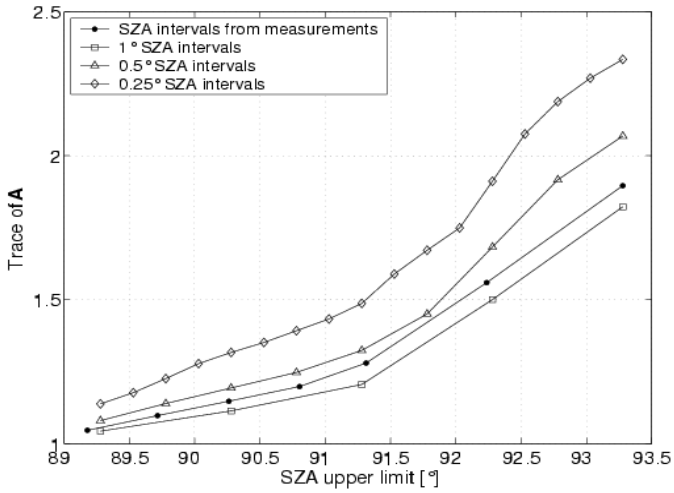

Application of the NERC-BAS retrieval suite to INTA results

Figure 6.3.1-55. *Retrieved profiles for selected days from INTA measurements (blue) at Izaña (28ºN) in 1999 (squares), 2000 (triangles) and 2001 (stars). SAGE II data for the same periods is in other colours.*

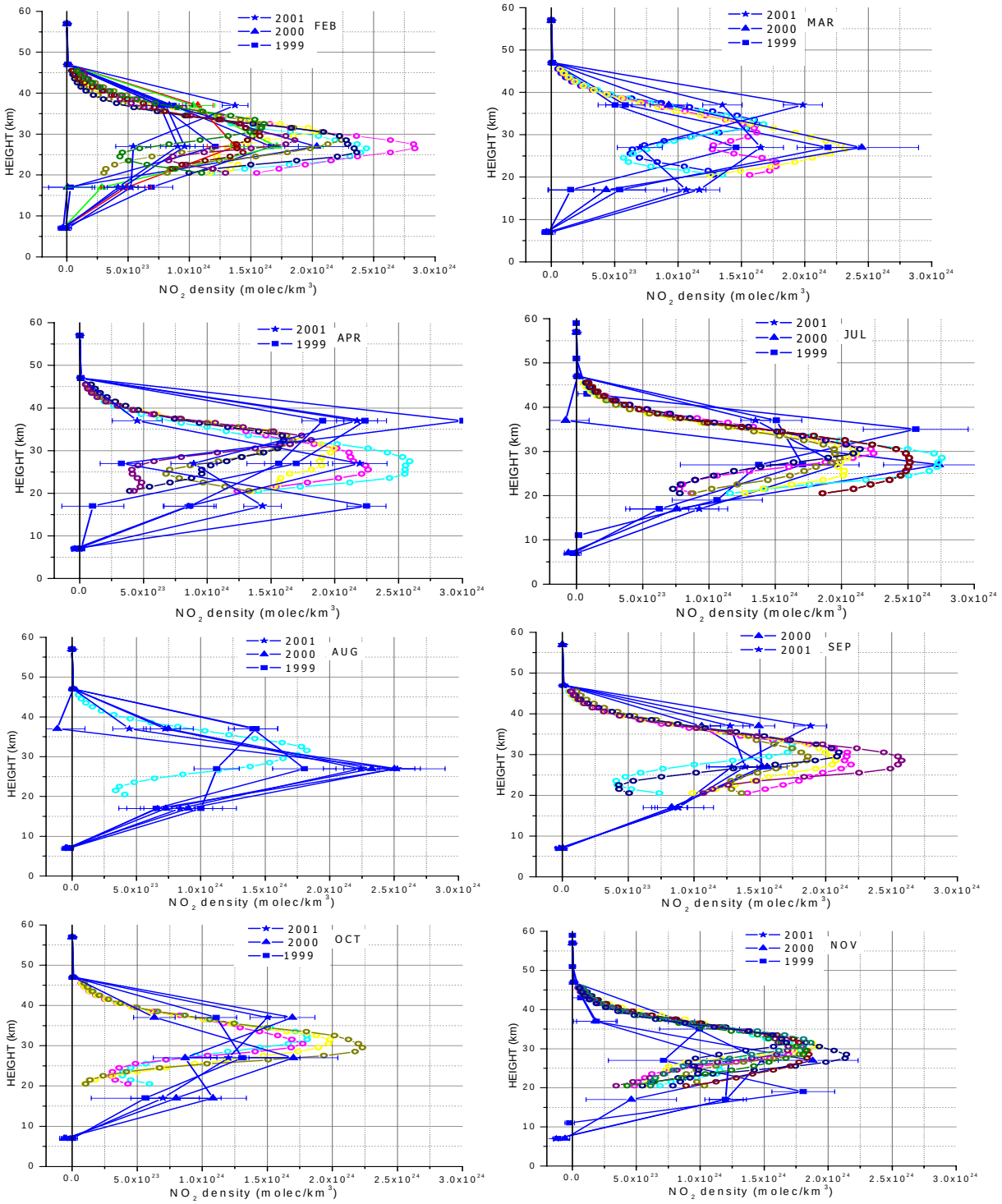

To test the NERC-BAS suite as an operational tool, INTA applied it to the slant column measurements from 1999 to 2001 by the INTA visible spectrograph (RASAS) at the subtropical Observatory of Izaña (28ºN, 16ºW). Slant columns for the SZA range 70º to 93º at intervals of about 0.5° were used, and the retrieval output was at 10 km intervals between 7 to 57 km. Days with small residuals in the spectral fit were chosen. The instrument did not always reach the largest SZA required for optimal retrieval, nevertheless the suite was successfully run for cases covering all seasons in each of the 3 years.

The results in Figure 6.3.1-55 are grouped by month, and include for comparison SAGE II profiles measured within 5º of the observatory. In the figure, the profile shapes are often bimodal rather than the unimodal we might expect from NO2 climatologies. This behavior is also observed in some coincident SAGE II profiles (e.g. March 2003), but in other cases the main maximum is located unrealistically high which we ascribe to instability in the retrieval method, a common problem. The unimodal retrieved profiles have a maximum between 25 and 30 km during the whole year, in agreement with SAGE II data.

Figure 6.3.1-56. *Vertical columns from integrating the retrieved profiles at Izaña (pink am, green pm), together with the vertical columns deduced from the same instrument in the conventional way (red am, blue pm).*

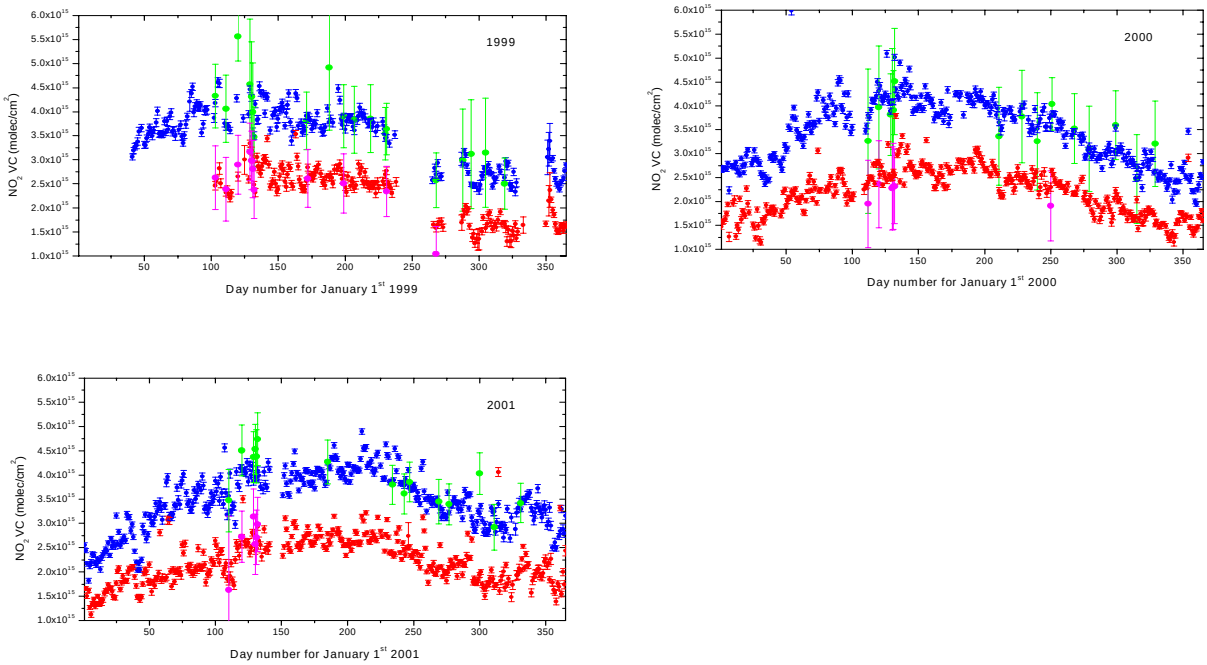

In Figure 6.3.1-56, the columns deduced from the retrieved profiles agree well with those determined without retrieval, showing that the instability is not relevant to the more important goal of self-consistent vertical columns – instability arises from lack of information content, so the bimodality of the profile does not change the resultant vertical column.

During 2000, sudden short-duration increases in NO_2 vertical column were observed. Defining a spike as an increase in column by greater than 10% of the same twilight on adjacent days, a number of spikes were identified (Figure 6.3.1-57). Possible explanations of the spikes are:

(a) Surface pollution in broken inversion episodes

(b) Abrupt change of stratospheric meridional circulation

(c) Stratospheric intrusions

(d) Long-range pollution coming from America

(e) Regional production of NO_2 in thunderstorms

Information on which of these possibilities takes place could be obtained from the height at which the spike occurs, even a distinction between stratosphere and troposphere would be useful. Figure 6.3.1-57, 21 and 22 show a case study of a spike with low aerosol (optical depth at 500nm = 0.02).

Figure 6.3.1-57. *Slant columns on a day with a spike in the vertical column (12 May 2000, day 132) and slant columns from the same twilight on the previous day, their ratios, and ratios of calculated AMFs.*

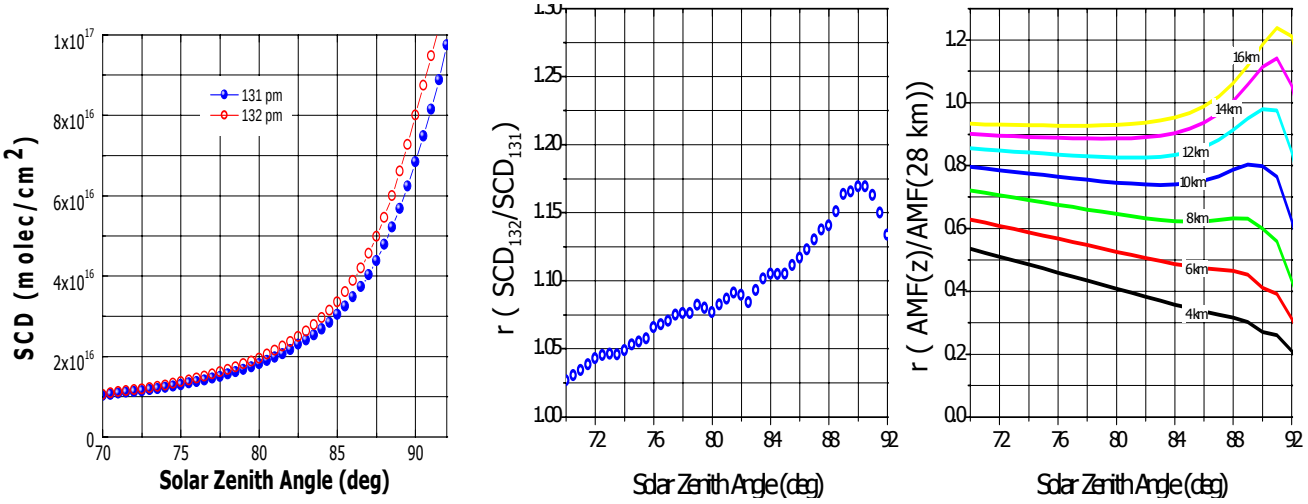

The ratio between the slant column densities (SCD) on day 132 and the previous day is given by:

$$r(sza) = \frac{SCD_{132}(sza)}{SCD_{131}(sza)} = \frac{VCD_{132}(sza)}{VCD_{131}(sza)} \cdot \frac{AMF_{132}(sza)}{AMF_{131}(sza)}$$

If the increase occurs in the stratosphere and the shape of the profile is not disturbed, then r should be constant with sza. Figure 6.3.1-57 shows this is not the case, instead r increases with sza, so either the NO_2 vertical column (VCD) was increasing, or the NO_2 enhancement takes place in the troposphere or lower stratosphere, modifying the air mass factor (AMF), or both.

Ratios of calculated AMFs in Figure 6.3.1-57 show that the variation of r with sza is consistent with an increase in NO_2 at 10 to12 km. Figure 6.3.1-58 shows the retrieved NO_2 profiles, but the expected maximum near 10 km does not occur.

Figure 6.3.1-58. *Profiles of NO_2 profiles on day 132 pm and the previous day retrieved with the operational suite at 10 km vertical intervals. The expected increase near 10 km on day 132 does not occur, perhaps because of the choice of starting altitude and vertical interval used in the retrieval.*

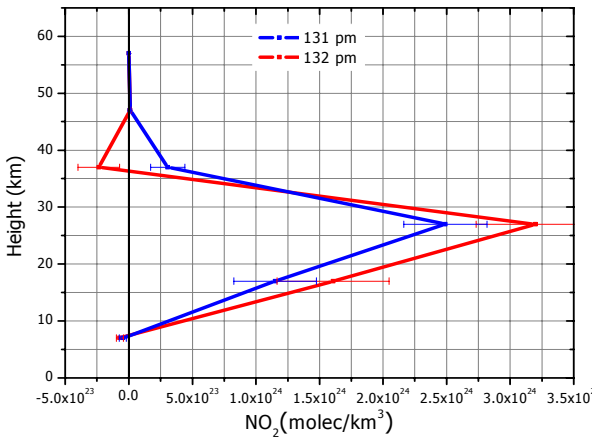

ISAC-CNR profile inversion and results

The method used for profile retrieving is that one suggested by McKenzie et al. 1991 based on the Chahine iterative retrieval. The Rodger (Rodger, 2000) approach has been used for the calculation of the error in the retrieved profile. The averaging kernels of our inversion model are shown in Figure 6.3.1-59 with the estimated percentage errors on the retrieved vertical profiles calculated using a mid-latitude climatological NO_2 profile. Sensitivity for altitudes higher than 32.5 km is very low and errors can reach values of up to 80%. Accurate *a priori* information is then necessary for these altitudes to give further stability to the solution. In the troposphere and the middle-low stratosphere, where the nitrogen dioxide variability is higher, the method is reasonably accurate with errors in the range of 12-38%. Full width at half maximum (FWHM) of the averaging kernel rows gives a possible estimation of the vertical resolution in the retrieved profile. From 2.5 up to 32.5 km the FWHM varies from 10 to 15 km so that a vertical step of 5 km is required at least to reproduce the retrieved signal without losing information. The sensibility of the retrieval to the NO_2 loading in the lowest troposphere was further investigated using synthetic measurements obtained with the RTM model AMEFCO. Three different scenario was used with NO_2 profiles constant in the stratosphere but with different tropospheric loading. The calculated slant columns were than used to retrieve the NO_2 profiles with the inversion model. Two positive results have been obtained: a) as suggested by the smoothing error calculation the retrieval has good sensibility in the lowest troposphere and b) no instability of the solution was observed when high NO_2 values in the troposphere were present.

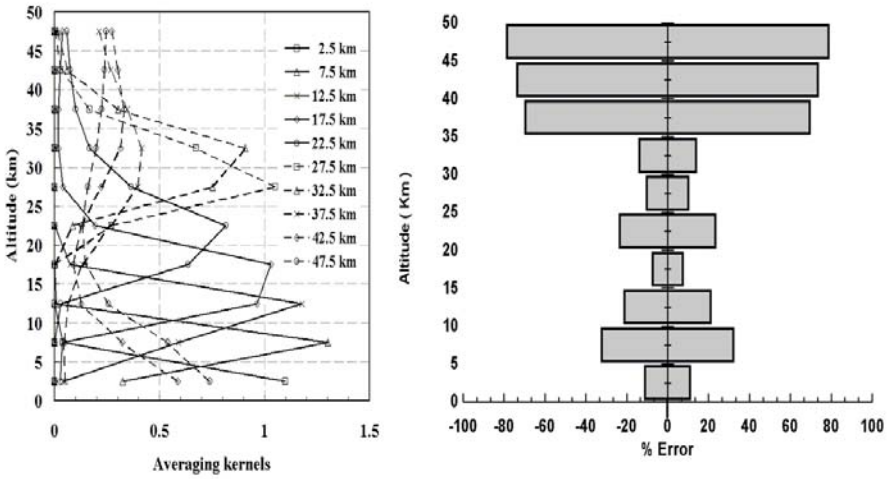

Figure 6.3.1-59. *On the left the averaging kernels of the inversion model used for nitrogen dioxide vertical profile retrieval from slant column measurements are shown. The estimated percentage error on the retrieval is shown on the right (see text for more details). The model can retrieve useful information on the vertical distribution of the gas up to 32.5 Km with errors ranging between 12% and 38%.*

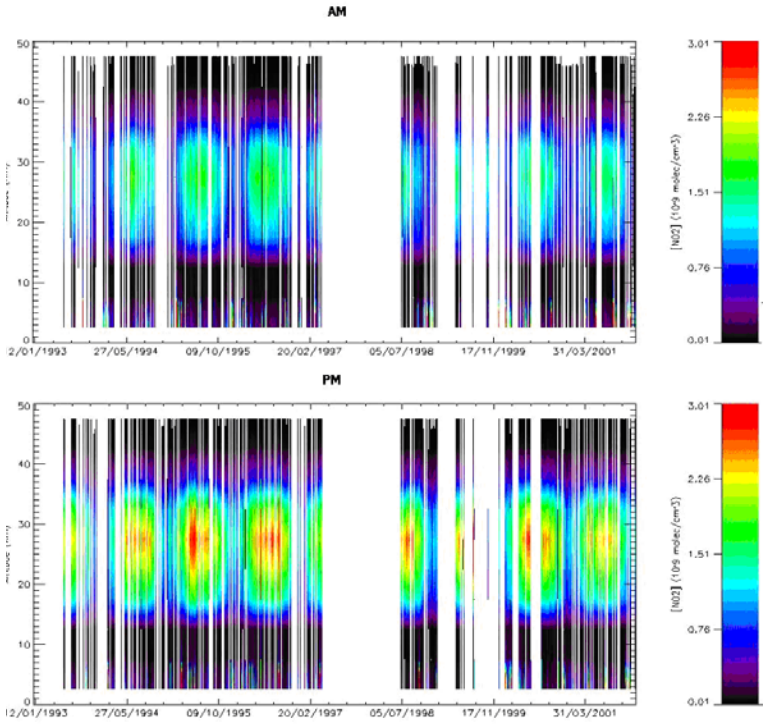

Figure 6.3.1-60. *NO_2 profiles at Mt. Cimone from 1993 to 2001.*

The inversion model has been than applied to the historical data set of NO_2 slant column measurements at Mt. Cimone (44 N, 11 E). Data from august 1993 to December 2001 was processed. Results are shown in Figure 6.3.1-60 separately for AM and PM observations.

The goal of the analysis was to study the trend of stratospheric NO_2 content neglecting any possible influence from tropospheric pollution. We used the NO2 concentration values at 27.5 Km to investigate thus the trend with a statistical model as suggested by Liley et al 2000. Results give an increased trend for stratospheric NO_2 at northern mid-latitudes of 3.5% and 4.4 % per decade for AM and PM respectively. Values are consistent with the trend of N_2O that is the main source of stratospheric nitrogen dioxide and that has been estimated with 3.6 ± 0.4 % increase per decade (WMO, 1998). Previous studies carried out on the same data set but considering slant column measurements at solar zenith angle of 90° (as done by Liley et al. 2000) reported substantially different results with an increasing trend per decade of 6% and 8% for AM and PM respectively (Petritoli et al., 2002).

The information retrieved on the tropospheric NO_2 amount was used to perform an intercomparison with NO_2 tropospheric column amount retrieved by GOME sensor in the Po valley area (Northern Italy) (Petritoli et al, 2004). The comparison of satellite columns with profiles retrieved by DOAS ground-based measurements carried out at Mt. Cimone (2165 m asl) provided good agreement (see Figure 6.3.1-61) when the troposphere was horizontally homogeneous enough to make the two measurements compatible. The strict selection criteria allowed only a selection of very few observations to be compared quantitatively. A set of nine episodes from the polluted days ensemble was selected according to the MC (mixing coefficient) parameter calculated using supplementary information on the tropospheric status and three of them were rejected because of clouds in the GOME FOV. Four of the remaining episodes showed a good linear correlation between GOME and GASCOD NO_2 tropospheric columns with R^2= 0.9 and the angular coefficient 0.86 while two cases (19/01/2000 and 17/02/2000), had a

GOME/GASCOD ratio of 0.68 and 0.55. The conclusion (see Petritoli et al. 2004) is that two different pollution sources were sampled by the satellite on 19/01/2000 and only one half of the GOME pixel was covered by the hot spot on the 17/02/2000. The data group with MC<<1 has also been studied and a reasonable interpretation of the discrepancy between the two instruments was found in cloud cover, lightning and strong gradients in the NO_2 column amounts in the Mt. Cimone area reflecting incomplete mixture of air masses sampled by GOME and GASCOD.

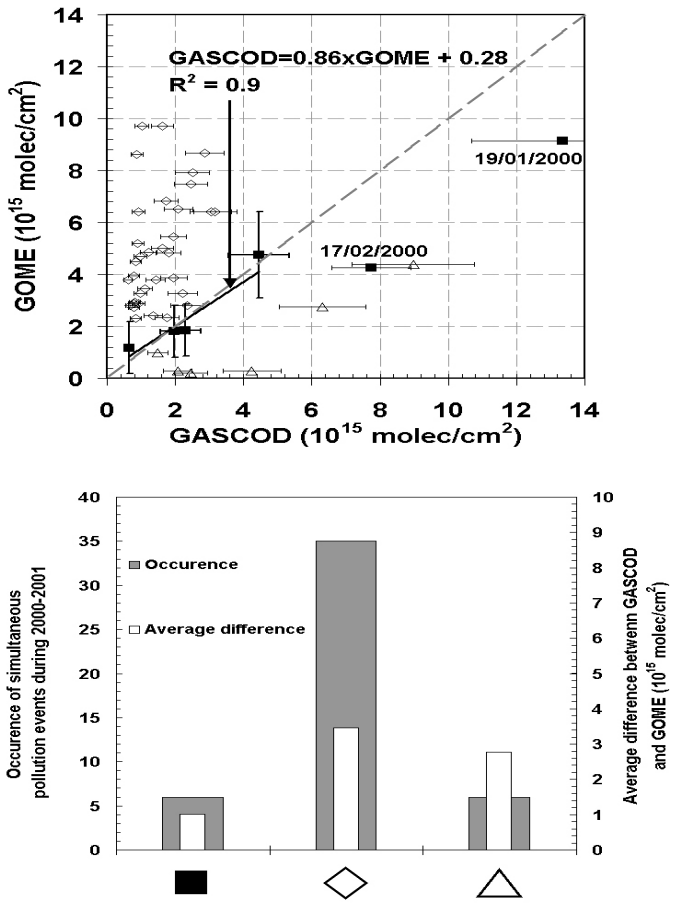

Figure 6.3.1-61. *Scatter plot between GOME and GASCOD tropospheric NO_2 columns (above) in the Mt. Cimone area. Different symbols are connected to the MC parameter as discussed in the text and in Table 2. The linear regression shown in the plot is calculated on the black filled squares excluding 19/01/2000, 17/02/2000 and the three cloudy days that are not included in the plot and in the analysis. Statistical summary of the pollution events analysed and the absolute average difference between GOME and GASCOD tropospheric NO_2 column are plotted in (below).*

Conclusions

Three new suites of NO_2 inversion software have been developed, one for operational use and two for research use. They have similar principles, though differ in detail. The operational suite is well documented, modular and portable. The research suite lend themself to testing different scientific and technical inputs.

The research suite has been used investigate errors and accuracy relative to satellite and balloon-borne instruments in a significant validation effort, and to examine details of vertical profiles in a polluted area

The operational suite has been distributed to QUILT partners. Its has already been used to investigate unusual NO_2 distributions at a subtropical station, and the trend in profile shape at an Antarctic station in summer - important because of the large apparent trend in total NO_2 there.

Main deliverables

- *Software suite for the retrieval of NO_2 profiles from ground-based slant columns at twilight, independent of the type of spectrometer or its location, distributed to the project partners and the NDSC*
- *Included in software suite; routine production of error statistics on the NO_2 profiles.*
- *Sample results of NO_2 profiles from a spectrometer with good signal-to-noise ratio and with poor signal-to-noise*

WP 2300: OClO algorithm development

Applied methodology and scientific achievements

Several activities have been carried out during the project to investigate the specific problems in retrieving OClO from UV/vis spectra. These activities include:

Acquisition of information

The first step was to systematically acquire information on the parameters used for the OClO analysis by the different groups. Like for the investigation of the BrO analysis during the OHP campaign (Alliwell et al., 2002) it turned out that also for OClO the settings of the various groups differed strongly. The details of the analysis parameters are summarised in Table 6.3.1-5. The collected information on the different OClO analysis properties as well as also on specific findings (see Table 6.3.1-6) of the different groups served as input for the systematic investigation of the impact of the algorithms settings on the OClO results.

Specific properties for the different measurement platforms

The influence of most OClO analysis parameters (see Table 6.3.1-7) on the retrieval is similar for DOAS observations from different platforms. Nevertheless, there exist also specific properties for measurements from different platforms, which will be briefly discussed in this section. Some of these differences are inherent for specific platforms (e.g. small signal to noise ratio for satellite observations). Others are caused by specific instrumental properties, e.g. due to undersampling of the detectors of GOME and SCIAMACHY. The specific properties for different platforms are summarised in Table 6.3.1-7.

Table 6.3.1-5. Details of the analysis parameters used for the OClO analysis by the different groups.

	NILU Ny-Ålesund/ Andøya	IASB Harestua	NIWA Arrival Heights	IUPHB Ny-Ålesund	IUPHD	Remarks
Spectral range (nm)	357 - 385	362.4 – 381 357.5 – 381	404 – 424 339 – 358.5	GB 355 – 390 GOME 363 – 392 Moon 397 – 424	GB 400.2-424.5 371.4-390.1 363.5-390.1 GOME 364 - 393	-Advantages for different ranges? -Differences in SCD OClO?
Ozone	GOME 202 & 241K	GOME 241K	GOME	GOME, BremFTS	-	Is ozone necessary?
NO_2	Harder 227K	Vand. 220&294K	Harder 227&294K	GOME, BremFTS	Vand. 220&294K	Differences in SCD OClO?
O_4	Hermans et al.	Hermans et al.	?	Greenblatt	Greenblatt	Differences in SCD OClO?
BrO	Wahner (227K)		?		-	Necessarry only in specific cases
OClO	Wahner (204K)		Wahner	Wahner, Bremen FTS	Wahner (204K)	Differences in SCD OClO?

	NILU Ny-Ålesund/ Andøya	IASB Harestua	NIWA Arrival Heights	IUPHB Ny-Ålesund	IUPHD	Remarks
Ring		calculated	measured	measured & calculated	Calculated (one / two spectra)	Differences in SCD OClO? How is it calculated? Is there a reference for the use of calculated or measured pectrum?
NO_2 tests	No	Harder, Vandaele (GOME summerOClO)	No		Different cross sections, different temps.	-temperature -Io-corr. -Filling-in
Io correction	Yes, Only small differences	Yes, for NO_2	Yes		Yes / no	Has to be investigated
Other corrections			Resol. change cross section			
Main problems	Signal to noise	Ring, offs., λ , Resolution changes, NO_2 cross sections	OClO, O_3 and NO_2 cross sections	O_4 cross section & shifts Instrumental artefacts (GOME)	NO_2 O_4 Fraunh. Ref.	

Table 6.3.1-6. Specific findings from OClO observations carried out by the different groups.

	NILU Ny-Ålesund / Andøya	IASB Harestua	NIWA Arrival Heights	IUPHB Ny-Ålesund	IUPHD	Remarks
HONO/CH2O	Not looked	Not looked	Not looked	Few cases HONO	HONO	What do we expect? -> models
AM / PM	AM > PM	AM = PM	AM < PM	AM=PM	AM=PM	What do we expect?
Outside vortex	NO	NO	later	later	Probably (GOME)	Different cases↑
Daytime	NO	?	later	-	SZA≥75° (GOME)	What do we expect? -> models
Summer	NO	VandaeleNO_2 YES	later	NO	Maybe.....	What do we expect? -> models

Table 6.3.1-7. Specific properties for OClO observations from different platforms.

Platform	Instrument	Problem	Potential solution
Ground based (partly also aircraft and balloon observations)		Fraunhofer reference spectrum contains OClO absorption, small difference between OClO absorption in both spectra	Very stable instruments and improved spectral analysis allow the use of Fraunhofer spectra from other seasons. Differential slant column density is compared to appropriate model output
Aircraft observations	AMAXDOAS	Strong dependence on the relative azimuth angle between viewing direction and sun	Improved spectral analysis and radiative transport modelling, investigation of the observed strength of the Ring effect.
Satellite observations	GOME/SCIAMACHY	Strong influence of the surface brightness and colour, especially on the Filling-in of Fraunhofer lines	Use of two or more Ring spectra, Use of Intensity offset as fitting parameter (Wagner et al., 2001b, 2002)
		Small signal to noise ratio	Improved spectral analysis, adding of spectra
		Undersampling	Spectral smoothing or modelling of the undersampling residuals, Use of an earth shine spectrum as Fraunhofer reference (Wagner et al., 2001a, 2002, Kühl et al., 2004a-c)
	SCIAMACHY	Polarisation	Takin into account the spectra of the polarisation responce of the instrument into the spectral fitting. (Wagner et al., 2004)

Systematic investigation of the analysis algorithms of the different groups using sythetic spectra.

Partner 2 (IASB) has provided synthetic spectra to the project partners for following purposes:

- •Check consistency of retrieval softwares
- •Support to optimisation of retrieval settings for BrO and OClO
- •Help in understanding possible sources of bias

The focus of these data sets were on:

- •Zenith-sky measurements at twilight (90° SZA)
- •UV-Vis region relevant for OClO and BrO retrieval (340 – 430 nm) – typical resolution of 0.7 nm FWHM
- •Include simple (Beer-Lambert) and more realistic simulations based on radiative transfer calculations with/without RRS

Four different data sets have been provided, each including simulations corresponding to following atmospheric scenarios:

1. Winter conditions, high OClO+BrO, low NO_2
2. Identical (1) + HCHO
3. Identical (1) + high NO_2
4. Identical (1), but without OClO
5. Summer conditions, high NO_2, no OClO
6. Identical (5) + HCHO

The agreement between the different groups is generally very good (better than a few percents). Largest differences have been generally found for SET3 (spectra with shift/stretch). One example of the comparison is shown in 6.3.1-62:

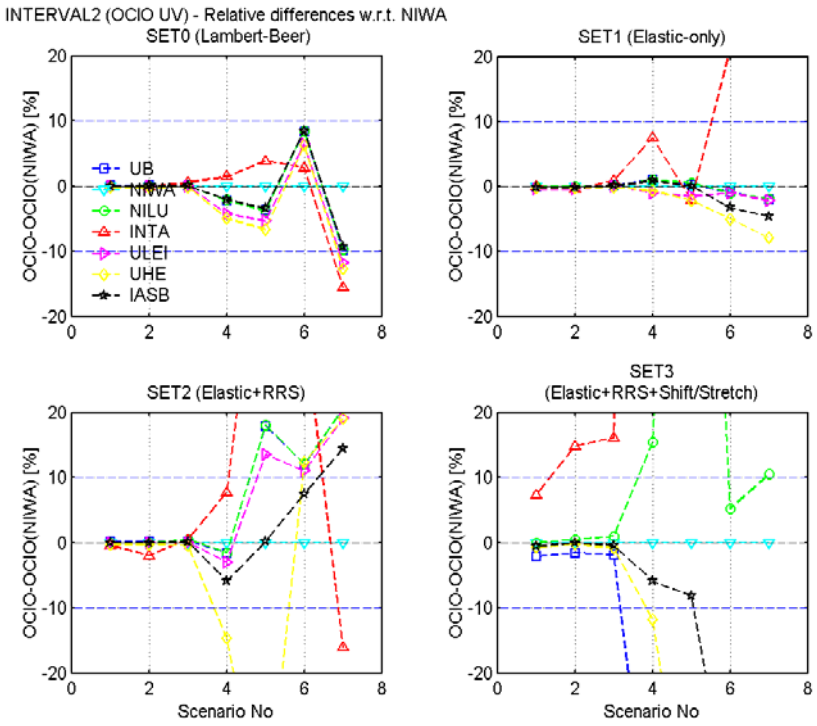

Figure 6.3.1-62. *An example of the comparison between OClO analysis performed by the different groups on the synthetic spectra provided by partner 7.*

In addition partner 2 has made some sensitivity tests to estimate the impact of various effects/settings:

- Solar I0 effect
- HCHO interference
- BrO fitting in OClO interval
- OClO UV versus Visible
- BrO fitting over larger wavelength interval
- Impact of molecular Ring fitting (e.g. adding Ring*O3 cross-section)

Some results are shown exemplarily in Figure 6.3.1-63.

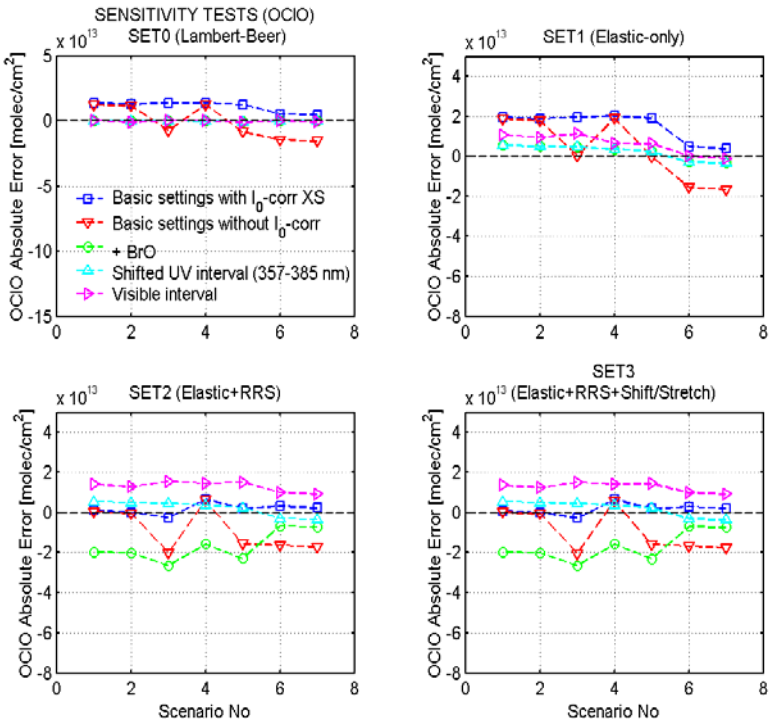

Figure 6.3.1-63. *Sensitivity tests on OClO analysis to estimate the impact of various effects/settings (performed by partner 2).*

References:

Aliwell, S.R., P.V. Johnston, A. Richter, M. Van Roozendael, T. Wagner, D.W. Arlander, J.P. Burrows, D.J. Fish, R.L. Jones, K. Karlsen TÆrnkvist, J.-C. Lambert, K. Pfeilsticker and I. Pundt, Analysis for BrO in zenith-sky spectra - an intercomparison exercise for analysis improvement, J. Geophys. Res., 107, 10.1029/2001JD000329, 2002.

Kühl, S., W. Wilms-Grabe, S. Beirle, C. Frankenberg, M. Grzegorski, J. Hollwedel, F. Khokhar, S. Kraus, U. Platt, S. Sanghavi, C. von Friedeburg and T. Wagner, Stratospheric Chlorine Activation in the Arctic winters 1995/96 to 2001/02 derived from GOME OClO Measurements, Adv. Space Res., 34, 798-803, 2004a.

Kühl, S., W. Wilms-Grabe, C. Frankenberg, S. Kraus, U. Platt and T. Wagner, First results on the DOAS – retrieval of OClO from SCIAMACHY nadir measurements, Proceedings of the ENVISAT & ERS Symposium, 6-10 September 2004, Salzburg, Austria, ESA publication SP-572, (CD-ROM), 2004b.

Kühl, S., Walburga Wilms-Grabe, Ulrich Platt, and Thomas Wagner, Polar Stratospheric Chlorine Activation in the years 1995 – 2003 derived from Measurements of OClO by GOME, Proceedings Quadrennial Ozone Symposium, 1-8 June 2004, Kos, Greece, 989-990, 2004c.

Wagner T., Leue C., Pfeilsticker K. and Platt U., Monitoring of the stratospheric chlorine activation by GOME OClO measurements in the austral and boreal winters 1995 through 1999, J. Geophys. Res., 106, 4971-4996, 2001a.

Wagner, T., K. Chance, U. Frieß, M. Gil, F. Goutail, G. Hönninger, P.V. Johnston, K. Karlsen-Tørnkvist, I. Kostadinov, H. Leser, A. Petritoli, A. Richter, M. Van Roozendael, U. Platt, Correction of the Ring effect and I0-effect for DOAS observations of scattered sunlight, Proc. of the 1st DOAS Workshop, Heidelberg, 13., 14. Sept., Heidelberg, Germany, 2001b.

Wagner T., Wittrock F., Richter A., Wenig M., Burrows J.P. and Platt U., Continous monitoring of the high and persistent chlorine activation during the Arctic winter 1999/2000 by the GOME instrument on ERS-2, J. Geophys. Res., 0.1029/

2001JD000466, 21 September 2002.

Wagner, T., S. Kühl, A. Richter, M. Bruns, J.P. Burrows, K.-P. Heue, B. Kirchoff, W. Wilms-Grabe, P. Wang, U. Platt, Preliminary validation of SCIAMACHY nadir OClO SCDs, Proceedings of the Second Workshop on the Atmospheric Chemistry Validation of ENVISAT (ACVE-2), see also at http://envisat.esa.int/workshops/acve2/contents.html, Frascati, Italy, 3 - 7 May, 2004.

Recommendations

We can conclude, that the solar I0 correction has a small impact, but seems to stabilise the OClO results. Best accuracy seems to be obtained in the 363-391 nm fitting interval, without including BrO in the fit (BrO-OClO interference effect in presence of Ring). The OClO fitting in visible window tends to be positively biased.

Main deliverables

- *Recommendations for the fitting parameters for a standard OClO DOAS algorithm*
- *Determination of the accuracy and precision of the standard OClO DOAS algorithm*
- *Recommendations for future improvements of the OClO retrieval*

WP 2400: Groundbased DOAS retrieval of IO

Applied methodology and scientific achievements

Introduction

During a former project (Stratospheric Ozone Destruction by Bromine), zenith-sky measurements in Ny-Ålesund have been analysed for absorption by iodine monoxide (*Wittrock et al., 2000*). If present in the stratosphere, iodine can provide rapid catalytic destruction cycles for ozone, in particular in the lowermost stratosphere. Iodine compounds add to ozone destruction by Cl_y and Br_y, but probably are not anthropogenic but primarily of natural origin. In two previous studies, small upper limits have been derived for IO and I_y, indicating that very little IO is present in the stratosphere. In contrast, analysis of the measurements in Ny-Ålesund provide evidence for stratospheric IO mixing ratios of 0.65 to 0.8 pptv in polar spring 1997, and similar values in other years.

Due to the fact that no other station has reported stratospheric IO so far, several tests have been carried out to exclude problems in the retrieval (also part of delivery D16). During this study following error sources have been ruled out to be responsible for an uncorrect IO retrieval: selection of the wavelength range, unproper correction of NO_2- absorptions, Ring correction, I_0-effect. As an example the following figure shows the difference in IO-DSCDs (differential slant column densities) between the standard evaluation and the retrieval taking into accout the temperature dependency of the NO_2 absorption cross section in the selected wavelength range.

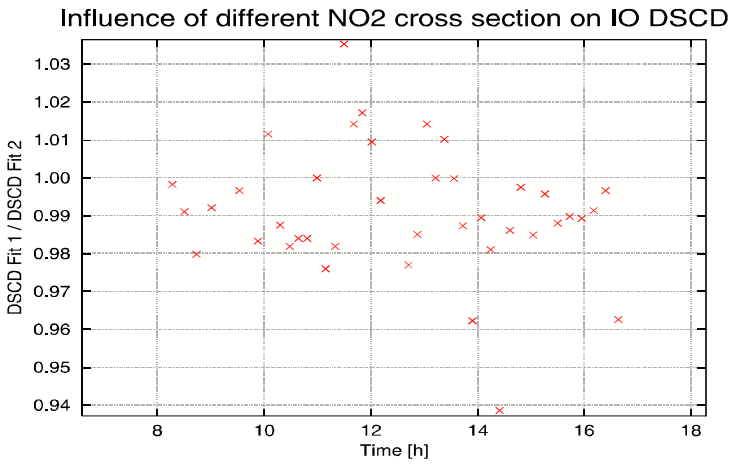

Figure 6.3.1-64. *Ratio of two different sets of IO DSCDs for 2 March 1997: one calculated taking into account two NO_2 temperatures (Fit2), the other one with one cross section measured at 221 K.*

Estimates of the stratospheric IO column under different conditions (D15)

IO DSCD at the subtropical observatory of Izaña (Partner 8)

At the end of 2001 a new UV DOAS INTA instrument was installed at subtropical Izaña Observatory (28ºN, 16ºW, 2370 m.a.s.l) for BrO DSCD measurements, this new instrument (ARTIST) covers the UV-Vis. range between 320 to 460 nm, and its resolution, 0.6 nm, allows us a improved attempt to evaluate IO DSCD.

The evaluation has been carried out over the days 1 to 290 of 2002, following the procedure described by Friess et al. The spectral range used for the retrieval was 415-450 nm, and O_3, NO_2, NO_2 T-dep I_0 corrected, O_4 and H_2O were included in the INTA analysis package. The cross sections were convolved and calibrated by WinDOAS software. The standard package has been modified in order to make an individual positioning and stretching of every spectrum respect to the cross sections and the reference spectrum This improvement, in addition to the best quality of data for IO retrieval, gives an appreciable reduction in the fit errors.

Up to now only one set of evaluation has been carried out between 80º and 90º sza.

Seasonal evolution evaluated between 80º-90º sza, is displayed in Figure 6.3.1-65. The standard deviation of the residuals for every day is shown in the top panel of the figure, days with a fit error larger than 3 10^{-4} have been removed, the other panel shown the DSCD of IO for am and pm. The mean values observed for IO DSCD are –1.062 10^{13} (sd 8 10^{12}) am and –1.25 10^{13} (sd 9 10^{12}) pm and as can be seen, the retrieved DSCDs are below the error bars.In both cases, am and pm, a different behavior after the day number 140 is observed in the DSCD of IO when the mean decreases to –1.3 10^{13} (sd 7 10^{12}) am and –1.7 10^{13} (sd 6 10^{12}) althought the grater values during the pm than in am are kept. The different behavior is surely related to the change of the field of view of the instrument, which occurred this day, from about 10º to 25º. This appears to be an unrealistic effect due to the change in the collecting optics.

To check whether or not the retrieved IO DSCD is correlated to the sd of the residuals, in Figure 6.3.1-66 the cross correlation between both magnitudes are plotted, and as can be observed, no clear dependence can be inferred. The main difference with the 2001 results is the pm values are greater than the am ones.Typical fit errors using the INTA analysis package are around 2 10^{-4}, for both datasets, am and pm. In Figure 6.3.1-67, the diurnal variation of the IO DSCD is shown for a particular day, 171, where the residuals are small. This is a clear sky day with very low aerosol loading. The intensity of the signal for the spectra collected for sza grater than 92º is in general very low and those spectra have been removed of the analysis.A slightly decrease is observed from 80º sza, coincident to larger sd of the residuals, but the DSCD never comes below 2 10^{13}, what is estimated to be the detection limit of the instrument.

From the analysis we conclude that no detectable levels of IO are present in the free troposphere of the subtropical Izaña Observatory, in agreement with the previous observations and the current accepted chemistry.

Figure 6.3.1-65. *IO DSCD between 80º and 90º sza during 2002 at Izaña station.*

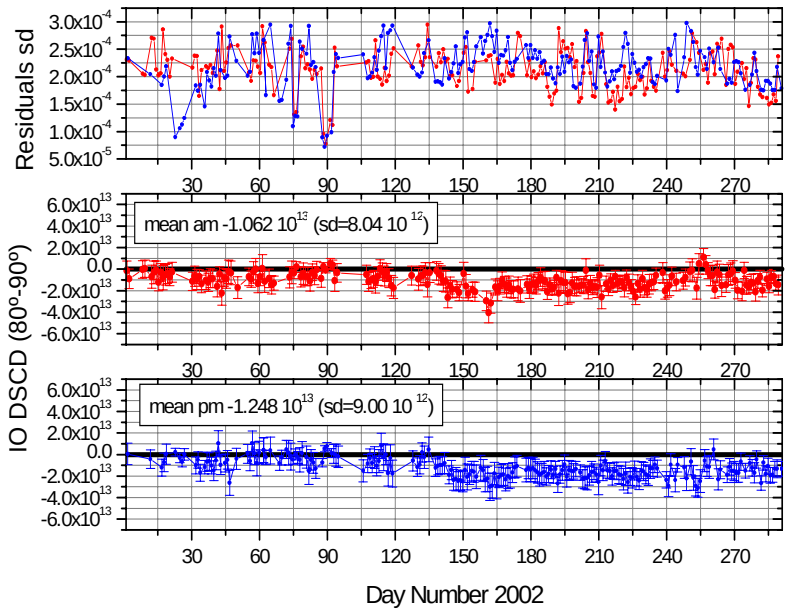

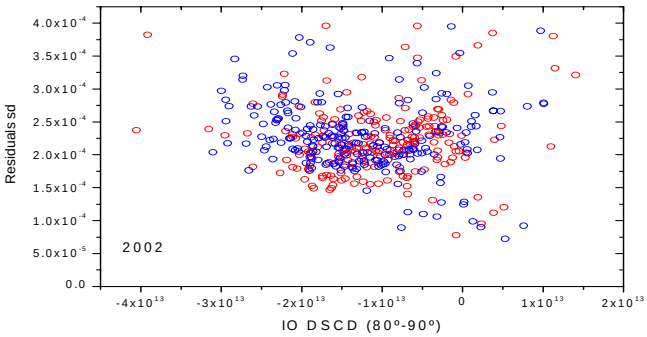

Figure 6.3.1-66. *Cross correlation between the sd of the residuals and the IO DSCD. Red circles are am data and blue ones pm data..*

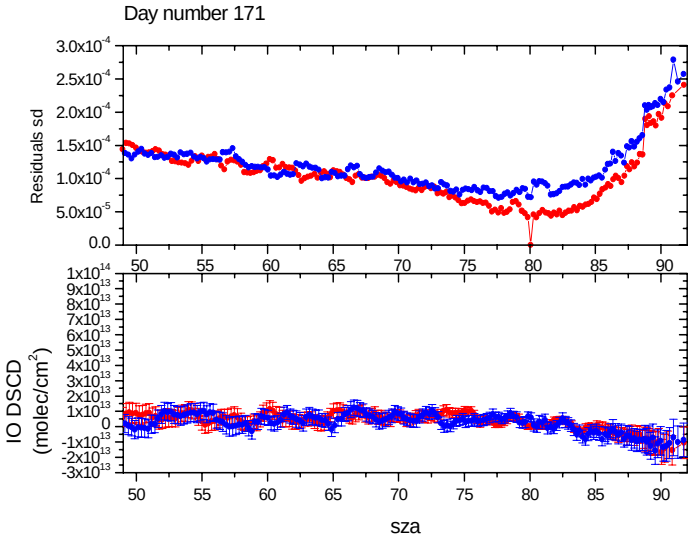

Figure 6.3.1-67. *Upper panel: residuals sd for IO DSCD for day number 171, am is in red and pm is in blue. Lower panels: IO DSCD for day number 171, am is in red and pm is in blue.*

Antarctica

Zenith sky DOAS measurements of iodine oxide (IO) were performed at Neumayer Station, Antarctica (70 S, 8 W) using a UV/Vis instrument that has been operating at this site continuously since March 1999 [Frieß et al., 2001]. The spectral signature of IO was clearly detected in the observed spectra (see below). A typical example of the diurnal variation of the IO dSCD observed at Neumayer is shown in Figure 6.3.1-68.

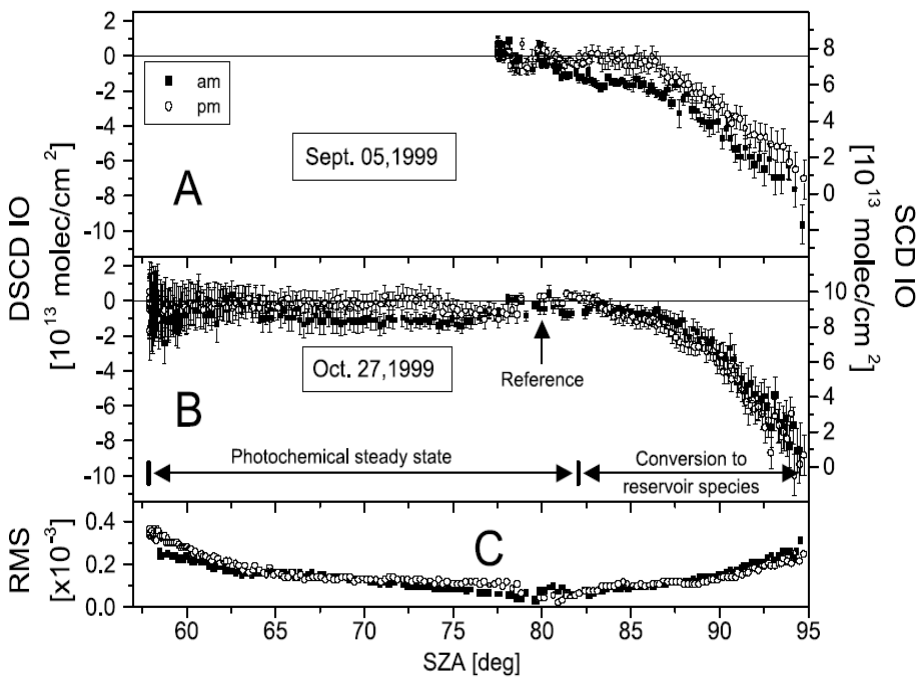

Figure 6.3.1-68. *Diurnal variation of the IO dSCD on September 5 (panel A) and October 27 (panel B), 1999. The position of the Fraunhofer reference spectrum is marked with an arrow. Left axis: inferred IO dSCD; Right axis: absolute IO SCD under the assumption that IO is totally removed from the atmosphere at a solar zenith angle of 95°. The error bars denote the 1 retrieval error. Panel C: RMS residual of the spectral retrieval on October 27.*

The diurnal variation of IO under clear sky conditions is characterised by a constant IO dSCD during day and a rapid decrease during twilight. The latter finding can be explained by the rapid conversion of iodine radicals to reservoir species ($IONO_2$, HOI) in the absence of sunlight. Based on radiative transfer calculations, we conclude from these measurements that the majority of the detected IO is located close to the surface: the airmass factor for IO located in the stratosphere strongly increases with increasing SZA. In contrast to the observed constant IO levels for SZA < 85°, this would lead to a significant increase in IO dSCD during twilight.

Further evidence for IO being located close to the surface is the fact that multiple scattering due to snowdrift has a significant impact on the IO dSCDs. This is illustrated in Figure 6.3.1-69. No pronounced diurnal variation of IO due to photochemistry is expected during this period since the solar zenith angle always remains below 86°. The IO dSCD has a constant value during a period of clear sky on December 14 and 15. A snowdrift on December 12 and 13 causes a strong variability of the light path, accompanied by a strong increase in IO dSCDs with values of up to 4 x 10^{13} molec/cm^2.

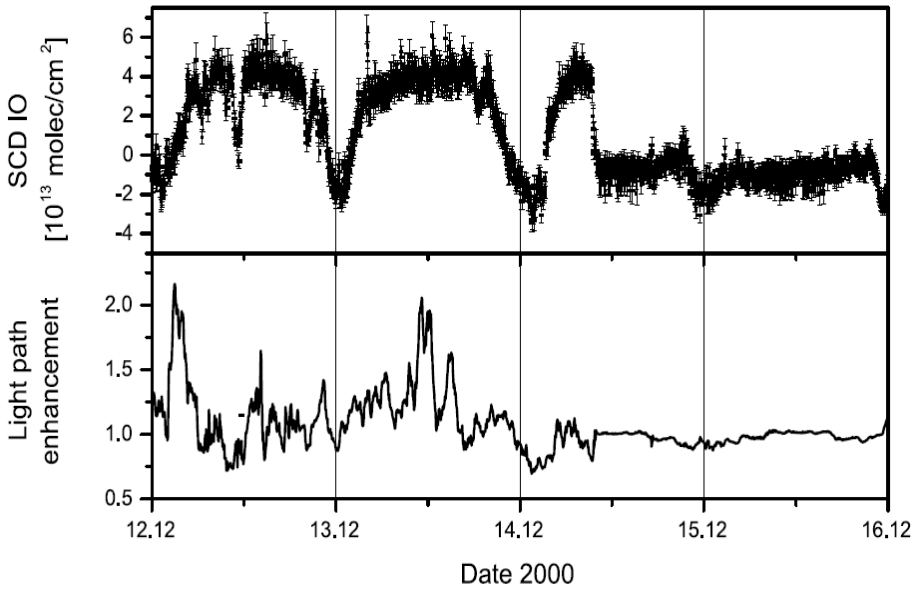

Figure 6.3.1-69. *dSCD IO from an analysis using a fixed Fraunhofer reference spectrum (upper panel) and the enhancement of the tropospheric light path as inferred from O_4 measurements (lower panel) between December 12 and 16, 2000.*

More direct evidence for the hypothesis that the observed IO is located in the boundary layer is provided by measurements using the new Multi-Axis telescope, which has been installed at Neumayer in early 2003. The new telescope allows to collect scattered light from different viewing angles. Compared to zenith sky measurements, observations from close to the horizon have a high sensitivity for absorbers located close to the surface due to the increased light path through the lower troposphere.

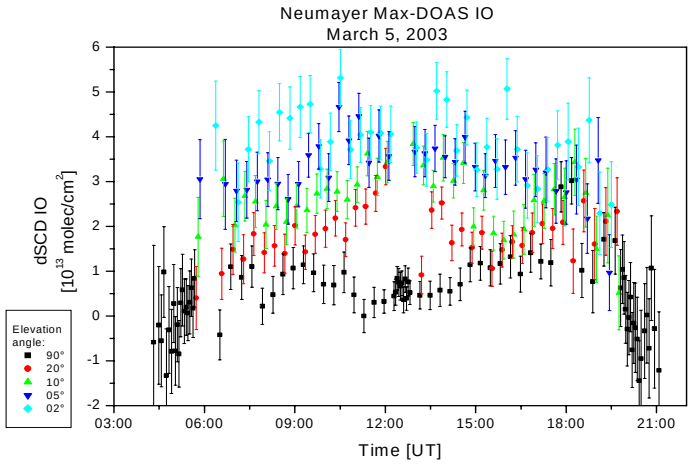

Figure 6.3.1-70. *Multi- Axis measurements of iodine oxide at Neumayer Station, Antarcita, on March 5, 2003. The elevation angles of the observations are indicated by different colours as denoted in the legend.*

Figure 6.3.1-70 shows the diurnal variation of the IO dSCD (relative to a zenith reference measured at noon) on a clear day in March 2003 for elevation angles of 90º (zenith), 20º, 10º, 5º, and 2º. A strong increase in IO dSCDs with decreasing elevation angle is observed, confirming that the detected IO is present in the boundary layer.

The zenith sky DOAS observations of IO at Neumayer Station can be summarised as follows:

- The spectral signature of iodine oxide has been clearly detected in the zenith sky spectra recorded at Neumayer station during 1999 and 2000.
- Although DOAS observations of zenith scattered sunlight provide no direct information on the altitude distribution of the observed trace gases, arguments based on radiative transfer model calculations and photochemistry indicate that the observed diurnal variation of the IO DSCD is caused by tropospheric rather than stratospheric IO.
- Assuming the observed IO to be located completely in the boundary layer leads to mixing ratios of roughly 5-10 ppt during summer, similar concentrations as typically found in the mid-latitude MBL.
- No evidence for stratospheric IO was found, mainly because the expected small stratospheric signature of IO may be masked by the strong tropospheric signal observed at Neumayer.
- The pronounced sensitivity of the IO dSCD to near surface multiple scattering due to snowdrift supports the conclusion that the bulk of IO is located close to the ground.
- More direct evidence for the hypothesis that the observed IO is located in the boundary layer is provided by analysis on measurements using the new Multi-Axis telescope. These MAX-DOAS measurements show a pronounced increase in IO dSCDs for low elevations.

Arctic

In spring 2002 a new developed MAX-DOAS setup was installed in Ny-Ålesund (see WP 2100). Having in 2002 only a UV part (325-412 nm), which is not able to detect IO, the system was supplemented with a second CCD-spectrometer device in March 2003. This was designed for the wavelength range from 390 – 570 nm, covering the spectral features from IO and OIO absorption. MAX-DOAS measurements during 2003 and 2004 from Partner 3 (UHB) in Ny-Ålesund have been analysed for IO absorption. Several settings have been tested according to suggestions by Wittrock, et al., 2000 and Friess, et al., 2001. Finally following parameter were chosen to analyse the spectra:

- Wavelength window: 416 – 439 nm;
- O_3, NO_2, IO , OClO, Ring;
- Polynomial: Degree 2;
- Background: Zenith noon

Throughout the year it was possible to find IO DSCDs above the detection limit. But this was the case for off-axis observations only. Usually the IO slant column follows the O_4 slant column, which is illustrated in Figure 6.3.1-71 and Figure 6.3.1-72. Radiative transfer model studies according to publications by [Heckel et al., 2004] and [Wittrock et al., 2004] were carried out to derive profile information for IO. This leads to volume mixing ratios of 1 ro 3.5 pptv from April to September within the boundary layer.

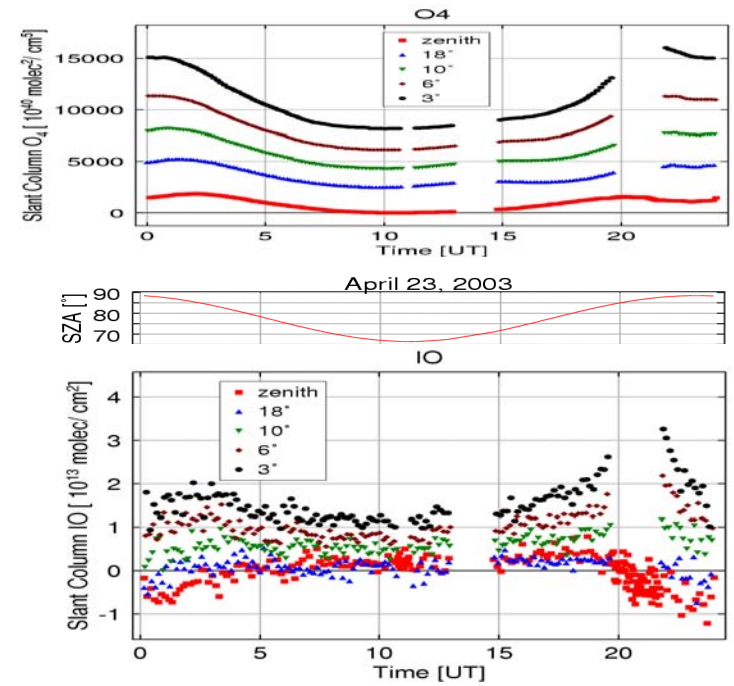

Figure 6.3.1-71. *Diurnal variation of the IO and O_4 DSCDs on April 23, 2003.*

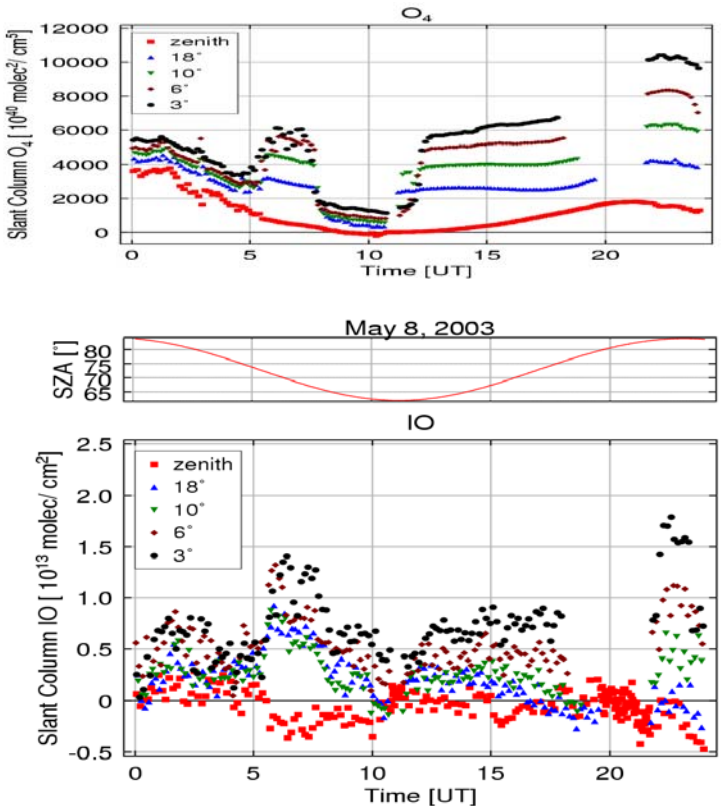

Figure 6.3.1-72. *Diurnal variation of the IO and O_4 DSCDs on May 8, 2003.*

Recommendations for the fitting parameters for an improved IO DOAS algorithm (Study from Partner 4)

Iodine oxide (IO) has been detected for the first time in Antarctica using a DOAS zenith sky UV/Vis instrument which has been operating at the German research station Neumayer (70 S, 8 W) since March 1999. The visible spectrometer of the Neumayer DOAS system covers the wavelength range between 400 and 650nm with a spectral resolution of 1nm FWHM. Zenith scattered light is observed by a telescope and dispersed using a holographic grating. A photo diode array with 1024 cannels serves as detector. The detector is cooled to -35ºC to minimise the dark current and detector noise,

The spectral signature of IO was clearly identified in the Neumayer spectra by observing five vibrational absorption bands located in the wavelength region between 415 and 461 nm. The cross sections used for the spectral retrieval of IO are listed in Table 6.3.1-8. In addition to IO, the cross sections of NO_2, ozone, O_4, OClO, H_2O and IO are included in the spectral retrieval. A polynomial of fourth degree is included in the fit to remove broad- band structures caused by Rayleigh and Mie scattering. Furthermore, a nonlinear offset to the intensity is allowed for in the analysis, which compensates for possible non-linearities of the instrument, such as instrumental stray light. The spectral analysis was performed using the WINDOAS software (M. van Roozendael and C. Fayt, IASB, pers. communication)

Table 6.3.1-8. Cross sections used for the retrieval of IO.

Trace gas	Temperatures	Reference
Ozone	221K, 271K	[Burrows et al., 1999]
NO_2	223K, 280K	[Voigt et al., 1999]
O_4	298K	Hermans, pers.comm.
OClO	233K	[Kromminga et al., 1999]
H_2O	273K	HITRAN database
IO		[Hönninger, 1999]
Ring spectrum		Synthetic spectrum

Since the optical density of IO is very small (typically below 10^{-3}), it is necessary to keep the signal to noise ratio of the spectral analysis as small as possible. Changes in the spectral resolution with time can strongly affect the spectral retrieval, since in this case the Fraunhofer structure cannot be removed properly by calculating the ratio of two spectra. Therefore, daily Fraunhofer reference spectra recorded at 80º SZA were used to analyse the twilight measurements of the respective dusk/dawn. This procedure has two shortcomings:

- Since the differential slant columns relative to a daily Fraunhofer reference spectrum have an unknown offset, which can vary from day to day, these measurements gain no direct information on the seasonal variation of iodine oxide but only on changes of the slant columns during twilight.
- The period of available data is restricted to those days were the solar zenith angle reaches less than 80. This leads to a gap in the time series between mid April and late August for our measurements at high southern latitudes.

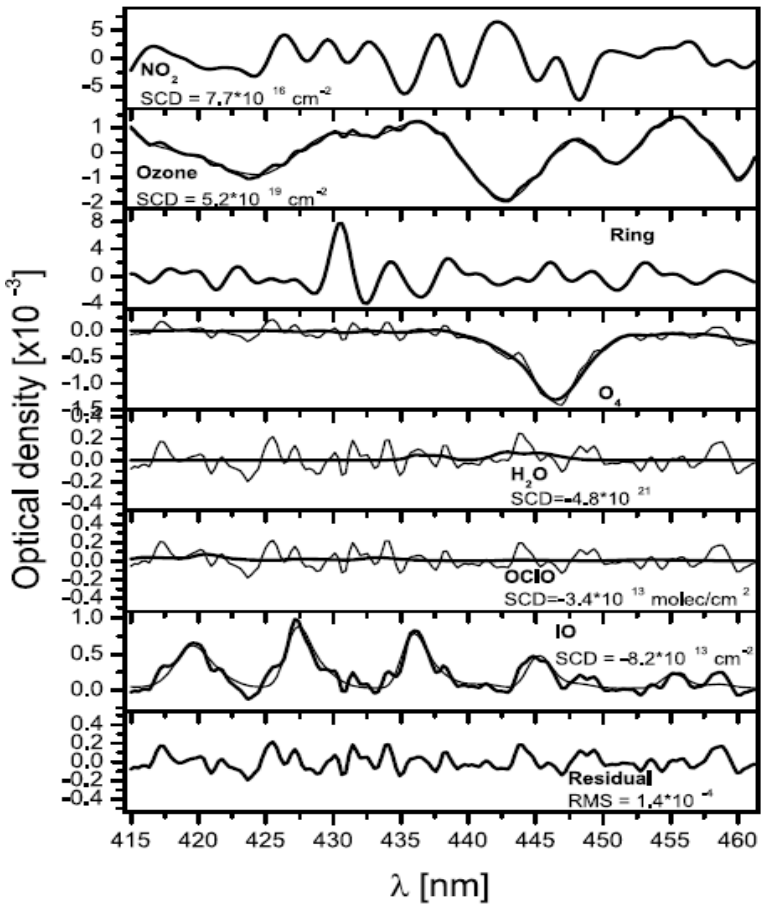

Figure 6.3.1-73. *Example for the spectral retrieval of IO on October 30, 1999 at 92° SZA. The Fraunhofer reference spectrum was recorded at 80° SZA on the same day.*

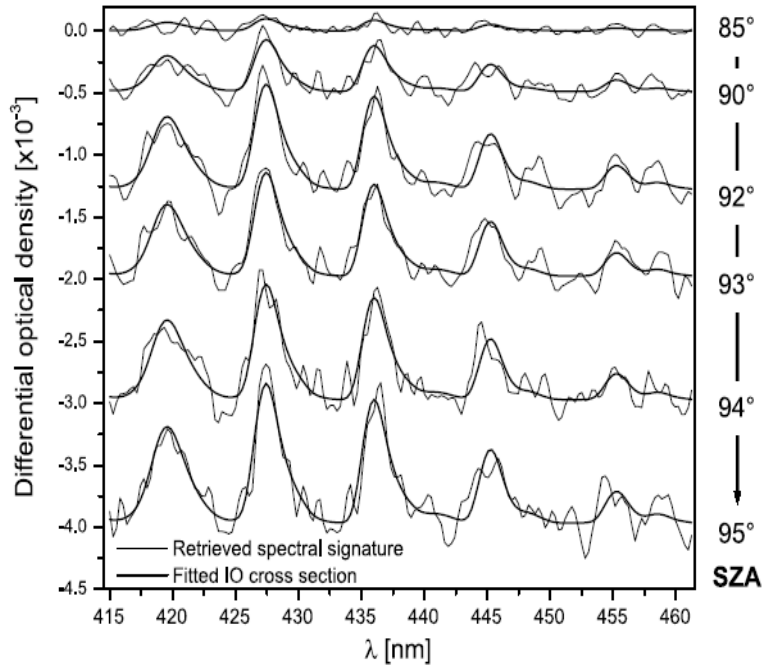

Figure 6.3.1-74. *Detected IO absorption structure during twilight as a function of SZA, observed on October 30, 1999. The Fraunhofer reference spectrum is recorded on the same day at 80° SZA. An offset is added to the individual absorption structures and the corresponding SZA is denoted at the right.*

Figure 6.3.1-73 shows an example for the spectral retrieval of iodine oxide. The five vibrational bands of the $A^2_{3/2}$ $X^2_{3/2}$ transition of IO in the wavelength region between 415 and 461.5 nm have an optical density of up to $1x10^{-3}$, while the residual RMS is only 1.4×10^{-4}. A negative IO dSCD is determined, which means that there is less IO abundant along the light path at 92 compared to 80 SZA. This is also illustrated in Figure 6.3.1-74: a strongly increasing negative spectral signature with increasing SZA is observed and IO can be clearly detected for solar zenith angles of up to 95.

Since the optical density of IO is very small, it must be guaranteed that the observed absorption structure is not an artefact. An element of uncertainty is a possible improper wavelength alignment of the reference spectra. Possible candidates for a spectral misalignment are the Fraunhofer reference spectrum, the cross sections for ozone [Burrows et al., 1999], for OClO [Wahner et al., 1987], and (to a small extend) for iodine oxide [Hönninger, 1999]. The influence of the uncertainty of the wavelength alignment was investigated according to the procedure recommended by Stutz and Platt [1996]: the cross sections and the Fraunhofer reference spectrum were shifted in wavelength by the uncertainty of their wavelength calibration. The change of the retrieved IO dSCD due to these wavelength shifts is a measure for the error caused by improper spectral alignment of the reference spectra.

These tests were performed in two separate ways: (1) by using a measured spectrum and Fraunhofer reference and (2) by using synthetic spectra. A synthetic Fraunhofer reference spectrum I_0 was created by convoluting a high-resolution Fraunhofer spectrum [Kurucz et al., 1984] to the resolution of the instrument. A second spectrum I was calculated by adding the absorption structure of the trace gases to the high resolution Fraunhofer spectrum prior to the convolution. To simulate the noise of the instrument, random noise was added to the synthetic spectra in order to obtain the same RMS residual as when analysing atmospheric spectra. The spectral analysis using the synthetic spectra I and I_0 was performed with the same settings as for measured spectra. Compared to the analysis of measured spectra, using synthetic spectra has the advantage that the 'true' IO fit coefficients are known and can be compared to the coefficients determined by the spectral analysis.

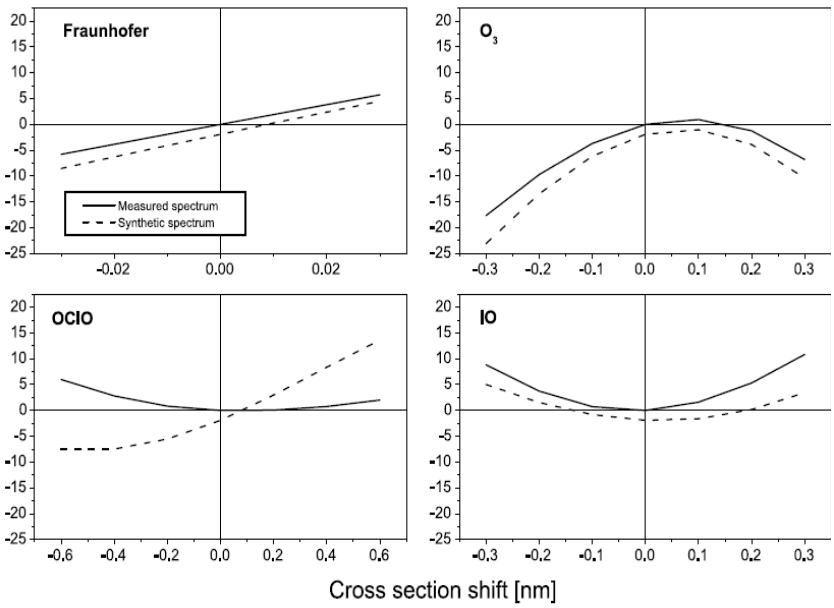

Figure 6.3.1-75. *Relative change in the IO fit coefficient (in percent) when shifting the ozone, OClO and IO cross sections and the Fraunhofer reference in wavelength. Solid lines: Results for a measured twilight spectrum from October 15, 1999 (92º SZA); dashed lines: Results for synthetic spectra, calculated as described in the text.*

Figure 6.3.1-75 shows how the IO fit coefficient changes when shifting the reference spectra in wavelength. The spectral retrieval of IO shows a remarkable stability when shifting the reference spectra in wavelength. The largest uncertainty is given by the spectral calibration of the ozone cross section.

Table 6.3.1-9 summarises the estimated errors of the IO dSCD due to improper wavelength calibration of the reference spectra. A total error of only about 3% is inferred, leading to the conclusion that errors in the wavelength calibration cannot cause artificial structures which would explain the observed IO absorption.

Table 6.3.1-9. Error in IO dSCD due to uncertainties in the wavelength calibration.

Reference spectrum	Wavelength uncertainty [nm]	Change in IO dSCD
Fraunhofer	0.02	2.0%
O_3	0.10	2.3%
OClO	0.20	0.5%
IO	0.01	0.1%
Total Error		**3.1%**

A further test of the reliability of the IO retrieval was performed by comparing the initial and retrieved IO dSCD using synthetic spectra. This was done in the following way:

1. A synthetic Fraunhofer reference spectrum I_0 was created by convoluting the high resolution Fraunhofer spectrum to the instrument's resolution.
2. A synthetic spectrum I with the absorption structures according to typical slant column densities of all absorbers was created. The initial IO slant column density in the synthetic spectrum was set to -8 x 10^{13} molec/cm^2. Two sets of 500 spectra each were calculated using the synthetic spectrum I:
   - a. by adding random noise (I_1)
   - b. by adding random noise plus the average residual structure of the spectral retrieval at 92º SZA during October 1999 (I_2)
3. In both cases, the variance of the noise was adjusted so that an average RMS residual of 2.5 x 10^4 was obtained in the spectral retrieval.
4. The IO dSCDs were determined by the spectral analysis procedure, performed using the Fraunhofer reference spectrum I_0 and both the sets of spectra I_1 and I_2.

Figure 6.3.1-76. *Histograms of the RMS residual (left) and relative fit error (right) of the IO retrieval for 91.5° SZA 92.5° for the measurements at Neumayer during 1999 and 2000.*

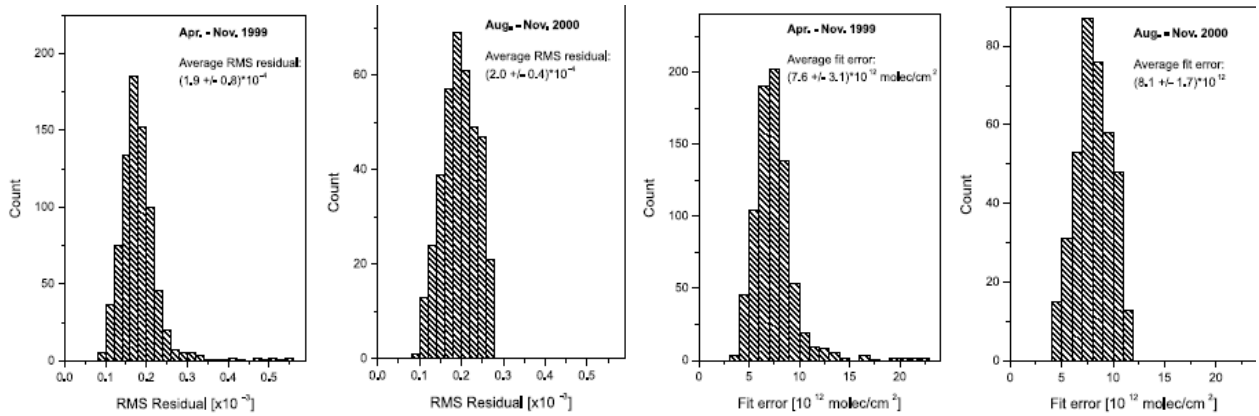

Table 6.3.1-76 shows the histogram of the retrieved IO dSCDs using the above described synthetic spectra. As expected, the average IO dSCD from spectra with pure random noise is close to the initial value of -8 x 10^{13} molec/cm^2, but the standard deviation of about 2.5 x 10^{13} molec/cm^2 is about twice as high as the fit error from measured spectra shown in Table 6.3.1-77. This is likely caused by the triangular smoothing applied to the spectra, which leads to an underestimation of the fit error since the smoothing causes a correlation of neighbouring pixels [Stutz and Platt, 1996]. When adding both random noise and the average residual to the synthetic spectra, the impact of systematic structure on the IO retrieval is simulated. In this case, the absolute value of the IO dSCD is underestimated by about 3.5%, while the standard deviation (1.5 x 10^{13}) is smaller compared to the case with pure noise, but still larger than the IO fit error of measured spectra.

Figure 6.3.1-77. *Histogram of the retrieved IO dSCDs using synthetic spectra with (a) random noise and (b) random noise plus the average residual of the IO retrieval at 92° SZA during October 1999. The synthetic spectra were created with an initial IO dSCD of –8 x 10^{13} molec/cm^2.*

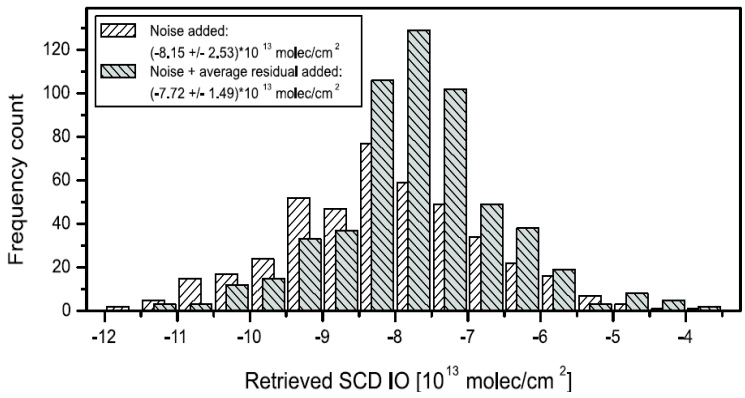

The influence of smoothing the spectra prior to the analysis was also tested using synthetic spectra with a modeled IO dSCD of -8 x 10^{13} molec/cm^2. As shown in Table 6.3.1-78, applying a single triangular smoothing has only a small impact of less than 1% on the retrieved IO dSCD.

A further uncertainty of the IO retrieval is given by possible nonlinearities of the instrument, which can be caused by an improper dark current correction or instrumental stray light. Those effects could cause artificial structures and are compensated for by fitting a nonlinear offset to the intensity. To investigate this, synthetic spectra with a varying offset and a constant IO dSCD of 5 x 10^{13} molec/cm^2 were calculated. The result of the spectral retrieval using these spectra is shown in Table 6.3.1-79. It is obvious that a small intensity offset of only a few percent leads to completely wrong results if no nonlinear offset is fitted. The nonlinear offset fit, however, can compensate well for these nonlinearities.

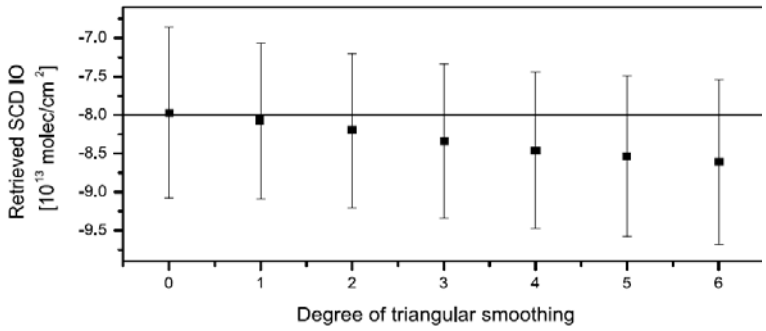

Figure 6.3.1-78. *Influence of smoothing on the spectral retrieval of IO using synthetic spectra with a modelled IO dSCD of –8 x 10^{13} molec/cm^2. The error bars represent the standard deviation of the data using 500 spectra with random noise.*

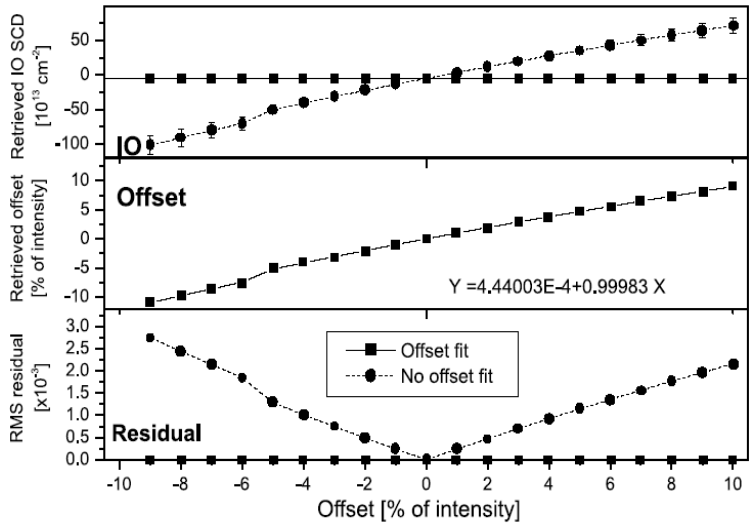

Figure 6.3.1-79. *Influence of the intensity offset on the spectral retrieval of IO using synthetic spectra with a modelled IO dSCD of –5 x 10^{13} molec/cm^2. The x axis denotes the intensity offset added to the synthetic spectra prior to the fit. Upper panel: Retrieved dSCD IO with (squares) and without (circles) accounting for an intensity offset in the analysis. Middle panel: Retrieved intensity offset; Bottom panel: RMS residual with (squares) and without (circles) accounting for an intensity offset in the analysis.*

The following can be concluded from the above sensitivity tests:

1. The RMS residual of the IO retrieval is typically in the order of 2 x 10^{-4}, while optical densities of more than 1 x 10^{-3} are observed with our instrument at Neumayer station. This leads to typical IO retrieval errors of 8 x 10^{12} molec/cm^2, compared to maximum IO dSCDs of more than 1 x 10^{14} molec/cm^2. However, the tests using synthetic spectra indicate that the retrieval algorithm may underestimate the error of the IO dSCD by a factor of two.
2. The detection limit of IO is 1 x 10^{13} molec/cm^2 (according to the definition of Stutz and Platt [1996])
3. Systematic residual structures have a relatively small impact on the retrieved IO dSCDs.
4. Changes of the instrument properties have only a small impact on the IO retrieval when using daily Fraunhofer reference spectra.

5. The IO retrieval is insensitive to possible wavelength misalignments of the reference spectra.
6. Possible nonlinearities of the instrument, e.g. caused by instrumental straylight, can have a large impact on the IO retrieval. Including a non-linear intensity offset in the retrieval can compensate for these effects.

The IO retrieval is found to be quite robust regarding changes of the analysis settings. The above findings give confidence that the observed absorption structure in the spectra measured at Neumayer station is related to the abundance of iodine oxide along the observed light path.

Summary and Conclusions

Several partners have analysed both ground-based and ballon-borne measured sunlight spectra for signatures of IO absorption. Case studies have shown, that the IO retrieval is quite robust to changes in the analysis settings (which is in contast to e.g. the BrO retrieval). The detection limit for the analysis is in the range of 5 10^{12} to 2 10^{13} molec/cm^2 in DSCD depending on site conditions and instrument.

Recommendations for the fitting parameters for an improved IO DOAS algorithm (D16)

Following table summarized the recommendated fitting parameter for an improved IO DOAS retrieval.

Wavelength window	At least 4 bands between 419 and 461 nm	
Polynomial	2 to 3	
Further corrections	Straylight (ground-based) Solar-center-to-limb-darkening (balloon-borne)	
Cross section included	Temperatures	Reference
Ozone	221K	[Burrows et al., 1999]
NO_2, two temperatures	223K, 280K	[Voigt et al., 1999]
O_4	298K	[Greenblatt et al., 1990] wavelength corrected or [Hermans, pers.comm].
OClO, for polar sites	233K	[Kromminga et al., 1999]
H_2O	273K	HITRAN database
IO		[Hönninger, 1999] or [Spietz, 1999]
Ring spectrum		Synthetic spectrum, e.g. SCIATRAN

Table 6.3.1-10. Recommendations for the fitting parameter for an improved IO DOAS algorithm.

Estimates of the stratospheric IO column under different conditions (D15)

An oberview of IO studies within the QUILT project is given below. They have been published at least partly in one of the project reports.

Group	How?	Where?	Trop.?	Strat.?	When?	Comments
Bremen	ZS DOAS MAX DOAS	**Arctic:** Ny-Ålesund Ny-Ålesund	Yes Yes (<3.5ppt)	Yes(<0.8ppt) No (< 0,3 ppt)	1995-1998 2003 – 2004	Stratospheric IO for high SZA only Tropospheric IO in BL
NILU	ZS DOAS	**Arctic:** Ny-Ålesund Andoya	Yes Yes	No No	95-97 98-	strat. signal possibly masked by trop.
Heid.	ZS-/MAX-DOAS	**Antarctica:** Neumayer	Yes (<10ppt)	No	1999	strat. signal possibly masked by trop. Tropospheric IO in BL
Heid.	DOAS	**Northern Mid-Latitudes:** Mace Head (Ireland)	Yes (<7 ppt)	-	1997	
Heid.	Ballon-borne DOAS	**Arctic and Mid-Latitudes:** Kiruna, Gap, Leon	-	No, < 0.1 ppt for lower stratosphere	1996 – 2000	
INTA	ZS DOAS	**Subtropics:** Izana	No	No	2002	

Combining all studies it is most likely, that the amount of IO is very small throughout the stratosphere (< 0.1 ppt). Only Wittrock et al. [2000] have reported IO differential slant columns larger than the detection limit, attributing them to small stratospheric amounts (<0.8 ppt). These observations couldn't confirmed from the Bremen group for measurements in 2003 and 2004 on the same site. Only IO DSCDs caused by tropospheric amounts have been found. These findings are in good agreement with measurements from Friess et al. in Antarctica.

One might speculate about the reasons for the disagreement between measurements in Ny-Ålesund from 1995 to 1998 and those in 2003 and 2004. Several tests have been carried out to exclude possible errors in the retrieval of the data. [Bösch et al.] have introduced the solar-center-to-limb-darkening effect (CLD) in the analysis of balloon-borne data. Even if it is in respect to the different viewing geometry of the ground-based measurements very unlikely, further investigations are necessary to exclude a possible influence of this effect on zenith sky measurements. More likelihood is an explanation, taking into account a combination of a varying amount of IO in the troposphere and instrumental problems under low-light conditions.

Recommendation for the format (SZA range, VCD/SCD/DSCD) of a standard IO product (D17) and for the future improvements of the IO retrieval (D18)

Because no clear evidence for stratospheric IO has been found during the project, deliverable D17 became obsolete. It is recommended to further investigate the CLD effect on zenith sky measurements.

Main deliverables

- *Estimates of the stratospheric IO column under different conditions*
- *Recommendations for the fitting parameters for an improved IO DOAS algorithm*
- *Recommendations for future improvements of the IO retrieval*
- *Daytime BrO, NO_2 and IO slant columns measured at sites using both off-axis viewing and zenith-sky geometry (part of D5).*

WP 2500: Radiative transfer interface

Applied methodology and scientific achievements

The objective of the WP2500 was to improve the accuracy of the different model/measurement radiative transfer (RT) interfaces used in the QUILT consortium for interpreting ground-based and GOME DOAS observations.

It has been achieved through an intercomparison exercise between the RT codes existing within QUILT. This exercise has been performed within the framework of a workshop on QUILT RT modelling activities held at IASB-BIRA on October 3-4, 2002.

The characteristics and fields of application of the RT models existing within QUILT are summarized in Table 6.3.1-11.

In order to test their consistency, these RT models have been involved in several SCDs calculations comparison tests performed using identical settings for all the models. Both ground zenith-sky (trace gases: BrO, NO_2, and OClO) and off-axis geometries (trace gases: BrO, NO_2, and HCHO) have been considered for these tests, the photochemical enhancement being taken into account only in the zenith-sky geometry. The main tests and their corresponding settings are the following:

1. Calculations of BrO, OClO, and NO_2 SCDs in zenith-sky geometry, photochemistry included
   - Fixed BrO, OClO, and NO_2 diurnal variation matrices, O_3, NO_2, p, T and total number density profiles
   - Fixed altitude grid: 0-120 km/1km layer thickness
   - Fixed wavelengths: 352 nm (BrO), 368 nm (OClO), and 422 nm (NO_2)
   - Fixed ground albedo value (0.20)
   - Fixed cross sections sets
   - Aerosol scattering and refraction not included
   - Calculation in single scattering (SS) mode + multiple scattering (MS) mode if possible

2. Calculations of BrO, NO_2, and HCHO SCDs in off-axis geometry, photochemistry not included
   - Initialization: same as exercise 1 except that single profiles are used (see Figure 6.3.1-80); wavelength for HCHO SCD calculations: 356 nm.
   - Calculations in MS mode (the only relevant mode in this geometry) for 0° and 90° of azimuthal angle of line of sight (AzLOS) and for 5°, 10°, 20°, 30°, 40°, and 90° (zenith) of elevation.

Partner	Model main features	Applications			
		SCD zenith, nadir static (O_3)	**SCD zenith, chemistry coupling (BrO, NO_2, OClO)**	**SCD off-axis**	**Weighting functions calculation**
UBRE (IUP-Bremen)	SCIATRAN model: –Combining Differential-Integral approach using the Picard-Iterative approximation (CDIPI) –Treatment of MS in a full spherical geometry including refraction –Chemistry included (2D array of profile variation with SZA) –Treatment for aerosol and clouds scattering, and ground albedo –Raman scattering included	YES	YES	YES	YES
UHEI (IUP-Heidelberg)	TRACY model: –Monte Carlo approach –Treatment of MS in a full spherical geometry including refraction –Chemistry included (2D array of profile variation with SZA) –Treatments for aerosol and cloud scattering, and ground albedo –Raman scattering included	YES	YES	YES	Under develop.
NILU, IASB-BIRA	–UVspec/DISORT package including chemistry (2D array of profile variation with SZA) –Discrete ordinate method –Treatment of MS and refraction in a pseudo-spherical geometry (direct beam only) –Treatment for aerosol and clouds scattering, and ground albedo	YES	YES	YES	YES
ISAC-CNR	–Single scattering model in a 2-D atmosphere –Treatment for refraction, aerosols scattering, and ground albedo	YES (zenith)	YES	YES	YES
NERC	–Forward ray tracing –2nd order of scattering in a full spherical geometry –Treatment for aerosols and PSC scattering, and ground albedo	YES (zenith)	YES	NO	YES
NIWA	–Single scattering model in a 2-D atmosphere –Treatment for refraction and aerosols scattering	YES (zenith)	YES	NO	YES

Table 6.3.1-11. Description and fields of application of the RT models existing within the QUILT consortium.

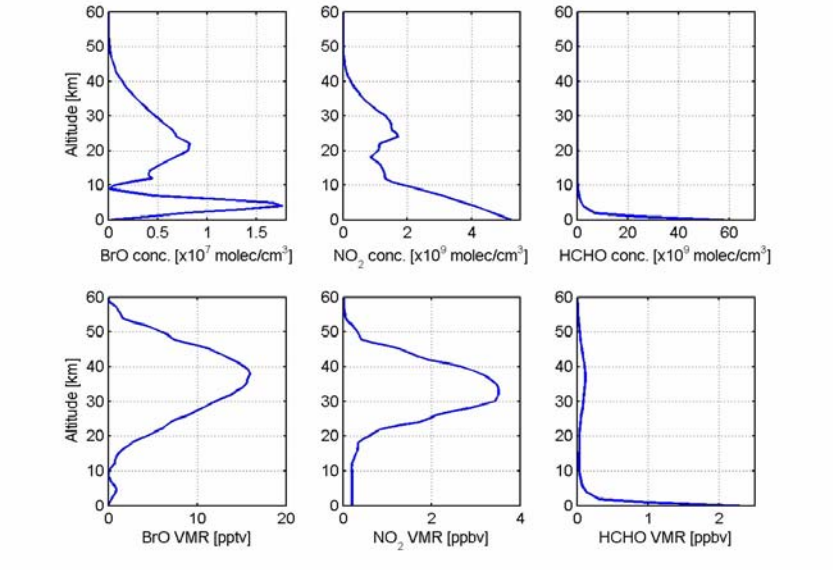

Figure 6.3.1-80. *Profiles in concentration (upper plots) and VMR (lower plots) used to initialize the RT models in the comparison tests in off-axis geometry.*

3. Test on the impact of the aerosol scattering in off-axis geometry: calculation of NO_2 and HCHO SCDs in off-axis geometry, aerosol scattering included and photochemistry not included
   - Initialization: same as exercise 2
   - Fixed aerosol profiles (extinction coefficient and phase function)
   - Calculation in MS mode (the only relevant mode in this geometry) for 30°, 60°, 90° and 120° of AzLOS and for 5°, 10°, 20°, 30°, 40°, and 90° (zenith) of elevation
4. Test on the impact of ground albedo in off-axis geometry: calculation of NO_2 and HCHO SCDs in off-axis geometry for different ground albedo values, aerosol scattering and photochemistry not included
   - Initialization: same as exercise 2
   - Fixed ground albedo values: 0, 0.30, 0.60, and 0.90
   - Calculations in MS mode (the only relevant mode in this geometry) for 0° and 90° of AzLOS and for 5°, 10°, 20°, 30°, 40°, and 90° of elevation

The results from test 1 (zenith-sky geometry) are presented in Figure 6.3.1-81. Since the findings are similar for both sunrise and sunset, only the results for sunset are shown and discussed here.

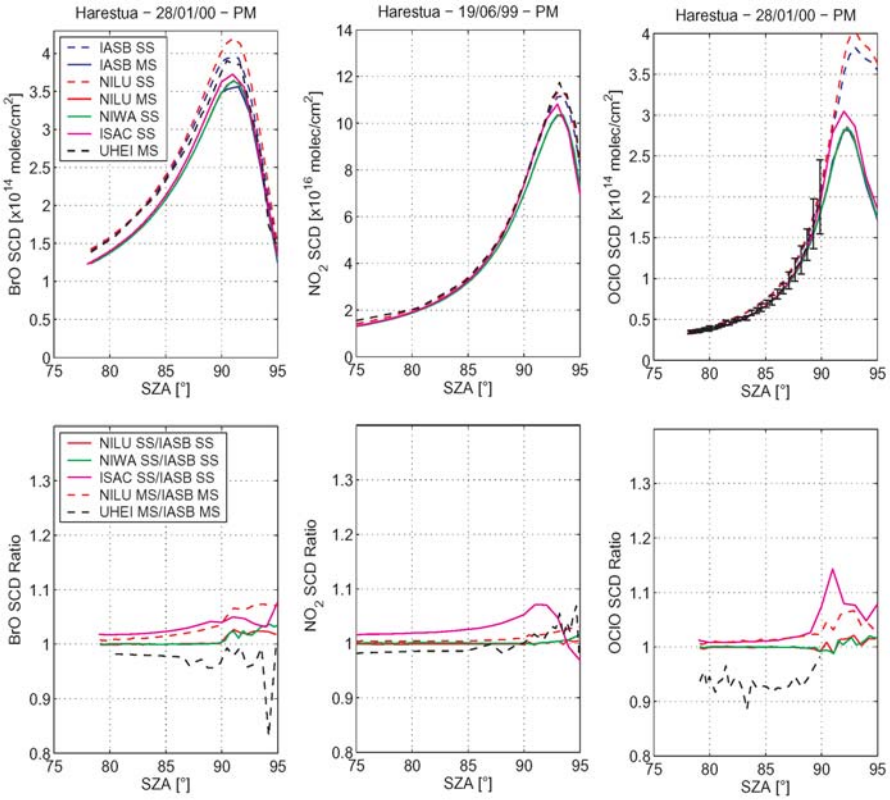

Figure 6.3.1-81. *Sunset BrO, NO_2, and OClO SCDs calculated for test 1 (zenith-sky geometry). The upper plots correspond to the SCDs and the lower plots to the ratios between the results from the different models and the IASB model arbitrarily chosen as the reference model. Two different scenarios have been considered: Harestua (Norway, 60°N) in summer (NO_2) and in winter where chlorine activation occurs (BrO and OClO). Solid and dashed lines are corresponding to calculations in SS and MS modes, respectively.*

A good agreement is observed between the NIWA, IASB, and NILU models in SS mode for the three species: the relative difference between the NIWA and NILU models and the IASB one – arbitrarily taken as the reference model - is smaller than 1% below 90° SZA and smaller than 3% above 90° SZA. These results indicate that the consistency between the three models about the way the photochemical effect has been implemented is very good. Concerning the ISAC-CNR calculations, the relative difference with the IASB model reaches larger values over the whole SZA range for the three species: between 1% and 5% below 90° SZA and up to 14% above 90° SZA (OClO at sunset). Since (1) the relative difference increases with increasing SZA, (2) the largest relative difference is observed for OClO above 90° SZA, and (3) this species varies rapidly at such large SZAs, this suggests that the way the photochemical effect is taken into account in the ISAC-CNR model differs from the other models. Concerning the calculations in MS mode, the agreement between NILU and IASB is quite good even if the difference between both models (up to 8% at large SZA) is larger than the one observed in SS mode. The relative difference between the UHEI and IASB models in the MS mode is smaller than 5% for BrO and NO_2 and 10% for OClO below 93° SZA. Above this SZA value, larger relative differences are observed: up to 16% and 8% for BrO and NO_2, respectively (UHEI calculations for OClO are missing in this SZA range). These results, at least those for BrO and NO_2, show that a very good consistency can be obtained up to 93° SZA between the SCDs calculated with the IASB and UHEI models despite the differences existing between both codes (i.e., the method of solving the RT equation and the treatment of the sphericity; see Table 6.3.1-11).

It should be noted that this comparison test has allowed to greatly improve the consistency between the different RT models in both scattering modes. This improvement is illustrated in Figure 6.3.1-82 where the first comparison results and the current results - obtained after modifying and optimizing the RT codes - are shown. The modifications in the RT codes have mainly concerned the way the photochemical enhancement is handled and the treatment of the forcing of photons into the sun in the case of the UHEI model (Monte Carlo approach).

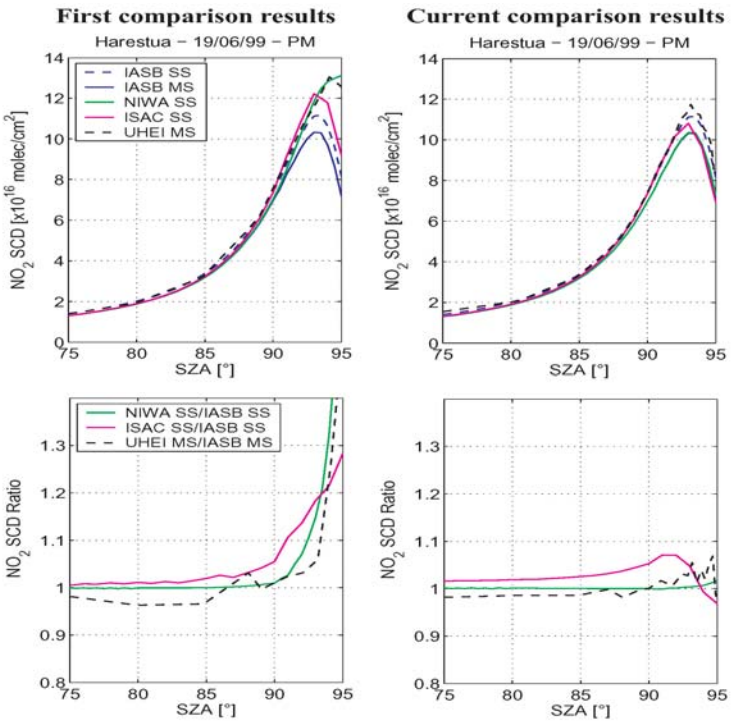

Figure 6.3.1-82. *First comparison results (left plots) and current results obtained after modifying and optimizing the RT codes (right plots). The upper plots correspond to the SCDs and the lower plots to the ratios between the results from the different models and the IASB model arbitrarily chosen as the reference model. Solid and dashed lines are corresponding to calculations in SS and MS modes, respectively.*

Figure 6.3.1-83 shows the results of test 2 (off-axis geometry) for HCHO. These correspond to calculations for 5°, 20°, and 40° of elevation and for 90° AzLOS.

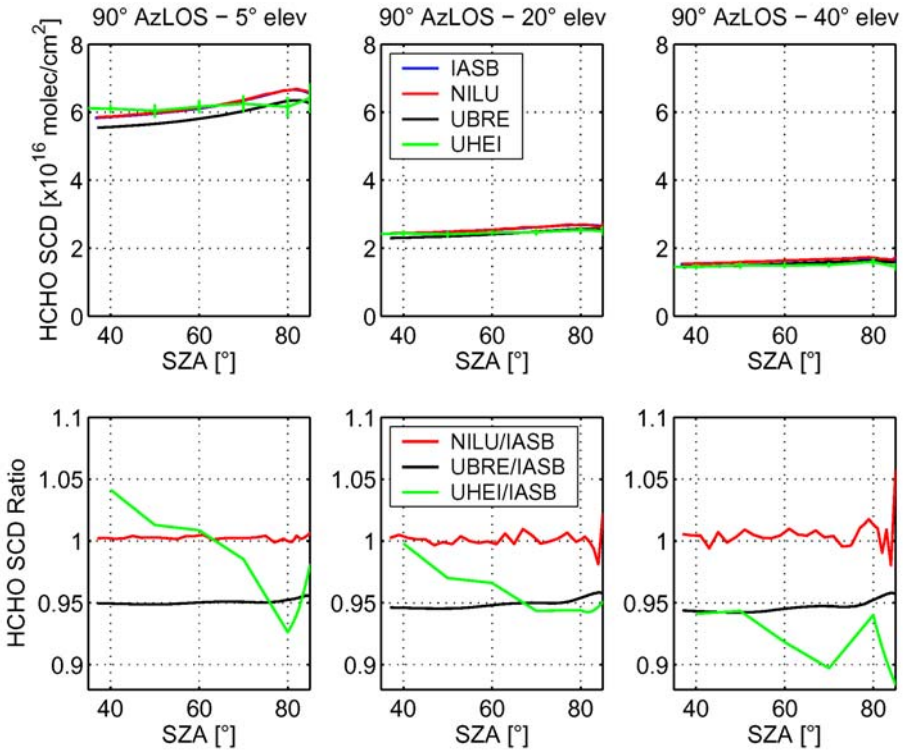

Figure 6.3.1-83. *HCHO SCDs calculated by the NILU, UBRE, IASB, and UHEI models in MS mode for test 2 (off-axis geometry). Upper plots correspond to the SCDs and the lower plots to the ratios between the results from the different models and the IASB model arbitrarily taken as the reference model. Results for 90° AzLOS and for 5°, 20°, and 40° of elevation are plotted here.*

The agreement between the IASB, NILU, UBRE, and UHEI models is very good for 5° and 20° of elevation: the relative differences between the NILU, UBRE, and UHEI models and the IASB one (reference model) are smaller than 2%, 6%, and 7%, respectively. In the case of the UBRE and NILU models, the relative difference is also almost constant over the entire SZA range whereas the relative difference between the UHEI and IASB models displays a large SZA dependence. A similar feature is observed at 40° of elevation. However, larger relative difference values are observed at this elevation, especially for the NILU and UHEI models at high SZA (relative difference values of +6% and -12 %, respectively). The comparison of calculations for both values of AzLOS (0° and 90°) also shows that the impact of the AzLOS is rather small: SCDs calculated for 90° AzLOS are maximum 10% larger than those calculated for 0° AzLOS and this for all four models.

Similar features are observed for BrO and NO_2 (results not shown here). However, the relative differences between NILU, UBRE, and UHEI models and the IASB one are smaller for these species than for HCHO.

A preliminary comparison test between the IASB, NILU, and UBRE models has also illustrated the impact of the resolution of the HCHO cross sections and altitude grid. Using high resolution HCHO cross sections and an altitude grid of 0-120 km/1km thick leads to large discrepancies between the UBRE model and the two other models based on the UVspec/DISORT package as it can been shown in Figure 6.3.1-84. These discrepancies have been resolved mainly by smoothing the high resolution HCHO cross sections used for this test, thus reducing the interpolation effects. To a much lesser extent, decreasing the layer thickness where the concentration changes rapidly with the altitude in the HCHO profile (layer thickness of 0.2 km instead of 1 km between 0 and 3 km) has also reduced interpolation effects and has improved the consistency between the models. This new altitude grid and the smoothed HCHO cross sections have been therefore adopted for the comparison tests involving HCHO.

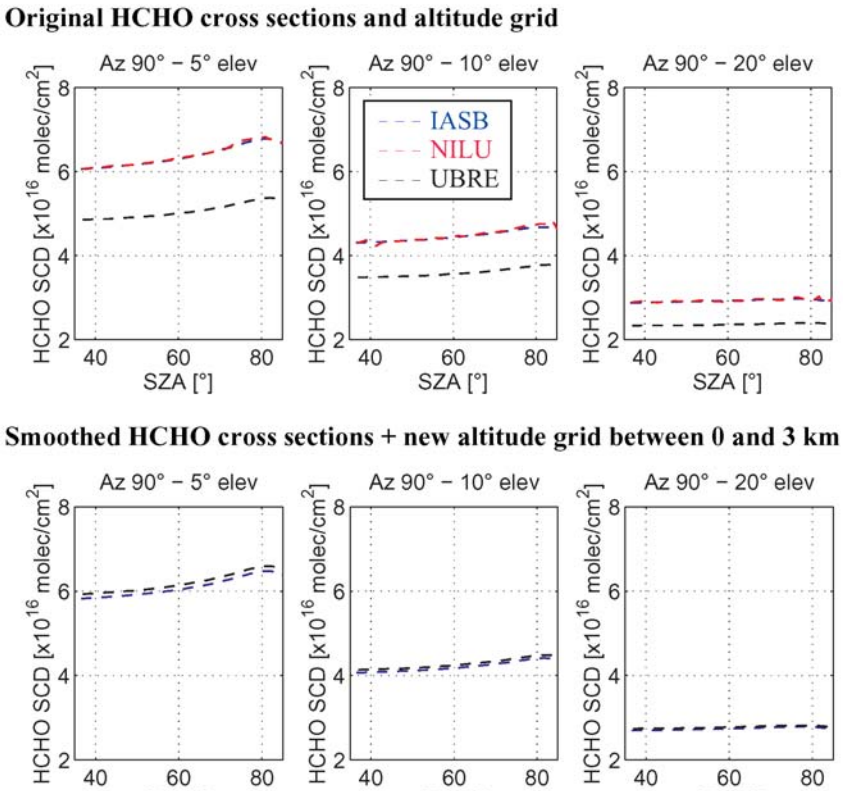

Figure 6.3.1-84. Impact of the resolution of the HCHO cross sections and altitude grid on the HCHO SCDs calculated by the UBRE and IASB models in off-axis geometry (comparison test 2). The upper plots and lower plots correspond to the SCDs calculated with the original HCHO cross sections and altitude grid and with smoothed HCHO cross sections and new altitude grid between 0 and 3 km, respectively. Results for 90° AzLOS and for 5°, 10°, and 20° of elevation are plotted here.

Figure Figure 6.3.1-85 shows the impact of aerosol scattering on NO_2 SCD calculations in off-axis geometry (test 3). The results presented here are corresponding to 30° of AzLOS for which the impact of the aerosol scattering is the largest.

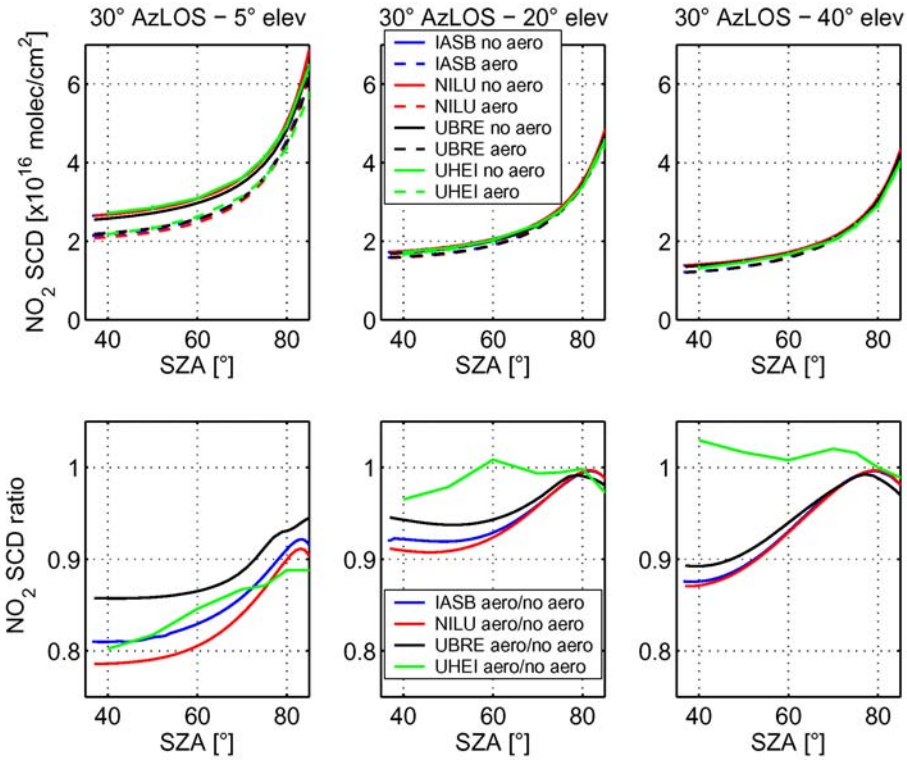

Figure 6.3.1-85. *NO_2 SCDs calculated by the NILU, UBRE, IASB, and UHEI models in MS mode for test 3 (impact of aerosol scattering in off-axis geometry). The upper plots correspond to the SCDs and the lower plots to the ratios between SCDs calculated with and without aerosol scattering. Results for 30° AzLOS and for 5°, 20°, and 40° of elevation are plotted here.*

Large discrepancies are observed between the ratios of NO_2 SCDs calculated with and without aerosol scattering. Since the models have been initialized with the same aerosol profiles (extinction coefficient and phase function), this indicates that the treatment of aerosol scattering differs in each model. Further investigations are needed to explain this feature. It is also observed that the consistency between the IASB, NILU, and UBRE models becomes clearly better when the SZA and the elevation but also the AzLOS (not shown here) increase. Concerning the impact of elevation degree, an opposite behaviour is observed for the UHEI model results: the consistency between this model and the others is the worst for high elevation degree values. Similar discrepancies between model results are observed for HCHO (not shown here). However, the impact of the aerosol scattering on HCHO SCDs is smaller: the ratio between calculations with and without aerosol scattering is comprised between 0.87 and 1.05 for all elevation degrees, SZA, and AzLOS.

The results of test 4 on the impact of ground albedo on HCHO SCD calculations in off-axis geometry are presented in Figure 6.3.1-86. At 80° SZA, an increase of the ground albedo from 0.0 to 0.9 leads to an increase of the HCHO SCD of about 20% and 80% for 5° and 40° of elevation, respectively. The corresponding increases for the NO_2 SCD are 5% and 18%, respectively (not shown here). These increases of HCHO and NO_2 SCD values are similar for the UBRE, NILU, and IASB models whereas they are systematically larger for the UHEI model. The larger impact of the ground albedo on the HCHO SCDs is expected since HCHO, in contrast to NO_2, is mostly located in the lower part of the troposphere (between 0 and 5 km) and is therefore more sensitive to the ground albedo. It is also observed that the impact of the ground albedo becomes larger as the SZA decreases.

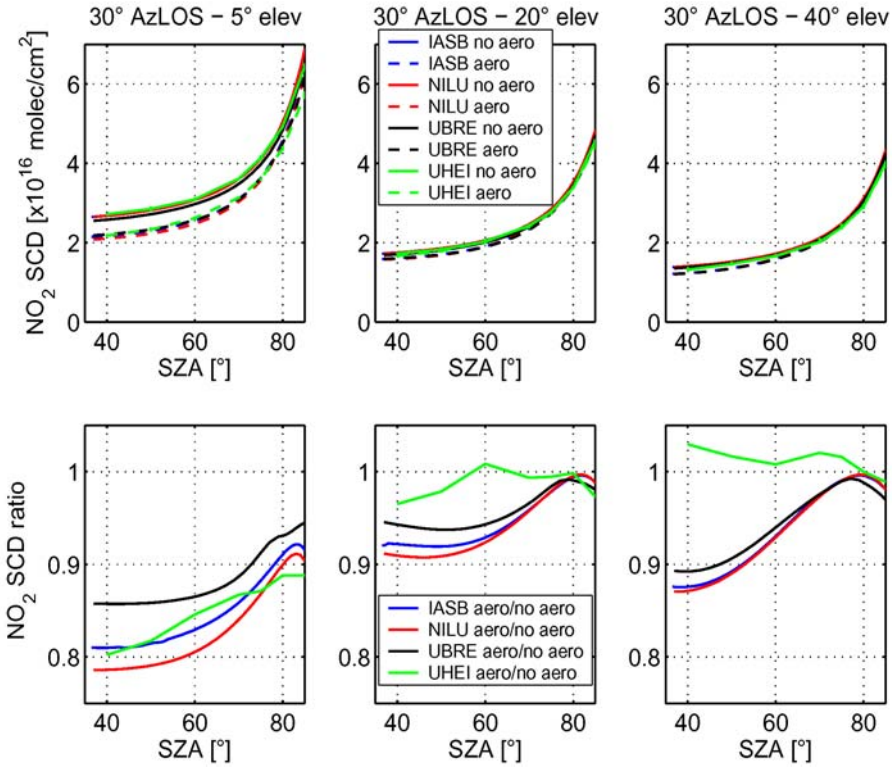

Figure 6.3.1-86. *HCHO SCDs calculated by the NILU, UBRE, IASB, and UHEI models in MS mode for test 4 (impact of ground albedo in off-axis geometry). The upper plots correspond to the SCDs and the lower plots to the ratios between SCDs calculated with ground albedo values of 0.9 and 0. Results for 90° AzLOS and for 5°, 20°, and 40° of elevation are plotted here.*

Conclusions

The present intercomparison exercise has allowed the determination of the consistency between the QUILT RT models used for interpreting the ground-based DOAS and MAX-DOAS observations. The main results are the following:

- The consistency between the QUILT RT models has been greatly improved for zenith-sky BrO, NO_2, and OClO SCD calculations in both SS and MS modes. However, some discrepancies still persist at large SZA (>90°) and need further investigations.
- A good overall agreement is obtained between IASB, NILU, UBRE, and UHEI models in MS mode for the calculation of BrO, NO_2, and HCHO SCDs in off-axis geometry.
- The impact of the aerosol scattering and ground albedo on off-axis NO_2 and HCHO SCDs has been quantitatively determined. The results clearly show that the treatment of aerosol scattering differs in each model whereas a reasonably good consistency is obtained between IASB, NILU, UBRE, and UHEI models concerning the impact of ground albedo.
- The WP2500 deliverable - consisting of a RT model validation package - has been made publicly available through the QUILT website. This package integrates all the initialization data and results of the present intercomparison exercise. Its purpose is to enable the testing of RT codes aiming to the calculation of AMFs (air mass factors)/SCDs as required for ground-based DOAS and MAX-DOAS applications.

6.3.2 WP 3000: Historical data set revision

Introduction

The aim of WP 3000, as defined in the QUILT DOW, is to optimise the exploitation of the existing European UV-visible monitoring systems by which ozone and the related active radicals NO_2, BrO and OClO can be measured from the ground, balloon and satellite. Over the past decade, a large amount of atmospheric measurements of these compounds have been performed at a number of sites covering high and mid-latitudes in both hemispheres. The existing network has also been extended during recent years (mostly towards tropical and equatorial regions where a lack of observational means has long been recognised), with the installation of several new UV-Vis instruments owned by different European institutes. In the current stage of the evolution of the NDSC, the need to establish methods to improve and consolidate the existing measurements has been identified and defined as an important objective of the QUILT project. This involves the selection of state-of-the-art retrieval algorithms (see results from WP 2000), and their application to available time-series of measurements in order to produce required homogeneous data sets for each relevant trace gas. Such high quality data can then be used by end user communities for testing and validating state-of-the-art chemical transport models, and ultimately synthesising information required by legislative authorities responsible for public health issues and by the general public as a whole.

Within WP 3000, there are three main work packages based on the analysis of data from respectively ground-based, balloon and satellite platforms. In this section, the efforts made by the QUILT partners during the whole project to extend their measurement capabilities, homogenise data sets and better exploit available measurements of O_3, NO_2, BrO, OClO and IO column measurements are described.

WP 3100: Ground-based DOAS revision

Applied methodology and scientific achievements

WP 3100 is dedicated to the consolidation of column measurement data series at the stations of the QUILT network (Table 6.3.2-12). As can be seen, most stations are part of the NDSC, as primary or complementary site. All latitudinal bands in between Arctic and Antarctic regions are covered. All stations provide O_3 and NO_2 columns, with data records of various lengths some of them extending back to eighties. An increasing number of sites also provide slant column measurements of BrO and OClO, the latter molecule being measurable only in polar regions. At some stations, zenith-sky observations are complemented by Multi-Axis DOAS (MAX-DOAS) observations, a novel development of the DOAS technique, which also enable the measurement of tropospheric trace gases (NO_2, BrO and HCHO). During the QUILT project, efforts have concentrated on establishing homogeneized time-series of the relevant QUILT trace species at the various stations. Although data consolidation activities were essentially carried out individually at each station, under responsibility of various data providers, results from the third NDSC intercomparison campaign of UV-visible spectrometers, held at Andoya, Norway, in March 2003, provided a significant contribution to WP 3100 in establishing new standards for high quality NO_2 slant column measurement. New NDSC certification criteria were also defined for this molecule. Therefore we start this section by a summary of main results from the Andoya 2003 campaign. The current status of the QUILT network is then outlined with a

description of main consolidation work performed. Examples of geophysical studies based on the resulting homogenised data series are finally given.

Table 6.3.2-12. The QUILT network of ground-based UV/Visible spectrometers.

Station	Lat.	Long.	Institute	Instrument type	Dates
Ny-Alesund, Spitzbergen [1, 4]	78.9°N	11.9°E	NILU	SAOZ	1990 – 2004
Ny-Alesund, Spitzbergen [1, 4]	78.9°N	11.9°E	UBremen	MAX-DOAS *	1995 – 2004
Summit, Greenland [4]	72.5°N	38°W	UBremen	MAX-DOAS *	2003 – 2004
Scoresbysund, Greenland [2]	70.5°N	22.0°W	CNRS	SAOZ	1991 – 2004
Andoya, Norway [2]	69.3°N	16.0°E	NILU	SYMOCS	1998 – 2004
Kiruna, Sweden [2]	67.8°N	21.1°E	UHeidelberg	DOAS	1994 – 2004
Sodankyla, Finland [2]	67.4°N	26.7°E	CNRS	SAOZ	1990 – 2004
Salekhard, Siberia [2]	66.7°N	66.7°E	CNRS	SAOZ	1998 – 2004
Zhigansk, Russia [2]	66.7°N	123.4°E	CNRS	SAOZ	1991 – 2004
Harestua, Norway [2]	60.2°N	10.8°E	BIRA	DOAS	1994 – 2004
Bremen, Germany	53.1°N	8.9°E	UBremen	MAX-DOAS *	1993 – 2004
Aberystwyth, UK [2]	52.0°N	4.1°W	UWales	SAOZ	1990 – 2004
Jungfraujoch, Switzerland [1]	46.6°N	8.0°E	BIRA	SAOZ	1990 – 2004
OHP, France [1]	43.9°N	5.7°E	CNRS	SAOZ	1992 – 2004
OHP, France [1]	43.9°N	5.7°E	BIRA	MAX-DOAS *	1998 – 2002
Mt Cimone, Italy	44.2°N	10.7°E	CNR	GASCOD	1993 – 2004
Bologna, Italy	44.5°N	11.3°E	CNR	GASCOD	1997 – 1998
Stara Zagora, Bulgaria	42.4°N	25.0°E	CNR	GASCOD	1999 – 2004
Izana, Canaries [2]	28.3°N	16.5°W	INTA	ARTIST	1993 – 2004
Merida, Venezuela	21.0°N	99.5°W	UBremen	MAX-DOAS *	2003 – 2004
Paramaribo, Suriname [2]	5.8°N	55.2°W	UHeidelberg	MAX-DOAS *	2003 – 2004
Tarawa, Kiribati Republic [2]	1.4°N	172.9°E	CNRS	SAOZ	1992 – 2004
Nairobi, Kenya	1.3°S	36.8°E	UBremen	MAX-DOAS *	2003 – 2004
Reunion Island [2]	21.1°S	55.5°E	CNRS	SAOZ	1994 – 2004
Reunion Island [2]	21.1°S	55.5°E	BIRA	MAX-DOAS *	2004
Bauru, Brazil [2]	22.4°S	49.0°W	CNRS	SAOZ	1995 – 2004
Lauder, New Zealand [1]	45.0°S	169.7°E	NIWA	DOAS	1980 – 2004
Kerguelen Island [2]	49.4°S	70.3°E	CNRS	SAOZ	1995 – 2004
Dumont d'Urville, Antarctica [1]	66.7°S	140°E	CNRS	SAOZ	1988 – 2004
Marambio, Antarctica	64.3°S	56.7°W	INTA	DOAS	1994 – 2004
Faraday, Antarctica [2]	65.3°S	64°W	BAS	SAOZ	1990 – 1995
Rothera, Antarctica [2]	67.6°S	68.1°W	BAS	SAOZ	1996 – 2004
Neumayer, Antarctica [2, 3]	70.7°S	8.3°W	Uheidelberg	DOAS	1999 – 2004
Terra Nova Bay, Antarctica [3, 4]	74°S	164°E	CNR	GASCOD	1996 – 2004
Arrival Heights, Antarctica [1, 3, 4]	77.8°S	166.7°E	NIWA	MAX-DOAS *	1998 – 2004

* includes low elevation bright-sky viewing, thereby also measuring tropospheric trace gases
[1] primary NDSC station
[2] complementary NDSC station
[3] often inside the edge region of the Antarctic stratospheric vortex
[4] maximum solar zenith angle in midsummer too small for reliable NO_2 measurements in midsummer

Third NDSC intercomparison of UV/Visible spectrometers, Andoya, Norway, 2003

Within the framework of the NDSC, an intercomparison campaign of ground-based zenith-sky viewing UV-visible spectrometers was held at the Andøya Rocket Range at Andenes, Norway from 14 February to 7 March 2003. The chosen site is classified as a complementary NDSC site. Eight groups from seven countries participated in the exercise. All of them are involved in the NDSC network. The purpose of this exercise is primarily to verify and ensure the high quality and the consistency of the data distributed through the NDSC. Criteria for acceptance of data have already been defined by the NDSC in the case of NO_2. However those definitions were made some years ago, during the previous NDSC intercomparisons in 1992 (Hofmann et al., 1995) and 1996 (Roscoe et al., 1999) and were characteristic of mid-latitude conditions. It was therefore deemed necessary to analyse their pertinence for high-latitude conditions and with instruments modified to take advantage of the technology developed since then. The campaign focused on the measurements of slant columns of NO_2, BrO, and OClO, with main focus on measurements of the NO_2 and BrO slant columns. For OClO, the weather conditions were such that very low levels of OClO were observed, therefore limiting the interest of the exercise for this molecule.

Different analysis criteria were investigated during the campaign. These included the use of fitting parameters as chosen by each group to provide what they considered to be optimised retrievals. Additional sets of imposed parameters were also used by each group including the wavelength interval, absorption cross sections, and species fitted. In practice the comparison focused on the use of three different sets of analysis parameters (TC), which allowed the characterization of the differences existing between the instruments. These differences were highlighted through the analysis of (a) regression between the groups and a common reference, (b) fractional differences relative to the reference, and (c) histograms of the absolute differences in measurements. The choice of the reference data was based on the methods established in Roscoe et al. (1999) and considered linear regressions between pairs of instruments in order to select a subgroup of instruments which performed comparably.

From the analysis of the results obtained under the different TCs, it appears that almost all instruments agreed within 5% or better when the analysis parameters are imposed, and using the 425-450 nm spectral interval (TC1). This agreement degrades to 9% when retrieving NO_2 in the 400-418 nm region and to 7% if each instrument uses its preferred choice of parameters. For the sake of uniformity it was recommended that all instruments preferably use a set of prescribed analysis parameters for their NDSC measurements. In particular, it is recommended to derive NO_2 slant columns from the 425-450 nm spectral region. Spectra should be calibrated in wavelength using a high-resolution solar spectrum (Kurucz et al., 1984). In this region, O_3, O_4, and H_2O should also be fitted on top of NO_2. High-resolution absorption cross sections of NO_2 are available in the literature at different temperatures (Harder et al., 1997; Vandaele et al., 1998). Both sets were obtained with Fourier transform spectrometers leading to a very accurate wavelength calibration. The O_3 temperature-dependent cross section of Bogumil et al. (2000) has been considered owing to its high signal to noise ratio and accurate wavelength calibration. In the NO_2 interval it is not necessary to take more than one temperature (223 K) into account. The O_4 absorption cross-section of Greenblatt et (1990), after correction for shift and stretch, should be used in this spectral region. The water vapour reference spectra was obtained by considering the line parameters listed in the HITRAN 2000 database (Rothman et al., 2003). However better correction could possibly be obtained using the measured absorption cross-sections of Harder and Brault (1997). The importance of the solar I_0 effect was already stressed in Aliwell et al. (2002). The O_3 and NO_2 absorption cross sections should therefore be corrected for this effect.

In comparison to previous exercises in 1992 and 1996, the 2003 Andoya NO_2 Intercomparison had different measurement conditions, with a limited range of solar zenith angles due to latitude and season, mainly cloudy conditions and little tropospheric contamination. The Andoya Intercomparison produced the best results so far, probably owing in part to more favourable conditions. However what stands out between the 1996 OHP and 2003 Andoya campaign, is the much closer agreement of all participants which should lead to a real improvement in the accuracy of NDSC global coverage. A major conclusion of the exercise is, that both instruments and analysis have improved since 1996. Some of this arises from e.g., the understandings about instrument polarisation effects, but also from the widespread use of WinDOAS analysis software which facilitates a more "standardised" approach to NO_2 measurements of adequate accuracy for NDSC.

2003 Intercomparison NO_2 Certification

Previous intercomparison exercises had led to the definition of acceptance criteria for NDSC-qualified NO_2 measurements, based on an assessment of the current state of the art in 1992 and 1996. On distinguished between two types of acceptance criteria:

Previous Type 1 (Long term Measurements):

Residual <= 0.10 x 10^{16} cm^{-2}, Slope = 1.00 ±0.05, Intercept <= ±0.15 x 10^{16} cm^{-2}.

Previous Type 2 (Process Studies):

Standard Deviation <= 0.05, Ratio = 1.00 ±0.10, Offset <= ±0.25 x 10^{16} cm^{-2}.

For this Intercomparison a single acceptance criteria was recommended as followed:

Residual <= 0.05 x 10^{16} cm^{-2}, Slope = 1.00 ±0.05, Intercept <= ±0.10 x 10^{16} cm^{-2}

With this criteria 7 out of the 8 participating groups have been certified. A possibility of later certification is proposed to the eighth group, upon submission and acceptance by the NDSC Steering Committee of a report demonstrating adequate improvement of the instrument performances.

Network status and long-term data series consolidation

In this section, the main activities carried by individual partners in view of optimising the quality and consistency of their reprocessed ground-based data sets are briefly described. The overall status of this consolidation work is summarised in Figure 6.3.2-13.

Partner 1: NILU

NILU operates zenith-sky instruments at two stations: Andøya (69.3°N,16.0°E) and Ny-Ålesund (78.9°N, 77.9°E). The time-series of NO_2 and O_3 column measurements recorded from 1991 until 2004 with the SAOZ instrument at Ny-Ålesund has been entirely reprocessed using the latest version of the CNRS analysis software. The data have been submitted to the QUILT data base. Unconsolidated SYMOCS observations of NO_2, O_3, BrO and OClO at Andøya are available from 1998 until 2004. Re-processed, harmonized data sets from Andøya will be added to the QUILT data base within a few weeks.

Partner 2: BIRA-IASB

BIRA-IASB has performed zenith-sky and (some) multi-axis DOAS observations at four stations of the QUILT network: Harestua, Jungfraujoch, OHP and Reunion Island. At the Jungfraujoch, SAOZ observations of NO_2 and O_3 total columns have been performed since 1991. In Harestua, measurements of O_3, NO_2, OClO and BrO columns have been started in 1994 (on a campaign basis) and continued without interruption over the period from 1998 until 2004. At OHP, zenith-sky measurements of BrO and NO_2 have first been conducted from June 1998 until December 2000, then a modified bi-axis DOAS instrument was installed and operated for BrO, NO_2 and HCHO monitoring until July 2002. More recently, in July 2004, a MAX-DOAS spectrometer was installed at Reunion Island after its qualification for NDSC was obtained during the Andøya campaign.

The complete data set of measurements of NO_2 and O_3 vertical columns, as well as BrO and OClO differential slant columns performed in Jungfraujoch, OHP and Harestua has been revisited within the QUILT project. Raw data have been re-processed using most recent analysis settings agreed during the Andøya Campaign with the aim to produce consistent and homogenized time-series of all QUILT-relevant trace species. These results have been incorporated in the QUILT data base and delivered to QUILT Partner 6 for comparison with model simulations. For O_3 and NO_2, the NDSC data base has also been updated using most recent evaluations.

Partner 3: University of Bremen

The University of Bremen currently maintains monitoring activities at five sites of the QUILT network: Bremen, Ny-Ålesund, Nairobi, Summit and Merida. Continuous raw data from these stations are available for Bremen since 1993, Ny-Ålesund since 1995, Nairobi since September 2002, and Summit since August 2003. The instrument for Merida has been set up in March 2004.

Wherever the instrument set up permits the retrieval of the slant columns of NO_2, BrO and OClO, data are analysed as agreed on the intercomparison campaign in Andøya, Norway.

Ozone columns in the ultraviolet wavelength region are derived by using the concept of extended DOAS: Instead of cross sections slant optical densities are fitted to compensate not only for the strong dependence on wavelength for the ozone air mass factor but also the temperature dependence of the absorption cross section.

Air mass factors are calculated using the newest version of the full-spherical radiative transfer model SCIATRAN (Rozanov et al. 2001). Where possible, these calculations are based on co-located ozone profiles provided by sonde measurements. Also the treatment of aerosols in the model is improved by using the extinction profile information obtained by MAX-DOAS measurements of the oxygen dimer O_4.

The analysis of data from Ny-Ålesund has been finalised and submitted to the QUILT database soon. For Bremen and Nairobi which are highly polluted sites, more work is needed especially for NO_2 vertical columns which are strongly affected by the varying tropospheric NO_2 concentrations.

Partner 4: CNRS-SA

CNRS has re-analysed the data from its 10 SAOZ instruments on the period 1988-2003. In addition to revision and homogeneisation of the NO_2 and O_3 slant column data sets according to results from the Andøya campaign, Artic, mid-latitude and tropical AMFs have been modelled using O_3 and NO_2 profiles from the balloon-borne SAOZ which will result in more accurate and consistent vertical columns. The consolidated data set is available on the CNRS-SA website (http://

www.aerov.jussieu.fr/~fgoutail/SAOZ-consol.html). This site has a direct link to the QUILT home web page.

Partner 6: University of Heidelberg

Within the QUILT project, DOAS measurements at Kiruna (Sweden), Neumayer (Antarctica) and Paramaribo (Suriname) were analysed and revised. The instruments of the latter two stations perform Multi-Axis DOAS observations (at Neumayer since 2003), while the measurements in Kiruna are still conducted in the zenith-sky geometry.

The entire dataset of zenith-sky UV observations in Kiruna/Sweden (68°N, 21°E) has been re-analysed. A consistent dataset of high quality of BrO and OClO dSCDs is now available for the period from 1997 until spring 2003. The data set from Neumayer Station, Antarctica (70°S, 8°W) comprises consistent time series of O_3 and NO_2 vertical columns, as well as BrO and OClO dSCDs from 1999 until summer 2003.

Partner 7: BAS

BAS has been operating a SAOZ instrument in Faraday from 1990 until 1995. Since 1996 this spectrometer has been moved and operated in Rothera. The times-series of NO_2 and O_3 columns from Faraday has been finalised and distributed. Measurement data in Rothera have been acquired until 2004 and all spectra have been analysed to slant columns with both SAOZ447 and Windoas softwares. O_3 values have been reworked and finalised, but not yet sent to NDSC data base. NO_2 values are still preliminary as routine chemically-modified Langley plot software is not yet written. NO_2 profiling has been started.

Partner 7: INTA

INTA maintains zenith-sky DOAS spectrometers at two ground-based sites: Izaña (28°N, 17°E) and Marambio (64°S, 57°W). Total columns of NO_2 and O_3 have been continuously monitored since 1993 at Izaña, and since 1994 at Maramabio. Since 1999, the Izaña spectrometer has been replaced by an improved version allowing for BrO differential slant column measurements, in addition to NO_2 and O_3 vertical columns.

Data sets from both stations have been revised as part of WP 3100, based on ecommendations issued during the NDSC Andøya Campaign (March 2003). Consolidated time series of NO_2 and O_3 vertical columns have been submitted for inclusion in the QUILT data base, as well as BrO differential slant columns measured in 2002 and 2003 at the tropical station of Izana. The complete consolidated NO_2 dataset for Izaña is however still under progress due to the need for a re-evaluation of errors in the scanning spectrometer (1993-1998). Nevertheless the dataset of the Diode Array instrument in Izaña (1999-2004) has been uploaded to the QUILT database.

Partner 10: ISAC-CNR

ISAC-CNR has produced ozone and NO_2 data sets from four ground-based stations, Mt. Cimone (Italy), Bologna (Italy), Stara Zagora (Bulgaria) and Terra Nova Bay (Antarctica). All the ground-based stations are equipped with GASCOD type UV/Vis spectrometers, with a spectral resolution of about 0.5 nm in the spectral range 290-600 nm, an NMOS Hamamatsu linear sensor and a f/5 Cassegrain input telescope. All the spectrometers work, as nominal mode, in the 410-464 nm spectral interval. The entire data set of zenith sky spectral measurements with GASCOD Uv-Vis spectrometers installed at Mt. Cimone, Stara Zagora and Terra Nova Bay has been reprocessed with the state of the art DOAS algorithm resulting

in a homogenous database of NO_2 and ozone total column from the above mentioned research stations.

Table 6.3.2-13. Status of ground-based UV-visible data set processing at QUILT stations.

Station	88	89	90	91	92	93	94	95	96	97	98	99	00	01	02	03	04
Ny-Alesund, NILU				X	X	X	X	X	X	X	X	X	X	X	X	X	X
Ny-Alesund, Ubremen								X	X	X	X	X	X	X	X	X	X
Summit, UBremen																X	X
Scoresbysund, CNRS				X	X	X	X	X	X	X	X	X	X	X	X	X	X
Andoya, NILU											X	X	X	X	X	X	X
Kiruna, UHeidelberg							X	X	X	X	X	X	X	X	X	X	X
Sodankyla, CNRS			X	X	X	X	X	X	X	X	X	X	X	X	X	X	X
Salekhard, CNRS											X	X	X	X	X	X	X
Zhigansk, CNRS				X	X	X	X	X	X	X	X	X	X	X	X	X	X
Harestua, BIRA							X	X	X	X	X	X	X	X	X	X	X
Bremen, UBremen						X	X	X	X	X	X	X	X	X	X	X	X
Aberystwyth, UWales				X	X	X	X	X	X	X	X	X	X	X	X	X	X
Jungfraujoch, BIRA				X	X	X	X	X	X	X	X	X	X	X	X	X	X
OHP, CNRS					X	X	X	X	X	X	X	X	X	X	X	X	X
OHP, BIRA											X	X	X	X	X		
Mt Cimone, CNR						X	X	X	X	X	X	X	X	X	X	X	X
Bologna, CNR										X	X						
Stara Zagora, CNR													X	X	X	X	X
Izana, INTA						X	X	X	X	X	X	X	X	X	X	X	X
Merida, UBremen																X	X
Paramaribo, UHeidelberg															X	X	
Tarawa, CNRS					X	X	X	X	X	X	X	X					
Nairobi, UBremen																X	X
Reunion Island, CNRS							X	X	X	X	X	X	X	X	X	X	X
Reunion Island, BIRA																	X
Bauru, CNRS								X	X	X	X	X	X	X	X	X	X
Lauder, NIWA	X	X	X	X	X	X	X	X	X	X	X	X	X	X	X	X	X
Kerguelen, CNRS								X	X	X	X	X	X	X	X	X	X
Dumont d'Urville, CNRS	X	X	X	X	X	X	X	X	X	X	X	X	X	X	X	X	X
Marambio, INTA							X	X	X	X	X	X	X	X	X	X	X
Faraday, BAS			X	X	X	X	X	X									
Rothera, BAS									X	X	X	X	X	X	X	X	X
Neumayer, UHeidelberg												X	X	X	X	X	X
Terra Nova Bay, CNR									X	X		X	X	X	X	X	X
Arrival Heights, NIWA											X	X	X	X	X	X	X

X data set fully homogeneised
X data set produced but not fully homogeneised
X data set available from external partner (not funded by QUILT)

Ground-based data dissemination

Final consolidated data records have been collected for inclusion in the QUILT data base at NILU, and a link to the QUILT web site (http://nadir.nilu.no/quilt/) has been established. In addition a Data Consolidation Document (DC-Doc), which includes details on measurements performed at each station, as well as relevant information on instruments, retrieval algorithms and ancillary data used by each group, has been compiled and associated to the data base.

Geophysical exploitation of homogenised data series at particular stations

In this section, results of some interesting studies performed at QUILT stations based on the use of the homogenised data sets are described.

Trend analysis of 8 years of NO_2 columns at Mt. Cimone

Recent studies have pointed out difficulties to give a correct interpretation to measured long term trend of stratospheric NO_2. Several atmospheric phenomena may alter the NO_2 content in stratosphere and each of them should be taken into account to evaluate the NO_2 trend. A study on the NO_2 trend performed on DOAS measurements obtained at Mt. Cimone station (44°N, 11°E, 2165 m asl) in the Northern Italy was performed. A first evidence of the NAO influence on the NO_2 stratospheric amount has been observed and investigated. Understanding the trend of NO_2 in the stratosphere is an important task for atmospheric science. The long-term evolution of stratospheric NO_2 is thought as being mainly modulated by the N_2O produced at the ground. Nevertheless southern hemisphere mid-latitudes observations (Liley et al, 2000) have found out a decade increase in NO_2 column amount measured during twilight of about 5% that is more than expected if compared with N_2O trend (that is around 3.4% per decade). Fish et al. (2000) tentatively explain such discrepancy by an indirect effect due to the trend in stratospheric aerosol. On the other hand, McLinden et al. (2001) demonstrate how the study of such trends performed with DOAS measurements during twilight periods is critical and requires a correct interpretation of chemistry. Here DOAS measurements performed at the Mt. Cimone station have been used by CNR-ISAC to show how the NO_2 column amount at northern mid-latitudes can be modulated by the pressure field patterns, which can be modelled with the NAO index. Other authors have found a correlation between NAO index and stratospheric ozone (Appenzeller et al. 2000, Weiss et al., 2001) and with other atmospheric parameters such as meridional heat flux, zonal winds and temperature (Gimeno et al, 2002, Zhou et al., 2001).

Zenith scattered UV/Vis radiation measurements are performed daily at Mt. Cimone since August 1993. One year and half of observations between 1997 and 1999 are missing. We have used AM and PM slant column values between 1993 and 2003 interpolated at fixed Solar Zenith Angle (SZA) values of 88° and 90°. As already shown in Liley et al. 2000, Appenzeller et al., 2000 and Weiss et al., 2001, one possible approach to the NO_2 trends in the stratosphere is to model the natural variations with known predictors. In this work we have used the following model:

$$\text{Model\_SC}_{NO_2} = \text{cost} + \sum_i a_i P_i$$

where Model_SC_{NO2} is the NO_2 slant column amount obtained by the model, P_i are the predictors (annual cycle, QBO, semiannual cycle, solar cycle) expressed with sinusoidal functions and a_i their relative coefficients. A non-linear fitting algorithm has been used to force the model to reproduce the observations in the least-squares sense. Any information related to sources of long-term NO_2 modulation not accounted for in the model will therefore show up in the residuals.

The slant column amounts have been filtered from pollution episodes by using NO_2 vertical profiles retrieved from the same measurements (Petritoli et al., 2002). Further, twilight periods with non-monotonous increasing slant columns have been removed because likely affected by local pollution transport (not considered in profiles retrieval) and/or cloudy sky conditions. The remaining data set has been monthly averaged in order to smooth out the natural high frequency variations of the NO_2 column (that our model can not reproduce properly) and therefore better capture the long-term (low-frequency) variations of the stratospheric NO2. This time scale also turns out to be adequate to study trends in dynamical processes (e.g. planetary wave activity) connected to the NAO index (Zhou et al., 2001). Monthly averages have been considered as representative only if they were obtained from at least 15 days measurements. These were used to perform correlations with the NAO index, as obtained from the NOAA Climate Prediction Center (http://www.cpc.ncep.noaa.gov/). A check on the stability of these correlations was performed using two different data sets for morning and evening measurements, respectively at SZA=88° and SZA=90°.

In Figure 6.3.2-87 and Figure 6.3.2-88 the scatter plots of the NO_2 residuals are plotted against the NAO index, for AM and PM at 88° and 90° for two distinct annual periods: January, February, March, April (JFMA) and September, October, November, December (SOND). The respective linear coefficients and their errors are reported in Table 6.3.2-14. During JFM, the NAO index represents the modulation of the tropopause height that has been demonstrated to modify the total ozone column (Appenzeller et al., 2000). AM results for JFMA are consistent with no-correlation at all, while PM results show a slightly negative correlation of the order $0.14\text{-}0.19 \times 10^{16}$ molec/cm^2/NAO. This means that during winter when NAO absolute oscillations of the order of 2-3 can be observed, the NO_2 slant column may be modulated by up to about 0.5×10^{16} molec/cm^2, which is in the range of 6-12% of the NO_2 slant column in winter and early spring period. The NO_2 modulation in AM slant column is expected to be much lower than that in PM and may have been hidden by the errors in our fitting model. The correlation in the SOND period appears to be slightly different. For this period, *Weiss et al.* (2000) reported a positive correlation between ozone measurements in the middle stratosphere obtained by ozone soundings at Payerne (Switzerland) and NAO. This was supposed to be correlated with variability in the middle stratospheric quasi-horizontal transport of ozone that leads to transport of ozone-rich air from high latitude during positive NAO phase and ozone-poor air from low latitude during negative NAO phase connected to upward propagation of Rossby waves that is favoured in SOND period. What we obtain for the NO_2 column is different in AM and PM observations.

Figure 6.3.2-87. *Linear correlation between NO_2 residuals and NAO index during JFMA. Error bars are the standard deviation of monthly average value.*

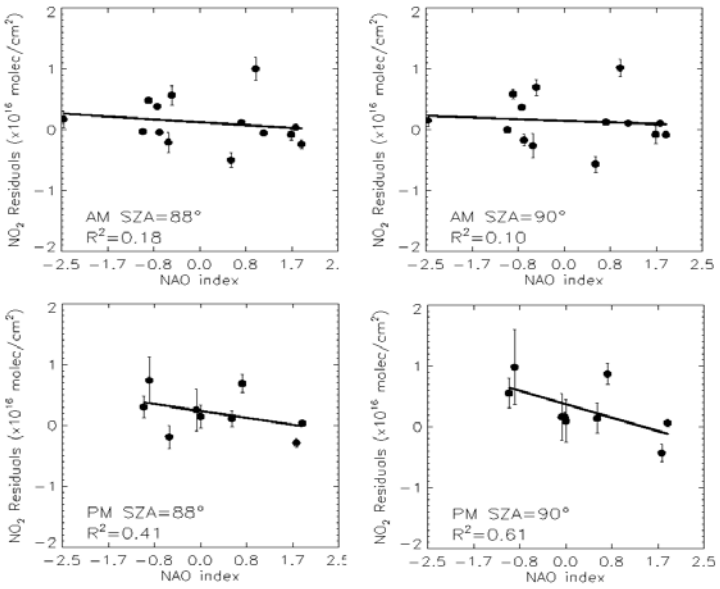

Figure 6.3.2-88. *Linear correlation between NO_2 residuals and NAO index during SOND. Error bars are the standard deviation of monthly average value.*

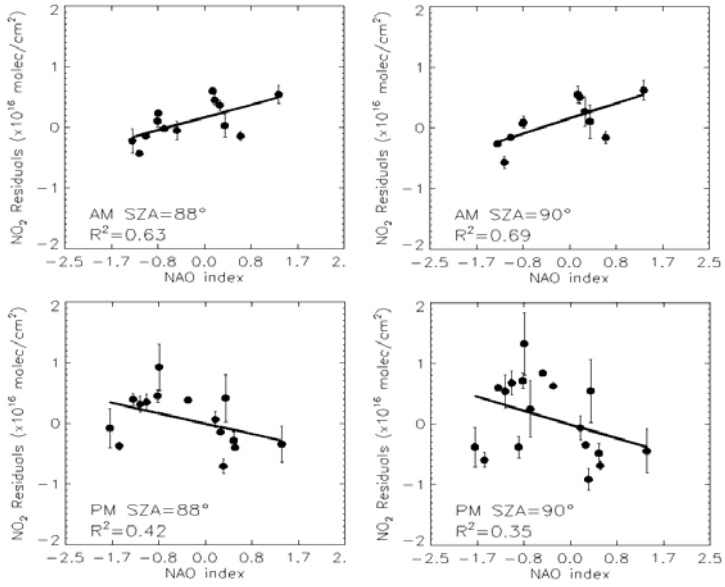

Table 6.3.2-14. Linear coefficients and respective errors of the NO_2 residuals versus NAO index..

	JFMA	**SOND**
AM 88°	-0.07 ± 0.09	0.25 ± 0.09
AM 90°	-0.04 ± 0.09	0.30 ± 010
PM 88°	-0.14 ± 0.11	-0.20 ± 0.12
PM 90°	-0.19 ± 0.12	-0.27 ± 0.17

The former show a positive correlation between 0.25-0.30 x10^{16} molec/cm^2/ NAO, the latter a weak negative correlation in the range of 0.20-0.27x10^{16} molec/ cm^2/NAO with a larger scatter. At mid-latitudes the daily variation of the NO_2 column is strictly linked to the catalytic ozone destruction cycle and to the slow re-

lease of NO_2 from the N_2O_5 nocturnal reservoir. AM observations are in agreement with ozone behaviour: at sunrise the NO_X-O_3 equilibrium is rapidly achieved and higher O_3 also means higher NO_2. The weak negative correlation in PM observation linked to the positive one in morning measurements means that the (NO_2PM - NO_2AM) difference tends to be higher during negative NAO phase (air coming from the low latitudes) and lower during positive NAO phase (air coming from high latitudes). Such consideration is in agreement with the natural NO_2 diurnal variation in the regions where stratospheric air comes from, but the new chemical equilibrium found after the transport has occurred could be not linear if compared to the transport event (NAO index). This seems to be confirmed by the large errors in linear PM coefficients.

Differential tropospheric NO_2 retrieval based on simultaneous observations in Bologna and Mt. Cimone

For 3 years between 1996 and 1998 a GASCOD spectrometer was operated by ISAC-CNR in Bologna (46 m asl) for zenith sky scattered solar radiation measurements. Bologna is located in the middle of the Po valley that is one of the region with highest NO_2 emission all around the world. The idea is to try to retrieve the NO_2 column amount in the lowest troposphere by comparing the measurements in Bologna with similar ones performed at Mt. Cimone that is located just on the border of the Po valley in the northern Apennines (2165 m asl). Spectra acquired at Mt. Cimone do not contain information on the atmospheric composition below 2165 m while spectra from Bologna do (see Table 6.3.2-89). The atmospheric air up to 2165 m contains for almost 90% of the days of the year all the PBL where pollutants are confined. So assuming that the stratospheric signal in the measurements are the same (as it seems reasonable since the horizontal distance between Bologna and Mt. Cimone is about 50 km) the difference of the slant column amount taken at the same solar zenith angle gives the slant column amount of the measured trace gases in the tropospheric portion between 46 m and 2165 m. All data available have been made homogeneous so that no significant bias due to data processing could come out from the difference. The method has then been tested using particular days during 1996 with different meteorological conditions:

- NO_2 polluted day with PBL extending above Mt. Cimone altitude (30-10-1996)
- NO_2 polluted day with PBL confined within 2165 m (12-12-1996)
- NO_2 pollution free day (02-06-1996)

Slant columns obtained are plotted in Figure 6.3.2-90 as well as their difference (Bologna-MtCimone). For the case a) NO_2 was transported also at Mt. Cimone reaching than the free troposphere. Here NO_2 has a longer lifetime so what we expected from the column between 46 and 2165 m is no significant changes during the measurement period. We checked this hypothesis with model calculation.

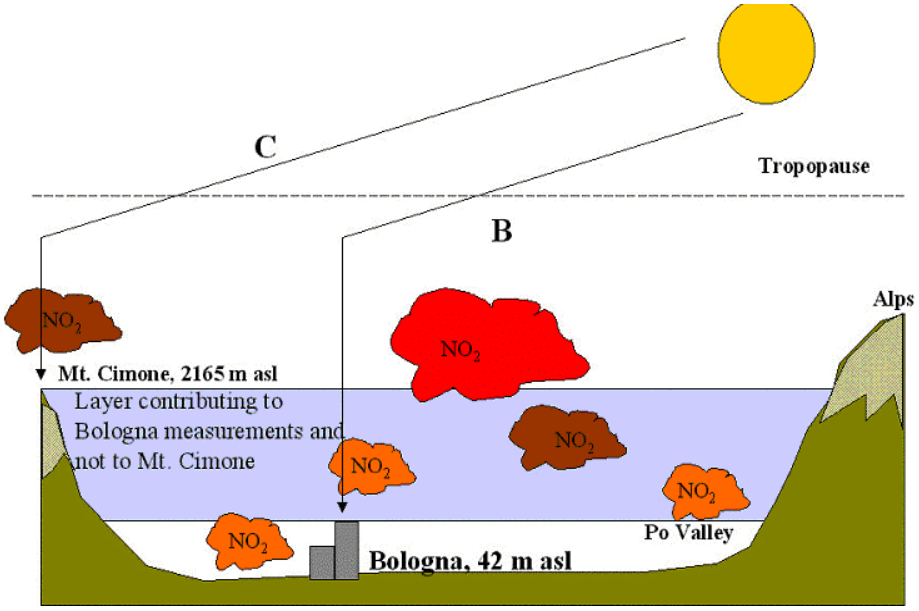

Figure 6.3.2-89. *Comparison between the geometry of the GASCOD instruments installed in Bologna and Mr. Cimone. Slant column measurement in Bologna contain information on the NO_2 in the PBL .*

From the measurements at Mt. Cimone we retrieved the NO_2 vertical profile of concentration (work performed within the WP 2200). The value at 2.5 km, 4.3 x 10^9 molec/cm^3, was used as a boundary condition to guess a NO_2 profile extending down to the ground with an exponentially increasing shape. The reconstructed profile was used to calculate, with the RTM AMEFCO, the expected slant column in the atmospheric layer within 46 and 2165 m. Results, shown in figure 3.4 (upper plot red line) are consistent with a constant NO_2 column between Bologna and Mt. Cimone. Case b) was useful to estimate the possible rate of change ($\Delta NO_2/\Delta t$) when PBL filling up with NO_2 is still in progress. A maximum value of the order of $3x10^{15}$ molec/(cm^2 x min) was found. Case c) was instead a good test to verify the presence of any bias due mainly to data processing. The difference between the slant column was zero (within the experimental error) during the entire measurement period.

This sort of feasibility study has demonstrated that the comparison of measurements performed in different stations can provide further information on the vertical distribution of NO_2

Figure 6.3.2-90. *Sample cases of the comparison between simultaneous NO_2 slant column measurements at Bologna and Mt. Cimone (see text for more details).*

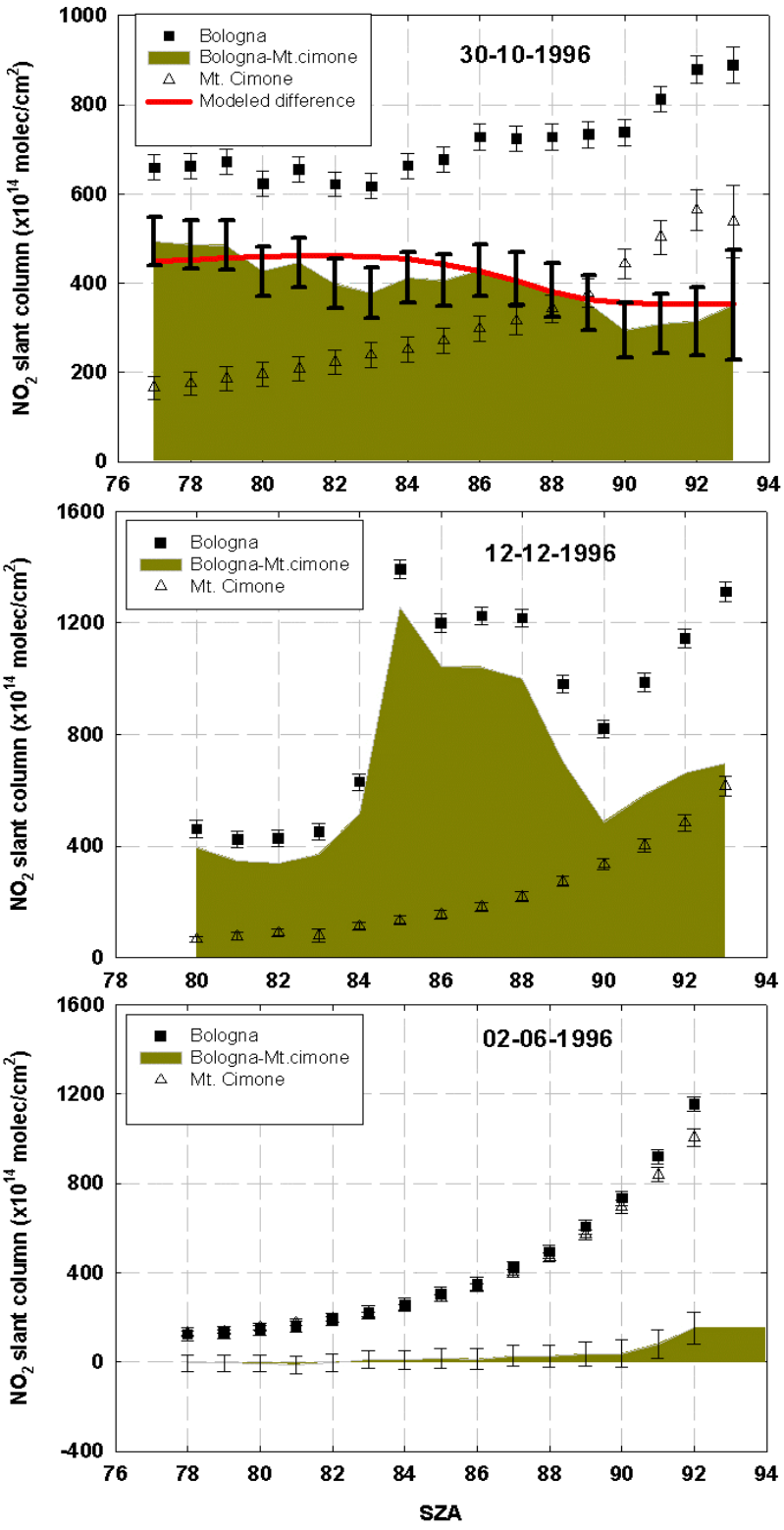

Comparison with the 3D-CTM SLIMCATat Izaña and Marambio stations

The NO_2 recorded by INTA at Izaña has been compared with the SLIMCAT 198 run (Figure 6.3.2-91). There are unrealistic features in autumn of 1997 in the model and a smaller annual wave, but in general the magnitude and seasonal dependence are well reproduced by the model.

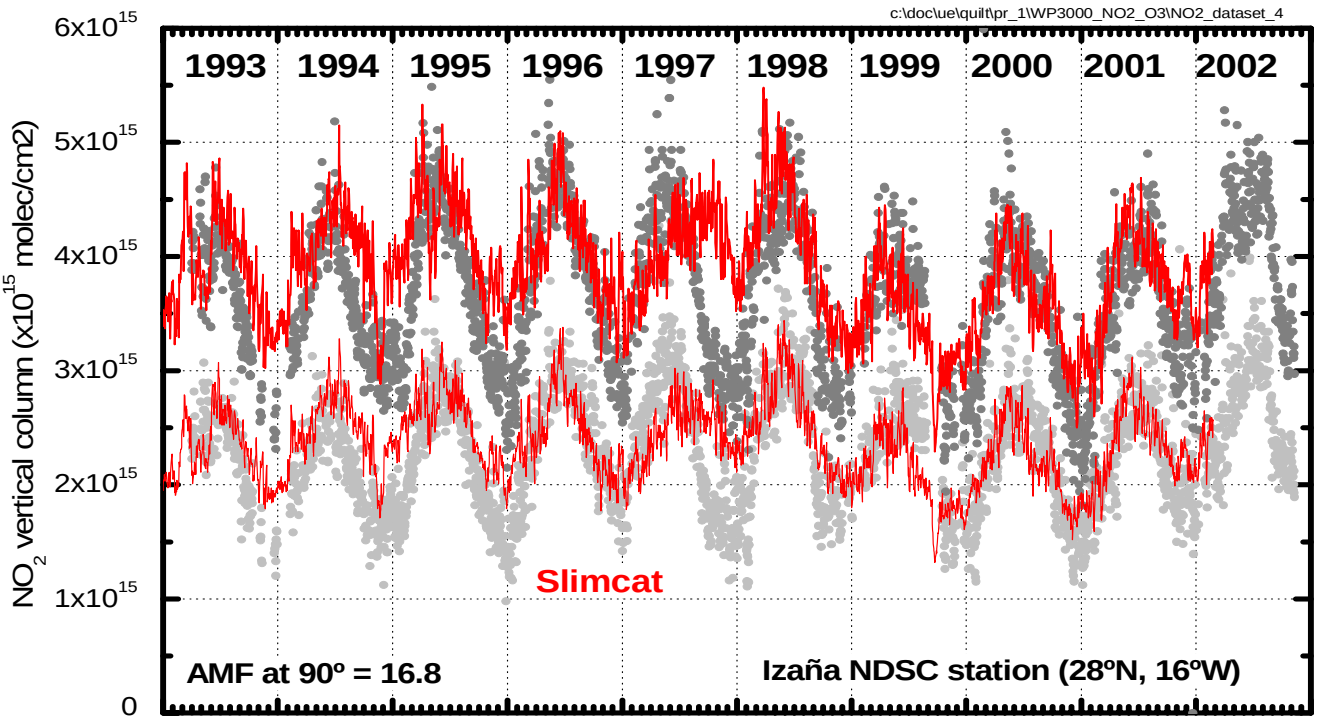

Figure 6.3.2-91. *NO_2 vertical columns measured at Izaña with the RASAS instrument (grey circles), and calculated with the SLIMCAT model (blue lines)*

Likewise, the NO_2 data series of Marambio have been compared with the output of the SLIMCAT run 198 in multi-annual mode forced by UKMO from 1994 to 2002. Results are presented in Figure 6.3.2-92, in terms of monthly means to reduce the day-to-day scattering. Despite the coarse grid used by SLIMCAT, which might lead to difficulties at the edge of the Antarctic vortex where meridional gradients can be large, the model reproduces well the seasonal evolution and the year-to-year variability during summer. The negative trend in the maxima from the summer 1997-1998 is also observed in the SLIMCAT data. Note that this result is apparently not consistent with the positive trend reported at mid latitude southern hemisphere by Liley et al. [2001], as well as by the SAOZ instrument located in the nearby station of Faraday/Rothera [Roscoe, private communication]. When analysing the differences in more details it can be seen that SLIMCAT provides lower values than EVA in autumn (Figure 6.3.2-93). Seasonal differences from the accumulated data clearly reflect the autumn disagreement (Figure 6.3.2-94).

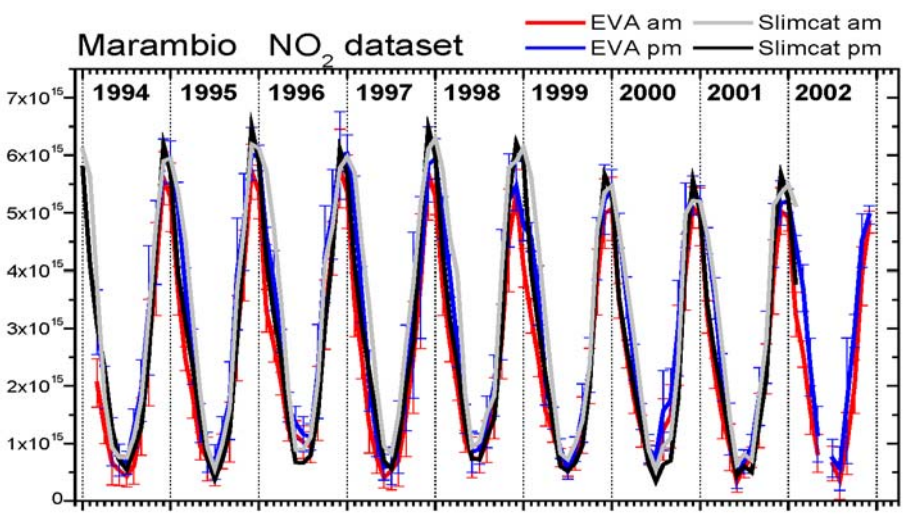

Figure 6.3.2-92. *Monthly means of the NO_2 DOAS EVA spectrometer and SLIMCAT run for the Marambio station (Antarctica).*

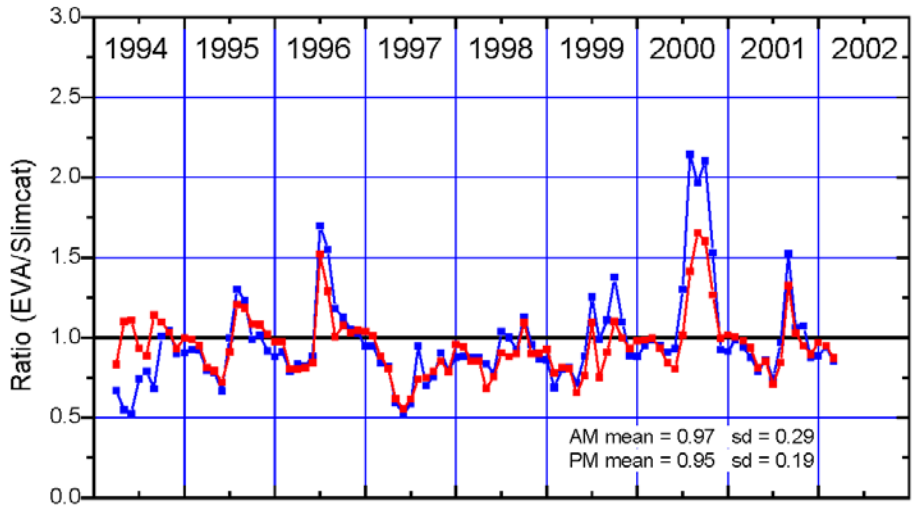

Figure 6.3.2-93. *Ratio of EVA to SLIMCAT NO_2 vertical columns at Marambio, Antarctica.*

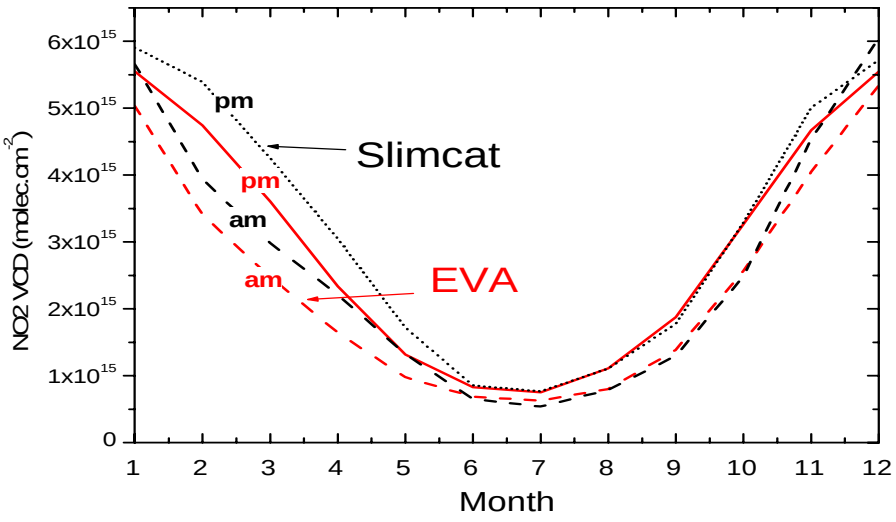

Figure 6.3.2-94. *Monthly mean of accumulated NO_2 data for EVA and SLIMCAT.*

Trend analysis of 10 years of BrO slant column measurements at Harestua, Norway

BrO is a key trace species involved in the destruction of stratospheric ozone. Following the Montreal Protocol and its subsequent amendments, decisions have been taken to implement the progressive phase-out of the production of all anthropogenic substances that deplete the ozone layer. Despite complete phase-out production of the Halons (the main Br-containing substances released by human activities) by 1994, total anthropogenic bromine has continued to increase consistently in the atmosphere; likely due to the large banking of these compounds in developed countries, and also to some authorized production and consumption in developing countries.

Since January 1994, measurements of BrO differential slant columns have been performed by BIRA-IASB at the complementary NDSC station of Harestua, Norway. Owing to the geometry of twilight observations, BrO differential slant columns are only weakly sensitive to the troposphere and therefore can be considered as directly proportional to the total stratospheric BrO content at twilight. As part of the QUILT project, the complete data set of homogenised BrO measurements retrieved for the period from 1994 until 2004 has been evaluated for long-term changes. In order to allow considering for this analysis early measurements (1994-1997) acquired only during winter-spring periods, the full data set has been first deseasonalised using a cyclic function derived from analysis of the well-sampled 1998-2002 time-series. Deseasonalised differential slant columns, representative of yearly mean values, were subsequently converted to approximate vertical columns at 80° of solar zenith angle using appropriate air mass factors calculated with proper account of the twilight BrO photochemical variation (see present report, WP 2500).

The resulting deseasonalised stratospheric BrO vertical column data set is represented in Figure 6.3.2-95. After regression analysis over the period 1994-2004, a significant positive rate of change is obtained for the period from 1994 until 2000, while the trend is found to be insignificant for the remaining period (from 2000 until 2004), suggesting a possible stabilisation of the stratospheric bromine loading over recent years. Accounting for a mean delay of about 4 years to transport air from the surface to the altitude of the bulk of BrO (20 km), the BrO change determined in this study can be related to changes in bromine content at the surface in the period 1990-2000. From surface measurements of the main Halons during the period from 1980 until 1996 (see EUR 19867) a systematic increase of the atmospheric bromine loading has been reported that is consistent with our stratospheric observations over the 1994-2000 period. More recently however, surface observations by Yokouchi et al. (2002) and Montzka et al. (2003) have lend evidence for a stabilisation and even a decline of surface methyl bromide contents that started around year 2000. Accounting for the 4 years time delay to transport air masses from the surface to the stratosphere, such a decline is expected to show up in our zenith-sky BrO observations from year 2004 onward. Continued monitoring is therefore needed to verify whether observed changes in the bromine sources at the surface are consistent with our observations of the long-term evolution of the stratospheric BrO content.

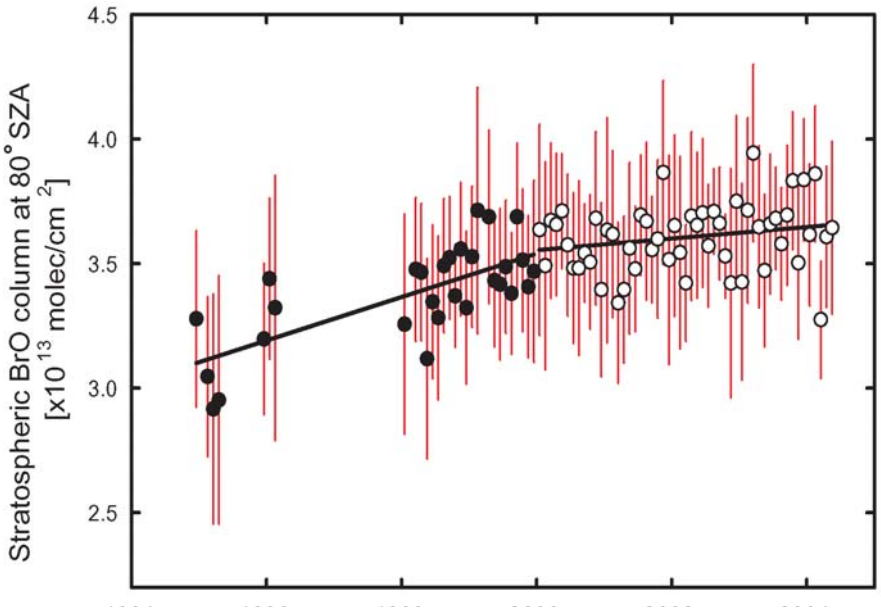

Figure 6.3.2-95. *Monthly averaged stratospheric BrO columns retrieved at Harestua (60°N) from 1994 to 2004. The seasonal variation of the BrO column has been removed using a cyclic function derived from observations in the period 1998-2002. Measurements indicate a stabilisation of the stratospheric bromine content in recent years.*

Main deliverables

- *Homogeneous, quality controlled time series of O_3, NO_2, BrO, OClO and colour index measurements at project network ground-based stations*
- *Data product quality description (including history) at each ground-based site*
- *Web based interface for public access to the created ground-based data set and documentation*

WP 3200: Balloon data set revision

Applied methodology and scientific achievements

The work in WP 3200 focused on the consolidation of O_3, NO_2, BrO, OClO, IO, and OIO vertical profiles mainly arising from an existing series of balloon-borne UV/visible measurements. The data set stems from a large series of stratospheric balloon flights conducted by either the SAOZ (Systeme d'Analyse par Observation Zénithale from partner 4, CNRS-SA) or LPMA/DOAS payloads (Laboratoire de Physique Moléculaire et Applications/ Differential Optical Absorption Spectrometry from partner 5, IUP-Heidelberg). Earlier data from about 100 SAOZ balloon flights and 13 LPMA/DOAS balloon flights were reprocessed including the most recent available information on (a) the balloon trajectories, (b) the spectral retrieval (as recommended by Aliwell et al., 2002 and Bösch et al., 2003), (c) absorption cross sections, and (d) the radiative transfer (for details see the section 'Data revision studies'). After the data have been reprocessed, they were carefully inter-compared with simultaneous or quasi-simultaneous measurements obtained from independent sensors (for details see the section 'Data quality check and inter-comparison' below).

Data revision studies

According to the details outlined below, the revision and the improvement of the balloon data required the consideration of known and only recently identified sources of errors and uncertainties. In general, it is crucial to consider a state of the art spectral retrieval (i.e., Aliwell et al., 2002) using recent updates of absorption cross sections, and accounting for:

- The solar center-to-limb darkening effect for the retrieval of very low sun measurements (i.e., Bösch et al., 2003).
- The residual absorption in the Fraunhofer reference spectrum. It has been shown (i.e. Dorf et al., 2004) that the most suitable method to infer the residual absorption in the Fraunhofer reference spectrum comes from a Langley plot in which the measured absorption is plotted as a function of total air mass. The residual absorption is then given by the intercept of the regression line to zero total air mass.
- The potential T-dependence of the absorption cross-sections (i.e., for NO_2, BrO, and OClO). This effect was usually taken into account by calculating an effective temperature for each line of sight measurement. The effective temperature is given by the actual stratospheric temperature in a certain altitude range or layer weighted with the slant column amount absorption in that particular layer.
- The re-calculation of the balloon trajectory files including all available information taken on the payloads or by remote sensors tracking the payloads
- The re-calculation of the ray tracing (for the solar occultation experiments) or RT of the limb measurements by a validated RT model (i.e. Weidner et al., 2004).
- The most recent profile inversion tools (Rodgers, 2000), including least-square unconstraint profile inversion technique or the optimal estimation (maximum a posteriori) solution technique.

As demonstrated below, if all these issues are carefully taken into account, the results of the various balloon measurements converge into largely consistent data sets.

Data quality check and inter-comparison studies

The achieved quality and consistency of the reprocessed balloon data can be demonstrated by tight inter-comparison studies using observations obtained from independent sensors flown either on the same payload, or obtained by other means (i.e., by collocated overpasses of satellite instruments which measure the same species, or by simultaneous ground-based observations). Examples of such inter-comparisons are described below. They demonstrate the quality of the balloon UV/visible solar occultation technique, its high potential for very reliable stratospheric investigations, and finally they open perspectives for new applications of aeronomical interest (e.g. the mini-DOAS Limb measurements is particularly sensitive for trace gas detection in the UT/LS region, or for cloud studies). The conclusions on the findings and still possible improvements are separately given at the end of each section for each of the considered trace gases.

A. O_3 profile inter-comparison

Within the present project, the O_3 profile inter-comparison studies included studies of measured ozone concentrations from the same payload (Section A.1), and inter-comparisons of ozone measured from the balloon and collocated satellite observations (Section A.2).

A.1. O_3 measurements from the same platform

Checks of quality and inter-comparisons of measured ozone can be straightforwardly performed from the LPMA/DOAS payload which in its standard configuration accommodates (1) an UV/Vis grating instrument (Ferlemann et al., 2000), (2) a near-IR FT-spectrometer (Camy-Peyret et al., 1993), both analyzing the direct sun light in the same light beam, (3), the mini-DOAS instrument which analyzes scattered skylight (Weidner et al., 2004), and (4) an electrochemical cell (ECC) ozone sonde which measures the ozone concentration in the vicinity of the payload. Accordingly, the inter-comparison is organized as follows:

A.1.1. O_3 absorption analysed within the same line of sight (UV/Visible versus IR)

Slant column densities of O_3 (O_3-SCD) (measured in the same light beam taken from the balloon gondola to the sun) as a function of flight time are regularly retrieved from LPMA observations within the 3040.03-3040.85 cm^{-1}, 2914.36-2915.16 cm^{-1}, and 1933.89-1940.00 cm^{-1} wavenumber ranges and from UV/vis DOAS observations within the 545 nm – 615 nm wavelength range. They provide the primary information on the atmospheric ozone concentration (see example in Figure 6.3.2-96)

Intercomparison exercises allow us to check the quality and consistency of both independent measurements, and particularly the quality of spectral retrievals and the consistency of the used absorption cross sections and their T- and p- dependencies in the near IR. Generally a good agreement (within ±5 %) is found for the inferred O_3-SCD with the larger error usually coming from the near-IR O_3 measurements, due to strong interferences with CO_2, H_2O, CH_4, and NO_2.

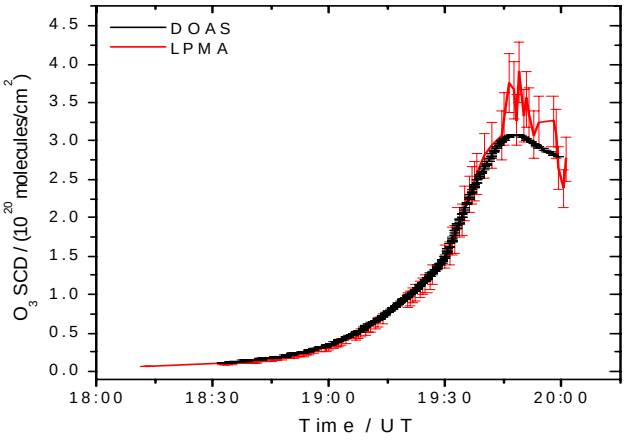

Figure 6.3.2-96. *Measured slant column densities of O_3 (O_3-SCD) as a function of flight time retrieved by LPMA (red) within the 3040.03 - 3040.85 1/cm, 2914.36 - 2915.16 1/cm and 1933.89 - 1940.00 1/cm wavenumber ranges and DOAS (black) within the 545 nm – 615 nm wavelength range for balloon ascent measurements at Kiruna on Aug. 21, 2001 (adopted from Butz et al., 2004).*

Another issue that complicates the direct inter-comparison results from the larger sampling rate of the UV/Vis (several seconds) compared to the near-IR (1 min) measurement. In general, this leads to a much better height resolution for the UV/vis vs the near-IR measurements which finally renders an inter-comparison of inferred O_3 profiles difficult, if the UV/vis observations are not smoothed to the same time/height resolution before profile inversion. Inspecting simultaneous O_3 measurements from a total of 13 LPMA/DOAS balloon flights leads us to conclude on the following errors for the O_3-SCD measurements: 1 – 3% for UV/vis DOAS, and up to 5 % for near-IR.

A.1.2. O_3 profile measured by direct-sun versus Limb (UV/Vis) and LPMA/DOAS payload

Further the O_3 profiles measured by direct sun UV/vis observations can also be compared with ozone measured in limb geometry using the novel mini-DOAS instrument (Figure 6.3.2-97 adapted from Weidner et al., 2004). Since for these measurements the same spectral interval (mini-DOAS O_3 is retrieved in the 490-520 nm wavelength interval, DOAS O_3 in the 545-615 nm wavelength range) and hence absorption cross section is used, the small discrepancies mostly arise from the different observation geometries (direct sun versus limb observation with a 90° azimuth and an elevation angle of 0.5°) and horizontal inhomogeneities in the probed ozone field.

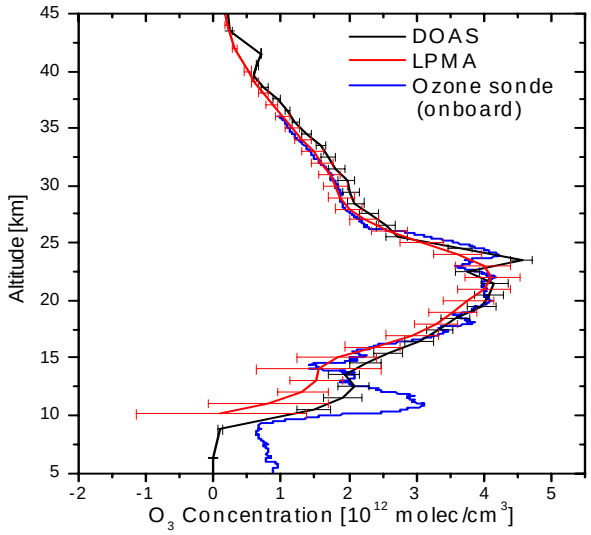

Figure 6.3.2-97. *Comparison of inferred O_3 profiles from (a) Limb observations (filled squares) at an azimuth angle of 90° and elevation angle of 0.5°, (b) the direct sunlight DOAS measurements (open circles), and two ECC ozone sondes (c) deployed on the same gondola (full line) and (d) from the stand-alone launched ECC-sonde for the Kiruna, March 23, 2003 flight.*

A.2. UV/Vis versus ECC

Finally, the measured UV/vis ozone profile can also be compared with ozone measured by an ECC ozone sonde deployed aboard (Figure 6.3.2-98). Again the measured UV/vis and near-IR ozone profiles compare well, in particular in the middle and upper stratosphere. In the lowermost stratosphere where ozone laminae do exist, however, the limited vertical resolution of the optical sensors become apparent, with the near-IR ozone measurement having the coarsest vertical resolution, while the UV/vis observation are able to capture some of the secondary ozone maximum due to its higher sampling rate. Also worth noting is that, by applying the recent update of the ECC sonde pump correction, the optical and chemical ozone measurements agree to better than 5% above 25 km.

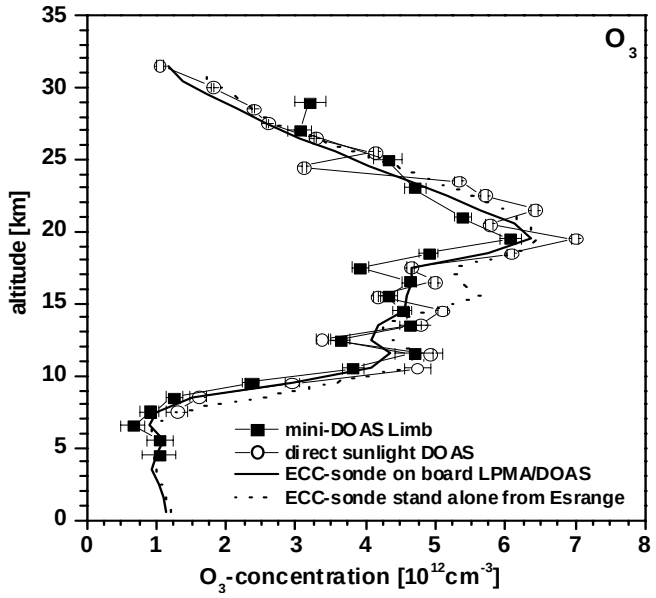

Figure 6.3.2-98. *Comparison of inferred O_3 profiles from simultaneous solar occultation observations by (a) UV/vis DOAS (black line), (b) near-IR LPMA (red line), and (c) by an ECC-sonde for the Kiruna flight on August 21, 2001.*

A.3. O_3 profile inter-comparison with co-located satellite measurementes (POAM III, ILAS I, SAGE III, ODIN/OSIRIS, GOME, SCIAMACHY)

Finally the quality of the UV/vis balloon measurements (as well as of the involved satellite instruments) has also been checked with space-borne measured ozone profiles of collocated satellite overpasses (Lumpe et al. 2002; Sioris et al., 2003; Sugita et al., 2002; Von Savigny et al., 2004, and others). The direct intercomparison of the ozone measured from both platforms, however, is hindered by more or less large spatial and temporal mismatches in both sets of observations. Therefore, in the tight inter-comparison studies performed within the present project, the air mass trajectory matching technique has been, and needs to be employed (Lumpe et al., 2002; Butz et al., 2004; Dorf et al., 2004). If this is done carefully, then the optical ozone measurements from the balloons and from the satellites are generally seen to agree well in the lower stratosphere, but not always in the lowermost stratosphere mainly due to the limited sensitivity of the satellite instruments there. An example of such a comparison is shown in Figure 6.3.2-99, which clearly indicates the reliability of the balloon and satellite measurements and the involved trajectory modeling.

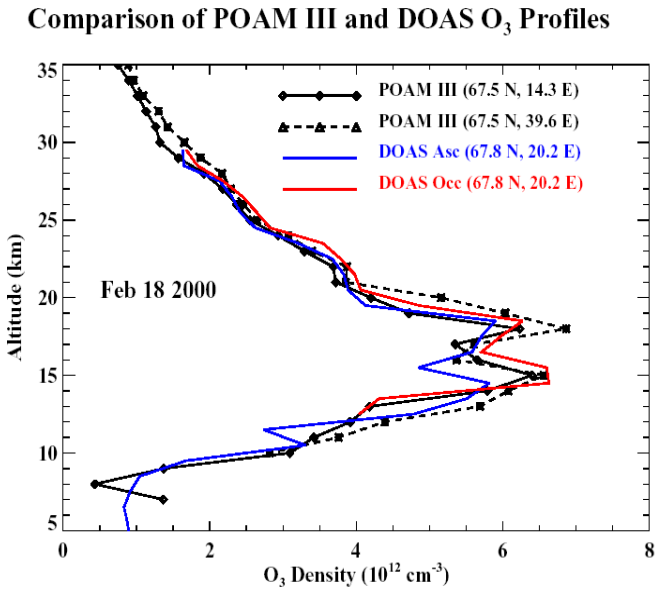

Figure 6.3.2-99. *Comparison of O_3 profiles inferred from simultaneous solar occultation observations by (a) UV/vis DOAS (black line), (b) near-IR LPMA (red line), and (c) by an ECC-sonde for the Kiruna flight on Feb 18, 2000.*

Conclusions

In conclusion, our inter-comparison studies on ozone profiling by balloon-borne UV/visible spectrometry with ozone measured by other means indicate that the optical ozone measurements in the Chappius band very likely provide the most accurate method (± 3%) to measure the ozone profile throughout the stratosphere, however, compared to in-situ measured ozone (from the ECC sonde) it inherently suffers from a limited height resolution. It can be concluded therefore that, the UV/Vis ozone profiling has evolved into a state-of-the-art method.

B. NO_2 profile inter-comparison

As it is shown with the ozone measurements, the validation of the NO_2 measurements involves similar techniques, instruments and tools, except that in some intercomparisons the photochemical variation of NO_2 has to be taken into account.

B.1. NO_2 measurements from the same platform

As before, we first inspect the slant column densities of NO_2 (NO_2–SCD) measured in the UV/vis and near-IR respectively, from aboard the LPMA/DOAS payload, then we inspect the NO_2 simultaneously measured by other means.

B.1.1. NO_2 absorption analysed within the same line of sight (UV/Visible versus IR)

Figure 6.3.2-100 shows the NO_2-SCD simultaneously measured in the 435-485 nm wavelength range and in two micro-windows of the near IR at 2914.36 - 2915.16 $cm^{-1}$and 2944.72-2945.11 cm^{-1} (Dufour et al., 2004). Similar to the ozone inter-comparisons above, the major discrepancy is due to the different sampling rate of both observations, but spectroscopic information (cross section, band strength and line broadening parameters) going into both retrievals are obviously consistent within the given error bars.

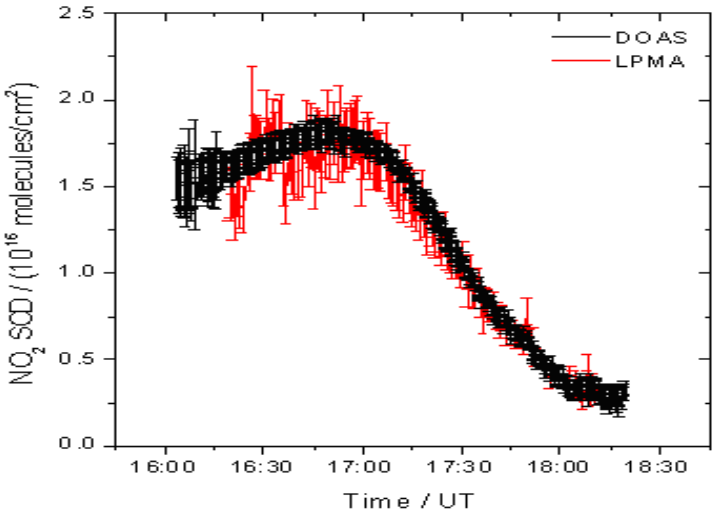

Figure 6.3.2-100. *Measured slant column amounts of NO_2 (NO_2-SCD) as a function of flight time retrieved by LPMA (red) within the 2914.36 - 2915.16 cm^{-1}, and 2944.72 - 2945.11 cm^{-1} wavenumber ranges and DOAS (black) within the 435 - 485 nm wavelength range for the balloon ascent measurements at Kiruna, on Aug. 21, 2001 (adopted from Butz et al., 2004).*

B.1.2. NO_2 profile measured by direct-sun versus Limb (UV/Vis) and LPMA/DOAS payload

Figure 6.3.2-101 inter-compares the NO_2 measured by direct sun spectroscopy and Limb (at an azimuth angle of 90° and elevation angle of 0.5° during the ascent of the LPMA/DOAS payload at Kiruna on March 23, 2003 (Weidner et al., 2004)). Clearly the seen consistency of both measurements demonstrates the reliability of the employed methods, which is particularly promising with respect to the current debate on the amount of NO_2 present in the lowermost stratosphere during polar winter, which is most likely due to artifacts in the employed methods.

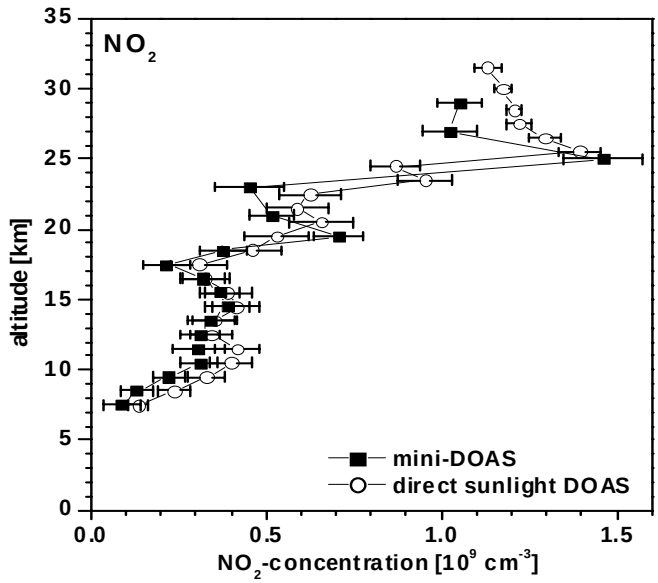

Figure 6.3.2-101. *Comparison of inferred NO_2 profiles from (a) Limb observations (filled squares) for an azimuth angle of 90° and elevation angle of 0.5°, and (b) from direct sunlight DOAS measurements (open circles) during balloon ascent at Kiruna on March 23, 2003 (adopted from Weidner et al. 2004).*

B.2. NO_2 profile inter-comparison with collocated satellite measurementes (POAM III, ILAS I, SAGE III, ODIN/OSIRIS, GOME, SCIAMACHY)

As with ozone, the balloon-borne measured NO_2 profiles were also inter-compared with overpasses of corresponding satellites (i.e., Randall et al. 2002; Sioris et al., 2003; Von Savigny et al., 2004, and others). Here the most direct inter-comparison is between the balloon-borne measurements and the POAM III observations since both sensors measure in the same observation geometry (solar occultation), which avoids the need of photo-chemically correcting the measurements (Randall et al., 2004). Figure 6.3.2-102 clearly demonstrates the consistency of both the balloon and satellite measurements for the observation over Kiruna on Feb. 18, 2000, which for that particular date shows an unusual secondary NO_2 maximum around 25 km. Corresponding to this maximum extremely low N_2O values were measured from aboard LPMA/DOAS, a finding which clearly points to a high in NO_x intrusion from the mesosphere. As for ozone, the inter-comparison also demonstrates that, the satellite is largely insensitive to NO_2 in the lowermost stratosphere.

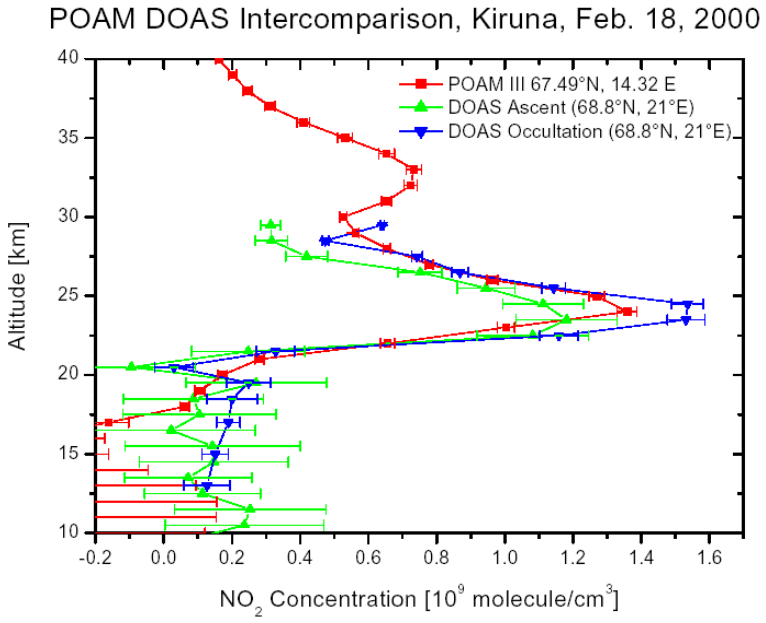

Figure 6.3.2-102. *Comparison of measured NO_2 profiles from (a) POAM III (red line), and (b) from direct sunlight DOAS measurements during balloon ascent (green line) and solar occultation (blue line) over Kiruna on Feb. 18, 2000 (adopted from Randall et al., 2002).*

B.3. Comparison with NO_2 profiles from ground-based instrumentation

Within the present project, the balloon-borne NO_2 profile measurements have also been compared with NO_2 profiles inferred by ground-based measurements in reasonable vicinity of the balloon measurements (Hendrick et al., 2004). Details of this comparison are given in the studies performed within WP 2200.

Conclusions

The studies within the present project clearly demonstrate that throughout the whole stratosphere NO_2 can be measured on a better than ±10 % level, however only if the optical measurements are performed with well defined light path (solar occultation) or accurate RT modeling (SAOZ and limb-DOAS), which excludes uncertainties due to the radiative transfer corrected for T-dependence of the NO_2 absorption cross section photo-chemically corrected for SZA > 88° and for the diurnal variation of stratospheric NO_2. If all these issues are carefully considered, then the UV/vis balloon instruments are able to measure NO_2 profiles on a < ± 5

% precision level, and including uncertainties of the NO_2 absorption cross section, an accuracy of < ± 7 % can be obtained.

C. BrO profile inter-comparison

C.1. BrO measurements from the same platform

As for O_3 and NO_2 the quality of the optical BrO measurements can best be checked by two independent measurements from aboard the same payload. Within the present project, the optical BrO measurements using the solar occultation technique were validated against Limb BrO measurements performed on the LPMA/DOAS payload.

C.1.1 BrO profiles measured by direct-sun versus Limb (UV/Vis) and LPMA/DOAS payload

Figure 6.3.2-103 shows one example of such a simultaneous BrO measurement from two independent sensors (solar occultation vs. Limb) conducted over Kiruna on March 24, 2004 (Weidner et al., 2004). Both measurements agree within the given error bars of each of the measurements, indicating the reliability of both methods.

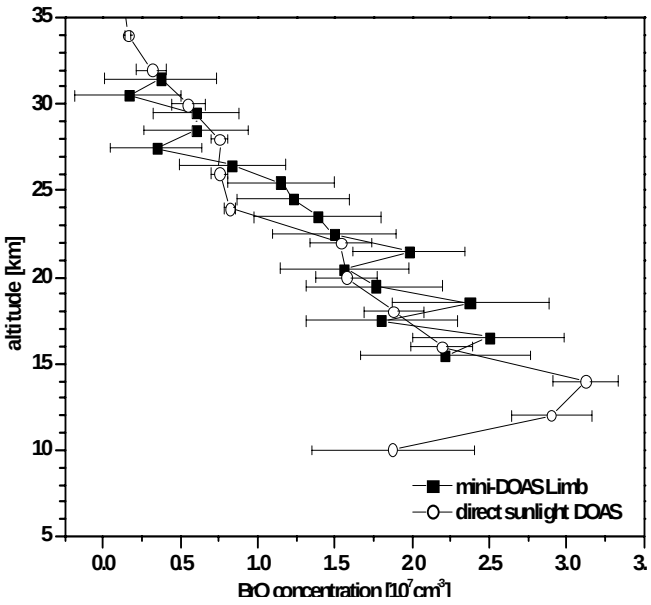

Figure 6.3.2-103. *Comparison of inferred BrO profiles from (a) Limb observations (filled squares) for an azimuth angle of 90° and elevation angle of -1.5°, and (b) from direct sunlight DOAS measurements (open circles) during balloon ascent at Kiruna on March 24, 2004 (adopted from Weidner et al. 2004).*

C.2 BrO profile inter-comparison with co-located ENVISAT/ SCIAMACHY measurements

Within the framework of the project, an inter-comparison study of BrO profile measurements from three different balloon borne sensors (by optical means with the LPMA/DOAS and SAOZ payloads, and by the resonance fluorescence from TRIPLE) with Limb BrO measured by the recently launched ENVISAT/SCIAMACHY satellite has also been started (Dorf et al., 2004). Overall the inter-comparison is promising, in particular above 20 km, but some problems still exist concerning the sensitivity of the SCIAMACHY measurements in the lowermost stratosphere.

Conclusions

According to the discussion above, stratospheric BrO profile measurements by optical means have evolved into a standard state-of-the-art technique within the present project. Recent improvements of the optical method (Aliwell et al., 2002; Harder et al 2000; Weidner et al., 2004) provide compelling confidence that

throughout the whole stratosphere BrO can be measured on ±10 % precision level, however only if the optical measurements are performed with well defined light path (solar occultation) or accurate RT modeling (SAOZ and limb-DOAS), which excludes uncertainties due to the radiative transfer corrected for T-dependence of BrO absorption cross section photo-chemically corrected for SZA > 88° for the diurnal variation of stratospheric BrO.

It is worth noting that for the time being, the major uncertainties in optical BrO measurements come from the uncertainty in the absorption cross section (±10 %), as indicated in Figure 6.3.2-104. Therefore, significant improvement in the accuracy in atmospheric BrO measurements will require a more accurate BrO cross section than presently existing.

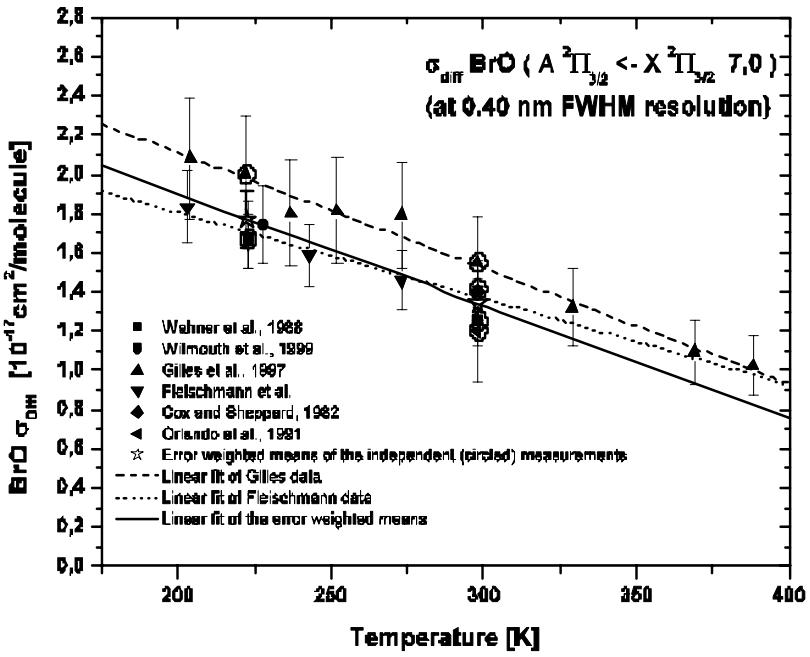

Figure 6.3.2-104. *Compendium of independent BrO cross section measurements in the UV, and the corresponding T-dependence.*

D. IO and OIO measurements

The UV/vis balloon measurements of LPMA/DOAS were also inspected for any signs of absorbing IO and OIO. Both gases could not be detected during the inspected solar occultation data gained from 10 balloon flights, which covered mid- and high latitudes during all season. The Bösch et al., (2003) study leads to the following conclusions, which are widely consistent, but tighter than earlier results (Wennberg et al., 1997, Pundt et al., 1998) on stratospheric iodine, except for the contracting results of the Wittrock et al., (2000) study. The abstract of the Bösch et al. (2003) paper reads as follows:

We report upper limits of lower stratospheric IO (inferred lowest values: 0.10 ppt, 0.07 ppt, and 0.06 ppt at 20, 15, and 12.5 km, respectively) and OIO (inferred lowest values: 0.10 ppt, 0.06 ppt, and 0.04 ppt at 20, 15, and 12.5 km, respectively) inferred from balloon-borne solar occultation UV/visible spectroscopy. The spectra were recorded during a series of Laboratoire de Physique Moléculaire et Applications/Differential Optical Absorption Spectroscopy (LPMA/DOAS) balloon flights that were conducted at different geophysical conditions, i.e., inside the Arctic winter vortex, at mid-latitudes, and at high latitudes in spring, summer, and fall. Photochemical modeling that accounts for the iodine partitioning during the observations allows us to infer upper limits of total inorganic gas-phase iodine (I_y), i.e., I_y (<20 km) of < 0.10 ± 0.02 ppt and <0.07 ± 0.01 ppt, taking into account

and neglecting OIO photolysis, respectively. For the middle stratosphere, the inferred upper limits of total I_y are larger because of the smaller detection sensitivity there. These observations suggest that either much less iodine enters the stratosphere than the amount expected from the stratospheric entry level iodine concentrations (primarily the tropical upper troposphere) or it resides in other minor gaseous species or, eventually, in a nongaseous, i.e., particulate, form in the stratosphere. The implications of our iodine measurements for stratospheric ozone are also briefly assessed using a two-dimensional model. For the assumed loading of 0.1 ppt I_y the modeled ozone reduction was small compared to a model run without iodine, with a maximum decrease of around 1% in mid-latitudes to high latitudes when OIO photolysis is included.

Conclusions

In conclusion, the spectral retrieval exercises conducted within the Bösch et al. PhD thesis clearly indicated that for the setting sun observation from balloon platforms the center-to limb darkening of the solar photosphere needs to be considered in order to minimize the residual structures in the spectral retrieval while the other parameters (i.e. Ring effect, inferred IO) attain reasonable values. If such corrections are not undertaken, fake IO of the order of 1 ppt would have been detected by the LPMA/DOAS payload in the stratosphere.

Balloon data dissimination

Revised balloon profiles of O_3, NO_2, BrO, and OClO from partners 4 and 5 are being made available to scientific community through the www pages of the participating individual groups (http://www.aerov.jussieu.fr/~fgoutail/Flight-List.html andhttp://www.iup.uni-heidelberg.de/institut/forschung/groups/atmosphere/stratosphere/) and from www.ZARDOZ/Nilu.no. CNRS has re-analysed the data from more than 70 SAOZ balloon flights out of 120 over the period 1992-2004.

Main deliverables

- *Quality controlled balloon profile measurements of O_3, NO_2, BrO, OClO and IO*
- *Documentation of balloon data evaluation procedure, data quality and error estimates for the final data set*
- *Web based interface for public access to the created balloon data set and documentation*

WP 3300: GOME data revision

Within WP 3300, consolidated data sets of O_3, NO_2, BrO and OClO column measurements by the Global Ozone Monitoring Experiment (GOME), onboard the ERS-2 satellite since July 1995) have been established and provided for comparison with model predictions (see WP 5000). It is anticipated that the optimised retrieval methods developed/validated for GOME in QUILT will form a basis for application in the next generation of UV-visible space-based sensors (in particular SCIAMACHY on the ENVISAT platform). The GOME data analysis is shared by partners 2, 3 and 5. The status of the relevant QUILT products developed and operationally processed in each institute or available from the GOME Operational Data Processor (GDP) is given in .Figure 6.3.2-15

Table 6.3.2-15. Scientific and operational GOME data products available for the QUILT project. Notes on the notations used in table: All: available over complete life-time of GOME (1995-2004);Web: distributed on the web;Trop: tropospheric product available;NRT: near-real-time product.

Institute / Trace gas	IUP Heidelberg	IUP Bremen	BIRA-IASB	DLR/ESA (GDP)
NO_2	All, Web, trop	All, NRT, trop		All
OClO	All, Web	All, NRT		
BrO	All, Web	All, NRT	All, Web	
O_3				All

Instrument and data product consolidation

GOME is one of several instruments aboard the European research satellite ERS-2 (*Burrows et al.*, 1999). It consists of a set of four spectrometers that simultaneously measure sunlight reflected from the earth's atmosphere and surface in four spectral windows covering the wavelength range between 240 nm and 790 nm with moderate spectral resolution (0.2 - 0.4 nm). The satellite operates in a nearly polar, sun-synchronous orbit at an altitude of 780 km with a local equator crossing time at approximately 10:30 local time. While the satellite orbits in an almost north-south direction the GOME instrument sweeps in the perpendicular east west direction. During one sweep, three individual spectral scans are performed. The corresponding three ground pixels covering an area of 320 km (east-west) by 40 km (north-south) lie side by side (a western, a center and an eastern pixel). The Earth's surface is totally covered within three days, and polewards from about 70° latitude within one day.

From the raw spectra measured by GOME, the slant column density (SCD) is determined using the Differential Optical Absorption Spectroscopy (DOAS) technique [Platt, 1994]. From the inferred differential absorption and knowledge of the absorption cross sections, the SCD of the QUILT-relevant trace species (O_3, NO_2, BrO and OClO) can be determined.

Work on historical satellite data at University of Bremen, University of Heidelberg and BIRA-IASB focused on the homogenisation of the GOME NO_2, OClO and BrO time series.

GOME NO_2 data set consolidation

While instrumental drift is a minor problem for GOME NO_2 retrieval if daily solar measurements are used, the angle dependency of the diffuser plate used for irradiance measurements has a substantial impact on the measurement results.

One possible solution to this problem is to use a fixed solar background spectrum for the complete time series and to apply an offset correction on the slant columns for every day. The approach followed here is to assume that the vertical NO_2 column over an area in the remote Pacific is constant over season and from year

to year, and to derive the offset necessary to force the daily NO_2 columns in this region to the expected value (2.10^{15} molec cm^{-2}). This offset is then subtracted from all GOME NO_2 slant columns of the day (Richter and Wagner, 2001; Richter and Burrows, 2002).

When this correction is applied, the internal consistency of the GOME NO_2 time series is much improved, and comparison with ground-based measurements performed at the stations which are part of QUILT indicates improved accuracy. An example of a typical comparison using QUILT measurements at the Sodankyla station is shown in Figure . The assumption underlying the correction applied however introduces some uncertainties in the GOME NO_2 columns. In particular at high sun, the error can be significant, and first comparisons with ground-based measurements during Antarctic summer indicate that there might be an impact from El-Nino / La-Nina events. If this proves to be right, more sophisticated estimates such as from high-quality ground-based measurements or model simulations could be used as reference over the Pacific to further improve the accuracy of the GOME NO_2 time series.

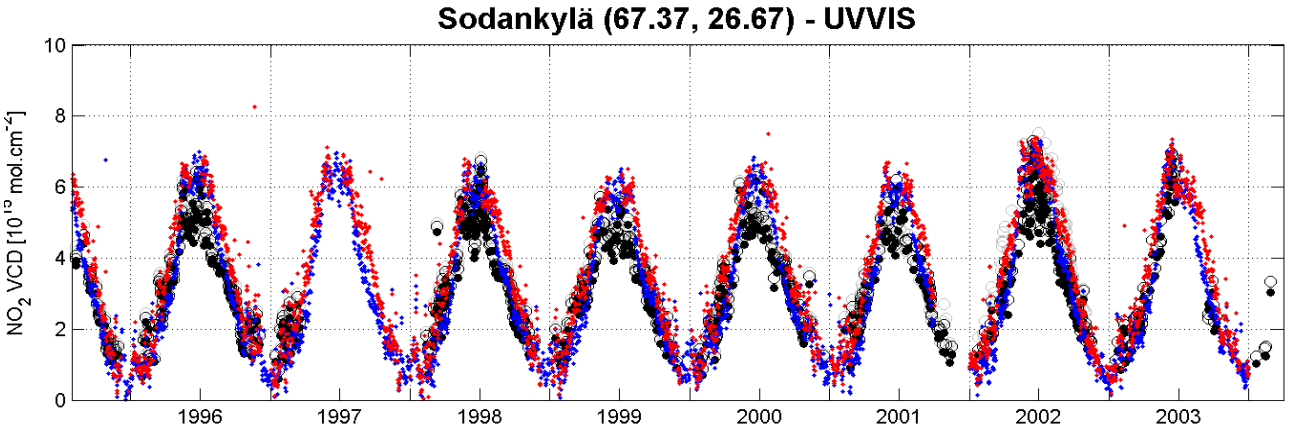

Figure 6.3.2-105. *Comparison between NO_2 total columns derived from GOME and from ground-based DOAS measurements at Sodankyla, Finland, from 1995 until late 2003. Accounting for the NO_2 photochemical variation between mid-morning (GOME) and twilight (ground-based) conditions, excellent agreement is found between satellite and ground-based data sets.*

GOME OClO data set consolidation and model comparison

The main analysis improvement regarding GOME OClO retrieval concerns the treatment of the Ring effect. Because the fitting to OClO differential structures has to be performed using a relatively large wavelength range, it was found that significant errors can be caused due to the wavelength dependence of the Ring effect, if this effect is not properly considered.

One way to account for the wavelength dependence of the Ring spectrum is to include more than one Ring spectrum in the DOAS analysis (Wagner et al., 2002). One Ring spectrum is calculated under the assumption that only Rayleigh-scattering contributes to the elastically scattered light. A second Ring spectrum is calculated assuming that the elastic scattered (or reflected) light originates from scattering on cloud tops or reflection on the (grey) surface of the earth (see Fig. 20). Including both Ring spectra in the DOAS fitting algorithm the portion for which each spectrum contributes for the correction of the Ring effect depends on the specific properties of a GOME observation (especially on the ground albedo and cloud cover). Especially for the GOME OClO analysis, which is applied to a relatively wide wavelength region (364-392 nm) in the UV, this improved method leads to significantly smaller (up to 35%) residual structures and thus smaller fitting errors compared to the standard evaluation.

In several studies the potential of GOME OClO observations for the characterisation of the evolution of stratospheric chlorine activation was demonstrated (e.g. Wagner et al., 2001). Due to its instrument stability and the global coverage it is in particular possible to investigate the onset and ending of the conversion of stratospheric chlorine to active species. During these periods it is interesting to compare the GOME OClO observations to model results in order to test the models ability to correctly describe the respective atmospheric processes.

A comparison between GOME and SLIMCAT OClO data is complicated by several aspects:

- GOME observations are sensitive to extended atmospheric volumes; thus different model values have to be considered for the comparison to a single GOME observation. This is in particular important for a chemically active species like OClO.
- Due to the strong dependence of the OClO photolysis on the solar zenith angle even small temporal differences between the measurements and model results can cause large deviations
- Since OClO observations can only be made at large SZA the latitudinal gradient for GOME observations can become very large and non-linear

All the above described aspects have to be taken into account for a detailed comparison. In a first attempt, OClO data from GOME were compared to SLIMCAT on a daily basis averaged over extended areas (zonal means between 64.5° and 69.5° latitude, see Figure 6.3.2-106). The temporal difference between the GOME observations and the model data is up to about 10 minutes (at 67° N GOME measures at 10:10 local time and is later than SLIMCAT). This should cause systematic smaller values of GOME compared to SLIMCAT.

Despite these limitations the resulting comparison shows a good qualitative agreement with respect to the general temporal evolution (at least for the winter 1999/2000). The onset and ending of the chlorine activation is nearly synchronous in both data sets; also the maxima appear during the same period. In general the GOME data are significantly lower compared to the SLIMCAT data (note the different scales). This can be largely attributed to the points discussed above. Especially during polar night the GOME observations were only possible (SZA < 92°) for the latitudes at the southern edge of the selected area. This will lead to an additional underestimation of the GOME OClO observations since this first comparison exercise also includes SLIMCAT data for SZA > 92°.

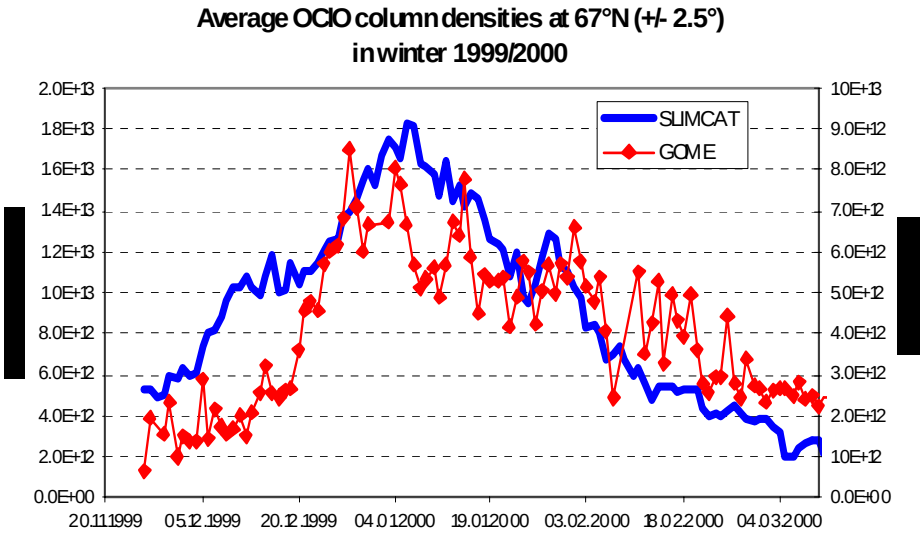

Figure 6.3.2-106. *Comparison of GOME and SLIMCAT OClO VCDs. The general evolution is well described by both data sets; the difference in absolute values (different scales) can be attributed to various shortcomings of this first comparison exercise (see text).*

GOME BrO data set consolidation

As for the NO_2 case, the main problem affecting the accuracy of GOME BrO retrieval is the spectral and angular dependency of the diffuser plate used for irradiance measurements. The impact of this instrumental deficiency is to introduce offsets in the retrieved BrO columns, the size of which depend on the solar spectrum used a reference in the analysis.

Since instrument degradation prevents the use of a fixed solar spectrum for analysis of long time series in the BrO spectral range, the solution adopted to minimise the impact of the diffuser problem is to use an equatorial earthshine spectrum as reference for BrO analyses, assuming that the small stratospheric BrO content above equatorial regions is approximately constant (5e13 molec/cm^2) and therefore can be added as a simple offset correction to the measured differential slant columns. As for NO_2, the internal consistency of the GOME BrO measurements is significantly improved after application of the equatorial offset correction. Comparisons with ground-based measurements (Van Roozendael et al., 2002) especially at the Harestua station (Figure 3.21) also support the reliability of the GOME BrO column evaluations.

As part of the QUILT project, the complete time-series of GOME BrO total columns has been reprocessed at BIRA-IASB using optimal settings, including the addition of a correction for formaldehyde absorption, which was found to be necessary over regions affected by bio-mass burning.

The resulting GOME BrO column data product has been compared to ground-based BrO VCD measurements performed at the Harestua stations in the period from August 2002 until June 2003 (Van Roozendael et al., 2004). To allow adequate matching of satellite and ground-based data, the ground-based BrO columns have been evaluated at noon time using a fixed reference spectrum and airmass factors have been calculated for both nadir and zenith geometries using the same assumptions on the BrO vertical distribution. As can be seen in Figure 3.21, both seasonal and day-to-day variations of the BrO column are captured in the same way by GOME and the ground-based measurements. Preliminary SCIAMACHY results, although more scattered and suffering from a lack of time coverage due to problems with the data distribution are also encouraging.

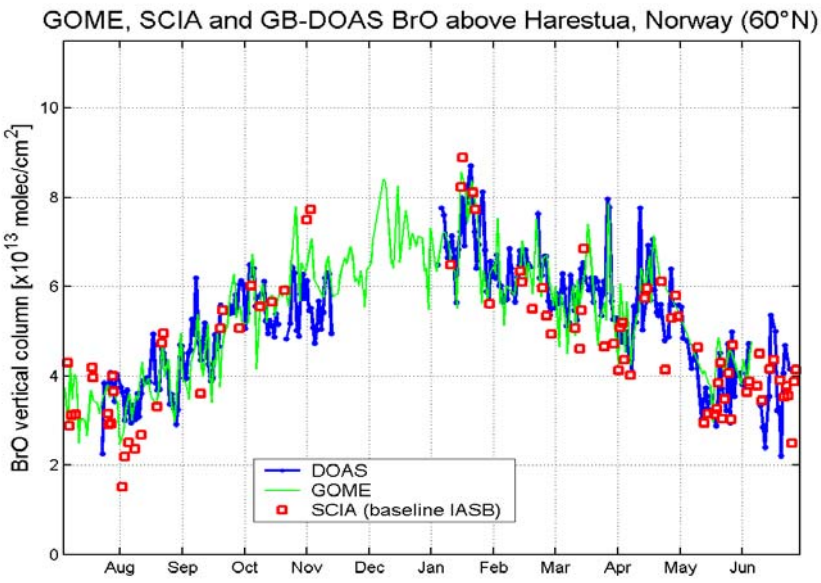

Figure 6.3.2-107. *Comparison of BrO vertical columns derived at Harestua (60°N, 8°E) from GOME, SCIAMACHY and ground-based zenith-sky measurements.*

Satellite data dissimination

The consolidated GOME BrO data produced at BIRA-IASB - at global scale and extracted for the QUILT stations (200 km radius overpasses) - can be downloaded in ASCII format from http://www.oma.be/BIRA-IASB/Molecules/BrO/index.html. Consolidated NO_2, BrO and OClO data retrieved using scientific algorithms from the University of Bremen and the University of Heidelberg can be obtained on the following web-sites:http://www.iup.physik.uni-bremen.de/gome/ ; and http://satellite.iup.uni-heidelberg.de/. In addition, GOME NO_2 data extracted at the University of Bremen for all QUILT stations can be downloaded in ASCII format fromhttp//www.doas-bremen.de/gome_no2_data_quilt.htm.

Main deliverables

- *Homogeneous, quality controlled time series of GOME columns of O_3, NO_2, BrO, and OClO for WP 4000 and WP 5000*
- *Documentation on GOME data evaluation procedures, data quality and error estimates for the final data set*
- *Web based interface for public access to the created GOME data set and documentation*

Socio-economic relevance and policy implication

European countries and the European Union have responsibilities under the Montreal protocol of the Vienna Convention, its amendments and the Framework Convention on Climate Change. Knowledge about the state and evolution of the ozone layer constitutes the basis for negotiations and decisions on the political level concerning the phase-out of ozone depleting substances. Long-term monitoring of chemical indicators of the status of the ozone layer is essential to verify the timely impact of regulations. This is especially important since, in addition to non-compliance, it is now established that there are others threats to the ozone layer: The increasing concentrations of greenhouse gases leads to a cooling of the stratosphere, which progressively will increase the probability for PSC formation

and hence halogen activation. For these reasons, it is essential that there is a strong, independent European scientific effort in stratospheric research. The research carried out within the QUILT WP 3000 contributes to improving the existing capabilities for long-term monitoring from the ground, balloon and satellite of several key-trace species that control the chemical budget of stratospheric ozone. The results of WP 3000 provide observational data sets suitable to assess current 3D models in their ability to reproduce these observations (as demonstrated in WP 5000). This leads to a better understanding of the mechanisms involved in ozone destruction in mid- to high latitude regions, thereby contributing to the knowledge which is necessary to formulate a sound environmental policy that aims at protecting the environment by quantifying chemically-induced ozone loss in the Arctic and at mid-latitudes.

Conclusion

This workpackage has been concerned with the data revision and homogeneisation of UV-visible trace gases measurements carried out by QUILT partners from ground-based stations, balloon-borne instruments as well as scientific data evaluations based on the GOME instrument on board of the ESA ERS-2 satellite platform.

At the end of the QUILT project, the network of ground-based spectrometers counts in total 31 stations all equipped with total ozone and NO_2 measuring zenith-sky spectrometers. Among these stations, 16 also offer capabilities to monitor BrO and (in polar regions) OClO slant columns. In a growing number of sites, additional instruments have been also set up for low elevation bright-sky viewing measurements (MAX-DOAS technique), which enable the simultaneous determination of stratospheric and tropospheric trace gases. In all cases, efforts have been made to produce final consolidated time series of column measurements of O_3, NO_2, BrO and OClO at the various stations based on most recent recommendations for data processing issued after the NDSC Andøya Campaign.

The ballooning groups have conducted similar consolidation and data homogenisation work. Intercomparison exercises already started previously have been continued to verify the overall consistency of the stratospheric trace gases profile measurements obtained with the different balloon instruments (SAOZ, LPMA-FTIR and Heidelberg-DOAS), in both UV-Visible and infrared regions. Resulting consolidated data sets have been made available on the local web-sites which have been linked to the central QUILT web-site.

Within WP 3300, consolidated GOME NO_2, BrO and OClO data sets have been produced over the full lifetime of GOME (1996-2004), and made available respectively on the Bremen, Heidelberg and BIRA-IASB web-sites. In order to assess the reliability of the consolidated data sets, comparisons of the GOME NO_2 and BrO columns with ground-based measurements have been performed by the Bremen University and BIRA-IASB for several stations of the QUILT network.

Examples of scientific studies based on the QUILT consolidated data sets have been given, which complement other more specific investigations presented in other parts of this final report.

References:

Aliwell, S.R., M. Van Roozendael, P.V. Johnston, A. Richter, T. Wagner, D.W. Arlander, J.P. Burrows, D.J. Fish, R.L. Jones, K. Karlsen-Tornkvist, J. C.Lambert, K. Pfeilsticker, and I. Pundt, Analysis for BrO in zenith-sky spectra: an intercomparison exercise for analysis, J. Geophys. Res., 0.1029/2001JD000329, 2002.

Appenzeller C., A. K. Weiss, J. Staehelin, North Atlantic Oscillation modulates Total Ozone Winter Trends, Geophy. Res. Lett., 27, 1131-1134, 2000.

Bogumil, K., J. Orphal and J. P. Burrows: Temperature-dependent absorption cross-sections of O3, NO2, and other atmospheric trace gases measured with the SCIAMACHY spectrometer, ERS-ENVISAT Symposium, ESA-ESTEC, 2000

Bösch, H., C. Camy-Peyret, M. Chipperfield, R. Fitzenberger, H. Harder, C. Schiller, M. Schneider, T. Trautmann, and K. Pfeilsticker, Inter comparison of measured and modeled stratospheric UV/vis actinic fluxes at large solar zenith angles, Geophys. Res. Lett, 28, 1179 - 1182, 2001.

Bösch, H., C. Camy-Peyret, M. Chipperfield, R. Fitzenberger, H. Harder, U. Platt, B. Sinnhuber, and K. Pfeilsticker, Upper Limits of Stratospheric IO and OIO Inferred From Center-to-Limb-Darkening-Corrected Balloon-Borne Solar Occultation Visible Spectra; Implications for Total Gaseous Iodine and Stratospheric Ozone, J. Geophys. Res. 108 (D15), 4455, doi: 10.1029/2002JD003078, 2003.

Burrows, J., M. Weber, M. Buchwitz, V. Rozanov, A. Ladstätter-Weißenmayer, A. Richter, R. DeBeek, R. Hoogen, K. Bramstedt, K-U. Eichmann, M. Eisinger, D. Perner, The Global Ozone Monitoring Experiment (GOME): Mission concept and first scientific results, J. Atmos. Sci., 56, 151-175, 1999.

Butz et al., Inter-comparison of stratospheric O3 and NO2 profiles by balloon-borne UV, vis and near-IR solar occultation and ENVISAT/SCIAMACHY Limb measurements, ACP (in prep.), 2004.

Canty, T., R.S. Salawitch, J.B. Renard, E.D. Reviere, K. Pfeilsticker, M. Dorf. R. Fitzenberger, H. Bösch, R.M. Stimpfle, D.M. Wilmouth, J.G. Anderson, E.C. Richard, D.W. Fahey, R.S. Gao, and T.P. Bui, Analysis of BrO, ClO, and nighttime OClO in the arctic winter stratosphere, J. Geophys. Res., (submitted), 2004.

Dorf et al., Balloon-borne stratospheric BrO measurements: Intercomparison with ENVISAT/SCIAMACHY BrO limb profiles, ACP (in prep.), 2004.

Dufour, G., S. Payan, F. Lefèvre, G. Berthet, M. Eremenko, A. Butz, P. Jeseck, Y. Té, K. Pfeilsticker and C. Camy-Peyret, 4D comparison method to study the NOy partitioning in summer polar stratosphere: Influence of aerosol burden, ACP (submitted), 2004.

EUR 19867, European Research in the Stratosphere 1996-2000, European Commission EUR 19867 – ISBN 92-894-1398-0, 2001.

Fish D. J., H. K. Roscoe, P. V. Johnston, Possible causes of stratospheric NO2 trends observed at Lauder, New Zealand, Geophys. Res. Lett., 27, 3313-3316, 2000.

Gimeno L., P. Ribera, R. Nieto, J. F. Perez,O. Vidal, L. de la Torre, D. Gallego , R. Garcia, E.Hernandez, Imprints of the North Atlantic Oscillation on four unusual atmospheric parameters, Earth Planet. Sci. Lett., 202, 677-692, 2002.

Greenblatt, G. D., J. J. Orlando, J. B. Burkholder and A. R. Ravishankara: Absorption measurements of oxygen between 330 and 1140 nm, J. Geophys. Res., 95, 18577-18582, 1990.

Gurlit, W., H. Bösch, H. Bovensmann, J. P. Burrows, A. Butz, C. Camy-Peyret, M. Dorf, K. Gerilowski, A. Lindner, S. Noel, U. Platt, F. Weidner, and K. Pfeilsticker, The UV-A and visible solar irradiance spectrum: Inter-comparison of absolutely calibrated, spectrally medium resolved solar irradiance spectra from balloon-, and satellite-borne measurements, submitted to ACPD, 2004.

Harder, J. W. and J. W. Brault: Atmospheric measurements of water vapor in the 442-nm region, J. Geophys. Res., 102, 6245-6252, 1997.

Harder, J. W., J. W. Brault, P. V. Johnston and G. H. Mount: Temperature dependent NO2 cross sections at high spectral resolution, J. Geophys. Res., 102, 3861, 1997.

Hendrick, F., B. Barret, M. Van Roozendael, H. Boesch, A. Butz, M. De Mazière, F. Goutail, J.-C. Lambert, K. Pfeilsticker, and J.-P. Pommereau, Retrieval of nitrogen dioxide stratospheric profiles from ground-based zenith-sky UV-visible observations: Validation of the technique through correlative comparisons, ACP, 4, 2867-2904,

2004.

Kurucz, R. L., I. Furenlid, J. W. Brault and L. Testerman: Solar flux atlas from 296 nm to 1300 nm. in Natl. Sol. Obs. Atlas 1, Harvard Univ., Cambridge, Mass., 1984.

Liley J. B., P. V. Johnston, R. L. McKenzie, A. J. Thomas, I. S. Boyd, Stratospheric NO2 variations from a long time series at Lauder, New Zeland, J. Geophys. Res., 105, 11633-11640, 2000.

Lumpe J. D., K. Hoppel, R. M. Bevilacua, E. Browell, W. B. Grant, T. McGee, J. Burris, L. Twigg, E. C. Richard, G. Toon, B. Sen, H. Boesch, R. Fitzenberger, and K. Pfeilsticker, Comparison of POAM III ozone measurements with correlative aircraft and balloon data during SOLVE, J. Geophys. Res., 107, 8316, doi:10.1029/2001JD000472, 2002.

McLinden C. A., S. C. Olsen, M. J. Prather, J. B. Liley, Understanding trends in stratospheric NOy and NO2, J. Geophys. Res., 106, 27787-27793, 2001.

Montzka, S.A., J.H. Butler, B.D. Hall, D.J. Mondeel, J.W. Elkins, A decline in tropospheric organic bromine, GRL, 30, 1826, doi :10.1029/2003GL017745, 2003

Petritoli A., Analisi quantitativa del biossido di azoto in stratosfera e troposfera nella regione della pianura padana mediante misure a rilevamento remoto ed in situ, Ph.D. thesis, Univeristy of Bologna, 2003.

Petritoli A., G. Giovanelli, I. Kostadinov, F.Ravegnani, D.Bortoli, P. Bonasoni, F. Evangelisti, U. Bonafè, F. Calzolari, Tropospheric and stratospheric NO2 amount deduced by slant column measurements at Mt. Cimone station, Adv. Space Res., 29, 1691-1695, 2002

Petritoli, A., G. Giovanelli, P. Bonasoni, I. Kostadinov, F. Ravegnani, D. Bortoli R. Werner, Study of the stratospheric NO2 trend at Mt. Cimone (44°N, 11°E), Italy: evidence of the NAO influence on the trace gas amount, Proceedings of the Quadrennial Ozone Symposium, Christos S. Zerefos, eds., University of Athens 2004, 1015-1016.

Petritoli, A., P. Bonasoni, U. Bonafè, D. Bortoli, F. Calzolari, F. Evangelisti, I. Kostadinov,, F. Ravegnani, G. Giovanelli, Seven Years of stratospheric NO2 Observations from DOAS Zenith Sky Measurements at Mt. Cimone Station (Italy), NDSC symposium, Arcachon (France), 2001.

Randall, C.E., J.D. Lumpe , R.M. Bevilacqua , K.W. Hoppel, E.P. Shettle, D.W. Rusch, L.L. Gordley, K. Kreher, K. Pfeilsticker, H. Boesch, G. Toon, F. Goutail, Validation of Polar Ozone and Aerosol Measurement (POAM) III NO2 Measurements, J. Geophys. Res., 107, 4432,10.1029/2001JD001520, 2002.

Richter, A., and J.P. Burrows, Retrieval of Tropospheric NO2 from GOME Measurements, Adv. Space Res., 29 (11), 1673-1683, 2002.

Richter, A., and T. Wagner, Diffuser Plate Spectral Structures and their Influence on GOME Slant Columns, Technical note presented at the GOME Science Advisory Group, Bremen (pdf-file, 360 kb, http://giger.iup.uni-heidelberg.de/thomas/publications.html), January 2001.

Roscoe, H. K., P. V. Johnston, M. Van Roozendael, A. Richter, A. Sarkissian et al., Slant column measurements of O3 and NO2 during the NDSC intercomparison of zenith-sky UV-Visible spectrometers in June 1996, J. Atm. Chem., 32, 281-314, 1999.

Rothman, L. S., A. Barbe, C. Benner, L. R. Brown, C. Camy-Peyret, et al., The HITRAN Molecular Spectroscopic Database: Edition of 2000 including updates through 2001, J. Quant. Spectrosc. Radiat. Transfer, 2003.

Sioris C. E., Craig S. Haley, C. A. McLinden, C. von Savigny, I. C. McDade, Wayne F. J. Evans, J. C. McConnell, N. D. Lloyd, E. Llewellyn, D. Murtagh, U. Frisk, T. P. Kurosu, Kelly V. Chance, K. Pfeilsticker, H. Bösch, and F. Weidner, Stratospheric profiles of nitrogen dioxide observed by OSIRIS on the Odin satellite, J. Geophys. Res., 108, NO. D7, 4215, doi:10.1029/2002JD002672, 2003.

Sugita, T., T. Yokota, H. Nakajima, H. Kanzawa, H. Nakane, H. Gernandt, V. Yushkov, K. Shibasaki, T. Deshler, Y. Kondo, S. Godin, F. Goutail, J.-P. Pommereau, C. Camy-Peyret, S. Payan, P. Jeseck, J.-B. Renard, H. Bösch, R. Fitzenberger, K. Pfeilsticker, M. von König, H. Bremer, H. Küllmann, H. Schlager, J.J. Margitan, B. Stachnik, G.C. Toon, K. Jucks, W.A. Traub, D.G. Johnson, I. Murata, H. Fukunishi, and Y. Sasano, Validation of ozone measurements from the Improved Limb Atmospheric Spectrometer (ILAS), J. Geophys. Res., 107, 8212, doi: 10.1029/2001JD000162, 2002.

Vandaele, A. C., C. Hermans, P. C. Simon, M. Carleer, R. Colin, S. Fally, M.-F. Mérienne, A. Jenouvrier and B. Coquart: Measurements of the NO2 Absorption Cross-section from 42000 cm-1 to 10000 cm-1 (238-1000 nm) at 220 K and 294 K, J. Quant. Spectrosc. Radiat. Transfer, 59, 171-184, 1998.

Van Roozendael, M., Richter A., Wagner T., Pundt I., Arlander D. W., Burrows J. P., Chipperfield M., Fayt C., Johnston P. V., Lambert J.-C., Kreher K., Pfeilsticker K., Platt U., Pommereau J.-P., Sinnhuber B.-M., Tørnkvist K. K. and Wittrock F., Intercomparison of BrO Measurements From ERS-2 GOME, Ground-Based and Balloon Platforms, Adv. Space Res., 29, 1661-1666, 2002.

Van Roozendael, M., I. De Smedt, C. Fayt, F. Wittrock, A. Richter, O. Afe, First validation of SCIAMACHY BrO columns, in Proc. Second Workshop on the Atmospheric Chemistry Validation of ENVISAT (ACVE-2), Frascati, Italy, 3 – 7 May, 2004

Wagner T., Wittrock F., Richter A., Wenig M., Burrows J.P. and Platt U., Continous monitoring of the high and persistent chlorine activation during the Arctic winter 1999/2000 by the GOME instrument on ERS-2, J. Geophys. Res., 0.1029/2001JD000466, 21 September 2002.

Wagner, T., C. Leue, K. Pfeilsticker, U. Platt, Monitorimg the stratospheric chlorine activation by Global Ozone Monitoring Experiment (GOME) OClO measurements in the austral and boreal winters 1995 through 1999, J. Geophys. Res., 106, 4971-4986, 2001.

Wagner, T., K. Chance , U. Frieß , M. Gil , F. Goutail , G. Hönninger , P.V. Johnston , K. KarlsenTørnkvist , I. Kostadinov , H. Leser , A. Petritoli , A. Richter, M. Van Roozendael , U. Platt, Correction of the Ring effect and I 0 effect for DOAS observations of scattered sunlight, 1st DOAS workshop, Heidelberg, 2001.

Weidner, F., H. Bösch, H. Bovensmann, J. P. Burrows, A. Butz, C. Camy-Peyret, M. Dorf, K. Gerilowski, W. Gurlit, U. Platt, C. von Friedeburg, T. Wagner, and K. Pfeilsticker, Balloon-borne Limb profiling of UV/vis skylight radiances, ozone and nitrogen dioxide: Technical set-up and validation of the method, ACPD (submitted), 2004.

Weiss A. K., J. Staehelin, C. Appenzeller, N. R. P. Harris, Chemical and dynamical contributions to ozone profile trends of the Payerne (Switzerland) balloon soundings, J. Geophys. Res., 106, 22685-22694, 2001.

Yokouchi, Y., D. Toom-Sauntry, K. Yazawa, T. Inagaki, T. Tamaru, Recent decline of methyl bromide in the troposphere, Atmos. Environ., 36, 4985-4989, 2002.

Zhou S., A. J. Miller, J. Wang, J. K. Angell, Trends of NAO and AO and their association with stratospheric processes, Geophys. Res. Lett., 28, 4107-4110, 2001.

6.3.3 WP 4000: Modelling Case Studies

This WP focused on specific, short-term modelling studies aimed at obtaining a better understanding of key processes that control stratospheric ozone. The 'case studies' investigated here complemented and supported the longer term 'trend' studies of WP 5000.

WP 4100: NO_2, IO short term modelling studies

U-Heidelberg analysed results from their balloon flights and derived new upper limits for the abundance of IO and OIO [*Boesch et al., 2002*]. As the total stratospheric inorganic iodine loading (Iy) is unknown, and therefore a free parameter in models, these observations can be compared with models to derive a value of Iy. This has been done and the results suggest that the Iy loading of the stratosphere may only be around 0.1 pptv. Furthermore, recent laboratory work has indicated that the species OIO may not photolyse. There is still a lack of certainty in the observational and kinetic database for iodine. Nonetheless, these balloon results have been used by UNIVLEEDS to compare with model calculations, and to constrain long-term simulations of the stratosphere.

UNIVLEEDS added a description of stratospheric iodine chemistry to the chemistry module of the SLIMCAT 3D CTM. This model contains the Iy species I, IO, OIO, HI, HOI, $IONO_2$, and IBr. The model also contains CH_3I as the Iy source gas. This scheme permits full 3D simulations of stratospheric iodine. However, given the large uncertainty in the chemistry of stratospheric iodine, which means it is necessary to perform many sensitivity tests, and the likely importance of iodine in the mid-latitude lower stratosphere, which requires long simulations, it was decided the best approach was initially to run the SLIMCAT CTM as a 2-D latitude-height model. To do this the SLIMCAT chemistry module was coupled to the isentropic 2D dynamical-radiative model of Kinnersley [1996]. This produced an efficient tool for performing a large number of sensitivity tests of this new chemical scheme.

The 2D model was integrated from 1970 until 2000. Time-dependent scenarios for halogen-containing source gases and other species (i.e. CH_4, N_2O, CO_2) were specified from scenario A3 of WMO [1999]. The loading of stratospheric aerosol was also taken from a dataset prepared for WMO [1999]. As the model calculates its own circulation using heating rates based on the model trace gas fields, small changes in e.g. O_3 can cause dynamical feedbacks which complicate the interpretation of the model results. Therefore, to allow us to diagnose the chemical effects of iodine cleanly, three 2D model runs were done over the last 6 years of the 30-year runs with fixed trace gas fields in the radiation scheme. One of these runs did not contain iodine. Two runs were performed with Iy=0.1 pptv - with and without OIO photolysis.

The effect of iodine on the calculated zonal mean distribution of ozone is shown in Figure 6.3.3-106. The changes are confined to the lower stratosphere below about 50 hPa; above this altitude the effect of iodine is minor and in the troposphere all of the model iodine is assumed to be in the form CH_3I. As Iy is released from its assumed source (CH_3I) rapidly it is relatively more important in the lowermost stratosphere. Overall, the impact on O_3 of including 0.1 pptv of Iy in the model is small. For the run which includes photolysis of OIO, the largest O_3 decreases of around -1% occur in the mid-high latitude spring near 300 hPa. The corresponding decrease in autum is around 0.6%. As well as these mid-high latitude changes, the model also predicts a decrease in O_3 of around 0.8% in the tropics just above the tropopause. When the photolysis of OIO is switched off the

calculated O_3 decreases are smaller everywhere and the maximum loss in the high latitude spring is 0.8%. These results are published in *Boesch et al*. [2002].

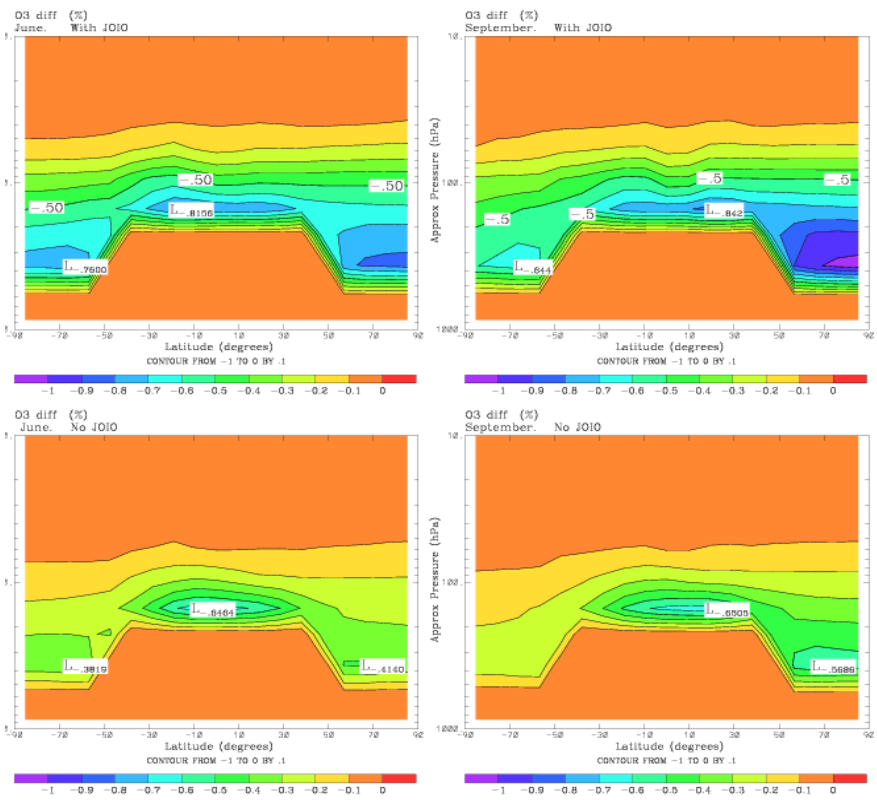

Figure 6.3.3-106. *Differences in zonal mean lower stratospheric O_3 for 1999 conditions between 2D model runs which included 0.1 pptv Iy compared to runs with no iodine for (a) June (including J_{OIO}), (b) September (including J_{OIO}), (c) June (including J_{OIO}), and (d) September (including J_{OIO}). The solid line indicates the location of the tropopause assumed in the 2D model.*

Next, the constant loading of 1 pptv Iy was included in long 3D model runs with observed trends in chlorine and bromine source gases. We investigated the impact of the Iy on the calculated column O_3 trend due to the other halogens and found the effect to be very small in the middle-latitudes (Figures 6.3.3-107 and 6.3.3-108).

Figure 6.3.3-107. *Differences in zonal mean O_3 for 2/11/1999 between 3D model run which included 1 pptv Iy compared to a run with no iodine.*

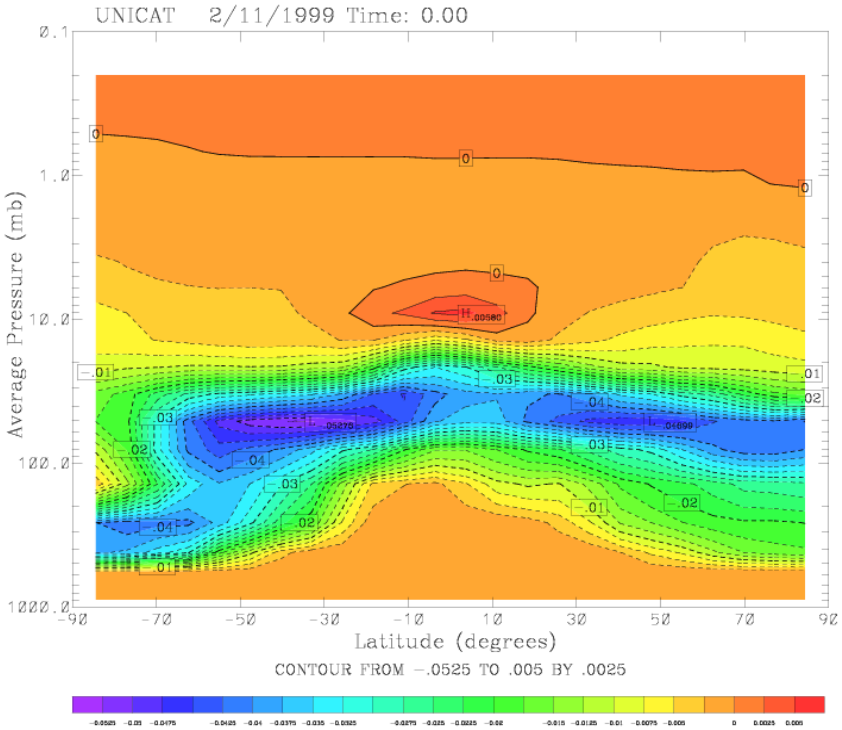

Figure 6.3.3-108. *Differences in zonal mean column O_3 for 1999 conditions between 3D model runs which included 1 pptv Iy compared to a runs with no iodinel.*

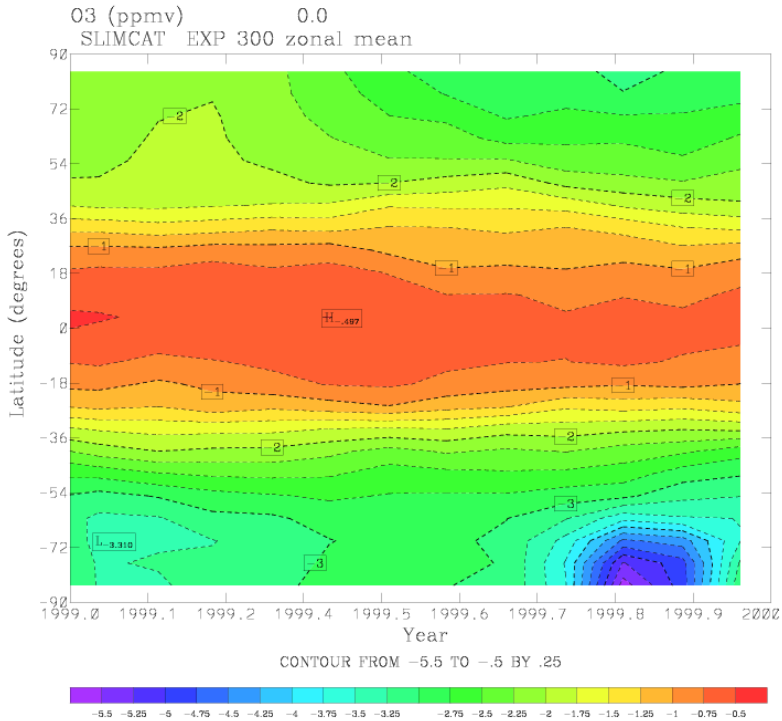

To study the relative efficiency of iodine for polar O_3 depletion a series of box model runs were done. This box model used the same chemistry scheme as the SLIMCAT 3D CTM and the final O_3 values for a range of simulations are shown in Table 6.3.3-16. These values can be used to work out the relative efficiency factors of bromine and iodine relative to chlorine. For Bry the efficiency (a local alpha factor) is ~89 while for iodine it is 178. This illustrates the potential importance of Iy for O_3 loss on a molecule-for-molecule basis.

Table 6.3.3-16. *Final values of O_3 (ppmv) for a series of Arctic box model runs at 50 hPa from November to March. The initial O_3 value was 2.5 ppmv. The final O_3 values are given as a function of Iy (pptv), Cly (ppbv) and Bry (ppytv).*

Iy=0				Iy=1				Iy=2			
Bry /Cly	**2.6**	**3.1**	**3.6**	Bry /Cly	**2.6**	**3.1**	**3.6**	Bry /Cly	**2.6**	**3.1**	**3.6**
10	1.61	1.46	1.33	**10**	1.56	1.42	1.28	**10**	1.52	1.37	1.24
15	1.48	1.33	1.20	**15**	1.43	1.29	1.15	**15**	1.38	1.24	1.11
20	1.36	1.21	1.08	**20**	1.31	1.16	1.03	**20**	1.26	1.12	0.98

Comparison of GOME NO_2 with SLIMCAT 3D CTM

UNIVLEEDS collaborated with UHB and UHEID to compare results from the SLIMCAT 3D CTM with GOME observations of NO_2, BrO and OClO in a quantitative way. Code was added to the SLIMCAT model to provide daily output of these species and the points of local GOME observations. The model was run from 1995 until 2003.

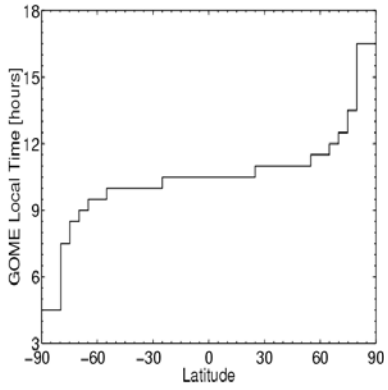

Figure 6.3.3-109. *Local time of the model output as a function of latitude, corresponding to the local time of the GOME measurements. (The temporal resolution of half an hour corresponds to the longitudinal resolution of the model of 7.5°.)*

The GOME instrument on-board the ERS-2 satellite is in a sun synchronous orbit. GOME thus measures at a constant local time, which needs to be taken into account when GOME measurements of species with a significant diurnal cycle (e.g., NO_2, BrO, OClO) are compared with models. In order to allow a direct comparison between GOME measurements and calculations from the SLIMCAT 3-D chemical transport model (CTM), the SLIMCAT model was modified to produce output of selected trace gases at the appropriate GOME local time. Figure 6.3.3-109 shows the local time of the model output as a function of latitude, according to the local time of GOME measurements.

GOME local time output was generated from two SLIMCAT model runs from October 1996 until February 1998. The difference between the two model runs is the treatment of the sulfate aerosol surface area, which has an important impact on the partitioning of reactive nitrogen compounds and thus on stratospheric chemistry in general. One of the model runs uses sulfuric acid mixing ratios, as calculated from a two-dimensional model (`standard run'). The other model run uses sulfuric acid mixing ratios that were reduced by a factor of 3 compared to the standard run, which is in better agreement with observed aerosol surface areas for the late 1990s. Both model runs were performed with a horizontal resolution of 5° latitude by 7.5° longitude.

For result of these model calculations, Figures 6.3.3-109 and 6.3.3-110 show a comparison of NO_2 vertical calculated by the model and observed by GOME for the two sites of Bremen (53°N) and Ny-Ålesund (79°N). The most striking feature of this comparison is the presence of an offset of about 1-2 x 10^{15} molecules/cm^2 between the observed and modelled NO_2 column for Bremen, which is largely absent for Ny-Aalesund. This is most likely due to tropospheric NO_2 at Bremen and much smaller amounts of tropospheric NO_2 at Ny-Ålesund. However, the analysis of the model calculations is still ongoing.

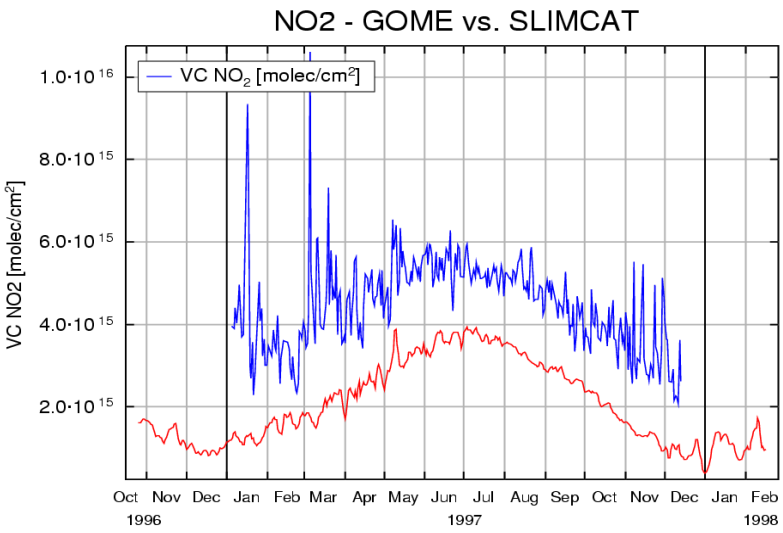

Figure 6.3.3-109. *A comparison of NO_2 vertical column densities from GOME measurements (blue) and the SLIMCAT model (red) at the location of Bremen. The model run is the `standard run' (see text) with model output at the corresponding local times of the observations. An offset between observations and model calculations is evident, which can be attributed to tropospheric NO_2.*

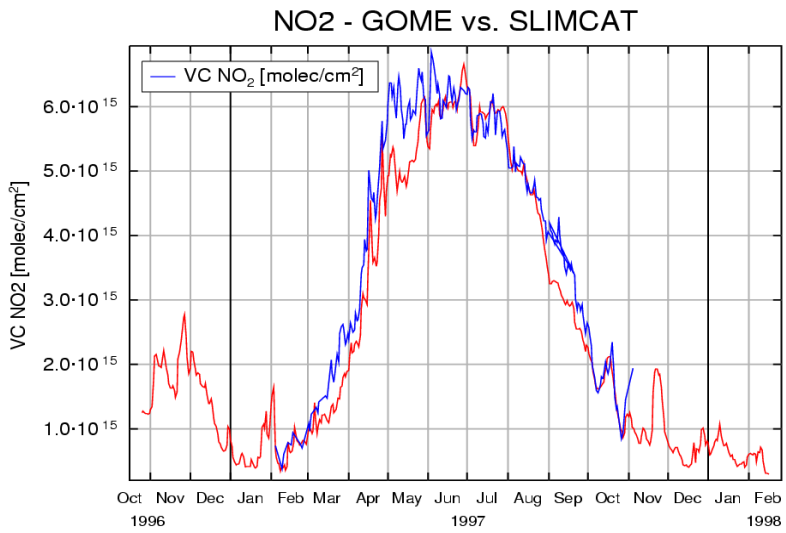

Figure 6.3.3-110. *Same as 6.3.3-109, but for Ny-Ålesund. The offset between observations and model is largely absent, indicating only very low amounts of tropospheric NO_2.*

Summary

We have studied the impact of iodine species on stratospheric ozone at both mid and high latitudes. Although on a molecule-for-molecule basis Iy species are efficient at destroying ozone, studies with a reasonable Iy loading of 0.1 pptv so only a very small¨effect on ozone, although the effect is largest in the very low-stratosphere. Overall it seems as Iy is not important for ozone depletion.Comparisons of model and observed NO_2 columns shows that the model peforms well in reproducing the diurnal cycle, in agreement with many previous studies.

Main deliverables

- *Comparison of the observed and seasonal diurnal variations in NO_2 with a 3D model.*
- *Comparison of observed and modelled abundances of IO.*
- *Updated assessment of the role of iodine in the chemistry of the lower stratosphere and O_3 depletion.*

WP 4200: Ozone Loss Studies

Work package 4200 was modified to focus on a comparison of one CTM (TM5) with GOME retrievals. The assessments of Arctic O_3 chemical loss and impact on lower latitudes was performed in WP 5300.

Validation of GOME O_3 profiles

In the first phase of this work package, SRON validated the improved model of Hasekamp and Landgraf [*Hasekamp and Landgraf, 2001, 2002; Landgraf et al., 2001; Hasekamp et al., 2004*] for ozone profile retrieval from GOME measurements with more then 750 ozone sonde measurements at different geo-locations. Table 6.3.3-17 gives an overview of the sonde stations used for the validation in the period 1996-1998.

For the validation it is essential to keep in mind that for an ill-posed problem like ozone profile retrieval from UV backscattered sunlight, it is in principle not possible to retrieve the complete ozone distribution in the probed atmosphere. Only that part of the profile can be retrieved about which information is present in the measurement. This means that we can only obtain smoothed profiles from GOME radiance measurements. Figure 6.3.3-111 shows a typical retrieval result. Besides a retrieved profile from a GOME observation, the figure also shows a collocated sonde measurement smoothed to the same vertical resolution as the retrieved profile. To illustrate the smoothing effect of the retrieval the non-smoothed sonde profile is also depicted. From the figure it appears that GOME is well capable to provide information about ozone in the lower stratosphere and troposphere. However, fine scale structures are clearly filtered out.

In Figure 6.3.3-112 the retrieved ozone concentration at 15 km altitude is compared in a time series with corresponding sonde profiles at Hohenpeissenberg, Germany, from spring 1996 to spring 1999. The daily and seasonal variability of the sonde profiles can be clearly seen in the smoothed sonde profiles as well, although the smoothing of the retrieval damps them. This indicates the utility of this kind of measurement for long-term trend studies of stratospheric ozone.

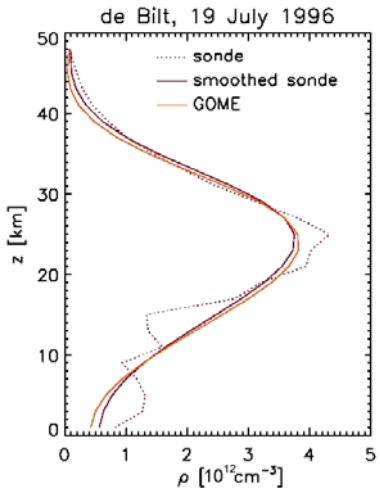

Figure 6.3.3-111. *Comparison of a retrieved ozone profile (orange line) from a GOME measurement from July, 19, 1996, with a coincident sonde profile over De Bilt, the Netherlands. The solid purple line indicates the sonde profile smoothed to the vertical resolution of the retrieval, whereas the dotted line indicates the sonde profile on the vertical model grid.*

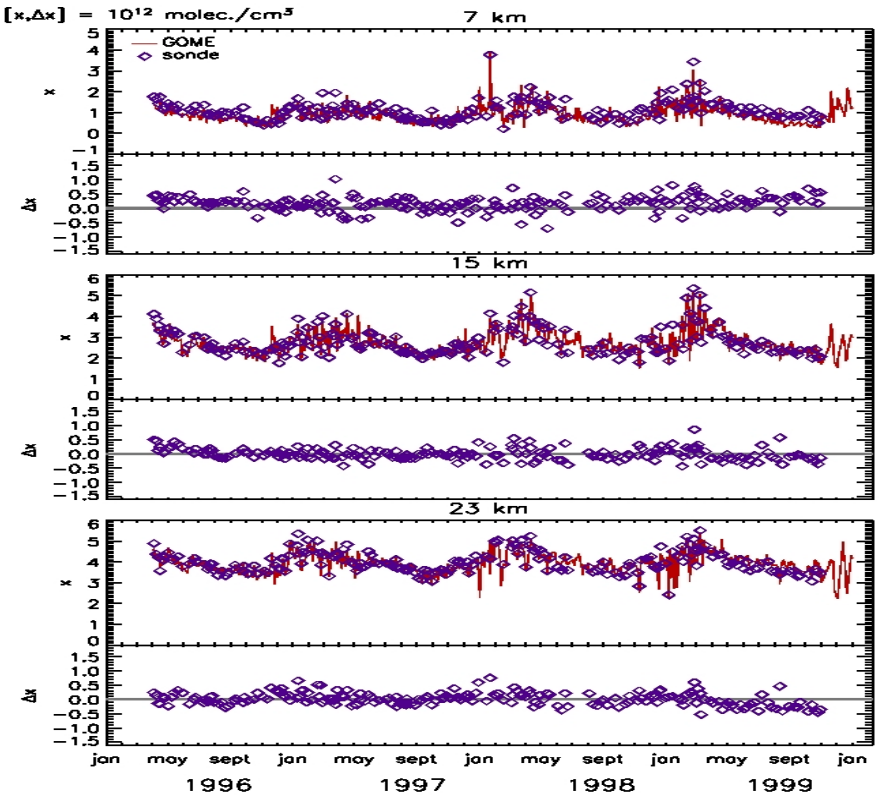

Figure 6.3.3-112. *Upper panel: Time series comparison of GOME profiles with sonde profiles over Hohenpeissenberg, Germany at 7, 15 and 23 km altitude. The purple squares represent the smoothed sondes. For validation this line should be compared with the red line indicating the retrieved ozone concentration. Lower panels: differences between the smoothed sonde and the retrieval concentration.*

The major conclusions from the comparison of the retrieved profiles for all stations as listed in Table 4.2 lead to the following results. An excellent agreement between GOME and sonde measurements was found at middle and high latitudes, both for the measured profile shape and variability. Within the tropics there exist small biases in the GOME O_3 profiles: tropospheric O_3 is slightly underestimated and stratospheric O_3 is overestimated, both by about 5-10 %. This bias does not affect the measured O_3 variability. These differences are an indication for potential biases in the forward model of the retrieval algorithm, although clouds, reduced sensitivity of the spectral measurements to the lower atmosphere and subpixel variability also play a role. Nevertheless, it was established that the achieved accuracy is sufficient to validate a chemical transport model.

Table 6.3.3-17. Sonde stations used for the validation of the GOME ozone profile including the number of collocations found with sonde measurements as well as the total number of measurements for the period spring 1996 to the end of 1998.

Station	(longitude,latitude)	Sonde-TM5
Sondankyla	(26.1°E, 67.3°N)	6-177
Sapporo	(141.3°E, 43.1°N)	40-426
Lerwick	(1.2°W, 60.1°N)	9-89
Wallops Island	(75.5°W, 37.9°N)	57-398
Churchill	(94.1°W, 58.8°N)	26-286
Tateno	(140.1°E, 36.1°N)	58-411
Edmonton	(114.1°W, 53.6°N)	55-439
Kagoshima	(130.6°E, 31.6°N)	35-371
Goose Bay	(60.34°W, 53.5°N)	37-316
Naha	(127.7°E, 26.2°N)	28-305
Legionowo	(21.0°W, 52.4°N)	64-491
Nairobi	(36.8°E, 1.3°S)	17-298
Lindenberg	(14.1°E, 52.2°N)	58-461
Ascension	(14.4°W, 7.9°S)	26-299
De Bilt	(5.2°E, 52.1°N)	64-493
Samoa	(170.6°W, 14.3°S)	29-243
Praha	(14.5°E, 50.0°N)	61-498
Laverton	(144.8°E, 37.9°S)	28-265
Hohenpeissenb.	(11.0°E, 47.1°N)	154-477
Macquarie Isl.	(159.0°E, 54.5°S)	17-409
Payerne	(6.6°E, 46.5°N)	197-432

Comparison of GOME and TM5 model results

In the second phase of the work package a comparison of TM5 model results with the GOME measurements was made. The TM5 model is a chemical transport model (CTM), i.e. wind fields that are obtained from a different source (ECMWF) are used to calculate transport of chemical species. This version of TM5 used a single O_3 tracer version based on the Cariolle scheme [*Cariolle and Deque, 1986; McLinden et al., 2000*]. It calculates O_3 variations as a function of temperature, in situ O_3 concentrations and O_3 columns above the model location. The O_3 dependence on these parameters was derived from a full-chemistry 2-D stratospheric chemistry model. The single tracer model is capable of simulating large-scale stratospheric O_3 chemistry. It is not suited to simulate tropospheric chemistry very well, especially close to the surface. The TM5 model was run with 33 vertical levels up to 60 km altitude. The period that was simulated was 1996-1998 on a global $2^o \times 3^o$ resolution.

Figure 6.3.3-9 shows the modelled and measured O_3 concentrations at 15 km altitude for Payerne, Switzerland. Note that the model bias for the lower stratosphere has been removed. There is an excellent agreement between modelled and measured variability, indicating that the model is well suited to simulate extratropical lower stratospheric O_3 variability. This agreement between modelled and measured variability was also found for other middle and high latitudes stations (also in the Southern Hemisphere). In addition, it was also found that the model bias was considerably smaller for the tropical stratosphere. Considering that the

tropical and mid-latitude stratosphere re coupled by the Brewer-Dobson circulation this provides an important clue for the explanation of the model bias.

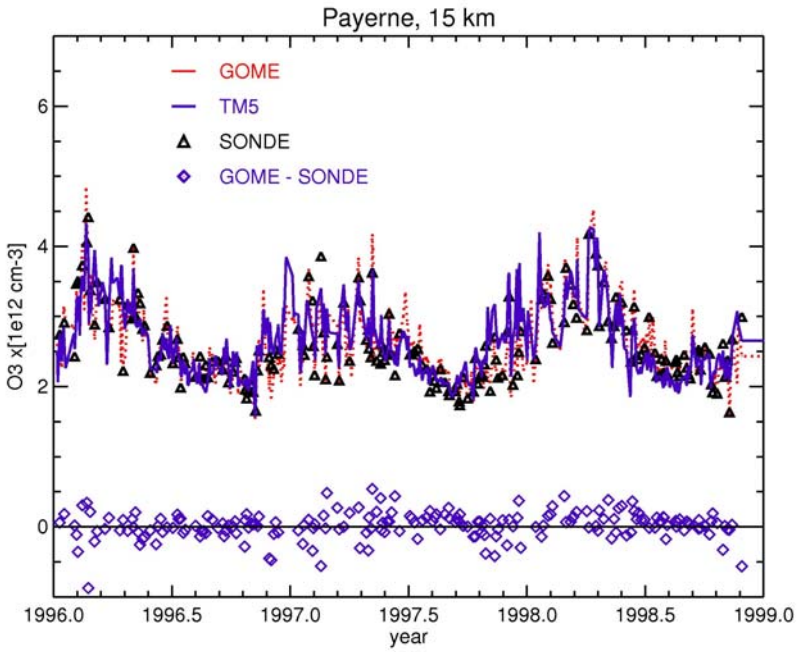

Figure 6.3.3-9. *GOME O_3 concentrations at 15 km altitude for Payerne, Switzerland (red line) and the corresponding (smoothed) TM5 O_3 concentrations at the GOME pixel (blue line) and sonde concentrations (black diamonds). Indicated are also the differences between GOME and sonde measurements (blue diamonds). For convenience the TM5 simulation results have been scaled such that the mean of the GOME concentrations equals the mean of the TM5 concentrations.*

The GOME sub-pixel variability was also studied with the TM5 model, which had been identified as a possible explanation for the differences between GOME and sonde measurements. Due to the large pixel size (960×80 km) it was expected that there might be a considerable amount of O_3 variability within this pixel and which complicates the validation of the GOME measurements with the sondes. The model results showed a significant amount of O_3 variability in the lower stratosphere and troposphere (up to 50% of the differences in between GOME and the sondes). It can be expected that there is even more variability than what was determined from the model results due to the inability of the model to simulate tropospheric O_3 chemistry. Although the GOME-TM5 comparison improved by taking the sub-pixel variability into account, the differences between GOME and TM5 only reduced by up to 20%, which is much less than the actual measured differences. There may be two explanations: clouds and tropospheric O_3, which is not accurately represented by TM5, but it is currently unclear how much each process may explain the existing differences.

The last part of the GOME-TM5 comparison was made for a latitude cross-section from North to South pole along 170°W (April-December 1996). The results provided a more consistent picture on the model biases, especially the lower stratospheric one. There was a clear latitudinal dependence of the bias with more O_3 in the lower stratosphere at middle latitudes and less O_3 in the tropical lower stratosphere. It was also established that the bias was confined tot the stratosphere below 30 km. It was therefore concluded that this bias was related to a too fast meridional stratospheric transport: O_3 production predominantly occurs in the tropical stratosphere, and is being transported towards higher latitudes by the Brewer-Dobson circulation. Thus, when transport is too fast, there is not enough accumulation of O_3 in the tropical stratosphere and too much accumulation of O_3 in the mid-latitude stratosphere. This is a known problem of chemistry-transport models and thus also significantly affects modeled stratospheric O_3 concentrations.

The results of the GOME-TM5 comparison have been written up in an article which is to going to be submitted [*de Laat et al., 2004*].

Summary

An O_3 profile retrieval algorithm for GOME measurements was validated against O_3 sonde measurements. The GOME O_3 profile measurements were in agreement with the O_3 sonde measurements. A comparison with CTM (TM5) model simulated revealed several biases, the most significant one being a stratospheric O_3 bias due to too fast stratospheric transport in the model.

Main deliverables

- *Comparison of a CTM (TM5) with GOME retrievals*

6.3.4 WP 5000: Model and data interpretation

This work package uses a combination of models and observations to study the long-timescale (i.e. multiannual) variability and trends of the key species NO_2, BrO and OClO. These long-term studies build on the shorter-term case studies of WP 4000 (especially WP 4100).

WP 5100: NO_2, BrO, OClO variability

Applied methodology and scientific achievements

A major aim of QUILT was to establish new, validated time series of ground-based observations of column NO_2, BrO and OClO (see WP 3000). Another aim was the improvement of 3D chemical models in response to studies performed in e.g. WP4000. Given these improvements in the observations and models we then compared the new observations with up-to-date simulations. The results for column NO_2, BrO and OClO are shown in Figure 6.3.4-114 - Figure 6.3.4-116 respectively

For NO_2 (see Figure 6.3.4-114) the model overestimates the column at high northern latitudes (e.g. Ny Alesund and Harestua). This is likely due to too large NO_y through strong descent in the lowermost stratosphere in the ERA-40 analyses used to force this new run. In general the agreement at middle latitudes is reasonable. However, using the model as a 'transfer standard' it is possible to shown that the column NO_2 observations at nearby stations are quite different. For example, around 1995 the observations at Mt Cimone are much larger than the model while for Jungfraujoch they agree. This may indicate tropospheric pollution in the Mt Cimone data, which is ignored in the model.

Comparisons of the differential slant column density (DSCD) for BrO are shown in Figure 6.3.4-115. The model, which is constrained by source gas loadings which yield about 21 pptv of Bry in the late 1990s, generally reproduces the magnitude of the observations well, although there are quite large differences at Tenerife where the observations show large variations than the model. These larger variations are similar to the model fields at high latitudes. It appears that the model tracer gradients in the subtropics might be too weak (due to excess transport in the analysed winds or low resolution) and this translates into low variability).

Observations of OClO are limited and Figure 6.3.4-116 just shows comparisons for Harestua and Neumayer. It is still difficult to draw quantitative conclusions for this species, but the model tends to capture the magnitude of the Arctic observations but overestimate the slightly large Antarctic observations.

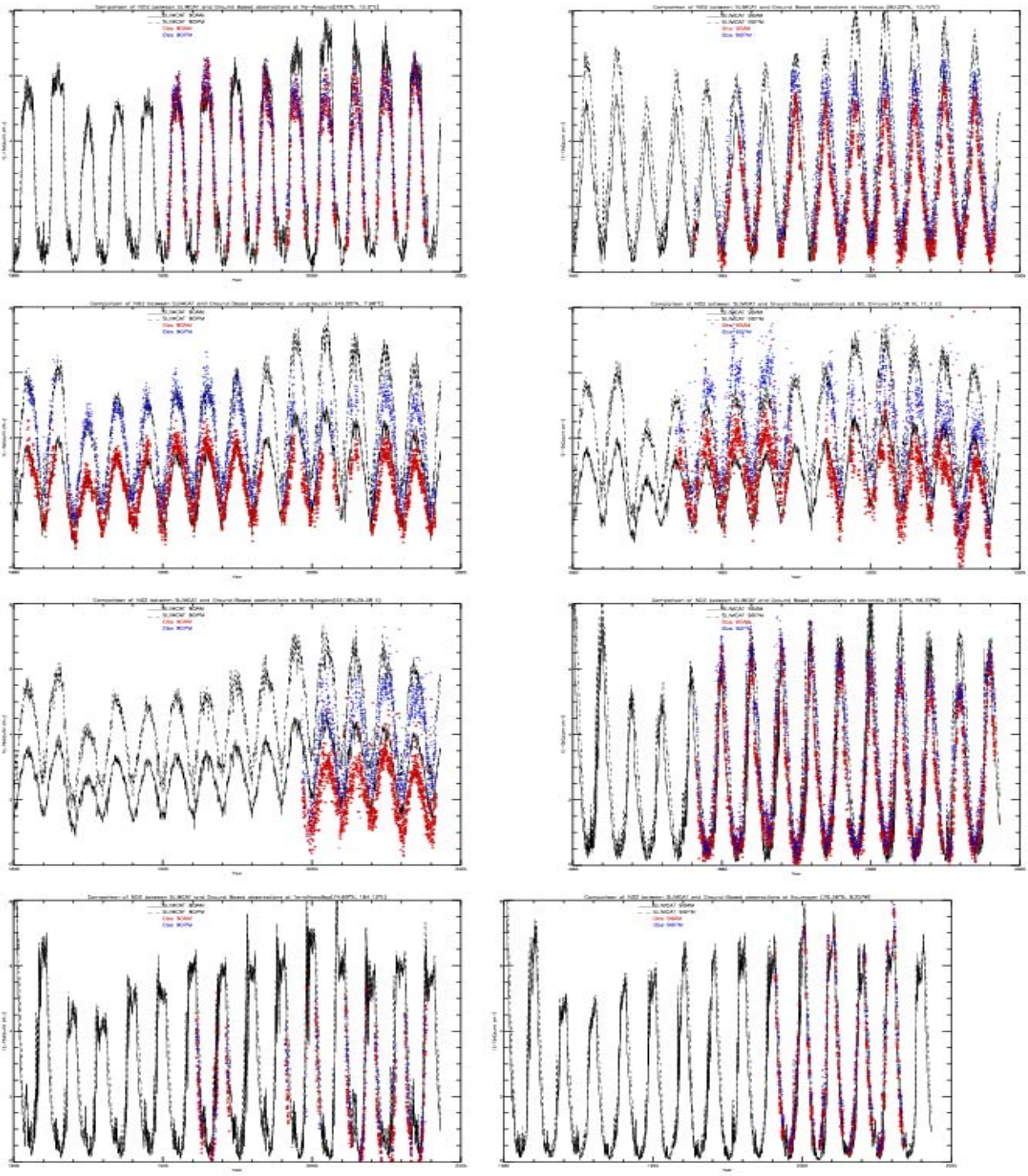

Figure 6.3.4-114. *Comparison of groundbased vertical column observations of NO_2 at 8 stations with calculations from the UNIVLEEDS SLIMCAT 3D CTM. The observations are shown for 90° am (red) and pm (blue). The model results are the lines for same times (am solid, pm dashed)*

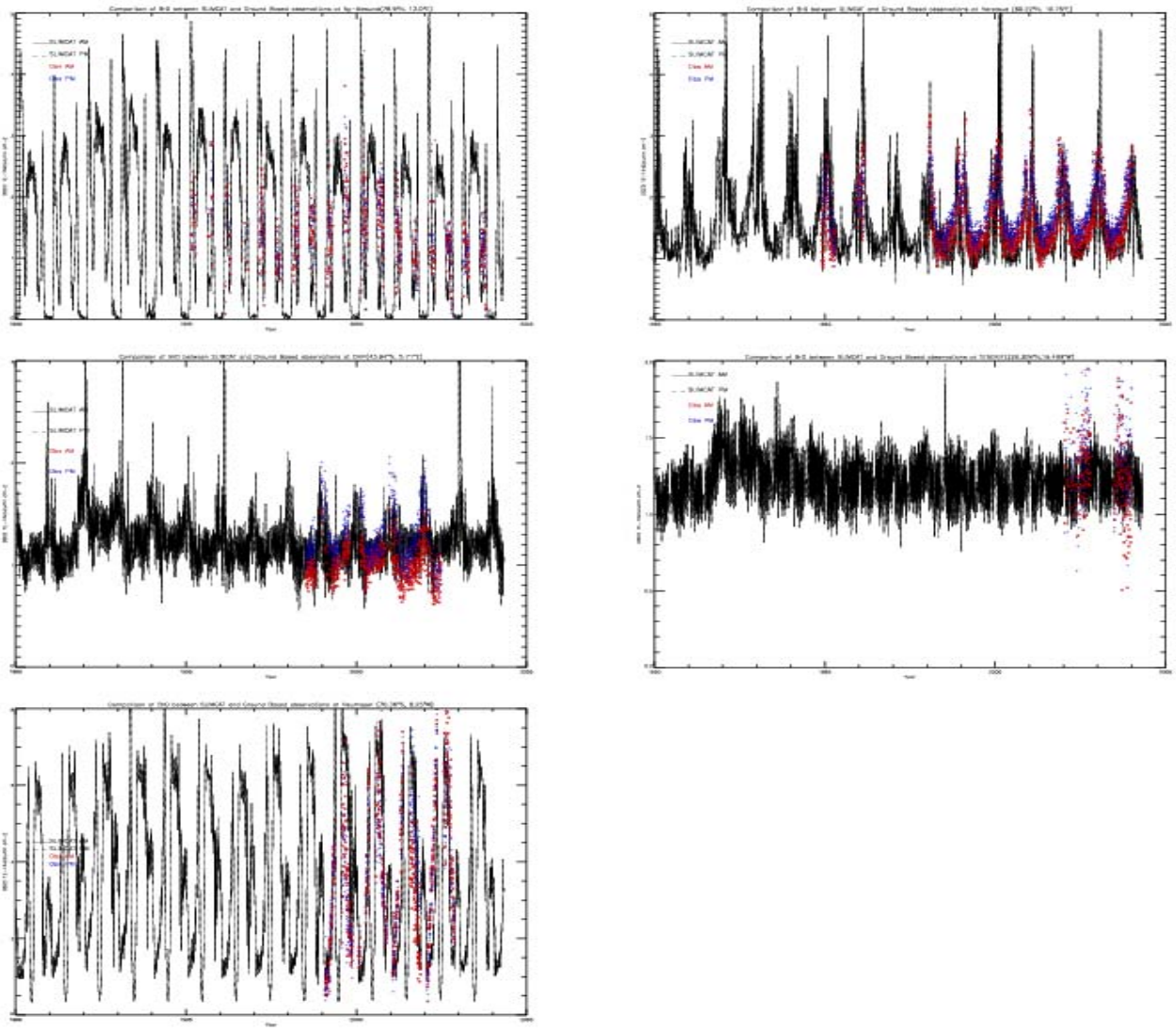

Figure 6.3.4-115. *Comparison of groundbased differential column observations of OClO at 5 stations with calculations from the UNIV-LEEDS SLIMCAT 3D CTM. The observations are shown for 90°–80° am (red) and pm (blue). The model results are the lines for same times (am solid, pm dashed). The model is converted to a slant column using the AMFs of: 5.3 at 80°, 22 at 90° in mid lats and polar summer, and 15.3 at 90° in polar winter.*

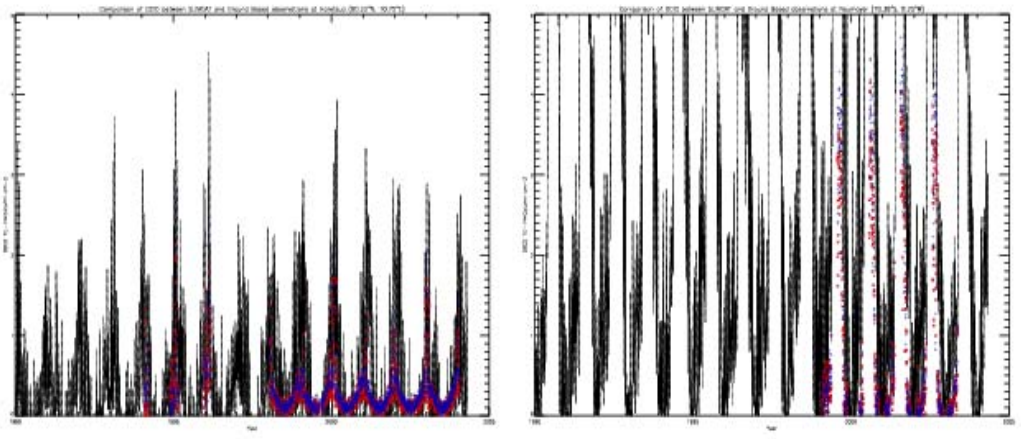

Figure 6.3.4-116. *Comparison of groundbased slant column OClO at 2 stations with calculations from the UNIVLEEDS SLIMCAT 3D CTM. The observations are shown for 90o am (red) and pm (blue). The model results are the lines for same times (am solid, pm dashed).*

Summary

The new QUILT validated time series of ground-based data (WP3000) have been compared with 3D CTM results. The model output acts as a transfer standard and shows large differences in column NO_2 measured at nearby stations - probably indicating tropospheric pollution at one site. At high latitudes the model overestimates column NO_2 due to strong transport in the ECMWF analyses. The BrO comparisons are consistent with a current stratospheric loading of around 21 pptv, although the model does not reproduce the sub tropical observations well. There is an inconsistency in the OClO comparisons: The model captures the magintude of the Arctic observations but overestimates the Antarctic ones.

WP 5200: NO_2 and BrO trends

Recent work at Lauder, New Zealand has indicated that there is a significant increasing trend in stratospheric NO_2 of around 6%/decade, which exceeds that expected from the increase in the source gas N_2O. It is important to confirm that this Lauder trend is representative of other locations and to understand the causes of this trend.

BAS have a fairly long record (since 1991, just before the large decrease due to Mt Pinatubo eruption) of Antarctic NO_2 observations from two site sites closely located (Faraday and Rothera). Figure 6.3.4-117 shows the recent retrievals of the am/pm NO_2 vertical column from this site. A trend has been applied to the summer data (when the NO_2 column is largest and the variability is small). This is shown in Figure 6.3.4-118 and indicates a positive trend of around 7.6%/decade, i.e. similar to Lauder, but based over a shorter time record. First comparisons of this dataset have been performed with UNIVLEEDS simulations (Figure 6.3.4-119). The basic model captures the observed annual cycle and some interannual variability. However, careful analysis is needed to verify the model variations are robust (e.g. the change in 1999 may be linked to changes in the UKMO assimilation system) before we can make conclusive statements on the trend.

Figure 6.3.4-117. *Observed times series of column NO_2 from the BAS station at Faraday/Rothera (65S/67S).*

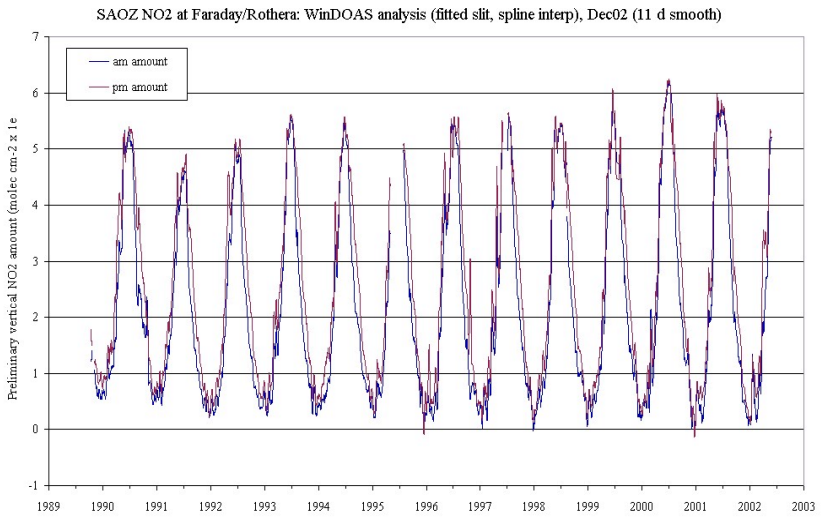

Figure 6.3.4-118. *NO_2 vertical column densities in summer at Faraday/Rothera. Also indicated is the result of a fitted trend of 0.76%/year (black circles).*

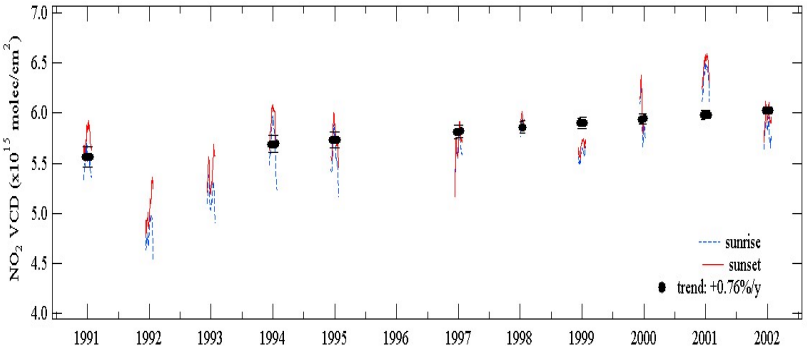

Figure 6.3.4-119. *Comparison of BAS NO_2 column observations at Faraday/Rothera with results from the UNIVLEEDS SLIMCAT 3D CTM for 1996 to 2002.*

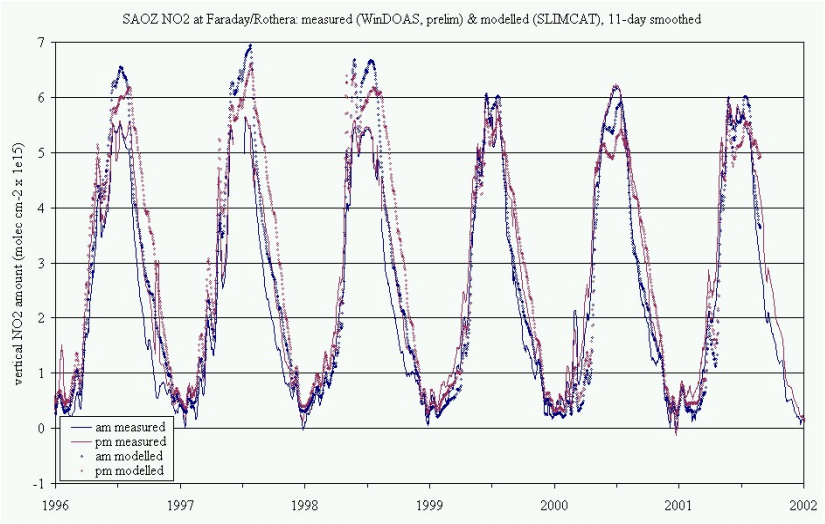

UNIVLEEDS have performed a number of runs with the SLIMCAT 3D CTM to study the cause of these observed trends. A basic model run (Run 311) was performed from 1989-2002 forced by ECMWF analysed (ERA40 until 1999 and then operational). The model had a full chemistry scheme. Boundary conditions for source gases (e.g. N_2O, CH_4, CFCs) were taken from *WMO [2003]*. The source of stratospheric NOy is N_2O which is increasing at around 3%/decade. Therefore, a similar model run (run 313) was done but with constant (1989 conditions) tropospheric N_2O.

Figure 6.3.4-120 compares the modelled NO_2 column at Lauder from runs 311 and 313 with ground-based observations. In general, the 3D model does an excellent job in reproducing the observed diurnal (am/pm) and seasonal variations (see WP 4100). Furthermore, the difference in column NO_2 between the two runs is relatively small compared to the increase in NO_2 from 1992 due to the decay of Pinatubo aerosols.

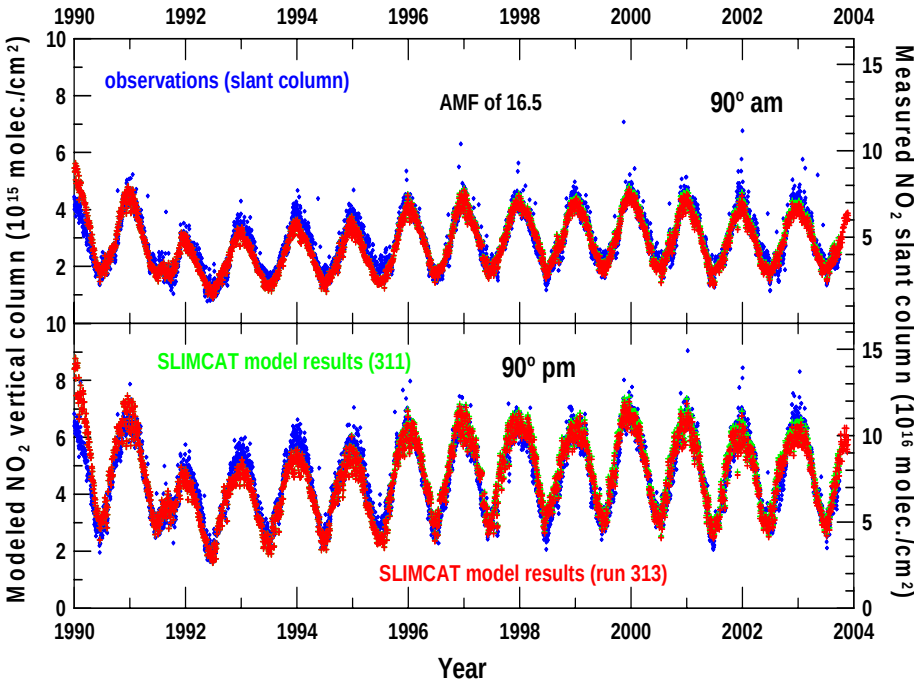

Figure 6.3.4-120. *Comparison of observed (NIWA) and modelled (SLIMCAT) column NO_2 at Lauder, New Zealand.*

The NO_2 trend from the two model runs, and the comparison with observations, have been quantified by applying the NIWA trend model (i.e. same model used for past analysis of observed time series). The trend model includes a linear term, QBO, solar cycle, El Nino term and offset annual cycle. For this work the trend model was also applied to the observations over the same modelled period (1/7/1990-30/9/2003). The results are shown in Table 6.3.4-18. For the model the trend model was also applied to column N_2O and NO_y.

Table 6.3.4-18. Calculated trends (%/decade) in NO2, NOy and N2O from two SLIMCAT model runs for morning (am) and evening (pm) twilight observations. Also include are the estimated trends from Lauder observations..

	Observed		**Model** (with N_2O trend – 311)		**Model** (without N_2O trend – 313)	
	AM	**PM**	**AM**	**PM**	**AM**	**PM**
NO_2	8.9 ± 0.4	7.8 ± 0.4	12.3 ± 3.3	9.9 ± 2.6	9.7 ± 3.3	7.5 ± 2.6
NO_y			-5.0 ± 2.3	-5.2 ± 2.2	-7.5 ± 2.3	-7.6 ± 2.2
N_2O			3.5 ± 0.3	3.5 ± 0.3	0.4 ± 0.3	0.4 ± 0.3

For N_2O the difference between the model trend from run 311 and 313 equals 3%/decade - i.e. the imposed N_2O trend in the surface mixing ratio. The fact that the N_2O trend in run 313 is not zero is a measure of the contribution of other factors (e.g. change in tropopause height) to this trend. The difference in NOy trend between runs 311 and 313 is around 2.5/%. This is less than the imposed N_2O trend indicating a feedback which reduces the impact of increased N_2O on NOy. In the absence of a forced N_2O trend the modelled NOy trend is around -7.5%/decade (with only a small am/pm difference as expected). This decrease in the NOy column could be due to an increase in tropopause height which also leads to the N_2O increase. The difference in NO_2 trend between run 311 and 313 is around 2.5%/decade - i.e. similar to the NOy trend difference. This value, the model's estimate of the direct effect of the N_2O trend on NO_2, is small compared to the overall modelled trend of 9.9/12.3 %/decade in run 311 and the observations of 8.9/7.8%/decade. This suggests the observed NO_2 trend is larger than can be explained directly by N_2O alone. However, the full model, with e.g. halogen, O_3, T trends, does capture the magnitude of the observed trend.

Summary

3D model runs have been performed to look at the observed long-term trend in groundbased NO_2 at sites such as Lauder, NZ. Over the period 1990-2003 the basic model does produce a trend similar in magnitude to the the observations of around 8%/decade over this time. The observed trend is clearly larger than the observed trend of 3%/decade in the NOy source gas, N_2O. There is a large contribution of decreasing aerosol loading during this period. However, the model agreement with the observed trend is also due to a 'dynamical' trend in the model NOy column (i.e. a trend which is present even in a run with constant NOy) and related to a change in the altitude of the NOy profile (e.g. change in tropopause height).

WP 5300: Ozone Loss Variability

The objective of this work-package is a better understanding of the stratospheric ozone depletion and an evaluation of its inter-annual variability.

As already done during previous winters [*Goutail et al, 1999, 2004*], CNRS-SA quantified the total ozone reduction inside the vortex during the winter of 2001/2002, 2002/2003 and 2003/2004. The analysis was based on the total ozone measurements of the Arctic SAOZ network from which the contribution of transport has been removed using the 3D CTM REPROBUS model.

CNRS-SA also compared experimental results since 1993/1994 to 3D CTM multi-annual simulations in order to verify the ability of models to reproduce the ozone loss in a variety of meteorological conditions (cold vortex early in the sea-

son with little sunlight or at the opposite, cold and persistent vortex until April, etc.) and chlorine loading.

Location of the instruments:

The data of the eight SAOZ UV-visible spectrometers located north of 60°N were used for this study. The location of the instruments is shown in Table 6.3.4-19

Table 6.3.4-19. Location of SAOZ Arctic stations.

Location	Country	Location	Property
Ny-Alesund	Spitzbergen	79 N, 12 E	NILU
Thule	Greenland	77 N, 68 W	DMI
ScoresbySund	Greenland	70 N, 2 W	CNRS/DMI
Zhigansk	East Siberia	67 N, 123 E	CNRS/CAO
Sodankyla	Finland	67 N, 27 E	CNRS/FMI
Salekhard	West Siberia	67 N, 67 E	CNRS/CAO
Harestua	Norway	60 N, 10 E	BIRA

Experimental and Model results

Winter 2001/2002:

Meteorological conditions:

The temperature at 475 K was below T_{NAT} from mid-December to early January (Fig. Figure 6.3.4-121). Otherwise, the temperature was warm. There was only few possibilities for PSC occurrences, during two periods as indicated on Figure Figure 6.3.4-123 (top), one in mid-December and one around January 10. That winter was a rather "warm" winter. The final warming occurred in early March.

Figure 6.3.4-121. *ECMWF minimum temperature in the Arctic at 475 K during the 2001/02 winter.*

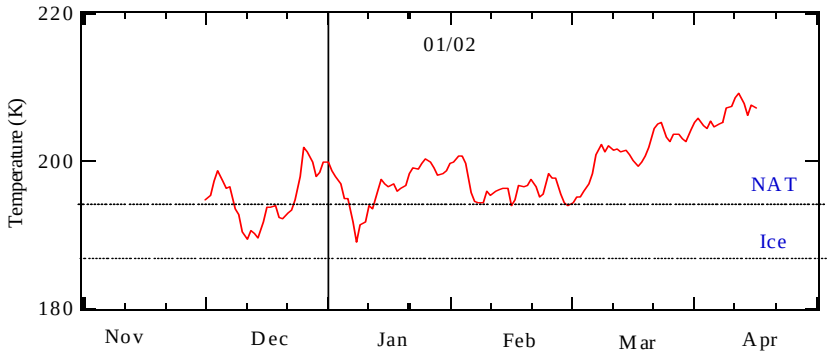

The vortex formed in December 2001 and persisted until early April (Figure 6.3.4-122). At that date, two lobes of the vortex were well separated (Figure 6.3.4-122, right).

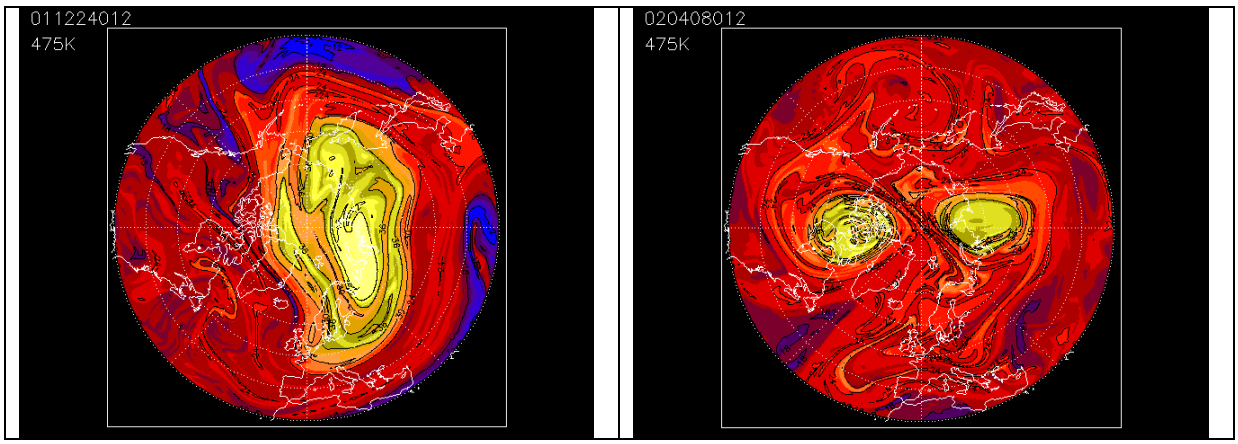

Figure 6.3.4-122. *Mimosa (Contour advection model) potential vorticity map at the 475K isentropic level. Red: low PV (outside vortex), yellow: high PV (inside vortex). Left:Dec 24, 2001; Right: April 8, 2002*

Experimental results:

Two periods of O_3 reduction are observed (Figure 6.3.4-123), one around mid-December and one in mid-February/early March. During that period the loss was at a rate of 0.25% per day. The cumulative loss at the end of the winter is 10 % which corresponds to ~ 46 DU.

Figure 6.3.4-123. *Bottom: Cumulative total ozone loss during winter 2001/02 from SAOZ network. Top: possible surface area of PSC at 475K*

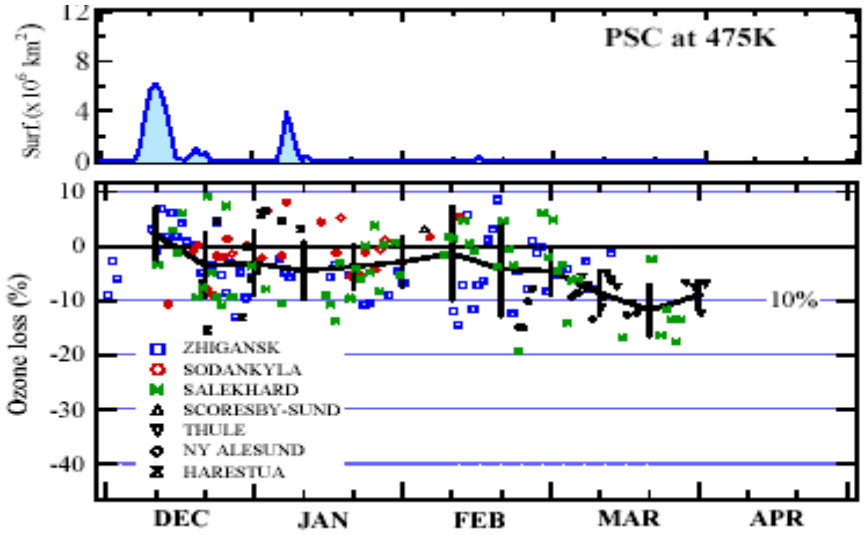

Model results:

The ozone loss simulated by two 3D CTM – Reprobus and SLIMCAT - has been studied. The ozone loss from the model is obtained using the difference between two consecutive run, one with ozone considered as a passive tracer and one with full photochemical reactions.

Reprobus:

During that "warm" winter Reprobus simulates a cumulative ozone loss of 8%, quite similar to the experimental results (Figure 6.3.4-124). Ozone decreases very slowly from December to end of February and almost half of the loss occurred in

March. In addition, Reprobus simulates more ozone loss above Zhigansk (Eastern Siberia) than above all the other stations. This is more difficult to see in the experimental data due to the larger dispersion.

Figure 6.3.4-124. *Reprobus cumulative total ozone loss during winter 2001/02 above SAOZ stations.*

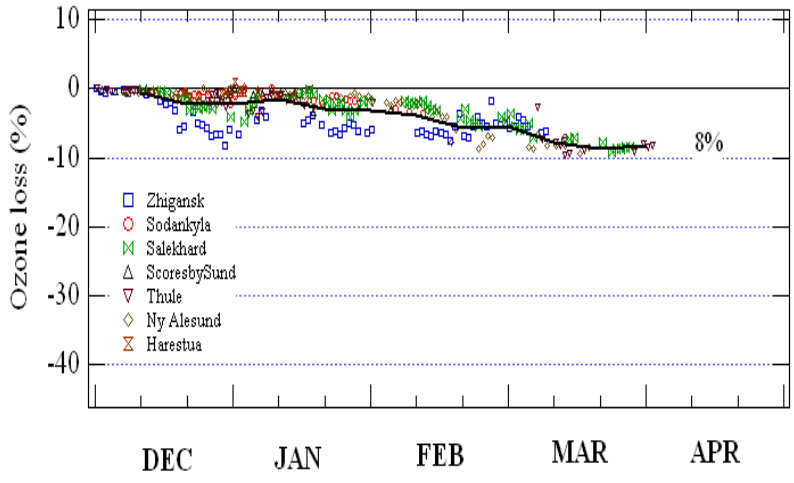

Slimcat:

During that "warm" winter Slimcat also simulates a small cumulative ozone loss of 6 %, quite similar to the experimental result obtained at the end of February (Figure 6.3.4-125). Ozone is decreases slowly from December to end of February. In accordance with the Reprobus results, Slimcat also simulates more ozone loss above Zhigansk (Eastern Siberia) than above all the other stations.

Figure 6.3.4-125. *.Slimcat cumulative total ozone loss during winter 2001/02 above SAOZ stations.*

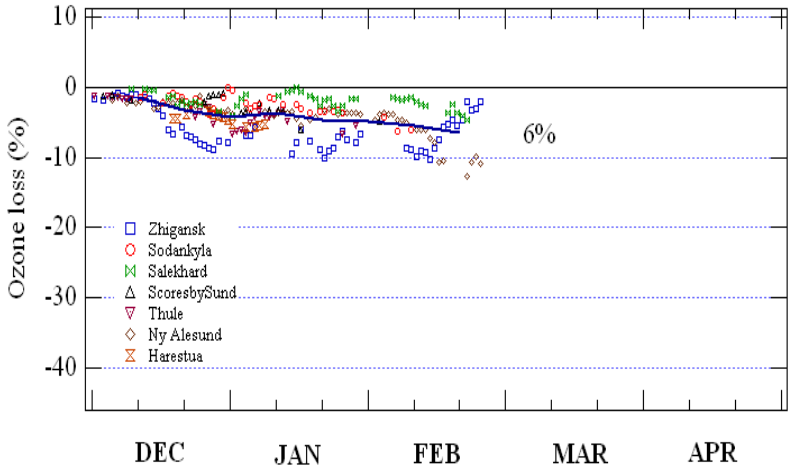

The inhomogeneity in the ozone loss is probably related to the vortex temperature inhomogeneity as it can be noticed on Figure 6.3.4-126. The temperature was warmer (red and orange) above Zhigansk (white star) than above Salekhard (red star) and Sodankyla (blue star) on the same day.

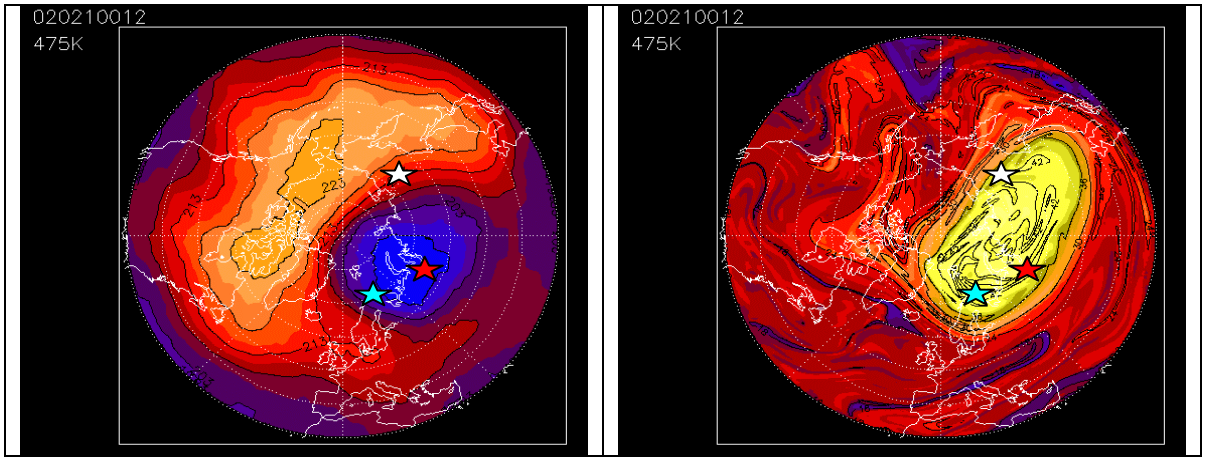

Figure 6.3.4-126. *Temperature and potential vorticity at 475 K on the February 10, 2002. Left: ECMWF temperature. Right: Mimosa PV Plot. The location of Zhigansk is indicated by a white star, Salekhard by a red star and Sodankyla by a blue star.*

Winter 2002/2003:

Meteorological conditions:

The temperature was below T_{NAT} at all levels from end of November to January 15, and the temperature was very cold, around T_{ICE}, at the beginning of December. The final warming occurred after March 22. The vortex was persisting until early April.

Figure 6.3.4-127. *ECMWF minimum temperature in the Arctic at 3 levels, 550 K, 475 K and 435 K during the 2002/03 winter.*

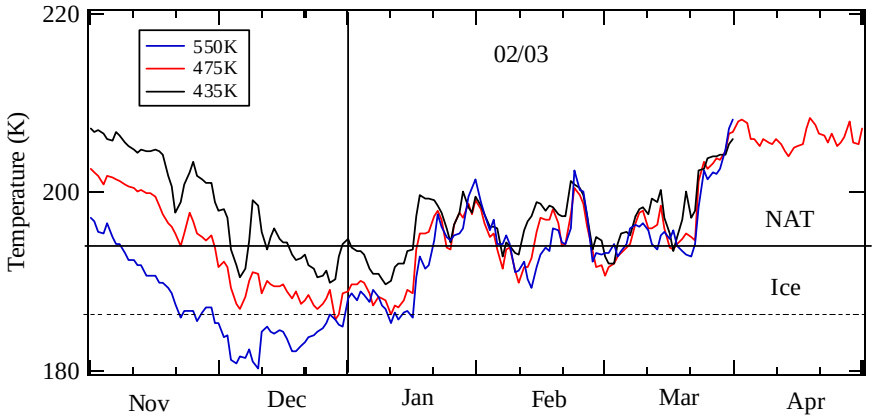

Experimental results:

Three periods of O_3 reduction are observed, one in December and one in January at a rate of 0.4% per day and one in end of February at a rate of 0.5 % per day. The cumulative loss at the end of the winter is 23 % which corresponds to ~90 DU.

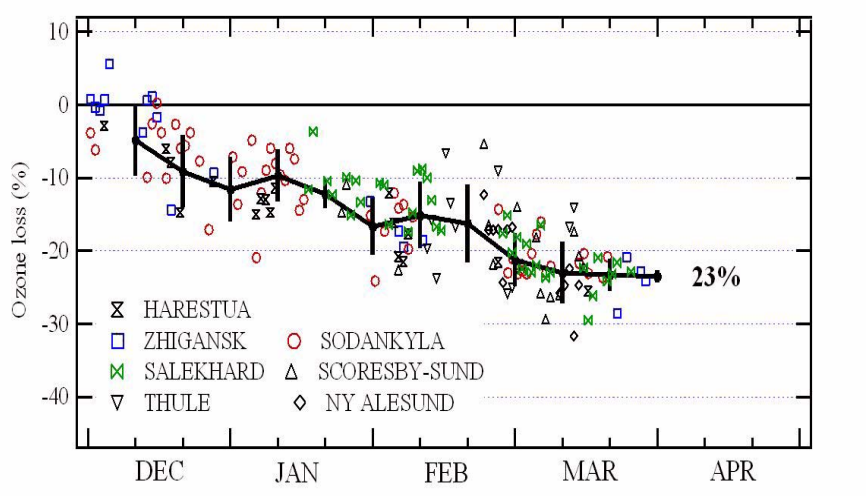

Figure 6.3.4-128. *Bottom: Cumulative total ozone loss during winter 2002/03 from SAOZ network.*

Model results:

Reprobus:

The REPROBUS simulations are shown in Figure 6.3.3.16. REPROBUS captures a loss at a rate of 0.3 % per day in December, then a plateau of about 20 days and again a loss at a rate of 0.2 % per day from January 20 until March 20. Its cumulative loss at the end of the winter is 20 % (or 80 DU). The timing and the amplitude of the loss are comparable to the observations. The current REPROBUS version correctly captures the December ozone destruction.

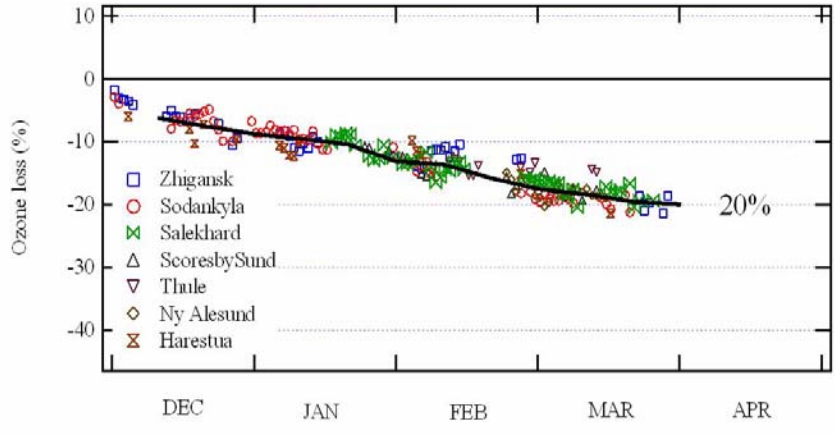

Figure 6.3.4-129. *Reprobus cumulative total ozone loss during winter 2002/03 above SAOZ stations.*

Slimcat:

The results of SLIMCAT simulations are shown in Figure 6.3.3.17. The early depletion is also captured at a rate of 0.3 % per day in December and January followed by a plateau of about 10 days in February and then by a loss again at a rate of 0.3 % per day from February 10 until March 10. At the end of the winter, the cumulative loss is 19 % (or 76 DU). The timing and the amplitude of the depletion are similar to that of REPROBUS.

Figure 6.3.4-130. *.Slimcat cumulative total ozone loss during winter 2002/03 above SAOZ stations.*

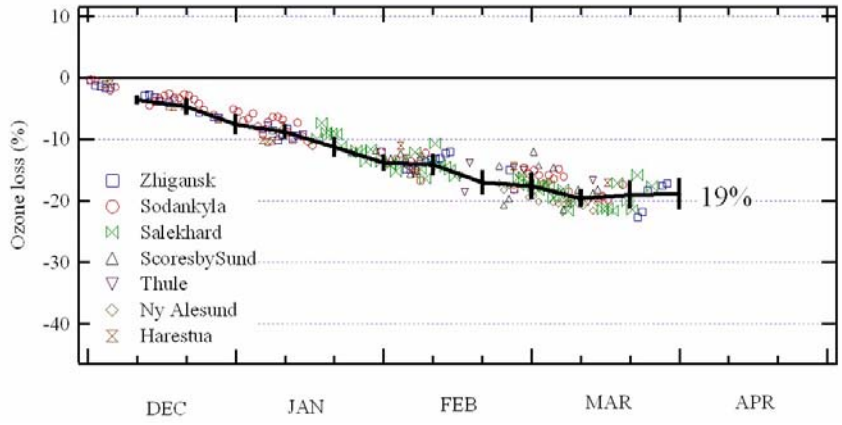

In summary, the 2002/03 REPROBUS and SLIMCAT simulations are in close agreement with each other, as well as with the SAOZ observations. In their current versions, both models appear to capture the early winter ozone depletion

Winter 2003/2004:

Meteorological conditions:

During the winter of 2003/2004, in early December, the vortex was compact and in coincidence with the cold temperature areas (Figure 6.3.4-131). On December 24, the vortex was elongated, extending down to Southern France, that is to sun-illuminated regions (Figure 6.3.4-132). The situation was very similar during the whole month of January. On January 30, the vortex was split in two lobes which recombined by mid-February. During the second part of February, the vortex was small, the temperature was increasing and cold surface area were vanishing. In March, the small remaining lobe of vortex is compact and centred on the pole. In April, the temperature was above 203 K at all levels.

Figure 6.3.4-131. *ECMWF minimum temperature in the Arctic at 3 levels, 550 K, 475 K and 435 K during the 2003/04 winter.*

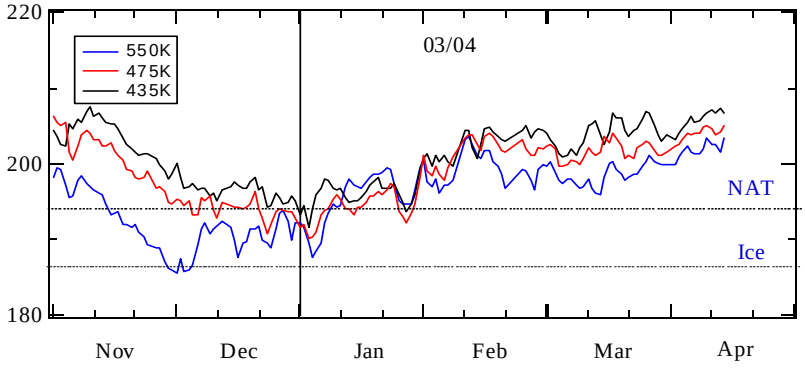

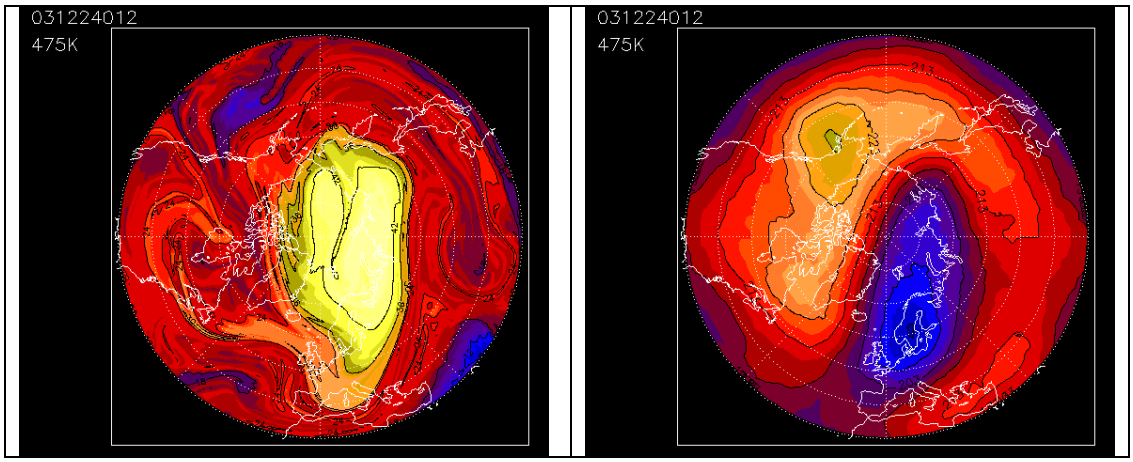

Figure 6.3.4-132. *Temperature and potential vorticity at 475 K on the December 24, 2003. Left: ECMWF temperature. Right: Mimosa PV Plot.*

Experimental results:

During the month of December, no loss was observed. A reduction at a rate of 0.3% /day was observed during the first 20 days of January, then the loss rate increased up to 0.5% /day between January 20 and February 10. No loss was observed after that date. The cumulative ozone loss during the winter is 18% corresponding to 90 DU.

Figure 6.3.4-133. *Bottom: Cumulative total ozone loss during winter 2003/04 from SAOZ network.*

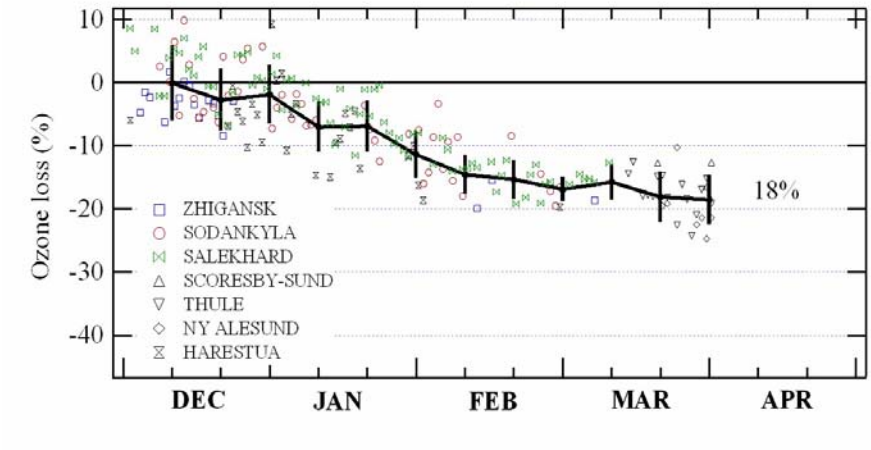

Model results:

Reprobus:

Reprobus simulates an ozone loss starting Mid- December 2003 and persisting during the whole period until end of March 2004 at a regular rate of 0.17% /day. The Reprobus cumulative loss is consistent with the experimental data within the error bars: -17% that is 85 DU.

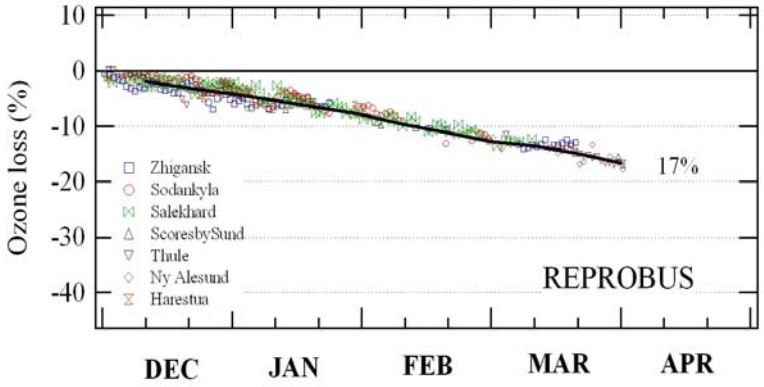

Figure 6.3.4-134. *Reprobus cumulative total ozone loss during winter 2003/04 above SAOZ stations.*

Slimcat:

Slimcat is also simulating a significant ozone loss, but with a smaller cumulative amount of 10%. In addition, Slimcat is simulating a larger scatter inside vortex, which is not present in the experimental data.

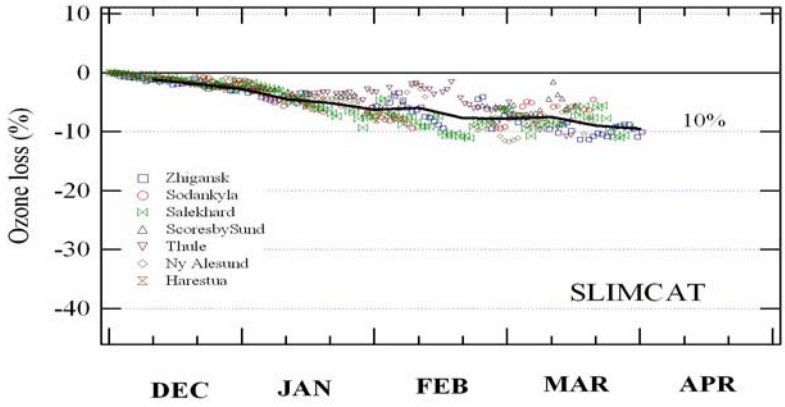

Figure 6.3.4-135. *Slimcat cumulative total ozone loss during winter 2003/04 above SAOZ stations.*

Comparison to previous winters

The winter loss observed during these three winters is smaller than the record ones – around 30% - reported in 1995 and 1996 and larger than the 5% reported in 1999. The observed cumulative loss for the eleven consecutive winters since 1993/94, the main period of ozone reduction during the season and the date at which 10 % loss was reached are displayed in Table 6.3.4-20.

Winter	Loss (%)	Loss (DU)	Period of loss	10% loss reached
1993/94	17	75	Dec 20 - Mar 20	Jan 20
1994/95	31	140	Dec 20 - Mar 20	Jan 20
1995/96	30	125	Dec 20 - Mar 10	Jan 20
1996/97	22	95	Jan 30 - Mar 30	Feb 20
1997/98	17	80	Dec 10 - Mar 1	Feb 10
1998/99	5	25	Jan 1 - Feb 20	---
1999/00	23	105	Jan 1 - Mar 10	Feb 10
2000/01	10	52	Jan 10 - Mar 1	Mar 10
2001/02	10	46	Dec 10 - Mar 30	Mar 30
2002/03	23	90	Dec 1 - Mar 10	Dec 30
2003/04	18	90	Jan 1 - Mar 1	Jan 30

Table 6.3.4-20. SAOZ Ozone loss.

In most cases, the ozone reduction is starting during the second half of December and 10 % loss is reached only on or after January 20. The winter 2002/03 with its 10 % loss at the end of December is an extreme case. For the first time in eleven years, a significant ozone loss has been observed very early in the winter, at low sun. The early activation is confirmed by the presence of high OClO levels observed in December by the UV-Visible spectrometer at Harestua in Southern Norway (Figure Figure 6.3.4-136) when the vortex was present above the station (bottom panel). The early ozone loss observed by the SAOZ in December 2002 is thus consistent with the cold ECMWF stratospheric temperatures and the high OClO over Harestua.

Figure 6.3.4-136. *Top: Time series of OClO Differential Slant Columns (91°-80° SZA) at Harestua, southern Norway, from December 1, 2002 until April 30, 2003. Bottom: Potential vorticity at 475 K and limit of the vortex.*

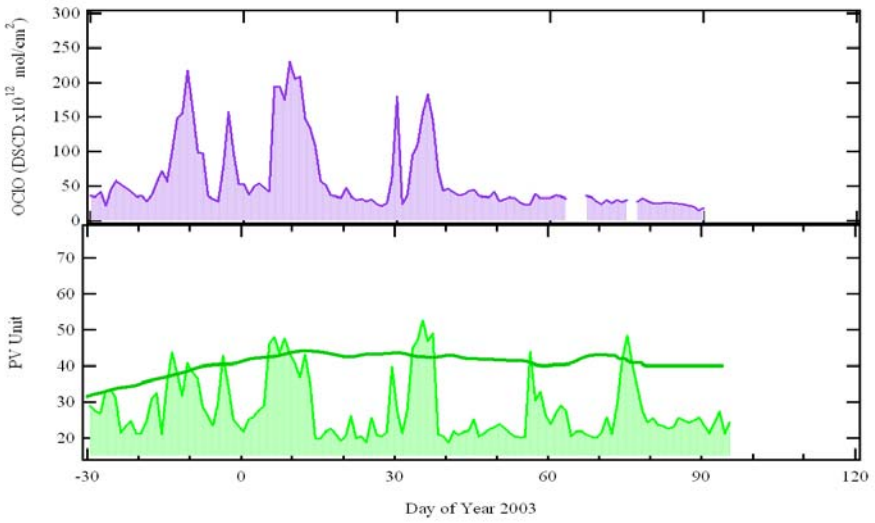

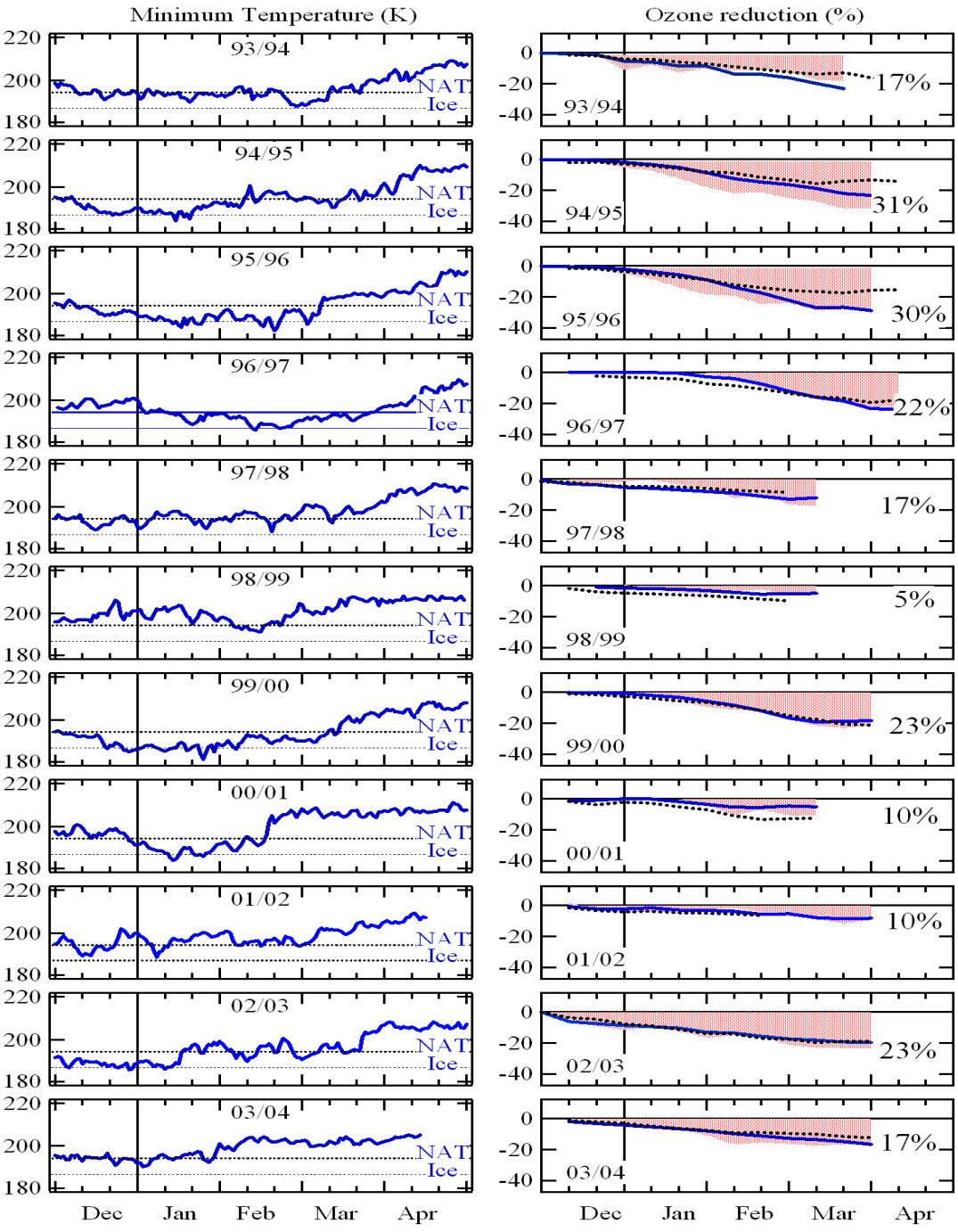

Figure 6.3.4-137. *Right: Total ozone reduction derived from the measurements of SAOZ network (hatched area) and modelled (full line: Reprobus, dotted line :Slimcat) on the left panel. Left: minimum temperature at 475 K north of 30°N and limit for NAT and ice PSC formation.*

Conclusions

The total ozone reduction inside the vortex has been quantified during the winter of 2001/2002, 2002/2003 and 2003/2004. The experimental results have been compared to 3D CTM REPROBUS and SLIMCAT. In their most updated version, both model are correctly reproducing the observed ozone loss.

References:

Cariolle, D. and M. Deque. Southern Hemisphere medium-scale waves and total ozone disturbances in a spectral general circulation model, J. Geophys. Res.,, 91, 10,825-10,846, 1986.

de Laat, A.T.J., J. Landgraf, B. Bregman and M. Krol, Validation of the TM5 model using GOME O3 profile measurements, (in preparation), 2004.

Goutail, F., J-P. Pommereau, E. Kyro, M. Rummukainen, P. Ericksen, S. Andersen, B-A. Kaastad-Hoiskar, G.O. Braathen, V. Dorokhov, V. Khattatov, M. van Roozendael and M. de Maziere, Total ozone reduction in the Arctic vortex during the winters of 1995/96 and 1996/97, Proc. 4th European Symposium on Polar Ozone, EC Air Pollution Research Report No. 66, eds. N.R.P. Harris, I. Kilbane-Dawe and G.T. Amanatidis, European Commission, 277-280, 1998.

Goutail, F., J-P. Pommereau, C. Phillips, C. Deniel, A. Sarkissian, F. Lefèvre, E. Kyro, M. Rummukainen, P. Ericksen, S. Andersen, B-A. Kaastad-Hoiskar, G. Braathen, V. Dorokhov and V. Khattatov, Depletion of Column Ozone in the Arctic during the Winters 1993-94 and 1994-95, J. Atmos. Chem., 32, 1-34, 1999.

Goutail, F., Pommereau, J.-P., and Lef`evre, F., Winter ozone loss in the Arctic and at mid-latitudes in 1998 and 1999 from the saoz ground-based network and balloon measurements, in Proc. 5th Europ. Symp., EU Air Pollution Res. Rep. 73, Saint Jean de Luz (France), 1999, edited by N. R. P. Harris, M. Guirlet, and G. T. Amanatidis, pp. 433–436, 2000.

Goutail, F., Pommereau, J.-P., and Lef`evre, F., Total ozone reduction in the Arctic during the winters 2001 and 2002 from the saoz network and comparison to previous winters, in Proc. 6th Europ. Symp., EU Air Pollution Res. Rep. 79, G¨oteborg (Sweden) 2002, edited by N. R. P. Harris, G. T. Amanatidis, and J. G. Levine, pp. 181–184, 2003.

Goutail, F., J.-P. Pommereau, F. Lefèvre, M. Van Roozendael, S. B. Andersen, B.-A. Kåstad Høiskar, V. Dorokhov, E. Kyro, M. P. Chipperfield and W. Feng. Early unusual ozone loss during the Arctic winter 2002/03 compared to other winters, ACPD, (accepted), 2004.

Hasekamp O.P., and J. Landgraf, Ozone profile retreival from backscattered ultraviolet radiances: The inversion problem solved by regularization, J. Geophys. Res., 106, 8077-8088, 2001.

Hasekamp O.P. and J. Landgraf, A linearized vector radiative transfer model for trace gas retrieval, J. Quant. Spectosc. Radiat. Transfer, in press, 2002

Hasekamp O.P., J. Landgraf, and R. van Oss: The need of polarization modeling for atmospheric constituent's retrieval, (in preparation), 2004.

Kinnersley, J.S., The climatology of the stratospheric THIN AIR model, Q. J. R. Meteorol. Soc., 122, 219-252, 1996.

Landgraf, J., O.P. Hasekamp, M.A. Box and T. Trautmann, A linearized radiative transfer model for ozone profile retrieval using the analytical forward-adjoint perturbation theory approach, J. Geophys. Res, 106, 27,291-27,305, 2001.

McLinden, C.A., S.C. Olsen, B. Hannegan, O. Wild, M.J. Prather and J. Sundet, Stratospheric ozone in 3-D models: A simple chemistry and the cross-tropopause flux, J. Geophys. Res., 105, 14,653-14,665, 2000.

Rex, M., R.J.Salawitch, P. von der Gathen, N.R.P. Harris, M.P. Chipperfield, and B. Nau-

jokat, Arctic ozone loss and climate change, Geophys. Res. Lett., 31, L04116, doi:10.1029/2003GL018844, 2004.

WMO, World Meteorological Organisation, Scientific assessment of ozone depletion: 1998, Global Ozone Research and Monitoring Project, No 44, 1999.

WMO, World Meteorological Organisation, Scientific assessment of ozone depletion: 2002, Global Ozone Research and Monitoring Project, No 44, 2003.

A study of the stratospheric chemistry of the Antarctic winter 2002 based on GOME observations and 3D-CTM calculations by the BASCOE FMR model (IASB-BIRA)

Introduction

In the middle of September 2002, the Antarctic vortex weakened into two parts and disappeared within a few weeks. This unique event prevented, at least partly, ozone depletion. The Antarctic winter 2002 presented aspects typical both of the Southern Hemisphere (single vortex) and of the Northern Hemisphere (weaker, episodic vortices with lower ozone depletion). This event was observed by the GOME instrument, which provided vertical column densities (VCD) of ozone and NO_2, but also slant column densities (SCD) of BrO and OClO. Although more difficult to interpret, these two species are rarely measured and give important clues about the processes leading to ozone depletion. In this contribution [Chabrillat et al., 2004] we focus on polar chemistry and stratospheric clouds. GOME observations are compared with co-located output from the BIRA-IASB 3D-model with the aim to:

1. Allow scientific exploitation of the GOME products of direct relevance to the QUILT project (BrO and OClO SCDs).
2. Validate our 3D-PSC-CTM model and assess the limits of such theoretical models.
3. Test our understanding of PSC microphysics and its effect on polar chemistry.
4. Evaluate the extent of winter chlorine activation and spring ozone depletion in 2002

BASCOE FMR: a 3D-PSC-Chemistry Transport Model

BASCOE is a 4D-VAR assimilation system of stratospheric chemistry developed at BIRA-IASB [Errera et al., 2001]. It is based on a 3D chemistry-transport model where Polar Stratospheric Clouds (PSC) microphysics and composition (SAT, STS, NAT and ICE particles) are explicitly treated. It is interactively coupled with chemistry and transport modules with a time step of 30 minutes. The model has a horizontal resolution of 3.75° x 5° and 37 (hybrid) pressure levels from the surface up to 0.1 hPa (subset of ECMWF vertical grid). It uses the temperature and wind fields from the 6-hourly ECMWF analyses.

In this study, it is used in a Free Model Run (FMR) mode, i.e. not constrained by observations. Simulations are started in January 2002 from initial conditions provided by the SLIMCAT 3D-CTM [Chipperfield et al., 2002]. The model state is interpolated by means of observation operators to the precise space and time of the GOME observations. A unique feature of the study is that the GOME observation operator computes the modeled BrO and OClO SCDs at GOME locations using altitude-dependent chemical air mass factors (AMFs). In this way, the quick variation of the species along the GOME viewing geometry is taken into account (see QUILT WP 2500 for a validation of the chemical AMFs). Results discussed in the present contribution are vortex averages, where the vortex edge is conventionally defined by the 65°S equivalent latitude on the 475K potential temperature level [Nash *et al.*, 1996].

Effects of PSC microphysics

According to ECMWF analyses (Table 6.3.4-138), minimum temperatures allowed NAT condensation during May 2002, but ICE particles appeared only in June. From the same ECMWF analyses, one also concludes that the ICE particles melted away in mid-August during an early warm-up of the vortex, while NAT particles disappeared briefly at the beginning of September, and definitely with the vortex split (Sept 21, 2002). The BASCOE FMR modeled distribution of water vapor was checked by comparison with measurements from the MIPAS instrument (ENVISAT) in July and September showing good agreement in the lower stratosphere and some underestimation in the middle stratosphere. This disagreement persists after the vortex split and could be due to a misrepresentation of vertical transport in the model, however it is also known that MIPAS observations of H_2O must be treated with caution in the presence of PSCs.

Figure 6.3.4-138. *ECMWF minimum temperature at the pressure level of 44.3 hPa, for equivalent latitudes lower than –65°.*

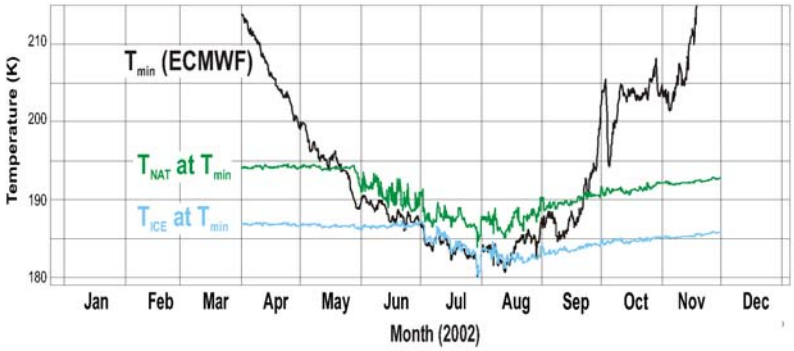

NO_2, BrO and OClO at the terminator

Since these species have large diurnal variations and possibly non-negligible tropospheric abundances, the comparison has been limited to GOME pixels around the terminator where the sensitivity of GOME to lowest atmospheric layers is minimized. BASCOE FMR and GOME observations of NO_2 VCD agree remarkably well (see Table 6.3.4-139), which suggests that the model correctly predicts denoxification processes. Starting in mid-August, the model slightly overestimates NO_2, probably because of exaggerated mixing (see mid-October drop).

In line with previous studies (see e.g. Final Report of the EU Stratospheric BrO project), the comparison of modeled BrO with GOME VCD observations reveals a systematic underestimation by the model (here approx. 35%), however the annual variation matches almost perfectly the GOME observations - except for a slight downward trend in the modeled BrO SCD during July, August and September. Since OClO at SZA=90° depends mainly on ClO abundance, it is a good indicator of chlorine activation [Wagner et al., 2001]. Modeled OClO SCDs first match GOME observations but decrease from mid-August (when ICE PSC disappear), while GOME shows that it remains constant until the vortex splits (Table 6.3.4-139b). This is a strong sign that some PSC-related process is not well understood.

Extent of ozone depletion

While the modeled ozone VCD is systematically overestimated by ~40 DU (cause currently under investigation), its spatial distribution captures perfectly the GOME maps as can be seen in Table 6.3.4-140.

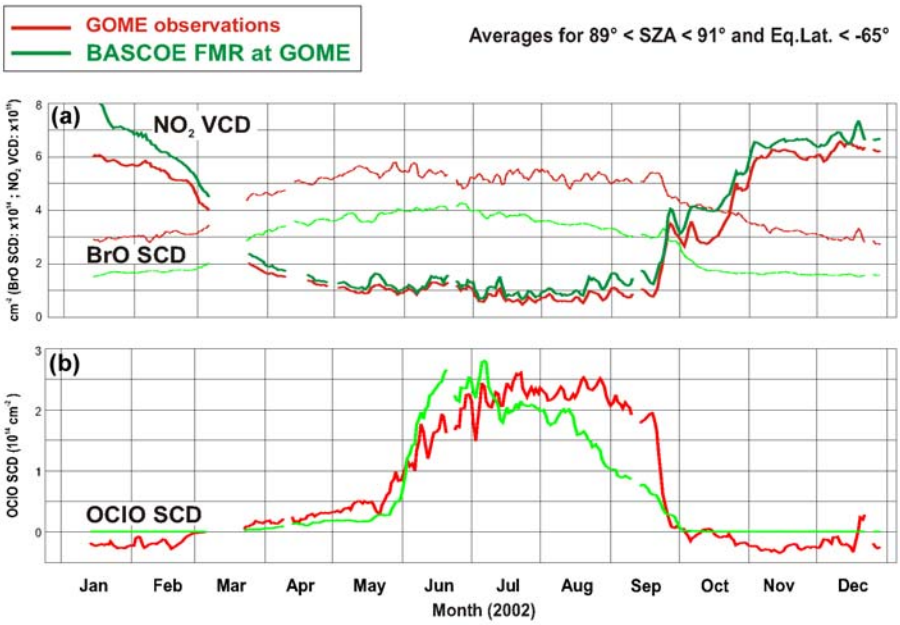

Figure 6.3.4-139. *Model values are interpolated to the precise space and time of the observations, accounting explicitly for the GOME nadir twilight geometry, by means of the BASCOE observation operators (see text).*

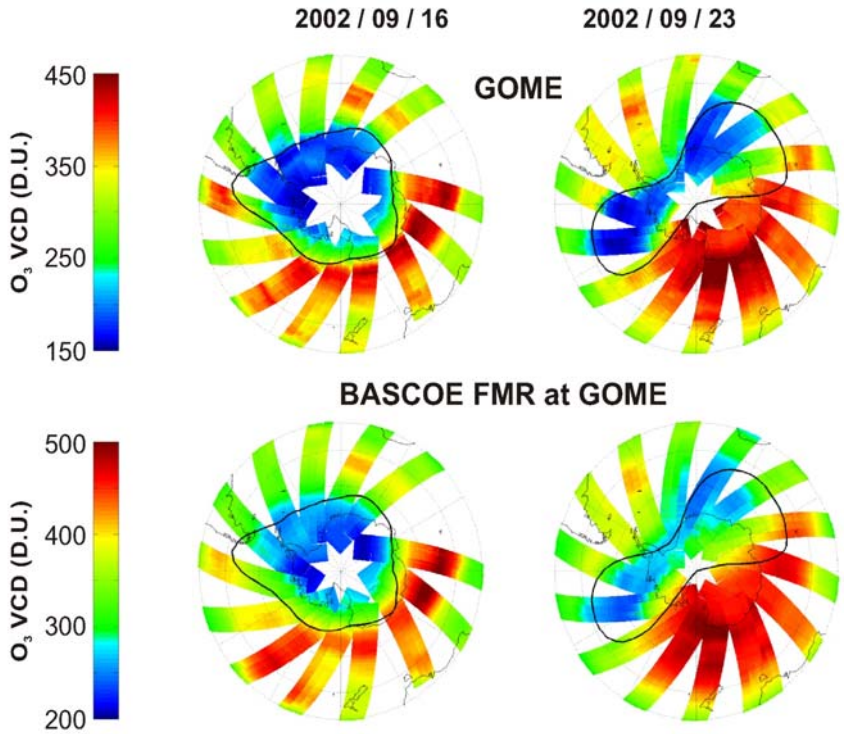

Figure 6.3.4-140. *Total ozone distributions measured by GOME and simulated by BASCOE FMR on 16 and 23 September 2002. A black line denotes the boundary of the polar vortex.*

This proves the quality of the advection module and observation operator, also shown by the good correlation between the modeled and observed time series (Table 6.3.4-141). Note that the downward trend from mid-July to mid-September is almost entirely due to a geometric effect. However a weak ozone depletion, not reproduced by the model, probably occurred during the first half of September. At that time indeed the disagreement between GOME and BASCOE FMR in-

creases significantly. Sensitivity tests currently under progress suggest that an excess of mixing occurs in the model due to the inadequate resolution of the BASCOE grid to account for fine polar structures. The limited resolution of the model could therefore be at the origin of an early disappearance of active chlorine in the simulations, resulting in a missing ozone loss. Other possibilities to explain the disagreement between model and observations are the following:

1. Ice PSC's could occur more frequently and at higher temperatures than currently predicted by theoretical models of PSC microphysics. Several other studies point to this possibility. This hypothesis should be checked against global observations of PSC's – if such observations exist.
2. The effect of denitrification, which delays the de-activation of active chlorine, could be more important in reality than computed by the model. It is quite difficult to check this hypothesis, as it depends on the history of the PSCs evolution during the months preceding the vortex split. The underestimation of denitrification is explained most easily by an underestimation of particle sedimentation rates.

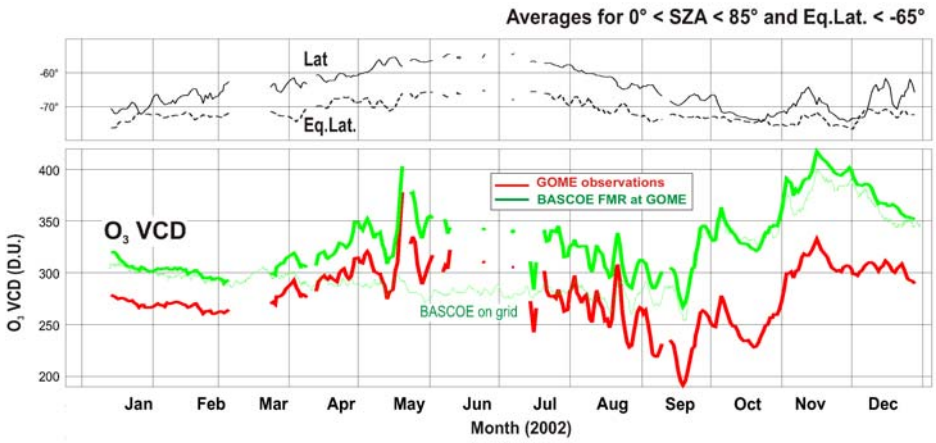

Figure 6.3.4-141. *Time series of calculated (green lines) and measured (red lines) ozone vertical columns, averaged around 90° SZA at the limit of the Antarctic terminator.*

Conclusions

This study provides three important advances in the exploitation of space-based observations of atmospheric chemistry and the understanding of the processes related to ozone depletion:

1. It allowed us to prepare efficiently the assimilation system BASCOE, validating the 3D-CTM and the observation operators, which are the basis of this system.
2. For the first time, space-based simultaneous observations of BrO, OClO, NO_2 and ozone have been compared quantitatively with model output.
3. This exercise also provides a clear illustration of the extent and the limits of our understanding of polar ozone depletion, providing a well-defined framework to test any future model of PSCs and stratospheric chemistry.

References

Chabrillat, S., D. Fonteyn, M. Van Roozendael, François Hendrick, Stratospheric Chemistry of the Antarctic winter 2002: GOME and MIPAS observations explained by a 3D-PSC-CTM, poster presentation at SPARC 2004,Victoria, Canada, 2004.

Chipperfield, M.P., et al., Sequential assimilation of stratospheric chemical observations

in a three- dimensional model , J.Geophys. Res., 107, 4585, 2002.

Errera, Q. and D. Fonteyn, Four-dimensional variational chemical assimilation of CRISTA stratospheric measurements, J. Geophys. Res., 106, 12,253-12,265, 2001.

Nash, E.R., et. al., An objective determination of the polar vortex using Ertel's potential vorticity, J. Geophys. Res., 101, 9471-9478, 1996

Wagner, T., C. Leue, K. Pfeilsticker and U. Platt, Monitoring of the stratospheric chlorine activation by Global Ozone Monitoring Experiment (GOME) OClO measurements in the austral and boreal winters 1995 through 1999, J. Geophys. Res., Vol. 106, 4971-4986, 2001

Total and tropospheric BrO columns based on the combined use of GOME observations and SLIMCAT model simulations

Introduction

Space nadir observations provide BrO columns with global coverage and might help to resolve ongoing science issues like:

1. the estimation of the stratospheric BrO trend to evaluate the impact of Montreal protocol regulations on bromine emissions.
2. the quantification of the polar BrO emissions and their impact on ozone at the regional scale.
3. the quantification of free-tropospheric BrO amounts including their latitudinal and seasonal variations and their impact on ozone at the global scale.

In order to reach these goals, total BrO columns must be resolved into their stratospheric and tropospheric contributions. As part of the QUILT project, attempts have been made at BIRA-IASB to extract total and tropospheric BrO columns based on a combination of GOME observations and calculations from the 3D-CTM SLIMCAT.

GOME – SLIMCAT tropospheric BrO residual approach

BrO slant columns have been retrieved from GOME in a quasi-operational mode as described in WP 3000, using settings given in Van Roozendael et al., 1999. The approach followed to infer tropospheric BrO columns is based on a residual technique, which consists in subtracting an estimation of the stratospheric column from measured total columns, accounting in a consistent way for the different air mass factors (AMFs) at stratospheric and tropospheric altitudes [Theys et al., 2004]. In contrast to the NO_2 case [see e.g. Richter et al., 2002], an estimation of the stratospheric BrO background cannot be easily obtained from GOME data alone because of the difficulty to find a reference sector free of tropospheric contamination. Instead the idea in the present contribution is to try and make use the 3D-CTM SLIMCAT model as a stratospheric BrO reference. The SLIMCAT model contains a detailed chemical scheme and simulates the distribution of all species involved in stratospheric ozone depletion. It has been optimized for bromine chemistry and to some extend validated by comparison with ground –based measurement [Sinnhuber et al., 2002]. A dedicated SLIMCAT output generated on purpose at the GOME overpass time has been provided to QUILT partners by M. Chipperfield. An illustration of the resulting residual tropospheric BrO product is presented in Table 6.3.4-142, for September 1997. Comparing with the distribution of total BrO columns (also shown in Table 6.3.4-142), one can see that strong bromine emissions characteristic of polar spring conditions are clearly visible and better isolated from the stratospheric background.

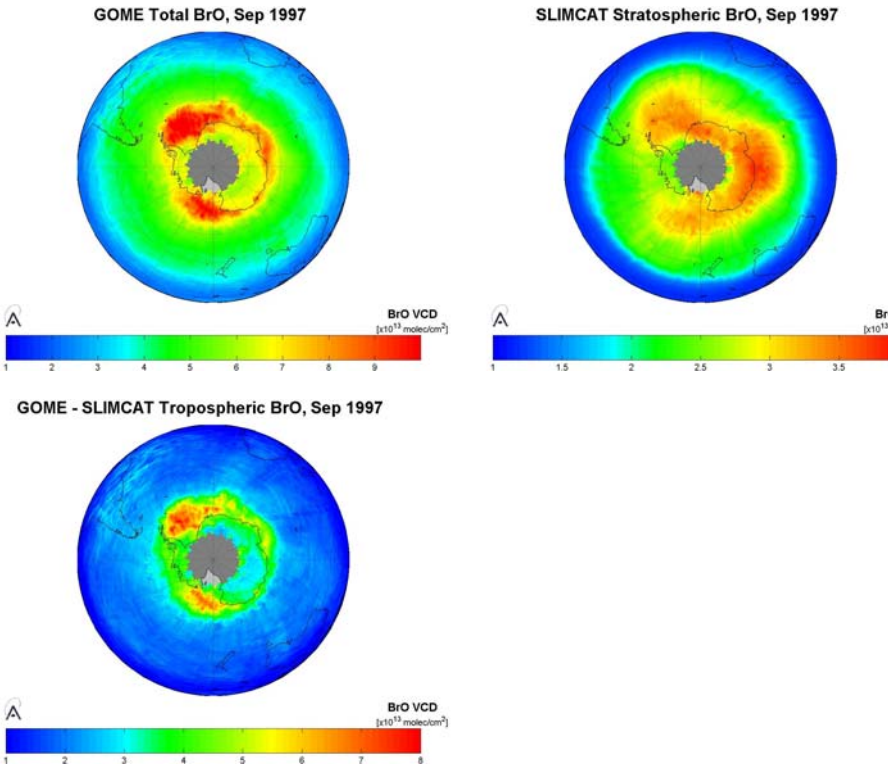

Figure 6.3.4-142. *GOME BrO columns resolved in their stratospheric and tropospheric contributions for September 1997, in the Southern Hemisphere.*

Discussion and conclusions

Using our residual analysis scheme, zonal averages of tropospheric BrO have been computed from all GOME measurements between 1997 and 2001 as displayed in Table 6.3.4-143. The resulting tropospheric BrO columns show significant seasonal variations and a strong latitudinal dependence in both hemispheres. Large BrO emissions in polar regions in spring are also evidently displayed.

A striking feature of the analysis is that non-zero residual tropospheric BrO contents are obtained in all conditions, whatever the latitude or the season. Stated in other words, BrO columns derived from GOME observations are always larger than simulated by the SLIMCAT model. Although such results might have a important consequences on the global chemistry of tropospheric ozone [von Glasow et al., 2004], it must be stressed that modeled columns are currently not constrained by any observations. Therefore the possibility of a systematic underestimation of the stratospheric BrO column by SLIMCAT, that would positively bias our tropospheric evaluations, cannot be ruled out at this stage. Such an underestimation could possibly result from the current neglect of several sources of inorganic bromine that may have a significant impact on the inorganic bromine budget in the lowermost stratosphere [see e.g. Pfeilsticker et al., 2000].

Although less important, additional problems may also arise due to the limited resolution of the model (5° x 7.5°), e.g.:

1. Fine structures in stratospheric bromine field not well captured by SLIMCAT may result in artifacts especially at high latitude during spring.

2. The twilight chemistry can be not adequately captured by the model output for regions close to the polar terminator.

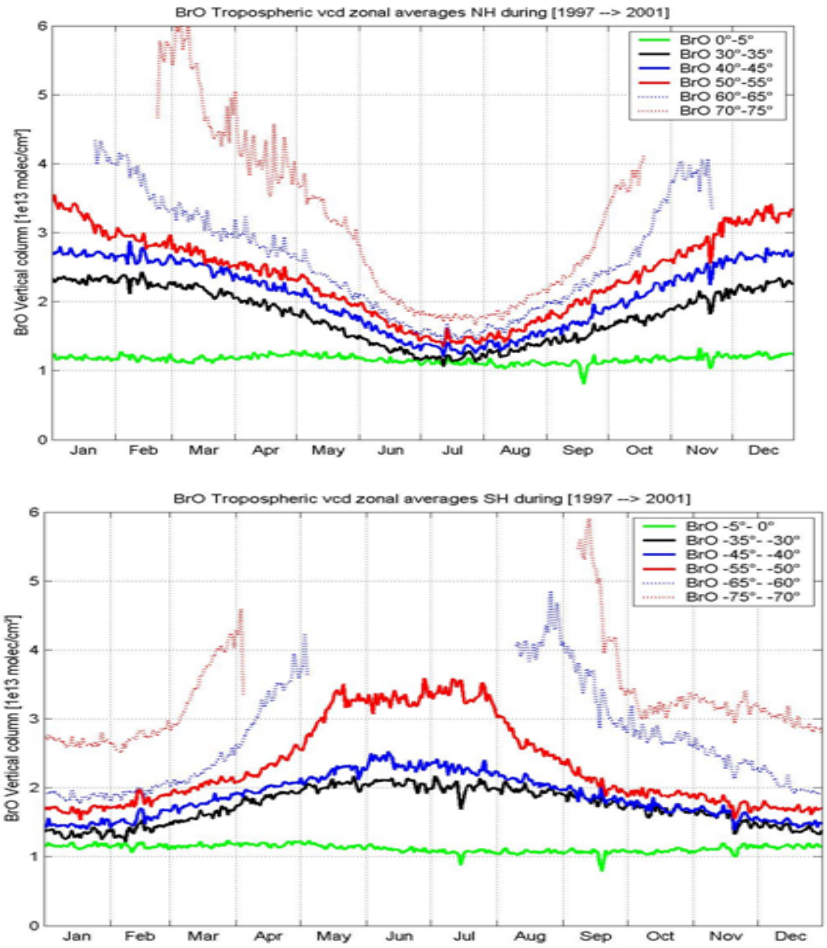

Figure 6.3.4-143. *Zonally averaged tropospheric BrO columns in Northern (left) and Southern (right) hemispheres derived from GOME observations and SLIMCAT simulations in the 1997-2001 period.*

Finally other sources of uncertainties can also be identified which will require to be further quantified: BrO slant column density errors, tropospheric AMFs uncertainties (tropospheric profile, surface albedo, cloud correction, snow/ice treatment). In the present state however, the main issue definitely concerns the reliability of the stratospheric correction as derived (here) from SLIMCAT results. In order to investigate the impact of using different model data, a preliminary comparison between SLIMCAT and the BIRA-IASB CTM BASCOE has been performed for one GOME orbit (see Table 6.3.4-144). For this exercise, the BASCOE output was obtained from a free run started on the 13 of January 2002 based on initial conditions provided by SLIMCAT. As can be seen in Table 6.3.4-144, BrO columns derived from SLIMCAT and BASCOE are reasonably consistent, which was to be expected since both models use the same assumptions on sources of stratospheric bromine (limited to methyl bromide and some halons coming from the troposphere). However, some significant differences are found in the Southern hemisphere (for this particular orbit). Clearly more investigations are needed to better understand the origin of these differences and in general to assess the robustness of stratospheric model calculations. Future work will focus on more systematic comparisons between available model and observations of BrO column and profile (ground based and balloon measurements, SCIAMACHY limb profiles).

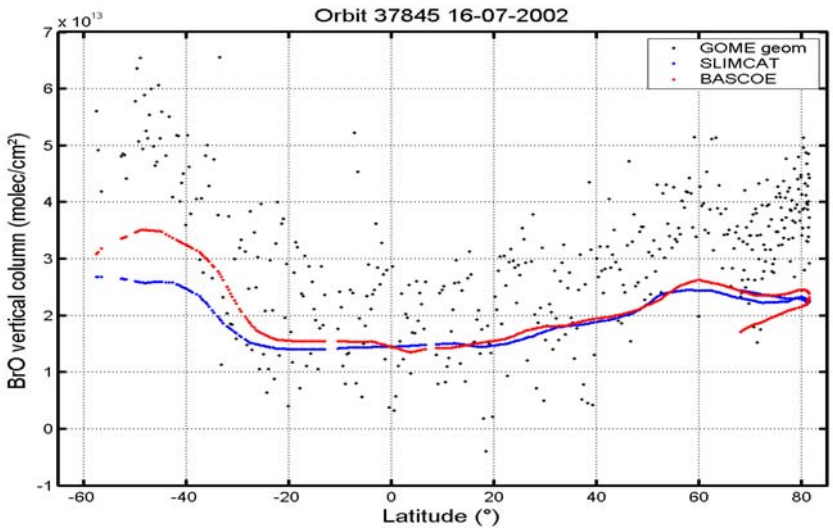

Figure 6.3.4-144. *BrO vertical columns derived from BASCOE and SLIMCAT models for a GOME orbit on 16 July 2002. GOME data are also displayed for comparison.*

Refereneces

Pfeilsticker K., W.T. Sturges, H. Bösch, C. Camy-Peyret, M.P. Chipperfield, A. Engel, R. Fitzenberger, M. Müller, S. Payan, and B.-M. Sinnhuber, Lower stratospheric organic and inorganic bromine budget for the arctic winter 1998/99, Geophys. Res. Lett., 27, 3305-3308, 2000.

Richter, A., and J.P. Burrows, Tropospheric NO2 from GOME measurements, Adv. Space Res., 29, 1673-1683, 2002.

Theys, N., I. De Smedt, M. Van Roozendael, C. Fayt, S. Chabrillat, M. Chipperfield, P. Post, R. van der A, Total and tropospheric BrO derived from GOME and SCIAMACHY as part of the TEMIS project, in proceedings of the ERS/ENVISAT 2004 Symposium, Salzburg, Austria, 6-10 September 2004 (in press)

Van Roozendael, M., C. Fayt, J.-C. Lambert, I. Pundt, T. Wagner, A. Richter, and K. Chance, Development of a bromine oxide product from GOME, in Proc. ESAMS'99-European Symposium on Atmospheric Measurements from Space, ESTEC, Noordwijk, The Netherlands, 18-22 January 1999, ESA WPP-161, p. 543-547, 1999.

von Glasow, R., R. von Kuhlmann, M. G. Lawrence, U. Platt, and P.J. Crutzen, Impact of reactive bomine chemistry in the troposphere, Atmos. Chem. Phys. Discuss.,4, 4877-4913, 2004.

Main deliverables

- *An assessment of of our understanding of the coupled chemistry of ClO and BrO through comparisons of OClO observed and modelled abundances of IO.*
- *An assessment of the the role of meteorological trends/variability on determining varisons in NO_2.and the likely cause of the apparent upward trend in observed stratospheric NO_2.*
- *Cummulative ozone loss from total column or integrated profiles since 1990.*
- *An assessment of the magnitude of the trend in lower stratospheric bromine inferred from the comparison of BrO in a CTM and groundbased observations (see WP 3100)*

6.3.5 WP 6000: WWW-NRT product services

The first objective of this work package is to provide the scientific community and the public with GOME and ground-based Near Real Time (NRT) measurements of ozone and halogen oxides throughout the winter/spring period when most of the stratospheric ozone destruction takes place (WP 6100). The second objective is to quantify in NRT of the ozone loss inside the polar vortex by comparison between measurements and modelled passive simulations (WP 6200). WP 6200 and WP 5300 (Ozone loss variability)have been merged and the scientific outcomes were presented in Section 6.3.4.

WP 6100: NRT ground-based and GOME data products

The objective of this work package is the provision in NRT of total ozone and NO_2 measurements from the ground-based UV-visible spectrometer network. Access to the ground-based data can be made via the project website. From the SAOZ network, morning and evening total column of ozone and NO_2 are received at the laboratory through Internet (most of the stations) or Argos satellite transmission (when internet is not available which is the case in Siberia and East Greenland) every day. A web site has been organised at CNRS. The measurements of the CNRS instruments have been checked and introduced on a daily basis on the web site: http://www.aerov.jussieu.fr/~fgoutail/SAOZ-RT.html

NRT data products from GOME have been published for the whole time period from January 2001 to June 2004. The webpage http://www.iup.physik.uni-bremen.de/gomenrt was continously supplemented with new features (e.g. different region selections) during the project period. The whole time series of GOME data since 1995 is available for all different data products, including column amounts of ozone, NO_2, BrO, OClO, formaldehyde and SO_2.

Due to a permanent failure of the ERS-2 tape recorder, the availability of GOME data coverage is limited to the region where ERS-2 is in direct contact with ground stations (North Atlantic sector and north polar region) starting 22nd June 2003. The Institute of Environmental Physics at the University of Bremen has fill this gap by providing scientific data products of the SCIAMACHY instrument onboard ENVISAT in real time (http://www.doas-bremen.de/sciamachy.htm, http://www.iup.physik.uni-bremen.de/scia-arc).

For further details and scientific outcomes see WP 5300 in Section 6.2.4.

Summary

The work carried out in WP6100 is an excellent example of the near-real time exploitation of satellite and ground-based UV-visible spectrometer (SAOZ) data. GOME data for the whole period 1995-present were available on the Univ. of Bremen web site; the SAOZ data were made available via the CNRS web site. The data provided through this WP has also been used for the Antarctic ozone bulletins issued by the World Meteorological Organization (WMO).

Main deliverables

- *Near Real Time maps of GOME O_3, NO_2, BrO, and OClO for the winter/ spring campaigns, available on the internet within hours after measurement*
- *GOME NRT data available for inclusion in the GOME data base WP 3300*

WP 6200: NRT ozone loss modelling

The objective of this work package is the quantification in Near Real Time of the ozone loss inside the polar vortex. The total ozone measurements are those from the ground-based UV-visible Arctic spectrometers, Thule, Ny-Alesund, ScoresbySund, Sodankyla, Salekhard and Zhigansk. The 3D-CTM, which have been used, are REPROBUS and SLIMCAT. NRT results from this work package are made available at the CNRS web page. A link to NRT modelling activities (MIMOSA/REPROBUS) at CNRS is also given.

http://www.aerov.jussieu.fr/~fgoutail/MIMOSA.html
http://www.aerov.jussieu.fr/~fgoutail/REPROBUS/Near_Real_Time/
http://www.aerov.jussieu.fr/~fgoutail/REPROBUS/Near_Real_Time 2002/
http://www.aerov.jussieu.fr/~fgoutail/REPROBUS/Near_Real_Time/ 2003/

For further details and scientific outcomes see WP 5300 in Section 6.2.4.

Summary

In WP 5300 and 6200 one has used a combination of observations and modelling (3D-CTMs: REPROBUS and SLIMCAT) to quantify in Near Real Time the degree of ozone loss in the Arctic. The total ozone reduction inside the vortex has been quantified during the winter of 2001/2002, 2002/2003 and 2003/2004. The experimental results have been compared to 3D CTM REPROBUS and SLIMCAT. In their most updated version, both model are correctly reproducing the observed ozone loss.

Conclusions including socio-economic relevance, strategie aspects and policy implications

The objective of WP 6100 was to provide the scientific community and the public with GOME and ground-based Near Real Time measurements of ozone and halogen oxides throughout the winter/spring period when most of the stratospheric ozone destruction takes place. These data are of specific interest for scientists during campaign planning but also to policy makers and the broader public as information on the status and development of ozone destruction in the Northern Hemisphere.

The objective of WP 6200 was to quantify in Near Real Time the degree of ozone loss inside the polar vortex by comparison between measurements and modeled passive simulations. This work can be seen in conjunction with the important question of “ozone recovery”. It is important to inform policy makers and the public on the state of the ozone layer in the North Polar regions and to verify model results against observations. It is through such verification that we can be confident that atmospheric chemistry models are able to predict the future development of the ozone layer. Model projections form the basis for EU and national policies on the phase-out of ozone depleting substances.

6.4 Main literature produced

Peer reviewed articles

Aliwell, S.R., M. Van Roozendael, P.V. Johnston, A. Richter, T. Wagner, D.W. Arlander, J.P. Burrows, D.J. Fish, R.L. Jones, K. Karlsen-Tornkvist, J. C. Lambert, K. Pfeilsticker, and I. Pundt., Analysis for BrO in zenith-sky spectra: an intercomparison exercise for analysis, J. Geophys. Res.,10.1029/2001JD000329, 2002.

Bhosale, C.S., G.S. Meena, A.L. Londhe, D.B. Jadhav, M. Gil y O. Puentedura,The variations of O3, NO2 and O4 densities in association with meteorological parameters during the winter/Spring of 1993-94 and 1994-95 at sub-arctic station, Indian Journal of Radio & Space Physics, submitted, 2004.

Bösch, H., C. Camy-Peyret, M. Chipperfield, R. Fitzenberger, H. Harder, U. Platt, B. Sinnhuber, and K. Pfeilsticker, Simultaneous Upper Limits of Stratospheric IO and OIO Inferred From Center-to-Limb-Darkening -Corrected Balloon-Borne Solar Occultation Visible Spectra; Implications for Total Gaseous Iodine and Stratospheric Ozone,J. Geophys. Res.,108 (D15), 4455, doi:10.1029/2002JD003078, 2003.

Borrell, P., John P. Burrows, Ulrich Platt, Andreas Richter and Thomas Wagner, New Directions: New Developments in Satellite Capabilities for Probing the Chemistry of the Troposphere, Atmospheric Environment, 37, 2567-2570, 2003.

Bracher, A., M. Weber, K. Bramstedt, S. Tellmann, J. P. Burrows, Long-term global measurements of ozone profiles by GOME validated with SAGE II considering atmospheric dynamics, J. Geophys. Res., accepted, 2004.

Bramstedt, K., J. Gleason, D. Loyola, W. Thomas, A. Bracher, M. Weber, and J. P. Burrows, Comparison of total ozone from the satellite instruments GOME and TOMS with measurements from the Dobson network 1996-2000, Atmospheric Chemistry and Physics 3, 1409-1419, 2003.

Bruns, M., S. Bühler, J. P. Burrows, K.-P. Heue, U. Platt, I. Pundt, A. Richter, A. Rozanov, T. Wagner, P. Wang, Retrieval of Profile Information from Airborne Multi Axis UV/visible Skylight Absorption Measurements, Applied Optics, 43 (22), 4415-4426, 2004.

Canty, T. R.S. Salawitch, J.B. Renard, E.D. Reviere, K. Pfeilsticker, M. Dorf. R. Fitzenberger, H. Boesch, R.M Stimpfle, D.M. Wilmouth, J.G. Anderson, E.C. Richard, D.W. Fahey, R.S. Gao, and T.P. BuiJ., Analysis of BrO, ClO, and nighttime OClO in the Arctic winter stratosphere, Geophys. Res. Lett., submitted, 2003.

Coldewey-Egbers, M., M. Weber, M. Buchwitz, and J.P. Burrows, Application of a modified DOAS method for total ozone retrieval from GOME data at high polar latitudes, Adv. Space Res. 34, 749-753, 2004.

DeBeek, R., M. Vountas, V. V. Rozanov, A. Richter, and J. P. Burrows, 2001, The Ring effect in the cloudy atmosphere, Geophys. Res. Lett., 28,721-72, 2001.

Denis, L., H.K. Roscoe, M.P. Chipperfield, M. Van Roozendael, F. Goutail, A new software suite for NO2 vertical profile retrievafrom groundbased zenith-sky spectrometers, J. Quant. Spectrosc. Radiat. Trans., submitted, 2004.

Denis, L., H.K. Roscoe, M.P. Chipperfield, M. Van Roozendael, F. Goutail, A new software suite for NO2 vertical profile retrieval from ground-based zenith-sky spectrometers, J. Quant. Spectrosc. Radiat. Trans., submitted, 2003.

Feng. W., M.P. Chipperfield, H.K. Roscoe et al.,Three-Dimensional Model Study of the Antarctic Ozone Hole in 2002 and Comparison with 2000, J. Atmos. Sci., (in press), 2004.

Frieß, U., J. Hollwedel, G. König-Langlo, T. Wagner, and U. Platt, Dynamics and chemistry of tropospheric bromine explosion events in the Antarctic coastal region, J. Geophys. Res., 109, doi: 10.1029/2003JD004133, 2004.

Frieß, U., J. Hollwedel, T. Wagner, G. König-Langlo, and U. Platt, Tropospheric bromine monoxide in the Antarctic coastal region, J. Geophys. Res., submitted, 2003.

Frieß, U., K. Kreher, P. V. Johnston, and U. Platt, Gound-based DOAS measurements of stratospheric trace gases at two Antarctic stations during the 2002 ozone hole period,

J. Atm. Sci., submitted, 2003.

Frieß, U., K. Kreher, P. V. Johnston, and U. Platt, Ground- based DOAS measurements of stratospheric trace gases at two Antarctic stations during the 2002 ozone hole period, JAS special issue on the Antarctic stratospheric sudden warming and split ozone hole of 2002, in press, 2004.

Frieß, U., T. Wagner, I. Pundt, K. Pfeilsticker, and U. Platt, Spectroscopic measurements of tropospheric iodine oxide at Neumayer station, Antarctica, Geophys. Res. Lett., 28, 1941-1944, 2001.

Gil M., M. Yela, E. Cuevas and V.Carreño, Sudden increases in the NO2 column caused by thunderstorms: A case study in the northern subtropical region,Journal of Physic and Chemical Research, in press., 2004.

Hansen, G., K. Bramstedt, V. Rozanov, M. Weber, and J.P. Burrows, Validation of GOME ozone profiles by means of the ALOMAR ozone lidar, Annales Geophysicae 21, 1879-1886, 2003.

Harris, N. P. R., M. Rex, F. Goutail, B.M. Knudsen, G.L. Manney, R. Müller, and P. von der Gathen, Comparison of Empirically Derived Ozone Losses in the Arctic Vortex , J. Geophys. Res., 107(D21), 10.1029, 2002.

Heckel, A., A. Richter, T. Tarsu, F. Wittrock, C. Hak, I. Pundt, W. Junkermann, and J. P. Burrows, MAX-DOAS measurements of formaldehyde in the Po-Valley, Atmos. Chem. Phys. Discuss., 4, 1151-1180, 2004.

Heue, K.-P., A. Richter, T. Wagner, M. Bruns, J.P. Burrows, . v.Friedeburg, W. D. Lee, U. Platt, I. Pundt, P. Wang, Validation of SCIAMACHY tropospheric NO2-columns with AMAXDOAS measurements, Atmos. Chem. Phys. Discuss., 4, 7513-7540, 2004

Heland, J., Schlager, H., Richter, A., Burrows, J. P., First comparison of tropospheric NO2 column densities retrieved from GOME measurements and in situ aircraft profile measurements, GRL, doi:10.1029/2002GL015528, 2002.

Hendrick, F., B. Barret, M. Van Roozendael, H. Boesch, A. Butz, M. De Mazière, F. Goutail, C. Hermans, J.-C. Lambert, K. Pfeilsticker, J.-P. Pommereau, Retrieval of nitrogen dioxide stratospheric profiles from ground-based zenith-sky UV-visible observations: Validation of the technique through correlative comparisons, Atmos. Chem. Phys., 4, 2091-2106, 2004.

Hild, L., Richter, A., Rozanov, V., and J. P. Burrows, 2001, Air Mass Calculations for GOME Measurements of lightning-produced NO2, Adv. Space Res., 29(11), 1685-1690, 2002.

Hollwedel, J., M. Wenig, S. Beirle, S. Kraus, S. Kühl, W. Wilms-Grabe, U. Platt, and T. Wagner, Year-to-year variations of spring time polar tropospheric BrO as seen by GOME, Adv. Space Res., accepted, 2003.

Hönninger G. and Platt U., The Role of BrO and its Vertical Distribution during Surface Ozone Depletion at Alert, Atmos. Environ. 36, 2481-2489, 2002.

Irie, H. , Y. Kondo, M. Koike, M. Y. Danilin, C. Camy-Peyret, S. Payan, J. P. Pommereau, F. Goutail, H. Oelhaf, G. Wetzel, G. C. Toon, B. Sen, R. M. Bevilacqua, J. M. Russell III, J. B. Renard, H. Kanzawa, H. Nakajima, T. Yokota, T. Sugita, and Y. Sasano, Validation of NO2 and HNO3 measurements from the Improved Limb Atmospheric Spectrometer (ILAS) with the version 5.20 retrieval algorithm, J. Geophys. Res., 107(D21),10.1029, 2002.

Lamsal, L. N., M. Weber, S. Tellmann, and J. P. Burrows, Ozone column classified climatology of ozone and temperature profiles based on ozonesonde and satellite data, J. Geophys. Res., accepted, 2004.

Leser, H., G. Hönninger, and U. Platt, MAX-DOAS measurements of BrO and NO2 in the marine boundary layer, Geophys. Res. Lett., 30, 1537, doi: 10.1029/ 2002GL015811, 2003.

Lu, J.Y, W. H. Schroeder, L. A. Barrie, A. Steffen, H. E. Welch, K. Martin, W. L. Lockhart, R.V: Hunt, G. Boila, A. Richter, Magnification of atmospheric mercury deposition to polar regions in springtime: the link to tropospheric ozone depletion chemistry, GRL, 28, 3219-3222, 2001.

Lumpe, J. D., Fromm, M, Hoppel K, Bevilacqua, R M., Randall, C E, Browell E, V., Grant, W B., McGee T, Burris, J. Twigg, L. , Richard, E. C., Toon, G., Margitan, J. J., Sen, B. , Pfeilsticker, K. , Boesch, H. , Fitzenberger, R. , Goutail F. , and J.P. Pommereau, Comparison of POAM III ozone measurements with correlative aircraft and balloon data during SOLVE, J. Geophys. Res.,107, 8316, doi:10.1029/

2001JD000472, 2002, printed: 108(D5), 2003.

Lumpe, D., K. Hoppel, R. M. Bevilacua, E. Browell, W. B. Grant, T. McGee, J. Burris, L. Twigg, E. C. Richard, G. Toon, B. Sen, H. Boesch, R. Fitzenberger, and K. Pfeilsticker, Comparison of POAM III ozone measurements with correlative aircraft and balloon data during SOLVE, J. Geophys. Res.,107, 8316, doi:10.1029/ 2001JD000472, 2002.

Kühl, S., W. Wilms-Grabe, S. Beirle, C. Frankenberg, M. Grzegorski, J. Hollwedel, F. Khokhar, S. Kraus, U. Platt, S. Sanghavi, C. v.Friedeburg, and T. Wagner, Stratospheric chlorine activation in the Arctic winters 1995/96 to 2001/02 derived from GOME OClO measurements, Adv. Space Res., accepted, 2003.

Müller, M.D., A.K. Kaifel, M. Weber, S. Tellmann, J.P. Burrows, D. Loyola, Ozone profile retrieval from GOME data using a neural network approach (NNORSY), J. Geophys. Res., 108, 4497, doi:10.1029/2002JD002784, 2003.

Müller, R.W., H. Bovensmann, J. W. Kaiser, A. Richter, A. Rozanov, F. Wittrock, and J.P. Burrows, Consistent Interpretation of Ground based and GOME BrO Slant Column Data, Adv. Space Res., 29(11), 1655-1660, 2002.

Petritoli, A., P. Bonasoni, G. Giovanelli, F. Ravegnani, I. Kostadinov, D. Bortoli, A. Weiss, D. Schaub, A. Richter, F. Fortezza, First comparison between ground-based and satellite-borne measurements of tropospheric nitrogen dioxide in the Po basin, J. Geophys. Res., Vol. 109, No. D15, D15307 10.1029/2004JD004547, 2004.

Petritoli, A., G. Giovanelli, I. Kostadinov, F.Ravegnani, D.Bortoli, , P. Bonasoni, F. Evangelisti, U. Bonafè, F. Calzolari, Tropospheric and stratospheric NO2 amount deduced by slant column measurements at Mt. Cimone station, Adv. Space Res., 29, 11, 1691-1695, 2002.

Petritoli, A., F. Ravegnani, G. Giovanelli, D. Bortoli, U. Bonafè, I. Kostadinov, A. Oulanovsky, Off-axis measurements of atmospheric trace gases by use of an airborne ultravilolet-visible spectrometer, Appl. Opt., 41, 27, 5593-5599, 2002.

Pundt, I., J.P. Pommereau, M.P. Chipperfield, M. Van Roozendael and F. Goutail, Climatology of the stratospheric BrO vertical distribution by balloon-borne UV-visible spectrometry, J. Geophys. Res., 107(D24), 10.1029, 2002.

Randall, C.E., J.D. Lumpe , R.M. Bevilacqua , K.W. Hoppel, E.P. Shettle, D.W. Rusch, L.L. Gordley, K. Kreher, K. Pfeilsticker, H. Boesch, G. Toon, F. Goutail, Validation of Polar Ozone and Aerosol Measurement (POAM) III NO2 Measurements, J. Geophys. Res., 107, 4432, 10.1029 2001JD001520, 2002.

Randall, C.E. , J.D. Lumpe, R.M. Bevilacqua, K.W. Hoppel, E.P. Shettle, D.W. Rusch, L.L. Gordley, K. Kreher, K. Pfeilsticker, H. Boesch, G. Toon, F. Goutail, and J.-P. Pommereau, Validation of POAM III NO2 Measurements, J. Geophys. Res.,107(D20), 10.1029, 2002.

Richter, A. and J.P. Burrows, Retrieval of Tropospheric NO2 from GOME Measurements, Adv. Space Res., 29(11) ,1673-1683, 2002 .

Richter, A., F. Wittrock, A. Ladstätter-Weißenmayer, and J.P. Burrows, GOME measurements of stratospheric and tropospheric BrO, Adv. Space Res., 29(11), 1667-1672, 2002.

Richter, A., F. Wittrock, M. Weber, S. Beirle, S. Kühl, U. Platt, T. Wagner, W. Wilms-Grabe, and J. P. Burrows, GOME observations of stratospheric trace gas distributions during the splitting vortex event in the Antarctic winter 2002 Part I: Measurements, accepted for publication in J. Atmos. Sci., 2004.

Roscoe, H.K., A review of stratospheric H_2O and NO_2, Adv. Space Res., C4.1-0007-02, in press, 2004.

Roscoe, H.K., The Brewer-Dobson circulation in the stratosphere and mesosphere - is there a trend?", submitted to Advances in Space Research, 2004.

Roscoe, H. K., K. Kreher, and U. Frieß, Ozone loss episodes in the free Antarctic troposphere, suggesting a possible climate feedback, Geophys. Res. Lett., 28, 2911-2914, 2001.

Schofield, R., B.J. Connor, K. Kreher, P.V. Jonston, and C. D. Rodgers, The retrieval of profile and chemical information from ground-based UV-visible spectroscopic measurements, J. Quant. Spec. & Rad. Trans., 86, 115 - 131, doi:10.1016/S0022-4073(03)00278-4 , 2004.

Sinnhuber, B.-M., M. Weber, A. Amankwah, and J.P. Burrows, Total ozone during the unusual Antarctic winter of 2002, Geophys. Res. Lett. 30, 1850, doi:10.1029/

2002GL016798, 2003.

Sinnhuber, B.-M., D. W. Arlander, H. Bovensmann, J. P. Burrows, M. P. Chipperfield, C.-F. Enell, U. Frieß, F. Hendrick, P. V. Johnston, R. L. Jones, K. Kreher, N. Mohamed-Tahrin, R. Müller, K. Pfeilsticker, U. Platt, J.-P. Pommereau, I. Pundt, A. Richter, A. M. South, K. K. Tørnkvist, M. Van Roozendael, T. Wagner, and F. Wittrock, Comparison of measurements and model calculations of stratospheric bromine monoxide, J. Geophys. Res., 107, doi:10.1029/2001JD000940, 2002.

Sioris C. E., Craig S. Haley, C. A. McLinden, C. von Savigny, I. C. McDade, Wayne F. J. Evans, J. C. McConnell, N. D. Lloyd, E.. Llewellyn, D. Murtagh, U. Frisk, T. P. Kurosu, Kelly V. Chance, K. Pfeilsticker, H. Bösch, and F. Weidner, Stratospheric profiles of nitrogen dioxide observed by OSIRIS on the Odin satellite, J. Geophys. Res.,108, D7, 4215, doi:10.1029/2002JD002672, 2003.

Sommar,J., I. Wängberg, T. Berg, K. Gårdfeldt, J. Munthe, A. Richter, A. Urba, F. Wittrock, W. H. Schroeder, Circumpolar transport and air-surface exchange of atmospheric mercury at Ny-Ålesund (79°N), Svalbard, spring 2002, Atmos. Chem. Phys. Disc., 4, 1727-1771, 2004.

Sugita, T., T. Yokota, H. Nakajima, H. Kanzawa, H. Nakane, H. Gernandt, V. Yushkov, K. Shibasaki, T. Deshler, Y. Kondo, S. Godin, F. Goutail, J.-P. Pommereau, C. Camy-Peyret, S. Payan, P. Jeseck, J.-B. Renard, H. Boesch, R. Fitzenberger, K. Pfeilsticker, M. von Koenig, H. Bremer, H. Küllmann, H. Schlager, J.J. Margitan, B. Stachnik, G.C. Toon, K. Jucks, W.A. Traub, D.G. Johnson, I. Murata, H. Fukunishi, and Y. Sasano, Validation of ozone measurements from the Improved Limb Atmospheric Spectrometer (ILAS), J. Geophys. Res., 107, 8212, doi: 10.1029/2001JD000162, 2002.

Tellmann, S., V.V. Rozanov, M. Weber, and J.P. Burrows, Improvements in the tropical ozone profile retrieval from GOME UV/vis nadir spectra, Adv. Space Res. 34, 739-743, 2004.

Vandaele, A.C., C. Fayt, F. Hendrick, C. Hermans, F. Humbled, M. Van Roozendael, M. Gil, M. Navarro, O. Puentedura, M. Yela, G. Braathen, K. Stebel, K. Tørnkvist, P. Johnston, K. Kreher, F. Goutail, A. Mieville, J.-P. Pommereau, S. Khaikine, A. Richter, H. Oetjen, F. Wittrock, S. Bugarski, U. Friess, K. Pfeilsticker, R. Sinreich, T. Wagner, G. Corlett, R. Leigh, An intercomparison campaign of ground-based UV-Visible measurements of NO2, BrO, and OClO slant columns. I. Methods of analysis and results for NO2, submitted to J. Geophys. Res. (2004).

Van Roozendael, M., T Wagner, A. Richter, I. Pundt, D.W. Arlander, J.P. Burrows, M. Chipperfield, C. Fayt, P.V. Johnston, J.C. Lambert, K. Kreher, K. Pfeilsticker U. Platt, J. P. Pommereau, B.M. Sinnhuber, K.K. Tornkvist, and F. Wittrock, Intercomparison of BrO Measurements from ERS-2 GOME, Ground-based and balloon platforms, Adv. Space Res., 29, 22, 1161-1666, 2002.

Velders, G. J. M.; C. Granier, R. W. Portmann, K. Pfeilsticker, M. Wenig, T. Wagner, U. Platt, A. Richter, and J. P. Burrows, Global tropospheric NO2 column distributions: Comparing 3-D model calculations with GOME measurements, JGR, D 106, 12643-12660, 2001.

Vountas, M., A. Richter, F. Wittrock, and J. P. Burrows, Inelastic scattering in ocean water and its impact on trace gas retrievals from satellite data, Atmos. Chem. Phys., 3, 1365-1375, 2003.

Werner, R., Iv. Kostadinov, D. Valev, At. Atanasov, G. Giovanelli, F. Ravegnani, A. Petritoli, D. Bortoli, Spectrometric mesurements of NO2 slant column amount at Stara Zagora station (42°N, 24°E), Adv. Space. Res., 31, 1473 - 1478, 2003.

Wagner, T., B. Dix, C. v. Friedeburg, U. Frieß, S. Sanghavi, R. Sinreich, and U. Platt, MAX-DOAS O_4 measurements - a new technique to derive information on atmospheric aerosols. (I) Principles and information content, J. Geophys. Res., in press., 2004.

Wagner, T., C. von Frideburg, M. Wenig, C. Otten, and U. Platt, UV/vis observations of atmospheric O_4 absorptions using direct moon light and zenith scattered sunlight under clear and cloudy sky conditions, J. Geophys. Res., 108, 4,424, doi: 10.1029/2001JD001026, 2002.

Wagner, T, F. Wittrock, A. Richter, M. Wenig, J.P. Burrows, and U. Platt, Continuos Monitoring of the high and persistent chlorine activation during the Arctic winter 1999/2000 by the GOME instrument on ERS-2, J. Geophys. Res., doi:10.1029/2001JD000466, 2002.

Wagner, T., C. Leue, K. Pfeilsticker, and U. Platt, Monitoring of the stratospheric chlo-

rine activation by GOME OClO measurements in the austral and boreal winters 1995 through1999, J. Geophys. Res.,106, 4971-4986, 2001.

Wagner, T., C. Leue, M. Wenig, K. Pfeilsticker, U. Platt, Spatial and temporal distribution of enhanced boundary layer BrO concentrations measured by the GOME instrument aboard ERS-2, J. Geophys. Res.,106, 24,225-24236, 2001.

Wang, P., A. Richter, M. Bruns, V. V. Rozanov, J. P. Burrows, K.-P. Heue, T. Wagner, I. Pundt, U. Platt, Measurements of tropospheric NO2 with an airborne multi-axis DOAS instrument, Atmos. Chem. Phys. Discuss., 4, 7541-7559, 2004.

Weber, M., S. Dhomse, F. Wittrock, A. Richter, B.-M. Sinnhuber, and J. P. Burrows, Dynamical Control of NH and SH Winter/Spring Total Ozone from GOME Observations in 1995 - 2002, Geophys. Res. Lett., 30(11), 10.1029/2002GL016799, 2003.

Weber, M., S. Dhomse, F. Wittrock, A. Richter, B.-M. Sinnhuber, and J.P. Burrows, Der Einfluss der Dynamik auf den Ozontransport und die Ozonchemie in hohen Breiten, Ozonbulletin des Deutschen Wetterdienstes Nr. 93, 25. Juni 2003.

Weber, M., K.-U. Eichmann, F. Wittrock, K. Bramstedt, L. Hild, A. Richter, J. P. Burrows, and R. Müller, The cold Arctic winter 1995/96 as observed by the Global Ozone Monitoring Experiment GOME and HALOE: Tropospheric wave activity and chemical ozone loss, Q. J. R. Meteorol. Soc.,128,1293-1320, 2002.

Wenig, M., S. Kühl, S. Beirle, E. Bucsela, B. Jähne, U. Platt, J. Gleason, and T. Wagner, Retrieval and Analysis of Stratospheric NO2 from GOME, J. Geophys. Res., revised, 2003.

Wittrock, F., H. Oetjen, A. Richter, S. Fietkau, T. Medeke, A. Rozanov, J. P. Burrows, MAX-DOAS measurements of atmospheric trace gases in Ny-Ålesund - Radiative transfer studies and their application, Atmos. Chem. Phys., 4, 955-966, 2004.

Wittrock, F., H. Oetjen, A. Richter, S. Fietkau, T. Medeke, A. Rozanov, and J. P. Burrows, MAX-DOAS measurements of atmospheric trace gases in Ny-Ålesund, Atmos. Chem. Phys. Disc., 3, 6109-6145, 2003.

Peer reviewed articles (in preparation)

Butz, A, H. Bösch, C. Camy-Peyret, M. Chipperfield, G. Dufour, M. Dorf, A. Rozanov, C. von Savigny, C. Sioris, S. Payan, F. Weidner, and K. Pfeilsticker, Inter-comparison of stratospheric O_3 and NO_2 profiles by balloon-borne UV, vis and near-IR solar occultation and ENVISAT/SCIAMACHY Limb measurements, in preparation for Atmos. Chem. Phys., 2004.

Dorf, M., A. Butz, H. Bösch, C. Camy-Peyret, M. Chipperfield, K. Grunow, S. Hrechanyy, B. Naujokat, A. Rozanov, C. Sioris, F. Stroh, F.Weidner, and K. Pfeilsticker, Balloon-borne stratospheric BrO measurements:Intercomparison with ENVISAT/SCIAMACHY BrO limb profiles, in preparation for Atmos. Chem. Phys., 2004.

Weidner, F., H. Bösch, A. Butz, C. Camy-Peyret, M. Dorf, K. Gerilowksi, W. Gurlit, and K. Pfeilsticker, Balloon-borne Limb profiling of UV/Vis skylight radiances, ozone and nitrogen dioxide: Technical set-up and validation of the method, in preparation for for Atmos. Chem. Phys., 2004.

Gurlit et al., Stratospheric solar irradiance in the UV-B, visible and near-IR spectral ranges: Inter-comparison with ground-based and satellite-borne measurements, Atmos. Chem. Phys., in prep., 2004.

Frieß, U., and U. Platt, Tropospheric IO in the Antarctic coastal region: Observations by Multi-Axis DOAS, to be submitted to Geophys. Res. Lett., 2003.

Frieß,U. and U. Platt, Absolute concentration measurements by DOAS in a highly scattering atmosphere, to be submitted to Geophys. Res. Lett., 2003.

Puentedura O., M. Gil, M. Navarro and C. López, BrO in the subtropics, to be submitted to Amos. Chem. Phys., 2004.

A.T.J. de Laat, J. Landgraf, B. Bregman and M Krol, The use GOME O_3 profile measurements for validation of chemistry-transport models, in preparation, 2004.

A.T.J. de Laat and J. Landgraf, Determining total tropospheric O_3 columns using GOME O_3 profiles and TOMS total O3 column measurements, in preparation.

Oetjen, H., F. Wittrock, A. Richter, and J.P. Burrows, Ten years of ground-based UV-Vis-

ible measurements at Ny-Ålesund (79°N, 12°E), in preparation for JGR, 2004.

Wittrock, F., S. Fietkau, T. Medeke, H. Oetjen, A. Richter, and J.P. Burrows, Observations of tropospheric BrO at different latitudes, in preparation for JGR, 2004.

Yela, M., S. Rodriguez, M. Gil, C. Parrondo, J. Araujo H. Ochoa, S. Díaz y G. Deferrari, The September 2002 Antarctic vortex major warming as observed by visible spectroscopy and ozonesoundings, to be submitted to Amos. Chem. Phys., 2004.

Conference proceedings

Blumenstock, T., A. Griesfeller, F. Hase, M. Scheneider, M. Gil, J.R. Moreta, U. Raffalski, U. Friess, G. Schwartz and E. Cuevas, Validation of MIPAS and SCIAMACHY data by ground-based spectroscopy at Kiruna, Sweden and Izaña, Tenerife Island (AO-191), First ENVISAT Validation Workshop, ESA/ESRIN, Italy, 9-13 Dec. 2002, Proceedings, ESA SP-531, 2003.

Bortoli , D., F. Ravegnani, I.K. Kostadinov, G. Giovanelli, and A. Petritoli, Stratospheric ozone and nitrogen dioxide amount obtained with GASCOD type DOASD spectrometer at Terra Nova Bay Station, (Antarctica) during December 2000 - Jannuary 2001, SPIE symposium, SPIE proceeding, 4485, 225-235, 2002.

Bortoli, D., G. Giovanelli, F. Ravegnani, I.K. Kostadinov, A. Petritoli, F. Calzolari, M.J. Costa, and A. M. Silva, Stratospheric nitrogen dioxide in Antarctic regions from ground based and satellite observations during 2001, SPIE symposium, SPIE Proceeding, 4882, 304-313, 2003.

Burrows, J.P. et al., Studies of NO_2 from Lightning and Convective Uplifting using GOME data, EUROTRAC symposium, March 2002.

Fietkau, S. et al., BrO measurements in Nairobi (1°S, 36°E) with the multi-axis DOAS method, EGU meeting, April 2004.

Fietkau, S. et al., One Year of Groundbased Multi Axis DOAS Measurements in Nairobi, 2nd International DOAS Workshop Heidelberg, September 2003.

Fietkau, S. et al., Multi-axis DOAS observations of atmospheric trace gases in Nairobi and Bremen, IGAC meeting, September 2002.

Gil, M., E. Cuevas, M. Yela, O. Puentedura, V. Carreñoy, and A. Redondas, Errors in backscattering satellite O3 measurements during absorbing aerosols Saharian Events, 3rd Asamblea Hispano Portuguesa de Geodesia y Geofísica, Valencia, España, 4 - 8 Febrero 2002, Books of Proceedings, ISBN 84-9705-297-8, edited 2003.

Goutail, F., A. Bazureau, and J.P. Pommereau, Validation of ENVISAT Products from SAOZ balloon flights in ESA/ACVT, ESA/ACVT First Envisat Validation Workshop, ESA/ESRIN, Frascati, Italy, 9-13 Dec. 2002, Proceedings, ESA SP-531, 2003.

Goutail, F., J. P. Pommereau and F. Lefèvre, Total Ozone Reduction in the Arctic during winters 2001 and 2002 from the SAOZ network and comparison to previous winters, Sixth European Symposium on Stratospheric Ozone, 2-6 Sept. 2002, Gothenburg, Sweden, Proceedings in: Air Pollution Research Report, Stratospheric Ozone 2002, N.R.P.Harris and G.T. Amanatidis (ed.), European Commission, 2003.

Goutail , F., L. Denis, J. P. Pommereau, F. Lefevre, and C. Deniel, Ozone loss, NOx and chlorine during the Arctic winter of 1999-2000 as reported by SAOZ, ground-based, short and long duration balloon flights, 15th ESA symposium on European Rocket and Balloon Programmes and Related Research, Biarritz, May 2001, Proceedings .

Lambert, J.-C., V. Soebijanta, Y. Orsolini, S. B. Andersen, A. Bui Van, et al., Coordinated ground-based validation of ENVISAT atmospheric chemistry with NDSC network data: Commissioning Phase Report, in Proc. First ENVISAT Validation Workshop, ESA/ESRIN, Italy, 9-13 Dec. 2002, ESA SP-531, 2003.

Lambert, J.-C., J. Granville, M. Allaart, T. Blumenstock, T. Coosemans, et al., Ground-based comparisons of early SCIAMACHY O3 and NO2 columns, in Proc. ENVISAT Validation Workshop, Frascati, 9-13 Dec. 2002, ESA SP-531, 2003.

Lambert, J.C., J. Granville, T. Blummenstock, F. Boersma, A. Bracher, et al., Geophysical Validation of SCIAMACHY NO2 Vertical Columns: Overview of Early 2004 Results, in Proc. Second Workshop on the Atmospheric Chemistry Validation of ENVISAT (ACVE-2), Frascati, Italy, 3 – 7 May, 2004

Lambert, J-C., M. Allaart, S.B. Andersen, T. Blumenstock, G. Bodeker, et al., First Ground-Based Validation of SCIAMACHY V5.01 O3 Column, in Proc. Second Workshop on the Atmospheric Chemistry Validation of ENVISAT (ACVE-2), Frascati, Italy, 3 – 7 May, 2004

Lambert, J-C., H.K. Roscoe, et al. (40 authors), Coordinated ground-based validation of Envisat atmospheric chemistry with NDSC network data: commissioning phase report, ESA/ACVT First Envisat Validation Workshop, ESA/ESRIN, Frascati, Italy, 9-13 Dec. 2002, Proceedings, ESA SP-531, 2003.

Lambert, J.-C., J. Granville , M. Allaart, T. Blumenstock, T. Coosemans, M. De Mazière, U. Friess, M. Gil, F. Goutail, D. V. Ionov, I. Kostadinov, E. Kyrö, A. Petritoli, A. Piters, A. Richter, H. K. Roscoe, H. Schets, J. D. Shanklin, V. T. Soebijanta, T. Suortti,M. Van Roozendael, and C. Varotsos, Ground-based Intercomparisons of early SCIAMACHY O_3 and NO_2 columns, ESA/ACVT First Envisat Validation Workshop, ESA/ESRIN, Frascati, Italy, 9-13 Dec. 2002, Proceedings, ESA SP-531, 2003.

Medeke, T. et al. , Multi-axis DOAS observations of atmospheric trace gases at the Greenland ice cap, 2nd International DOAS Workshop Heidelberg, September 2003.

Medeke ,T. et al. , Multi-axis DOAS observations of atmospheric trace gases in Bremen, DPG Frühjahrstagung, March 2003.

Mieville, A., F. Goutail, J.P. Pommereau, J-C. Lambert, V. Dorokhov, S. Khaikin, and D. Ignatiev, Consolidation of SAOZ ground-based O_3 and NO_2 column measurements in the Arctic and comparison with GOME, Sixth European Symposium on Stratospheric Ozone, 2-6 Sept. 2002, Gothenburg, Sweden, Proceedings in: Air Pollution Research Report, Stratospheric Ozone 2002, N.R.P.Harris and G.T. Amanatidis (ed.), European Commission, 2003.

Nüß, H. et al., Improvements of GOME NO_2 Retrieval, EGU meeting, April 2004.

Nüß, H. et al., GOME NO_2 Retrieval with individual AMF for Aerosol, Albedo, Orography and Profile, 2nd International DOAS Workshop Heidelberg, September 2003.

Nüß, H. et al., GOME NO_2 Retrieval with MOZART Profiles, IGAC meeting, September 2002.

Oetjen, H. et al., MAX-DOAS measurements in Ny-Ålesund and during the Andoya Campaign in 2003, 2nd International DOAS Workshop Heidelberg, September 2003.

Oetjen, H. et al., Observations of Atmospheric Trace Gases from 1994 to 2003, EGU meeting, April 2003.

Oetjen, H. et al., Multi-axis DOAS observations of atmospheric trace gases, Sixth European symposium on stratospheric ozone in Gothenburg, September 2002.

Petritoli, A., F. Ravegnani, I. Kostadinov, D. Bortoli, and G. Giovanelli, Development of a new methodology for the retrieval of in-situ stratospheric trace gases concentration from airborne limb-absorption measurements, SPIE symposium, SPIE proceeding, 4485, 486-492, 2002.

Petritoli, A., P. Bonasoni, U. Bonafe, D. Bortoli, F. Calzolari, F. Evangelisti, I. Kostadinov, F. Ravegnani, and G. Giovanelli, Stratospheric NO2 climatological trend at northern mid-latitudes from 8 years of ground based observations at Mt. Cimone station, Geoscience and Remote Sensing Symposium, 2002, Proceedings IEEE International, 4, 2331-2333, 2002.

Pfeilsticker, K., H. Bösch, A. Butz, C. Camy-Peyret, M. Dorf, W. Gurlit, K. Grunow, B. Naujokat, and F. Weidner, Balloon-Borne DOAS Measurements of SCIAMACHY Level 1 and 2 Data Products, 16th Symposium on European Rocket and Balloon Programmes and Related Research, St. Gallen, June 2.-5. 2003, Proceeding, 2003.

Richter, A. et al., Linking Tropospheric NO_2 Measurements from SCIAMACHY to the GOME Time Series, EGU meeting, April 2004.

Richter, A. et al., Cloud effects in Tropospheric NO_2 Columns retrieved from SCIAMACHY Nadir Measurements, DPG Frühjahrstagung, March 2004.

Richter, A. et al., First NO_2 Results from SCIAMACHY UV/vis Nadir Measurements, 2nd International DOAS Workshop Heidelberg, September 2003.

Richter, A. et al., First Results from SCIAMACHY UV/vis Nadir Measurements, DPG Frühjahrstagung, March 2003.

Richter, A. et al., Comparison of GOME BrO measurements with SLIMCAT model results, EGS assembly, April 2002.

Schmoltner, A.-M. et al., Retrieval of stratospheric and tropospheric ozone from SCIAMACHY limb and nadir observations, EGU meeting, April 2004.

Sierk, B. et al., Tropospheric trace gas amounts from combined limb/nadir analysis of SCIAMACHY data, DPG Frühjahrstagung, March 2003.

Wang, P. et al., AMAXDOAS NO_2 and HCHO measurements during the FORMAT Campaigns, EGU meeting, April 2004.

Wang, P. et al., AMAXDOAS measurements from the DLR Falcon Part1: north route, DPG Frühjahrstagung, March 2003.

Wetzel, G., T. Blumenstock, H. Oelhaf, G.P. Stiller, D.-Y. Wang, et al., Validation of Mipas-Envisat Version 4.61 Operational Data: NO2, in Proc. Second Workshop on the Atmospheric Chemistry Validation of ENVISAT (ACVE-2), Frascati, Italy, 3 – 7 May, 2004

Wittrock, F. et al., Ground-based UV/vis observations of atmospheric trace gases at different latitudes, 8th IGAC conference, September 2004.

Yela, M., S. Rodriguez, M. Gil, J. Iglesias, J. Araujo, S. Diaz, and M. Chipperfield, Seasonal evolution of NO2 and O3 outside, at the edge and inside the Antarctic Polar Vortex: Comparison with the SLIMCAT model, 3rd Asamblea Hispano Portuguesa de Geodesia y Geofísica, Valencia, España, 4 - 8 Febrero 2002, Books of Proceedings, ISBN 84-9705-297-8, edited 2003.

Van Roozendael, M., I. De Smedt, C. Fayt, F. Wittrock, A. Richter, O. Afe, First validation of SCIAMACHY BrO columns, in Proc. Second Workshop on the Atmospheric Chemistry Validation of ENVISAT (ACVE-2), Frascati, Italy, 3 – 7 May, 2004
Theys, N., I. De Smedt, C. Fayt, M. Chipperfield, P. Post, R. van der A, and M. Van Roozendael, Total and tropospheric BrO derived from GOME and SCIAMACHY as part of the TEMIS project, in Proc. of the ERS/ENVISAT 2004 Symposium, Salzburg, Austria, 6 – 10 September, 2004 (in press)

Van Roozendael, M., C. Fayt, C. Hermans, and J.-C. Lambert, Retrieval of tropospheric BrO ad NO2 from UV-visible Observations, in the “Annual Report 2001- TROPOSAT: The Use and Usability of Satellite Data for Tropospheric Research”, EUROTRAC-2 International Scientific Secretariat (ISS), GSF-National Research Centre for Environment and Health, Munich, Germany, pp. 67-71, May 2002.

Reports

Adukpo, D., Charactisation of a MAX-DOAS Instrument and Application to Satellite Validation, Masters Thesis, University of Bremen, September 2002.

Friedeburg, C. v., Derivation of trace gas information combining differential optical absorption spectroscopy with radiative transfer modelling, University of Heidelberg, Heidelberg, Germany, Ph.D. thesis, 2003.

Hönninger, G., Halogen oxide studies in the boundary layer by multi axis differential optical absorption spectroscopy and active longpath-DOAS, Ph.D. thesis, University

of Heidelberg, 2002.

Moreta J. R., NO2 column intercomparison: SCIAMACHY versus Ground based (Antarctica and Subtropics), Physics Science Faculty, Univ. Madrid, Spain, Diploma thesis, 2003.

Oetjen, H., Messungen atmosphärischer Spurengase in Ny-Ålesund. Diploma-Thesis, University of Bremen, September 2002 (in German).

Petritoli, A., Analisi quantitativa del biossido di azoto in stratosfera e troposfera nella regione della pianura padana mediante misure a rilevamento remoto ed in situ, University of Bologna, Spain, Ph.D. thesis, 2003.

Schlieter, S., Spurengasmessungen während der Nacht mittels Mondlichtspektroskopie im Vergleich mit Modellrechnungen. PhD-Thesis, University of Bremen, June 2001 (in German).

Sinreich, R.,Höhenprofilmessung von NO2 mit Multi-Axis-DOAS Messungen in Heidelberg, Univ. of Heidelberg, Heidelberg, Germany, Diploma thesis, 2003.